INVESTIGATION OF THE LIQUID STRUCTURE OF DIMETHYL SULFOXIDE-PYRIDINE MIXTURES WITH BRILLOUIN SPECTROSCOPY

THESIS FOR THE DEGREE OF PH.D. MICHIGAN STATE UNIVERSITY

MARY MARGARET TANNAHILL

1973

LIBRARY
Michigan State
University



ABSTRACT

INVESTIGATION OF THE LIQUID STRUCTURE OF DIMETHYL SULFOXIDE-PYRIDINE MIXTURES WITH BRILLOUIN SPECTROSCOPY

BY

Mary Margaret Tannahill

A Brillouin scattering study of binary solvent mixtures of dimethyl sulfoxide (DMSO) and pyridine was performed in order to gain insight into the structural changes occurring in solution as the composition was varied from pure pyridine to pure DMSO. Thirteen solutions, ranging from neat pyridine to neat DMSO, were examined spectrometrically at eight different temperatures between 20 and 60 °C. The light scattering and acoustical properties determined were the Brillouin shift, Brillouin linewidth, Landau-Placzek ratio, velocity of sound, sonic absorption coefficient and adiabatic compressibility. Density and refractive index data for the mixtures were also recorded.

Examination of the refractive index, Brillouin shift, velocity of sound, sonic absorption coefficient and Brillouin linewidth as a function of temperature revealed a linear relationship for each property. The refractive index and Brillouin linewidth were also found to be linear functions of composition in the temperature range from 20 to 60 °C.

Fluctuations in the velocity of sound and frequency-corrected absorption coefficient over the entire compositional region from neat pyridine to neat DMSO indicated changes in the degree of association in the liquid. Neat DMSO was ascertained to be a rather highly

structured liquid and appeared to possess a greater degree of organization than either neat pyridine or any of the binary mixtures. Neat pyridine, however, was also noted to possess a considerable degree of ordering.

Maximum disorganization of the liquid structure occurred at approximately the equimolar composition for each of the eight temperatures, implying that the associated species present in the DMSO-pyridine mixtures are aggregates of DMSO and/or pyridine rather than complexes between DMSO and pyridine. Infrared spectroscopic measurements of the S-O stretching frequency for mixtures of dimethyl sulfoxide and pyridine at 22 OC support the concept of self-association of DMSO.

The Landau-Placzek ratio was found to be a linear function of the temperature for each of the DMSO-pyridine mixtures investigated.

There was a distinct break, however, in the Landau-Placzek ratio-temperature curve for pure DMSO at 45 °C, indicating reorganization of the liquid structure at this temperature.

The overall variations in the Landau-Placzek ratio with composition gave supporting evidence to the interpretations of the velocity of sound and absorption coefficient data. In particular, a vast increase in association between 0.80 and 1.00 mole fraction DMSO was heralded by a significant decrease in the Landau-Placzek ratio in this region.

INVESTIGATION OF THE LIQUID STRUCTURE OF DIMETHYL SULFOXIDEPYRIDINE MIXTURES WITH BRILLOUIN SPECTROSCOPY

Ву

Mary Margaret Tannahill

A THESIS

Submitted to

Michigan State University

in partial fulfillment of the requirements

for the degree of

DOCTOR OF PHILOSOPHY

Department of Chemistry

686498

to the memory of my grandfather,

James S. Campbell

ACKNOWLEDGMENTS

The author wishes to express her thanks to the following people, without whose technical and/or intellectual expertise this work could not have been completed: Stuart Gaumer, designer of the Brillouin scattering spectrometer; Charles Hacker and Russell Geyer of the University Machine Shop; Keki Mistry, Jerry DeGroot and Andrew Seer, Jr. of the University Glassblowing Shop; Henny Seeuwen and Kathy Fagan, typists and Jo Llu Long, graphics illustrator, at the University of Texas Medical Branch in Galveston.

My sincere appreciation also goes to my mentor, Dr. Jack B.

Kinsinger, for his wisdom and humor during the course of the research,
and to my parents, Mr. and Mrs. C. F. Tannahill, for their unswerving
moral support during this endeavor.

TABLE OF CONTENTS

			Page
ı.	INT	PRODUCTION	1
II.	DES	CRIPTION OF LIGHT SCATTERING FROM INDEPENDENT PARTICLES	3
•	A.	General Concepts	3
	в.	Rayleigh Scattering	4
	c.	Fine Structure of the Rayleigh Peak: Brillouin	
		Scattering	6
		1. Brillouin scattering from a pure fluid	8
		2. Brillouin scattering from a two-component mixture	28
		a. Derivation of the spectral distribution of	
		light scattered from a binary liquid system	28
		b. Relationship between the Brillouin linewidth,	
		phenomenological coefficients and thermodynamic	
		parameters	37
	D.	Effects of Optical Properties of Polar Liquids on Light	
		Scattering	43
III.	EXP	PERIMENTAL INFORMATION	53
	A.	The Brillouin Spectrometer	53
	в.	Design and Characterization of the Temperature Control	
		Cell	56
	c.	Preparation of the Samples	63
	D.	Measurement of the Refractive Index	64

TABLE OF CONTENTS (Cont.)

			Page
IV.	RES	ULTS AND DISCUSSION	65
	A.	Variation of the Refractive Index with Temperature	
		and Composition	65
	В.	Molar Refractivity at 22.0 °C	71
	c.	Variation of the Brillouin Shift with Temperature and	
		Composition	76
	D.	Velocity of Sound and Related Quantities	91
	E.	Variation of the Brillouin Linewidth with Temperature	
		and Composition	114
	F.	Sonic Absorption Coefficient and Related Quantities	157
	G.	Variation of the Landau-Placzek Ratio with Temperature	
		and Composition	181
v.	CON	CLUSIONS	192
	LIS	T OF REFERENCES	194
	APP	PENDICES	199

LIST OF TABLES

TABLE		Page
1	Measured and Corrected Temperatures Obtained During Brillouin Scattering Measurements for Mixtures of DMSO and Pyridine	62
2	Nominal and Measured Compositions for Mixtures of DMSO and Pyridine	66
3	Refractive Index as a Function of Temperature for λ = 5890 and 5145 Å	67
4	Molar Refractivities for Mixtures of DMSO and Pyridine at 22.0 °C	75
5	Brillouin Shift as a Function of Temperature	84
6	Intercept and Slope for the Brillouin Shift-Temperature Relationship ν_B = A + BT	88
7	Brillouin Shift and Velocity of Sound as a Function of Temperature for Mixtures of DMSO and Pyridine	96
8	Intercept and Slope for the Sonic Velocity-Temperature Relationship $V_S = A + BT$	100
9	Squares of the Ideal and Experimental Velocities of Sound for 21.6 °C	101
10	Adiabatic Compressibility as a Function of Composition for 21.6 °C	104
11	Experimental and Calculated Intensities for the Central Peak of 0.80 Mole Fraction DMSO at 59.0 °C	122
12	Experimental and Calculated Intensities for the Left Brillouin Peak of 0.80 Mole Fraction DMSO at 59.0 °C	125
13	Experimental and Calculated Intensities for the Central Peak of Neat DMSO at 59.0 °C	131
14	Experimental and Calculated Intensities for the Left Brillouin Peak of Neat DMSO at 59.0 °C	133
15	Experimental and Calculated Intensities for the Central Peak of Neat Pyridine at 29.5 °C	135

LIST OF TABLES (Cont.)

TABLE		Page
16	Experimental and Calculated Intensities for the Right Brillouin Peak of Neat Pyridine at 29.5 OC	137
17	Linewidth of the Central Peak as a Function of Finesse	144
18	Comparison of the Linewidths of the Central Peaks of Neat DMSO, Neat Pyridine and 0.40 Mole Fraction DMSO at a Given Finesse	151
19	Brillouin Linewidth as a Function of Temperature for Mixtures of DMSO and Pyridine	152
20	Absorption Coefficient as a Function of Temperature for Mixtures of DMSO and Pyridine	160
21	Temperature Derivative of the Sonic Absorption Coefficient	167
22	Landau-Placzek Ratio as a Function of Temperature for Mixtures of DMSO and Pyridine	182
23	Temperature Calibration Data	199
24	Calculation of the Dispersion for Mixtures of DMSO and Pyridine at 26.4 °C	203
25	Calculation of $n_{5145\text{\AA}}^{\text{O}}$ for Mixtures of DMSO and Pyridine at 26.4 $^{\text{O}}\text{C}$	204
26	Temperature Dependence of the Refractive Index for λ = 5890 and 5145 R	205

LIST OF FIGURES

FIGURE		Pag e
1	The light scattering process	3
2	The Brillouin spectrometer	54
3	Sketch of the temperature control cell	57
4	Cross-sectional view of the temperature control cell	58
5	Calibration data for the temperature control cell	61
6	Refractive index versus temperature for mixtures of DMSO and pyridine	69
7	Refractive index versus temperature for neat DMSO	70
8	Variation of the temperature derivative of the refractive index with composition for mixtures of DMSO and pyridine	72
9	Refractive index versus composition for 30.1 °C	73
10	Refractive index versus composition for 22.0, 26.4 and 30.1 °C	74
11	Variation of the density with composition for 22.0 °C	77
12	Molar refractivity versus composition at 22.0 °C	78
13	Brillouin spectrum for 0.15 mole fraction DMSO at 34.5 °C	80
14	Brillouin spectra for neat DMSO at 29.5 and 59.0 °C	81
15	Brillouin spectra for 0.60 mole fraction DMSO at 39.4 and 59.0 °C	82
16	Brillouin spectra for neat pyridine at 21.6 and 59.0 °C	83
17	Brillouin shift versus temperature for neat DMSO	86
18	Brillouin shift versus temperature for neat pyridine, 0.10, 0.15, 0.30 and 0.50 mole fraction DMSO	87
19	Variation of the intercept of $v_B = A + BT$ with composition for mixtures of DMSO and pyridine	89

LIST OF FIGURES (Cont.)

FIGURE		Page
20	Variation of the slope of v_B = A + BT with composition for mixtures of DMSO and pyridine	90
21	Brillouin shift versus composition at 21.6 °C	92
22	Brillouin shift versus composition for 21.6, 29.5, 34.5 and 39.4 °C	93
23	Brillouin shift versus composition for 44.5, 49.3, 54.2 and 59.0 $^{\rm O}{\rm C}$	94
24	Temperature coefficient of the velocity of sound	102
25	Variation of the velocity of sound with composition for 21.6, 29.5, 34.5, 39.4, 44.5, 49.3, 54.2 and 59.0 °C	103
26	Square of the velocity of sound versus composition for 21.6 °C	105
27	Variation of the adiabatic compressibility with composition for 21.6 °C	107
28	Variation of the S-O stretching frequency with composition at 21.6 °C	109
29	Square of the velocity of sound versus composition for 21.6, 29.5, 34.5, 39.4, 44.5, 49.3, 54.2 and 59.0 °C	111
30	Portion of Brillouin spectrum for neat pyridine at 29.5 °C	117
31	Central peak of Brillouin spectrum for 0.80 mole fraction DMSO at 59.0 $^{\rm O}{\rm C}$	118
32	Left Brillouin peak of Brillouin spectrum for 0.80 mole fraction DMSO at 59.0 °C	119
33	Central peak of Brillouin spectrum for neat DMSO at 59.0 °C	120
34	Left Brillouin peak of Brillouin spectrum for neat DMSO at 59.0 °C	121
35	Left-hand side of central peak for 0.80 mole fraction DMSO at 59.0 °C fit to a Lorentzian	127
36	Right-hand side of central peak for 0.80 mole fraction DMSO at 59.0 °C fit to a Lorentzian	128

LIST OF FIGURES (Cont.)

FIGURE		Page
37	Left-hand side of left Brillouin peak for 0.80 mole fraction DMSO at 59.0 °C fit to a Lorentzian	129
38	Right-hand side of left Brillouin peak for 0.80 mole fraction DMSO at 59.0 °C fit to a Lorentzian	130
39	Laser-line instrumental profile, spectrum 1-b, August 17, 1971	139
40	Laser-line instrumental profile, spectrum 1-b, August 17, 1971, fit to a Gaussian	140
41	Left-hand side of laser-line instrumental profile, 1-b, August 17, 1971, fit to a Lorentzian	141
42	Right-hand side of laser-line instrumental profile, 1-b, August 17, 1971, fit to a Lorentzian	142
43	Linewidth versus finesse for central peak of neat DMSO	148
44	Linewidth versus finesse for central peak of neat pyridine	149
45	Linewidth versus finesse for central peak of 0.40 mole fraction DMSO	150
46	Brillouin linewidth versus temperature for mixtures of DMSO and pyridine	156
47	Brillouin linewidth versus composition for 34.5 °C	158
48	Brillouin linewidth versus composition for 21.6, 29.5, 34.5, 39.4, 44.5, 49.3, 54.2 and 59.0 °C	159
49	Absorption coefficient versus temperature for 0.20 mole fraction DMSO	169
50	Absorption coefficient versus composition at 21.6 °C	171
51	Absorption coefficient versus composition at 54.2 °C	172
52	Frequency-corrected absorption coefficient versus temperature for 0.70 mole fraction DMSO	173
53	Frequency-corrected absorption coefficient versus temperature for 0.05, 0.10, 0.30 and 0.50 mole fraction DMSO	174
54	Frequency-corrected absorption coefficient versus composition at 21.6 °C	176

LIST OF FIGURES (Cont.)

FIGURE		Page
55	Frequency-corrected absorption coefficient versus composition for 21.6, 29.5, 34.5 and 39.4 °C	177
56	Frequency-corrected absorption coefficient versus composition for 44.5, 49.3 and 54.2 °C	178
57	Velocity and absorption of sound for mixtures of DMSO and pyridine at 21.6 $^{\rm O}{\rm C}$	179
58	Absorption of sound and adiabatic compressibility for mixtures of DMSO and pyridine at 21.6 °C	180
59	Landau-Placzek ratio versus temperature for neat pyridine	185
60	Landau-Placzek ratio versus temperature for 0.80 mole fraction DMSO	186
61	Landau-Placzek ratio versus temperature for neat DMSO	187
62	Variation of the Landau-Placzek ratio with composition for 29.5, 34.5, 39.4, 44.5, 49.3, 54.2 and 59.0 °C	188
63	Variation of the Landau-Placzek ratio with β_S/ρ^2 for mixtures of DMSO and pyridine at 21.6 °C	190

I believe

that man will not merely endure

he will prevail

He is immortal

not because he alone among creatures has an inexhaustible voice

but because he has a soul

a spirit capable of compassion

and sacrifice and endurance

William Faulkner Nobel Prize Acceptance Speech Stockholm December 1950

I. INTRODUCTION

Decause of its unique solvation properties, dimethyl sulfoxide (DMSO) has been the subject of wide-ranging scientific investigations in the past twenty years (1). Specific chemical reactions of DMSO have been studied, as well as the physical properties, solvation effects and structure of this aprotic polar solvent.

It is generally accepted that liquid and solid DMSO are highly associated substances (cf. the physical properties listed on page 5 of Ref. 1), and that the forces responsible for this high degree of association arise from dipole-dipole interactions between the sulfur and oxygen atoms of adjacent molecules. It is postulated that there are several different structural forms in which molecular aggregates of DMSO exist (1), depending on the mole fraction of DMSO in a particular mixture of the liquid and on the amount of kinetic energy available.

These structural forms have been examined previously by a variety of methods:

- (1) infrared spectroscopy (2-5).
- (2) thermodynamic studies (6-9).
- (3) dielectric constant and refractive index measurements (6), (10), (11).
- (4) nuclear magnetic resonance spectroscopy (12).
- (5) density and viscosity measurements (6).
- (6) mass spectroscopy (6).

Many of these investigations were performed in binary solvent mixtures of DMSO, in the hope that the concentration dependence of the property under study would give some clue as to the type of DMSO aggregate formed as the mole fraction of DMSO increased. No publications have appeared, however, concerning the use of light scattering spectroscopy to characterize the structural forms of dimethyl sulfoxide in binary solvent mixtures.

The purpose of this brillouin scattering study of dimethyl sulfoxide-pyridine mixtures is to elucidate structural changes which are

postulated to occur in the liquid as the composition is varied from pure

pyridine to pure DMSO. Specifically, it is the author's intent

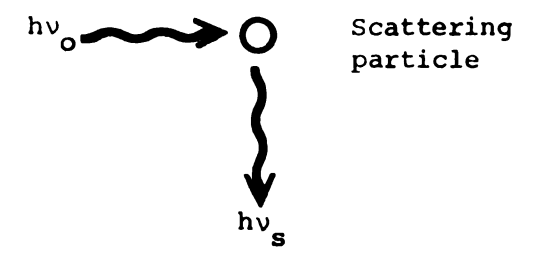
- (1) to present data on the velocity of sound in binary mixtures of DMSO and pyridine, and to attempt to correlate changes in the sonic velocity with changes in the liquid structure.
- (2) to show that structural changes are also manifest in the concentration and temperature dependence of other lightscattering parameters, namely, the Landau-Placzek ratio and the attentuation coefficient of sound waves in the liquid.
- (3) to correlate the data obtained from the light scattering experiments with data obtained by other physical-chemical methods.

II. DESCRIPTION OF LIGHT SCATTERING FROM INDEPENDENT PARTICLES

A. General Concepts

Light scattering from a system of independent particles occurs when an incident electromagnetic wave of frequency $\nu_{\rm O}$ strikes a scattering particle, inducing an oscillating electric dipole in a direction perpendicular to the electric vector of the incident radiation. This oscillating dipole then emits radiation of frequency $\nu_{\rm S}$ in a direction perpendicular to the direction of propagation of the incoming radiation. If the frequency of the scattered wave is equal to that of the incoming wave, elastic scattering is said to have taken place. Inelastic scattering occurs if the frequency of the scattered wave is not equal to the frequency of the incoming wave; this implies a scattered wave of different energy.

Pictorially, the light scattering process can be viewed in this manner:



 $v_0 = v_s$, elastic scattering process $v_0 \neq v_s$, inelastic scattering process

Figure 1. The light scattering process.

Rayleigh scattering is the term used to describe an elastic scattering process in which the size of the scattering particle is small compared to the wavelength of the incident radiation. In this process,

the scattering particle acts like a radiating linear dipole after impact with the incident electromagnetic wave. Mie scattering occurs when radiation of small wavelength (compared to the dimensions of the scattering particle) strikes a macromolecular system of large relative index of refraction. Here the scatterer can no longer be considered to be a simple oscillating dipole, and the intensity and distribution of the scattered light assumes a much more complicated form than for small-particle Rayleigh scattering.

B. Rayleigh Scattering

As outlined in Section A, light scattering occurs when an incident electromagnetic wave interacts with the polarizability of a scattering particle. The dipole moment induced in the x direction by an incoming beam traveling in the z direction is given by

$$\mu_{\mathbf{x}} = \alpha_{\mathbf{x}\mathbf{y}} \mathbf{E}_{\mathbf{y}} \tag{1}$$

where α_{xy} is the x-y component of the polarizability tensor and E_y is the magnitude of the electric vector of the incident radiation. In other words, an electric vector in the y direction causes an electric dipole in the x direction because of the distortability of the electron distribution in the molecule. The polarizability component, α_{xy} , is a measure of this distortability.

In general, the polarizability is a function of direction and must be regarded as a tensor of the second order:

$$\alpha = \begin{bmatrix} \alpha_{xx} & \alpha_{xy} & \alpha_{xz} \\ \alpha_{yx} & \alpha_{yy} & \alpha_{yz} \\ \alpha_{zx} & \alpha_{zy} & \alpha_{zz} \end{bmatrix}. \tag{2}$$

The subscripts x, y, and z denote the Cartesian coordinates of

the scattering system under consideration. For isotropic molecules, 1 the only terms of importance in the polarizability tensor are α_{xx} , α_{yy} , and α_{zz} . The off-diagonal elements are zero in the case of isotropic scattering particles.

The intensity of light scattered in the x direction by an incoming beam of light with the electric vector oscillating in the y direction is given by the relation

$$I_{x} = \frac{\omega^{4}}{3c^{3}} \left| \alpha_{yy} \right|^{2} E_{y}^{2}$$
 (3)

where ω is the angular frequency of the incident radiation and c is the velocity of light in vacuo.

Switching to polar coordinates, we have, for isotropic scattering particles of average polarizability, α , the Rayleigh equation (13) for the total intensity of radiation scattered in the direction θ from an unpolarized incident beam of light:

$$I_{\theta} = \frac{I_{0} 8\pi^{4} \left|\frac{-1}{\alpha}\right|^{2}}{\lambda^{4} r^{2}} \left(1 + \cos^{2}\theta\right). \tag{4}$$

In equation (4), I is the intensity of the incident radiation, α is the average isotropic polarizability (14), given by

$$\overline{\alpha} = \frac{1}{3} \left[\alpha_{xx} + \alpha_{yy} + \alpha_{zz} \right], \tag{5}$$

 θ is the angle between the direction of observation and the direction of propagation of the incident beam, r is the distance between the scattering particles and the observer, and λ^* is the wavelength of light in the medium.

We will assume in the ensuing discussion that we are dealing with isotropic molecules.

Also,
$$\lambda' = \frac{\lambda_{O}}{n} , \qquad (6)$$

where λ_0 is the <u>in vacuo</u> wavelength of the incident light and n is the index of refraction of the medium.

Ehagavantam (15) has derived a relationship for the average polarizability, α , for an isolated molecule treated as a dielectric sphere:

$$\overline{\alpha} = \frac{\Delta \varepsilon}{4 \, \text{Te}} \ . \tag{7}$$

Here $\Delta \epsilon$ is the fluctuation in the dielectric constant about the average value, ϵ , in the small spherical scattering volume, v.

Employing equation (7) for \overline{a} , the Rayleigh relation for the scattering of light from an isolated isotropic molecule can be written as

$$I_{\theta} = \frac{I_{0}\pi^{2} < (\Delta \epsilon)^{2} > (1 + \cos^{2}\theta)}{2\lambda^{4} r^{2} v^{2}}$$
 (8)

where < $\left(\Delta\epsilon\right)^2$ > is the mean square fluctuation in the dielectric constant. 1

 I_{Θ} , it should be recalled, is the total intensity of the light scattered in the direction θ . Specific expressions are derived in section C for the intensity spectrum of the Rayleigh-scattered light.

C. Fine Structure of the Rayleigh Peak: Brillouin Scattering
In 1922, almost ten years after initiating a theoretical investigation of the scattering of light from dense media, Leon Brillouin
published his theory concerning the fine structure of the Rayleigh peak
(16). Brillouin postulated the existence of three peaks for a highly

¹Introduction of $< (\Delta \epsilon)^2 >$ is justified by a consideration of the statistical treatment of the fluctuations in the dielectric constant.

resolved Rayleigh spectrum: a central peak (the Rayleigh peak itself) and two symmetrical Doppler-shifted side peaks.

Beginning with Debye's theory of the specific heat of solids (17) and Einstein's theory for the scattering of light from density fluctuations in an ideal gas (18), Brillouin derived a formula for the scattering of light from density fluctuations in a dense medium. Much to his amazement, he found that "... only one Debye vibration was responsible for the scattering of light [at given light frequency ν and scattering angle ω with hypersonic vibration ν_0 ... (19)." These unusual results were published as a note in the Comptes Rendus de l'Academie des Sciences of Paris in 1914 (20).

Before Brillouin had a chance to pursue these light scattering hypotheses to fruition, however, World War I commenced and he left with the French Army for the field. Upon returning to his theoretical papers in 1919, Brillouin decided to attack the problem of light scattering from a different point of view. He considered the passage of ultrasonic or hypersonic waves in a dense medium as creating "... a succession of planes of higher and lower density, moving along with sound velocity u ... (19)." Since each of the phonon planes of frequency v_0 reflects light waves of a specific frequency, v_0 , there is only one way in which the incident beam can be modified in frequency after an interaction with one of these planes: it must be Doppler shifted by an amount tv_0 from the incident frequency, v_0 . In other words,

$$\Delta v = \pm \left| v - v_0 \right| = \pm \frac{2v_{\text{nu}}}{c} \sin \omega / 2 , \qquad (9)$$

Note that Brillouin's symbols for the frequency of the incident photon and for the scattering phonon are exactly reversed with respect to the symbols which are used in subsequent portions of this work.

where Δv is the change in frequency exhibited by the Doppler-shifted side peaks, n is the refractive index of the medium and c is the velocity of light, in vacuo. Equation (9) is the principal equation of Brillouin scattering; it describes what happens when an electromagnetic wave of frequency v interacts with a sound wave of velocity u in the liquid.

1. Brillouin scattering from a pure fluid

Light is scattered by a pure fluid as a result of local fluctuations (inhomogenieties) in the optical dielectric constant, $<\Delta \varepsilon^2>$. The fluctuations in the dielectric constant are, in turn, dependent upon several factors: fluctuations in density, orientational fluctuations and fluctuations caused by dipole-induced-dipole interactions and by shear stresses and strains. Fluctuations caused by reorientation of nonspherical molecules, by dipole-induced-dipole interactions and by shear stresses and strains in the liquid are responsible for depolarized light scattering (21). According to Landau and Placzek (22), the density fluctuations that account for polarized scattering are divisible into two major components: isobaric entropy fluctuations, which produce a peak centered at the incident frequency (the Rayleigh peak) and isentropic pressure fluctuations, which give rise to two Doppler-shifted side peaks (the Brillouin peaks). The three peaks taken together are called a Brillouin spectrum; this polarized spectrum can also be considered to result from time-dependent fluctuations in the dielectric constant.

Several theoretical papers have been published concerning the intensity distribution of light scattered from density fluctuations in a pure fluid (22-29); however, only three of these (25-27) establish a

foundation for our later consideration of light scattering in a binary mixture. We begin with the pure thermodynamic fluctuation theory of Cummins and Gammon (25).

On the basis of thermodynamic arguments alone, Landau and Placzek (22) derived a theoretical expression for the rates of the intensity of the central peak, I_c , to the combined intensities of the Brillouin side peaks, $2I_R$:

$$\frac{\mathbf{I}_{\mathbf{C}}}{2\mathbf{I}_{\mathbf{B}}} = \frac{\mathbf{c}_{\mathbf{p}} - \mathbf{c}_{\mathbf{v}}}{\mathbf{c}_{\mathbf{v}}} = \frac{\beta_{\mathbf{T}} - \beta_{\mathbf{S}}}{\beta_{\mathbf{S}}}.$$
 (10)

In equation (10), c_p and c_v are the specific heats at constant pressure and volume, respectively, β_T is the isothermal compressibility and β_S is the adiabatic compressibility. Through the years it was found, however, that the Landau-Placzek equation did not match with experimentally determined values of $I_c/2I_B$ (25, 30, 31). By the introduction of a frequency-dispersion correction term, Cummins and Gammon (25) sought to alleviate this difficulty. They examined the classical fluctuation theory of light scattering and then modified the resulting equations to take into account the effects of dispersion (frequency dependence) on the thermodynamic properties of the system.

According to Einstein (18), the intensity, i, of light scattered by a small volume element, v, of a pure fluid when a plane polarized beam of light is incident on it at $90^{\circ 1}$ can be given by:

$$i_{90} = \frac{I_o \pi^2}{r^2 \lambda_o^4} v^2 < (\Delta \epsilon)^2 > .$$
 (11)

The scattering angle, θ , is always measured from the direction of propagation of the incident beam to the direction of observation of the scattered light.

In equation (11), i_{90} is the intensity of the scattered light, I_{0} is the intensity of the incident beam, r is the distance from the scattering element to the point of observation, and $<(\Delta\epsilon)^{2}>$ is the mean square fluctuation of the dielectric constant. This equation applies to a system of particles which are small (< one tenth) compared to the wavelength of the incident radiation. Furthermore, it is assumed that the random fluctuations in the local dielectric constant are uncorrelated from one volume element to another.

Einstein expressed the dielectric constant in terms of the intensive variables density, ρ , and temperature, T, such that

$$\Delta \varepsilon = \left(\frac{\partial \varepsilon}{\partial \rho}\right)_{T} \Delta \rho + \left(\frac{\partial \varepsilon}{\partial T}\right)_{\rho} \Delta T \qquad (12)$$

and

$$\langle (\Delta \varepsilon)^2 \rangle = \left(\frac{\partial \varepsilon}{\partial \rho} \right)_{\rm T}^2 \langle (\Delta \rho)^2 \rangle + \left(\frac{\partial \varepsilon}{\partial \rm T} \right)_{\rm O}^2 \langle (\Delta \rm T)^2 \rangle.$$
 (13)

Einstein then neglected the second term in equation (13) on the assumption that $(\partial \varepsilon/\partial T)_{\rho}$ is small compared to $(\partial \varepsilon/\partial \rho)_{T}$. Coumou, Mackor and Hijmans (32) have verified experimentally that $(\partial \varepsilon/\partial T)_{\rho} << (\partial \varepsilon/\partial \rho)_{T}$ so that indeed equation (13) reduces to

$$\langle (\Delta \varepsilon)^2 \rangle = \left(\frac{\partial \varepsilon}{\partial \rho} \right)_{T}^2 \langle (\Delta \rho)^2 \rangle.$$
 (14)

According to statistical mechanical fluctuation theory (33),

$$\langle (\Delta \rho)^2 \rangle = kT \beta_{T} \rho^2 / v. \tag{15}$$

By substituting (14) and (15) into (11), we obtain the following expression for the intensity of light scattered at 90° from the incident beam:

The cross terms involving $\Delta\rho$ and ΔT drop out because of the statistical independence of ρ and T.

$$i_{90} = \frac{I_o \pi^2}{r^2 \lambda_o^4} k T \beta_T v \left(\rho \frac{\partial \varepsilon}{\partial \rho} \right)_T^2 . \tag{16}$$

In these equations k is Boltzmann's constant.

Another method of evaluating $<(\Delta\epsilon)^2>$ is to choose entropy and pressure (22) as the independent variables for the dielectric constant, ϵ , and to write the fluctuations in ϵ as

$$\Delta \varepsilon = (\partial \varepsilon / \partial S)_{p} \Delta S + (\partial \varepsilon / \partial p)_{S} \Delta p.$$
 (17)

The cross terms involving Δs and Δp are also disregarded because of the statistical independence of p and S, so we are left with

$$\langle (\Delta_{\mathbb{C}})^2 \rangle = (\partial_{\varepsilon}/\partial S)^2_{p} \langle (\Delta S)^2 \rangle + (\partial_{\varepsilon}/\partial p)^2_{S} \langle (\Delta p)^2 \rangle.$$
 (18)

From statistical mechanical fluctuation theory we have

$$\langle (\Delta p)^2 \rangle = kT/v_{\beta_S}$$
 and $\langle (\Delta S)^2 \rangle = kc_{p}\rho v$. (19)

By using a simple mathematical transformation and thermodynamic identities, it is easy to show that the second term of equation (18) can be given by

$$\left(\frac{\partial \varepsilon}{\partial p}\right)_{S}^{2} < (\Delta p)^{2} > = \frac{k T \beta_{S} \rho^{2}}{v} \left(\frac{\partial \varepsilon}{\partial \rho}\right)_{S}^{2}. \tag{20}$$

Employing still another mathematical transformation and more thermodynamic relations one can write the first term of equation (18) as

$$\left(\frac{\partial \varepsilon}{\partial S}\right)_{p}^{2} < (\Delta S)^{2} > = \frac{kT^{2}}{c_{p}\rho v} \left(\frac{\partial \varepsilon}{\partial T}\right)_{p}^{2}.$$
 (21)

After substitution of expressions (20) and (21) into equation (11), the scattering intensity at 90° becomes

$${}^{1}90 = \frac{{}^{1}o^{\pi^{2}v}}{{}^{2}\lambda_{o}^{4}} \left[\frac{{}^{kT}^{2}}{{}^{\rho}c_{p}} \left(\frac{\partial \varepsilon}{\partial T} \right)_{p}^{2} + {}^{kT}\beta_{S} \left(\rho \frac{\partial \varepsilon}{\partial \rho} \right)_{S}^{2} \right], \qquad (22)$$

where the first term in the brackets is the Rayleigh component of the scattering intensity and the second term represents the total Brillouin scattering intensity. One final simplification results if we use the thermodynamic transformation

$$(\partial_{\varepsilon}/\partial_{\rho})_{S} = (\partial_{\varepsilon}/\partial_{\rho})_{T} + (T/c_{\mathbf{v}\rho}^{2})(\partial_{\rho}/\partial_{\rho}) (\partial_{\varepsilon}/\partial_{\rho})_{\rho}$$
 (23)

and neglect the second term (see Ref. 25):

$$i_{90} = \frac{I_o^{\pi^2 \mathbf{v}}}{r_o^{2} \lambda_o^{4}} \left[\frac{k \mathbf{T}^2}{\rho c_p} \left(\frac{\partial \varepsilon}{\partial \mathbf{T}} \right)_p^2 + k \mathbf{T} \beta_S \left(\rho \frac{\partial \varepsilon}{\partial \rho} \right)_T^2 \right]. \tag{24}$$

Because of the narrow Doppler shift of the Rayleigh peak observed experimentally, one can assume that the Rayleigh term (first term) represents slowly damped fluctuations. The Brillouin (second) term represents high frequency non-static pressure fluctuations. The first term can be accurately expressed in terms of the static values of the thermodynamic entities, while the variables in the second (Brillouin) term should be given the hypersonic values associated with the high frequency of the Brillouin shift. Equation (24), with a subscript "static" on the first term in the brackets and a subscript "hypersonic" on the second term, is the dispersion-corrected scattering intensity. The same equation with the subscript "static" on both terms is the original result of the Landau-Placzek theory.

As was stated earlier, the original theoretical prediction of the ratio of the intensity of the central component to the combined intensity of the Brillouin components is given by

$$\frac{I_{C}}{2I_{R}} = \frac{\beta_{T} - \beta_{S}}{\beta_{C}} , \qquad (10)$$

where the values of $\boldsymbol{\beta}_T$ and $\boldsymbol{\beta}_S$ are considered to be the equilibrium

(static) values. We have already derived an equation for the total scattering intensity from a pure fluid---equation (16); note that this equation is incorrect only with respect to the contribution of the Brillouin components. Therefore, if we subtract the static-value Brillouin term of equation (24) from the total scattering intensity, we should be left with a correct expression for the intensity of the central component:

$$I_{c} = I_{T} - 2I_{B_{static}} = \frac{I_{o} \pi^{2} v}{r^{2} \lambda_{o}^{4}} \left[kT \beta_{T} \left(\rho \frac{\partial \varepsilon}{\partial \rho} \right)_{T}^{2} \right] - \frac{I_{o} \pi^{2} v}{r^{2} \lambda_{o}^{4}} \left[kT \beta_{S} \left(\rho \frac{\partial \varepsilon}{\partial \rho} \right)_{T}^{2} \right]$$
static
$$(25)$$

Combining equation (25) with the second term (hypersonic limit) of (24), we obtain a dispersion-corrected expression for the Landau-Placzek ratio of a pure fluid:

$$\frac{I_{C}}{2I_{B}} = \frac{\left[k^{T}\beta_{T}\left(\rho\frac{\partial\varepsilon}{\partial\rho}\right)_{T}^{2} - k^{T}\beta_{S}\left(\rho\frac{\partial\varepsilon}{\partial\rho}\right)_{T}^{2}\right]_{Static}}{\left[k^{T}\beta_{S}\left(\rho\frac{\partial\varepsilon}{\partial\rho}\right)_{T}^{2}\right]_{hS}}$$
or
$$\frac{I_{C}}{2I_{B}} = \frac{\left[\left(\rho\frac{\partial\varepsilon}{\partial\rho}\right)_{T}^{2}\left(\beta_{T} - \beta_{S}\right)\right]_{Static}}{\left[\left(\rho\frac{\partial\varepsilon}{\partial\rho}\right)_{T}^{2}\beta_{S}\right]_{hS}}.$$

It should be pointed out that this dispersion correction is contingent on the choice of entropy and pressure as the independent variables. This choice enables us to divide the fluctuations into low- and high-frequency components and use the correct values of the thermodynamic variables in the theoretical expressions for the intensities of the various components.

In theory, then, it should be possible to correct the classical Landau-Placzek ratio for the effects of dispersion by introducing a value for the hypersonic adiabatic compressibility in the denominator and multiplying the resultant expression by the correction factor

$$\left(\rho\frac{\partial\epsilon}{\partial\rho}\right)_{T\ \text{static}}^{2} \ / \left(\rho\frac{\partial\epsilon}{\partial\rho}\right)_{T\ \text{hs}}^{2} \ . \ \text{The hypersonic adiabatic compressibility,}$$

 $\beta_S^{\mbox{\scriptsize hs}}$, is evaluated from the equation

$$\beta_{S}^{hs} = 1/\left(\rho v_{hs}^{2}\right) , \qquad (27)$$

where \mathbf{v}_{hs} is the hypersonic velocity as determined from the experimental Brillouin shift. The correction factor $\left(\rho\frac{\partial\epsilon}{\partial\rho}\right)_{T}^{2}$ static $\left(\rho\frac{\partial\epsilon}{\partial\rho}\right)_{T}^{2}$ hs is a difficult quantity to determine experimentally. The applicability of the Cummins-Gammon dispersion-corrected Landau-Placzek ratio is limited, therefore, to those liquids for which the values of $\left(\rho\frac{\partial\epsilon}{\partial\rho}\right)_{T}^{2}$ static

and
$$\left(\rho \frac{\partial \epsilon}{\partial \rho}\right)_{T_{hs}}$$
 are available.

A more preferable method to predict the magnitude and frequency dependence of the various components in a Brillouin spectrum was developed by Mountain using the linearized hydrodynamic equations of irreversible thermodynamics (24, 27). This theory provides the time dependence of the thermodynamic and hydrodynamic variables. Although Mountain employed this technique initially to derive the intensity distribution of the scattered light from a pure fluid near its critical point (24), he later extended the theory of the spectra of light scattered from pure fluids with a single mode of relaxation (27). In the context of the present paper, we shall examine only the theory in Ref. 27.

To facilitate the calculation of the spectrum of the light scattered by a pure fluid, Mountain assumes a model in which the fluid possesses internal degrees of freedom that are weakly coupled to the translational degrees of freedom, thereby affecting the decay of density fluctuations in the liquid. Because density fluctuations are responsible for the observed polarized light scattering spectrum of a liquid, the weak coupling of modes serves to modify this frequency spectrum. The modification occurs in such a manner that the classical Landau-Placzek ratio, $(c_p - c_v)/c_v$, is no longer valid. Mountain considers the specific case of coupling to a single thermal relaxation mode. He derives formulas for the frequency and intensity distributions of the scattered light, and compares his results to data from two liquids which are assumed to have single thermal relaxation times. The notation used in the following discussion of the problem is essentially due to Mountain, with minor changes introduced to aid in comprehension of the text.

Let us consider the light scattered from density fluctuations within a small volume element which contains N molecules of the scattering fluid:

$$i(\vec{R}, \omega) = \frac{I_0 N}{16\pi^2 R^2} k_i^4 \sin^2 \Phi \langle [\Delta \epsilon (k, \omega)]^2 \rangle . \qquad (28)$$

In equation (28), I is the intensity of the incident plane polarized wave of vector \overrightarrow{k}_i ; R is the point of observation of the scattered light intensity, $i(\overrightarrow{R}, \omega)$, and the scattering is considered to have taken place at the origin. The non-subscripted k in the equation refers to the change in the wave vector \overrightarrow{k}_i after scattering. The angle between the electric vector of the incident radiation and the obser-

vation point is Φ , while $\Delta\epsilon(k,\omega)$ is the Fourier component of the fluctuation in the dielectric constant; ω is the <u>shift</u> in the angular frequency of the scattered light. We can define the magnitude of the change in wave vector as $k = (4\pi n \sin\theta/2)/\lambda_0$ rad/cm for calculational purposes, where λ_0 is the wavelength of the incident radiation, n is the refractive index of the scattering medium, and θ is the scattering angle.

To avoid having to solve directly for $\Delta\epsilon(k,\,\omega)$, we invoke statistical mechanical fluctuation theory and express the dielectric constant in terms of the density and temperature:

$$\Delta \varepsilon = (\partial \varepsilon / \partial \rho)_{T} \Delta \rho + (\partial \varepsilon / \partial T)_{\rho} \Delta T.$$
 (12)

Again, we neglect $(\partial \varepsilon/\partial T)_{\rho}$ compared to $(\partial \varepsilon/\partial \rho)_{T}$, so that we can rewrite equation (28) as

$$i(R, \omega) = \frac{I_0 N}{16\pi^2 R^2} k_i^4 \sin^2 \Phi (\partial \epsilon / \partial \rho)_T^2 < [\rho(k, \omega)]^2 >.$$
 (29)

In this case, $\rho(k, \omega)$ is the Fourier component of the density fluctuations, and it must be evaluated over the ensemble average of the initial states of the system. For the evaluation of the mean square Fourier component of the density fluctuations, we must go to the linearized hydrodynamic equations of irreversible thermodynamics. It is necessary to solve the linearized hydrodynamic equations for $\rho(k, \omega)$ in terms of an initial fluctuation, $\rho(k)$; this can be accomplished by the elegant method of van Hove (34). In the subsequent analysis we assume that the transfer of energy from the internal degrees of freedom to the translational degrees of freedom occurs by a single relaxation process. The linearized hydrodynamic equations which must be solved are given below; details of the solutions, however, are omitted.

The continuity equation for the scattering system under consideration is

$$\partial \rho_1 / \partial t + \rho_0 \operatorname{div} \overrightarrow{v} = 0$$
, (30)

the energy transport equation can be written

$$\rho_{o} c_{v}(\partial T_{1}/\partial t) - \left[c_{v}(\gamma - 1)/\beta\right](\partial \rho_{1}/\partial t) - \lambda \nabla^{2} T_{1} = 0 , \qquad (31)$$

and the longitudinal portion of the Navier-Stokes equation is

$$\rho_{o} \frac{\partial \vec{v}}{\partial t} = -\left(\frac{c_{o}^{2}}{\gamma}\right) \operatorname{grad} \rho_{1} - \left(\frac{c_{o}^{2} \beta \rho_{o}}{\gamma}\right) \operatorname{grad} T_{1} + \left(\frac{4}{3} \eta_{s} + \eta_{v}\right) \operatorname{grad} \operatorname{div} \vec{v}$$

$$+ \int_{0}^{t} \eta'(t - t') \operatorname{grad} \operatorname{div} \vec{v}(t') \operatorname{dt'} . \tag{32}$$

In these equations, ρ_{O} and T_{O} are equilibrium values of the number density and temperature, $\rho = \rho_{O} + \rho_{1}$ is the number density, $T = T_{O} + T_{1}$ is the temperature, and η_{S} is the shear viscosity. The bulk viscosity consists of two parts, a frequency independent term, η_{V} , and a frequency dependent term that is the Fourier transform of $\eta'(t)$. The coefficient γ is the ratio of the specific heat at constant pressure, c_{p} , to the specific heat at constant volume, c_{V} ; β is the coefficient of thermal expansion, λ is the thermal conductivity, c_{O} is the low frequency (adiabatic) phonon velocity, and t is the time.

Before attempting a solution of the linearized hydrodynamic equations for $\rho(k, \omega)$, Mountain discusses the adaptation by Komarov and Fisher (35) of van Hove's theory of neutron scattering (34) to the problem of light scattering. Komarov and Fisher have shown that the intensity of light scattered by N molecules of a fluid with effective molecular polarizability, α , is

$$i(\vec{R}, \omega) = \frac{I_0 N}{2\pi R^2} \alpha^2 k_i^4 \sin^2 \phi S(k, \omega) , \qquad (33)$$

 $S(k, \omega)$ being the generalized structure factor. (The reader should be immediately cognizant of the similarity between equations (33) and (29)). The Fourier component of the density fluctuations is related to the generalized structure factor by

$$S(k, \omega) = \langle \rho(k, \omega) \rho(-k) \rangle. \tag{34}$$

Integration of $S(k, \omega)$ over the possible angular frequencies in the liquid yields the ordinary structure factor, S(k), which is, in turn, related to the initial density fluctuation, $\rho(k)$:

$$S(k) = \frac{1}{2\pi} \int_{-\infty}^{\infty} S(k, \omega) d\omega = \langle \rho(k) \rho(-k) \rangle. \qquad (35)$$

Obviously, if one can determine either $\rho(k, \omega)$ or $S(k, \omega)$, the other quantity can readily be evaluated. Mountain's ultimate goal in the ensuing analysis is to solve for $\rho(k, \omega)$ using the linearized hydrodynamic equations, then to ascertain $S(k, \omega)$ from the relationship above.

Upon solving for $\rho(k, \omega)$, Mountain finds that the initial density fluctuations are related to the generalized structure factor by a function $\sigma(k, \omega)$, which is the frequency distribution of the scattered light. Specifically,

$$S(k, \omega) = \langle \rho(k) \rho(-k) \rangle \sigma(k, \omega)$$
 (36)

where
$$\sigma(\mathbf{k}, \omega) = 2\text{Re} \left\{ \left[\frac{\langle \rho(\mathbf{k}, \mathbf{s}) \rho(-\mathbf{k}) \rangle}{\langle \rho(\mathbf{k}) \rho(-\mathbf{k}) \rangle} \right]_{\mathbf{S} = i\omega} \right\}$$
; (37)

s is the dummy variable utilized in the evaluation of the Laplace and Fourier transforms of the density fluctuations during solution of the linearized hydrodynamic equations.

Mountain solves for $\sigma(k, \omega)$ approximately by neglecting the

small terms in the expression for the inverse Laplace transform of the density fluctuations. He obtains an approximate expression for $\sigma(k, \omega)$; a consideration of this equation provides a better understanding of the intensity expressions which are set forth later in this work. Consequently, as a close approximation to $\sigma(k, \omega)$, we have

$$\sigma(k, \omega) \approx (1 - 1/\gamma) \left[\frac{2\lambda k^{2}/\rho_{o}c_{p}}{(\lambda k^{2}/\rho_{o}c_{p})^{2} + \omega^{2}} \right]$$

$$+ \left[\frac{(c_{\infty}^{2} - c_{o}^{2})k^{2} - (v^{2}/c_{o}^{2} - 1)(c_{o}^{4}/v^{4}\tau^{2} + c_{o}^{2}k^{2}(1 - 1/\gamma))}{c_{o}^{4}/v^{4}\tau^{2} + v^{2}k^{2}} \right]$$

$$\times \left[\frac{2c_{o}^{2}/v^{2}\tau}{c_{o}^{4}/v^{4}\tau^{2} + \omega^{2}} \right]$$

$$+ \left[\frac{1 - c_{o}^{2}/v^{2}(1 - 1/\gamma)}{c_{o}^{4}/v^{4}\tau^{2} + v^{2}k^{2}} \right]$$

$$\times \left[\frac{r_{B}}{r_{B}^{2} + (\omega - vk)^{2}} + \frac{r_{B}}{r_{B}^{2} + (\omega + vk)^{2}} \right].$$
(38)

 $\Gamma_{\rm B}$ is the half-width of a Brillouin peak, ${\bf v}$ is the phonon speed calculated from the Brillouin shift, c_{∞} is the infinite-frequency phonon speed and τ is the relaxation time of the thermal diffusion process responsible for the weak coupling of the internal degrees of freedom to the translational degrees of freedom.

As is easily seen from equation (38), all four of the components are Lorentzian in character. The first term represents the decay of a density fluctuation by a thermal diffusion process; this decay is recognized as a non-propagating (static) mode. The second

term is also a nonpropagating type of decay, and is related to the coupling of the internal degrees of freedom of the molecules. The last term is a propagating decay in the density fluctuation; it represents the phonon modes. Equation (38) for the frequency distribution of the light scattered from a fluid with thermal relaxation is valid only under the condition that the thermal decay process has but a single relaxation time associated with it.

The intensity of the Rayleigh component of the scattered light and the Brillouin intensities are ascertained by integrating the individual terms of equation (38) with respect to the shift in the angular frequency, ω . In general, the intensity ratio of the central peak to the Brillouin components is

$$\frac{\frac{1}{c}}{2I_{B}} = \frac{(1 - 1/\gamma) + (c_{\infty}^{2} - c_{o}^{2})k^{2} - (v^{2}/c_{o}^{2} - 1)\left[(c_{o}^{4}/v^{4}\tau^{2}) + c_{o}^{2}k^{2}(1 - 1/\gamma)\right]}{\left[1 - c_{o}^{2}/v^{2}(1 - 1/\gamma)\right]\left[v^{2}k^{2} + c_{o}^{2}/v^{2}\tau^{2}\right] - (c_{\infty}^{2} - c_{o}^{2})k^{2}}.$$
(39)

For low phonon frequencies (vk τ << 1), the relationship simplifies to the classical Landau-Placzek ratio, $I_c/2I_B = \gamma - 1$. For large phonon frequencies (vk τ >> 1), we obtain

$$\frac{I_{C}}{2I_{B}} = (\gamma - 1) \left[1 + \left(\frac{\gamma}{\gamma - 1} \right) \left(\frac{c_{\infty}^{2} - c_{O}^{2}}{c_{O}^{2}} \right) \right]. \tag{40}$$

Mountain has applied these equations to systems of carbon disulfide and carbon tetrachloride, for which much peripheral experimental data is available, and has obtained values for the intensity ratios that are in much better agreement with experimental data than are the classical Landau-Placzek ratios.

The most obvious difficulties in utilizing Mountain's results

for the Landau-Placzek ratio in experimental situations are: (1) one must have previous insight into the relaxational behavior of the liquid being studied, so that the single relaxational model can be applied, (2) one must have some method for estimating (vk_T) in order to use the simplified expressions for $I_C/2I_B$ and (3) if one is considering a liquid with more than one mode of relaxation available, a much more complicated derivation for the spectral distribution of the scattered light is needed.

The final technique to be appraised for the calculation of the intensity and frequency distribution of the light scattered by a pure fluid is a modification of Mountain's approach. Although Mountain treated the case of a singly relaxing liquid in scrutinizing detail, he did not consider the case of a liquid with more than one relaxation time. Montrose, Solovyev and Litovitz (26) have developed a formula for the spectral distribution function, $\sigma(k,\omega)$, for both a nonrelaxing and relaxing liquid in a manner analogous to Mountain's method of evaluation of $\sigma(k,\omega)$ for a singly relaxing fluid.

These authors consider first the case of a nonrelaxing liquid and view the light scattering to be a consequence of fluctuations in the optical dielectric constant. The authors also make the usual assumption that the contribution of the thermal fluctuations in dielectric constant are small compared to the contribution due to density fluctuations. Montrose, et al. express the spectral distribution function, $< \rho(k, t) \rho(-k) >$, which is determined by taking the appropriate values of the time derivative of the density. After solving the linearized hydrodynamic equations for the Laplace (time) and Fourier

(space) transform, (k, s), of the density fluctuation, $\rho(\vec{R}, t)$, leading that

$$\sigma(\mathbf{k}, \omega) = 2\operatorname{Re}\left\{\left[\frac{\langle \rho(\mathbf{k}, s) \rho(-\mathbf{k}) \rangle}{\langle \rho(\mathbf{k}) \rho(-\mathbf{k}) \rangle}\right]_{s = i\omega}\right\}. \tag{41}$$

(The reader will recognize this as being the same equation as (37),

Mountain's relation for the frequency distribution of light scattered

from a singly-relaxing fluid.)

The correlation function ratio of equation (41) is given by

$$\left[\langle \rho(k, s) \rho(-k) \rangle / \langle \rho(k) \rho(-k) \rangle \right] s = i\omega$$

$$= \left[\left(\mathbf{s}^{2} + \left[(\lambda/\rho_{o}^{c} \mathbf{v}) + (\eta_{o}/\rho_{o}) \right] \mathbf{s} \mathbf{k}^{2} + c_{o}^{2} \mathbf{k}^{2} (1 - 1/\gamma) + \lambda \eta_{o}^{c} \mathbf{k}^{4}/\rho_{o}^{2} \mathbf{c}_{\mathbf{v}} \right) \right]$$

$$\left(\mathbf{s}^{3} + \left[(\lambda/\rho_{o}^{c} \mathbf{v}) + (\eta_{o}/\rho_{o}) \right] \mathbf{s}^{2} + \left[c_{o}^{2} \mathbf{k}^{2} + (\lambda \eta_{o}^{c} \mathbf{k}^{4}/\rho_{o}^{2} \mathbf{c}_{\mathbf{v}}) \right] \mathbf{s} + \lambda c_{o}^{2} \mathbf{k}^{4}/\gamma \rho_{o}^{c} \mathbf{v} \right]$$

$$+ \lambda c_{o}^{2} \mathbf{k}^{4}/\gamma \rho_{o}^{c} \mathbf{v}$$

$$\left(\mathbf{s}^{3} + \left[(\lambda/\rho_{o}^{c} \mathbf{v}) + (\eta_{o}/\rho_{o}^{c}) \right] \mathbf{s} + \left[c_{o}^{2} \mathbf{k}^{2} + (\lambda \eta_{o}^{c} \mathbf{k}^{4}/\rho_{o}^{c} \mathbf{v}_{\mathbf{v}}) \right] \mathbf{s}$$

$$+ \lambda c_{o}^{2} \mathbf{k}^{4}/\gamma \rho_{o}^{c} \mathbf{v} \right)$$

$$\left(\mathbf{s}^{2} + \left[(\lambda/\rho_{o}^{c} \mathbf{v}) + (\eta_{o}/\rho_{o}^{c}) \right] \mathbf{s} + \left[(\lambda/\rho_{o}^{c} \mathbf{v}) + (\eta_{o}/\rho_{o}^{c} \mathbf{v}_{\mathbf{v}}) \right] \mathbf{s}$$

$$+ \lambda c_{o}^{2} \mathbf{k}^{4}/\gamma \rho_{o}^{c} \mathbf{v}_{\mathbf{v}} \right)$$

$$\left(\mathbf{s}^{2} + \left[(\lambda/\rho_{o}^{c} \mathbf{v}) + (\eta_{o}/\rho_{o}^{c}) \right] \mathbf{s} + (\lambda \eta_{o}^{c} \mathbf{k}^{4}/\rho_{o}^{c} \mathbf{v}_{\mathbf{v}} \right] \mathbf{s}$$

$$+ \lambda c_{o}^{2} \mathbf{k}^{4}/\gamma \rho_{o}^{c} \mathbf{v}_{\mathbf{v}} \right)$$

$$\left(\mathbf{s}^{2} + \left[(\lambda/\rho_{o}^{c} \mathbf{v}) + (\eta_{o}/\rho_{o}^{c}) \right] \mathbf{s} + (\lambda \eta_{o}^{c} \mathbf{k}^{4}/\rho_{o}^{c} \mathbf{v}_{\mathbf{v}} \right] \mathbf{s}$$

$$+ \lambda c_{o}^{2} \mathbf{k}^{4}/\gamma \rho_{o}^{c} \mathbf{v}_{\mathbf{v}} \right)$$

$$\left(\mathbf{s}^{2} + \left[(\lambda/\rho_{o}^{c} \mathbf{v}) + (\eta_{o}/\rho_{o}^{c}) \right] \mathbf{s} + (\lambda \eta_{o}^{c} \mathbf{k}^{4}/\rho_{o}^{c} \mathbf{v}_{\mathbf{v}} \right) \mathbf{s}$$

$$+ \lambda c_{o}^{2} \mathbf{k}^{4}/\gamma \rho_{o}^{c} \mathbf{v}_{\mathbf{v}} \right)$$

$$\left(\mathbf{s}^{2} + \left[(\lambda/\rho_{o}^{c} \mathbf{v}) + (\eta_{o}/\rho_{o}^{c} \mathbf{v}_{\mathbf{v}} \right] \mathbf{s} + (\lambda \eta_{o}^{c} \mathbf{v}^{c} \mathbf{v}_{\mathbf{v}} + (\lambda \eta_{o}^{c} \mathbf{v}^{c} \mathbf{v}_{\mathbf{v}} + (\lambda \eta_{o}^{c} \mathbf{v}_{\mathbf{v}} + (\lambda \eta_{o}^{c}$$

where λ is the thermal conductivity, $\eta_{_{\hbox{\scriptsize O}}}$ is the frequency independent longitudinal viscosity, and

$$s = -\lambda k^2 / \rho_0 c_p . (43)$$

Equation (42) is equivalent to Mountain's equation (13) in Ref. 24, and Montrose, et al. remark that up to this point, their treatment has been identical to Mountain's. The authors proceed, however, to decompose the correlation function ratio and calculate a spectral distribution function that is markedly different from Mountain's with respect to the Brillouin components.

Montrose, et al. first reduce the complexity of the denominator

 $^{^{1}}_{\rho}(\overset{\rightharpoonup}{R},\;t)$ is the departure at time t, of the density from its equilibrium value.

of equation (42) by estimating the relative magnitude of the terms present. Since $\lambda/c_{v} << \eta_{o}$ for most transparent liquids, the terms containing $(\lambda/c_{v}^{\eta})^{2}$ can be ignored. The denominator is then rewritten as

$$(s + \lambda k^{2}/\rho_{o}c_{p}) \left\{ s^{2} + \left[\frac{\eta_{o}}{\rho_{o}} + \frac{\lambda(1 - 1/\gamma)}{\rho_{o}c_{v}} \right] k^{2}s^{2} + c_{o}^{2}k^{2} \right\}.$$
 (44)

Furthermore, the factor $\lambda(1-1/\gamma)/\rho_{O}c_{V}$ has been found (36) to be less than one per cent of η_{O}/ρ_{O} for a wide variety of liquids, so that expression (44) can be reduced even more. Montrose, et al. define two terms, ω_{O} and Γ_{B} :

$$\omega_0 = c_0 k$$
 and $\Gamma_B' = \eta_0 k^2 / 2\rho_0$. (45)

 $\Gamma_{\rm B}^{'}$ is the true Brillouin half-width at half height, and is similar to Mountain's more complicated expression for $\Gamma_{\rm B}$ given on p. 216 of Ref. 27.

By eliminating the insignificant terms of equation (42), one arrives at a simplified expression for the correlation function ratio:

$$\left[\frac{\langle \rho(k, s) \rho(-k) \rangle}{\langle \rho(k) \rho(-k) \rangle}\right]_{s=i\omega} = \frac{s^{2} + 2\Gamma_{B}s + \omega_{O}(1 - 1/\gamma) + 2\Gamma_{B}\lambda k^{2}/\rho_{O}c_{v}}{(s + \lambda k^{2}/\rho_{O}c_{p})(s^{2} + 2\Gamma_{B}s + \omega_{O}^{2})}.$$
(46)

Montrose, et al. separate the right-hand side of equation (46) into partial fractions

$$\left[\frac{\langle \rho(k, s) \rho(-k) \rangle}{\langle \rho(k) \rho(-k) \rangle} \right]_{s = i\omega}$$

$$= (1 - 1/\gamma) \frac{1}{s + (\lambda k^2/\rho_0 c_p)} + \left(\frac{1}{\gamma}\right) \frac{s + 2\Gamma_B}{(s + \Gamma_B)^2 + (\omega_0^2 - \Gamma_B)} \tag{47}$$

and use (47) in equation (41) to calculate the spectral distribution function for a nonrelaxaing liquid:

$$\sigma(\mathbf{k}, \omega) = (1 - 1/\gamma) \frac{2\lambda k^{2}/\rho_{o}c_{p}}{\left[\lambda k^{2}/\rho_{o}c_{p}\right]^{2} + \omega^{2}} + \left[\frac{2c_{o}^{2}k^{2}}{\gamma}\right] \frac{2\Gamma_{B}'}{\left[2\omega\Gamma_{B}'\right]^{2} + \left[\omega^{2} - \omega_{o}^{2}\right]^{2}}.$$
(48)

The first term denotes the nonpropagating central component of the scattered light and the second term represents the propagating phonon modes (Brillouin peaks). Since the Brillouin peaks are considered to be caused by isentropic (adiabatic) pressure fluctuations, Montrose, et al. label the second term $\sigma_{\rm S}(k,\,\omega)$ and commence to examine it in detail.

Looking back at equation (34) and (36), which are valid for the Montrose, et al. treatment, as well as for Mountain's theory, from whence they came, we see that

$$\sigma_{S}(k, \omega) \propto \langle \rho_{S}^{2}(k, \omega) \rangle = \frac{\left(2\rho_{O}^{2}/v_{k}\right) k_{B} T \eta_{O}}{\left[\omega \eta_{O}\right]^{2} + \left[\rho_{O}\omega^{2}/k^{2} - \rho_{O}c_{O}^{2}\right]^{2}}.$$
 (49)

In equation (49), k_B is Boltzmann's constant and $\sigma_S(k,\omega)$ is considered to be the isentropic density fluctuation which is responsible for the phonon modes. The authors continue by making an interesting observation about equation (49): "... the form of $< \rho_S^2(k,\omega) >$ is the same as that for the spectrum of the displacement correlation function for a harmonic system under the action of a random (white noise) driving force ..." (Ref. 26, p. 120). What this implies is that the spectrum arising from spontaneous fluctuations is equivalent to the spectrum of a system driven by random forces. The density fluctuation phenomenon

•

is seen, therefore, to be completely analogous to the problem of a damped harmonic oscillator, ¹ with the Brillouin peaks being the results of the "resonant" frequencies of the density fluctuations that are driven by the thermal energy of the system.

In this particular situation, the Callen-Welten (37) fluctuation dissipation theorem can be applied to the problem to yield further information about the fluctuations in density as they are related to the dissipative (relaxation) processes which occur in the liquid in response to the external driving force (thermal energy). Piercy and Hanes (38) have made this application using the language of electric circuits and Nyquist logic, and have found, among other things, that the traditional neglect of temperature fluctuations of the dielectric constant can lead to serious errors in the analysis of Brillouin spectra (Ref. 38, p. 1007).

With these facts in mind, Montrose, et al. expand $\sigma_{\mbox{S}}^{}(k,\;\omega)$ into four partial fractions:

$$\sigma_{S}(k, \omega) = \frac{1}{\gamma} \left[\frac{\Gamma_{B}}{\Gamma_{B}} + \left(\omega - \omega_{4}\right)^{2} + \frac{\Gamma_{B}}{\Gamma_{B}} + \left(\omega + \omega_{4}\right)^{2} \right]$$

$$-\left(\frac{\Gamma_{B}}{\omega_{4}}\right)\frac{\omega - \omega_{4}}{\Gamma_{B}^{2} + \left(\omega - \omega_{4}\right)^{2}} + \left(\frac{\Gamma_{B}}{\omega_{4}}\right)\frac{\omega + \omega_{4}}{\Gamma_{B}^{2} + \left(\omega + \omega_{4}\right)^{2}}$$
(50)

in which ω_4 is the frequency of free oscillation of the damped system:

$$\omega_4 = \omega_0 \left[1 - \frac{1}{4} \left(\omega_0^2 n_0^2 / \rho_0^2 c_0^4 \right) \right]^{\frac{1}{4}} . \tag{51}$$

The damping or dissipative element can be shown to be the longitudinal viscosity, η_0 (Ref. 26, p. 122).

By definition, ω is the product of the low-frequency phonon velocity, c_0 , and the magnitude of the change in wave vector, k, and $\omega = 0$ is the center of the Brillouin spectrum. Equation (50) applies to the specific case of a nonrelaxing fluid.

If we replace ω_4 with ω_0 in the first two terms of equation (50), we obtain the same result as Mountain for a nonrelaxing fluid. The last two terms are present but somewhat obscure, in Mountain's theory for a single relaxation when $\tau \to 0$. As is recognized from equation (50), the first two terms are Lorentzian peaks centered at $\omega = \pm \omega_4$. The last two terms appear to be skewed Lorentzians which have the effects of asymmetrizing and shifting the original Brillouin peaks (the ones defined by the first two terms) toward the center of the spectrum (to $\omega = 0$). It should be noted, however, that when the individual terms of (50) are integrated in order to determine the intensity ratio of the Rayleigh to the Brillouin peaks, the integrals of the last two terms cancel out, so that they do not contribute to the Landau-Placzek ratio.

In the remainder of the theoretical discussion, Montrose, et al. turn their attention to the case of a relaxing liquid, utilizing the same basic method, the linearized hydrodynamic equations and the Piercy-Hanes electrical circuit approach, as they did for the nonrelaxing case. The basic difference in the derivation of the spectral distribution function for the case of a relaxing liquid is the inclusion of the time dependence (frequency dependence) of the various thermodynamic and viscoelastic parameters, such as the specific heat, c_{v} , the thermal expansion coefficient, β , the shear viscosity, η_{s} and the longitudinal modulus, M.

By applying the linearized hydrodynamic equations, the authors

find for a relaxing liquid that the spectral distribution function can be given by

$$\sigma(\mathbf{k}, \omega) = (1 - 1/\gamma) \left[\frac{2\lambda k^2 / \rho_o c_p}{\left(\lambda k^2 / \rho_o c_p\right)^2 + \omega^2} \right] + \frac{2M_o \left[\eta(\omega) + \eta_o \right]}{\gamma \left(\left\{ \omega \left[\eta(\omega) + \eta_o \right] \right\}^2 + \left[\rho_o \omega^2 / k^2 - M'(\omega) \right]^2 \right)}$$
(52)

where $\eta(\omega)$ is the frequency dependent longitudinal viscosity and M'(ω) is the real part of the frequency dependent modulus of elasticity. For the special case of a singly relaxing fluid

$$\eta(\omega) = \rho_0 \left[\frac{\left(c_{\infty}^2 - c_{0}^2\right)\tau}{1 + \omega^2 \tau^2} \right] \text{ and } \mathbf{M}'(\omega) = \rho_0 \left[\frac{c_{0}^2 + c_{\infty}^2 \omega^2 \tau^2}{1 + \omega^2 \tau^2} \right], \tag{53}$$

which leads to the formula

$$\sigma(\mathbf{k}, \omega) = (1 - 1/\gamma) \left[\frac{2\lambda \mathbf{k}^2/\rho_o c_p}{\lambda \mathbf{k}^2/\rho_o c_p} \right]^2 + \omega^2$$

$$+ \left[2M_o \left\{ \rho_o \left[\left(c_{\infty}^2 - c_o^2 \right) \tau / \left(1 + \omega^2 \tau^2 \right) \right] + \eta_o \right\} \right]$$

$$\left[\gamma \left\{ \omega \left[\rho_o \frac{\left(c_{\infty}^2 - c_o^2 \right) \tau}{1 + \omega^2 \tau^2} + \eta_o \right] \right\}^2$$

$$+ \left\{ \rho_o \omega^2 / \mathbf{k}^2 - \rho_o \left(c_o^2 + c_{\infty}^2 \omega^2 \tau^2 \right) / \left(1 + \omega^2 \tau^2 \right) \right\}^2 \right].$$
 (54)

This is similar to the expression from Mountain's theory, equation (38).

As in the case of a nonrelaxing liquid, Montrose, et al. then attempt to apply the Piercy-Hanes equivalent electric circuit theory to this problem. The situation for a relaxing liquid is much more complicated than for a nonrelaxing liquid, however, so that they can only approximate the form of $\sigma_S(k,\omega)$ for the special case of a singly relaxing liquid exhibiting small dispersion (i.e., for $\left(c_\infty^2-c_0^2\right)/c_0^2<<1$).

In other situations, the errors inherent in the evaluation of the frequency dependent portion of the modulus of elasticity, $M'(\omega)$, become too great to obtain a meaningful expression for $\sigma_S(k,\omega)$. In spite of these imposing difficulties, one interesting observation is made for the experimental situation in which the liquid possesses a single relaxation time, small dispersion and small thermal conductivity: a density fluctuation in the liquid can be regarded as being composed of an oscillatory and a nonoscillatory portion, giving rise to the Brillouin peaks and the Rayleigh peak, respectively. The macroscopic relaxation time, τ , is assumed to be the sum of the rates at which the oscillatory and nonoscillatory portions of the density fluctuations are damped. The explicit division of density fluctuations into these component parts is the subject of a second paper by Litovitz and his colleagues (23), with specific application to a relaxing viscous liquid which can form a glass

Although it can be seen that several theoretical expressions are available for the intensity distribution of light scattered from a pure fluid, it should be noted that none of these equations has as yet been fully tested. This is because of the lack of information on the various thermodynamic entities in the equations, and because of the high degree of accuracy required for the extraction of the Brillouin scattering parameters from experimental spectra.

- 2. Brillouin scattering from a two-component mixture
 - a. Derivation of the spectral distribution of light scattered from a binary liquid system

Because of the complexity of the theoretical analysis of the spectral distribution of light scattered from multicomponent systems,

very few papers dealing with this subject have appeared in the literature (39-44). Of the papers which have appeared, only one (44) is of interest to our immediate problem of light scattering from the binary system DMSO and pyridine.

Fishman and Mountain (44) consider the spectral distribution of light scattered by a binary mixture with internal degrees of freedom (i.e., thermal and/or structural relaxation) in much the same manner as Mountain and Deutch (43) determined the spectral distribution of light scattered from a binary solution possessing no internal relaxational modes. They use linearized hydrodynamic equations to calculate the relative magnitude of the modes by which the relaxing system returns to equilibrium, and thermodynamic fluctuation theory for initial estimates of the correlation functions for the thermodynamic variables.

For both relaxing and nonrelaxing fluids, the authors consider the intensity of the scattered light to be related to the Laplace-Fourier transform of the auto-correlation function of the optical dielectric constant. The Laplace-Fourier transform is evaluated by making use of the linearized hydrodynamic equations and thermodynamic fluctuation theory in a manner analogous to that described in section C-1 for a pure liquid. The basic difference in the method of evaluation of $<\Delta\epsilon(k,\,\omega)^2>$ for a binary mixture is the inclusion of the concentration dependence of the dielectric constant. As was done previously with the dielectric constant for a pure fluid, we express ϵ in terms of certain macroscopic (thermodynamic) variables, and proceed to analyze the fluctuations in ϵ in terms of the fluctuations of these variables.

From the Gibbs Postulate (45), we know that any intensive property 1 of the thermodynamic state of a system is a function of $\kappa+1$ intensive properties, κ being the canonical component number of the system. The dielectric constant is an intensive property, and for a homogenous binary solution, $\kappa=2$, so that ϵ can be expressed in terms of three intensive variables. In order to achieve the simplest possible arrangement for calculational purposes, we want to choose three intensive variables that are statistically independent, so that their fluctuation cross terms go to zero. The obvious choices for the three thermodynamic variables are pressure, temperature and concentration, quantities which are easy to measure experimentally. If we express the dielectric constant $\epsilon(p,T,c)$ in terms of space and time (r and t), we can relate the fluctuations in ϵ to the fluctuations in pressure, temperature and concentration:

$$\delta \varepsilon(\mathbf{r}, t) = (\partial \varepsilon / \partial \mathbf{p})_{\mathbf{T}, c} \delta \mathbf{p}(\mathbf{r}, t) + (\partial \varepsilon / \partial \mathbf{T})_{\mathbf{p}, c} \delta \mathbf{T}(\mathbf{r}, t) + (\partial \varepsilon / \partial c)_{\mathbf{p}, \mathbf{T}} \delta c(\mathbf{r}, t).$$
(55)

The linearized hydrodynamic equations are constructed, as usual, but this time they are modified to include a frequency-dependent volume viscosity which relaxes with a single relaxation time, ³ and a diffusion

An intensive property is defined at every point in the system (e.g., temperature); it is also the ratio of two extensive properties, such as $\rho = dm/dV$.

The symbol δ is used instead of Δ for the fluctuation terms to indicate that we are dealing with space-time functions of the thermodynamic variables.

This single relaxation mechanism is usually visualized as thermal relaxation.

equation. We have for the continuity equation and the modified Navier-Stokes equation

$$\partial \rho / \partial t + \rho div v = 0$$
 (56)

and

$$\frac{\partial \operatorname{div} \mathbf{v}}{\partial t} = -\frac{1}{\rho_0} \nabla^2 \mathbf{p} + \eta_0 V^2 \operatorname{div} \mathbf{v} + \left[c_{\infty}^2 - c_0^2 \right] \int_0^{t - t'/\tau} V^2 \operatorname{div} \mathbf{v}(t - t') dt', \tag{57}$$

respectively. The energy transport equation (58) and diffusion equation (59) can be written

$$\rho_{o} c_{p} (\partial T/\partial t) - \rho_{o} k_{T} (\partial \mu/\partial c)_{p,T} (\partial c/\partial t) + \rho_{o} T_{o} (\partial S/\partial c)_{T,c} 2p/\partial t = \lambda \nabla^{2} T$$
 (58) and

$$(\partial c/\partial t) = D \left[\nabla^2 c + (k_T/T_0) \nabla^2 T - \left(\left[(p_0/\rho_0)^2 (\partial \rho/\partial c)_{p,T} \right] / (\partial \mu/\partial c)_{p,T} \right) \nabla^2 p \right].$$
(59)

In these equations, μ is the chemical potential of the mixture, as defined by Landau and Lifshitz (46) to be

$$\mu = \mu_1/m_1 - \mu_2/m_2 \tag{60}$$

where μ_1 and μ_2 are the chemical potentials and m_1 and m_2 are the masses of the two species in one gram of solution. The concentration, c_i , is equal to $n_i m_i$, where n_i is the number of molecules of substance i in one gram of solution. Returning to equation (59), D is the diffusion coefficient for the binary mixture, k_T is the thermal diffusion ratio, and the subscript o indicates an equilibrium value.

Examining equations (56-59), we see that there are four equations and five unknowns; this necessitates the assumption that local thermodynamic equilibrium prevails in the system, so that the fluctuations in density can be written

$$\delta \rho = (\partial \rho / \partial p)_{T,C} \delta p + (\partial \rho / \partial T)_{p,C} \delta T + (\partial \rho / \partial C)_{p,T} \delta C$$
 (61)

and equation (61) can be used for $\delta\rho$ in the continuity equation. The four equations are solved by the use of Fourier-Laplace transforms to obtain the initial values (t = 0) of the functions p(r, t), T(r, t) and c(r, t). The generalized structure factor, S(k, ω), can then be evaluated from the expression for $\delta\varepsilon(r, t)$, since S(k, ω) is related to $\delta\varepsilon(r, t)$ by

$$S(k, \omega) = 2Re \int_{0}^{\infty} dt \int_{V} \langle \delta \varepsilon(r + r', t) \delta \varepsilon(0, 0) \rangle \exp \left[i(kr - \omega t) \right] dr dr'.$$
(62)

After performing these calculations, Fishman and Mountain arrive at this expression for the generalized structure factor, $S(k,\;\omega)^{-1}:$

Corrections have been made to the original equation to compensate for an incorrect thermodynamic expression borrowed by these authors from Miller (39).

$$\begin{split} \mathbf{s}(\mathbf{k}, \ \omega) &= \left[\frac{2\epsilon}{3c_{D}} \right]^{2} \frac{k_{B} \sigma}{\mathbf{p}_{A}} \left\{ \frac{22k^{2}}{4} + \frac{1}{\omega^{2}} + \left(\frac{\kappa_{K1}}{2}\right)^{2} + \frac{c_{O} \sqrt{4}}{4} - \left(\frac{c_{O} \sqrt{4}}{2}\right)^{2} \left[\frac{2c_{O}^{2} \sqrt{2}}{4} + \frac{1}{\omega^{2}} \right] \\ &+ \left[c_{O} \sqrt{2} \right]^{2} \left[1 - c_{O}^{2} \sqrt{2} \right] + (v_{K1})^{2} \left[1 - c_{O}^{2} \sqrt{2} \right] \\ &+ \left(v_{K1} \right)^{2} + \left(c_{O} \sqrt{2} \right)^{2} + (v_{K1})^{2} \left[1 - c_{O}^{2} \sqrt{2} \right] \\ &+ \left(c_{O} \sqrt{2} \right)^{2} \left[1 - c_{O}^{2} \sqrt{2} \right] + (v_{K1})^{2} \left[1 - c_{O}^{2} \sqrt{2} \right] \\ &+ \left[c_{O} \sqrt{2} \right]^{2} \left[1 - c_{O}^{2} \sqrt{2} \right] + (v_{K1})^{2} \left[1 - c_{O}^{2} \sqrt{2} \right] \\ &+ \left[c_{O} \sqrt{2} \right]^{2} \left[1 - c_{O}^{2} \sqrt{2} \right] + \left(v_{K1} \right)^{2} \left[1 - c_{O}^{2} \sqrt{2} \right] \\ &+ \left[c_{O} \sqrt{2} \right]^{2} \left[c_{O} \sqrt{2} \right] + \left(v_{K1} \right)^{2} \left[c_{O} \sqrt{2} \right] \\ &+ \left[c_{O} \sqrt{2} \right]^{2} \left[c_{O} \sqrt{2} \right] + \left(c_{O} \sqrt{2} \right] \\ &+ \left[c_{O} \sqrt{2} \right]^{2} \left[c_{O} \sqrt{2} \right] + \left(c_{O} \sqrt{2} \right] \\ &+ \left[c_{O} \sqrt{2} \right] + \left(c_{O} \sqrt{2} \right] \\ &+ \left(c_{O} \sqrt{2} \right)^{2} \left[c_{O} \sqrt{2} \right] + \left(c_{O} \sqrt{2} \right] \\ &+ \left(c_{O} \sqrt{2} \right)^{2} \left[c_{O} \sqrt{2} \right] \\ &+ \left(c_{O} \sqrt{2} \right)^{2} \left[c_{O} \sqrt{2} \right] + \left(c_{O} \sqrt{2} \right] \\ &+ \left(c_{O} \sqrt{2} \right)^{2} \left[c_{O} \sqrt{2} \right] \\ &+ \left(c_{O} \sqrt{2} \right)^{2} \left[c_{O} \sqrt{2} \right] + \left(c_{O} \sqrt{2} \right] \\ &+ \left(c_{O} \sqrt{2} \right)^{2} \left[c_{O} \sqrt{2} \right] \\ &+ \left(c_{O} \sqrt{2} \right)^{2} \left[c_{O} \sqrt{2} \right] \\ &+ \left(c_{O} \sqrt{2} \right)^{2} \left[c_{O} \sqrt{2} \right] \\ &+ \left(c_{O} \sqrt{2} \right)^{2} \left[c_{O} \sqrt{2} \right] \\ &+ \left(c_{O} \sqrt{2} \right)^{2} \left[c_{O} \sqrt{2} \right] \\ &+ \left(c_{O} \sqrt{2} \right)^{2} \left[c_{O} \sqrt{2} \right] \\ &+ \left(c_{O} \sqrt{2} \right)^{2} \left[c_{O} \sqrt{2} \right] \\ &+ \left(c_{O} \sqrt{2} \right)^{2} \left[c_{O} \sqrt{2} \right] \\ &+ \left(c_{O} \sqrt{2} \right)^{2} \left[c_{O} \sqrt{2} \right] \\ &+ \left(c_{O} \sqrt{2} \right)^{2} \left[c_{O} \sqrt{2} \right] \\ &+ \left(c_{O} \sqrt{2} \right)^{2} \left[c_{O} \sqrt{2} \right] \\ &+ \left(c_{O} \sqrt{2} \right)^{2} \left[c_{O} \sqrt{2} \right] \\ &+ \left(c_{O} \sqrt{2} \right)^{2} \left[c_{O} \sqrt{2} \right] \\ &+ \left(c_{O} \sqrt{2} \right)^{2} \left[c_{O} \sqrt{2} \right] \\ &+ \left(c_{O} \sqrt{2} \right)^{2} \left[c_{O} \sqrt{2} \right] \\ &+ \left(c_{O} \sqrt{2} \right) \\$$

In equation (63), c is the concentration of the solute, in moles, g_2 is the weight of solute in grams, α is the thermal expansion coefficient of the mixture, V is the small volume element responsible for the scattering and the terms subscripted with a zero denote equilibrium quantities. Also, c_p , ρ_o and β_S refer to values for the mixture. The terms in (63) which involve the quantities (vk + ω) and (vk - ω) are considered to be the Brillouin components; all other terms make up the central peak.

By integrating equation (63) with respect to the change in wave vector, k, and the frequency shift, ω , one obtains the intensity distribution of the scattered light. Dropping the subscripts for the equilibrium quantities, we find the intensity ratio of the Rayleigh peak to the Brillouin doublet 1 to be

$$\frac{I_{C}}{2I_{B}} = \left\{ J_{O} \left[1 + \frac{\left[c_{\infty}^{2} - v^{2} \right] k^{2} \tau^{2} + \left[c_{O} / v \right]^{4} - \left[c_{O} / v \right]^{2}}{\left(v k \tau \right)^{2} + \left[c_{O} / v \right]^{4}} \right] + \frac{\left[c_{\infty}^{2} - c_{O}^{2} \right] k^{2} \tau^{2} + \left[c_{O} / v \right]^{4} - \left[c_{O} / v \right]^{2}}{\left(v k \tau \right)^{2} + \left[c_{O} / v \right]^{4}} \right\} \right\} \right\}$$

$$\left\{ 1 - \frac{\left[c_{\infty}^{2} - c_{O}^{2} \right] k^{2} \tau^{2} + \left[c_{O} / v \right]^{4} - \left[c_{O} / v \right]^{2}}{\left(v k \tau \right)^{2} + \left[c_{O} / v \right]^{4}} - \left[c_{O} / v \right]^{2}} \right\} \right\}$$

$$- J_{O} \left[\frac{\left[c_{\infty}^{2} - v^{2} \right] k^{2} \tau^{2} + \left[c_{O} / v \right]^{4} - \left[c_{O} / v \right]^{2}}{\left(v k \tau \right)^{2} + \left[c_{O} / v \right]^{4}} \right] \right\}$$

$$(64)$$

This result differs somewhat from the equation set forth by Fishman and Mountain.

where
$$J_{o} = \left(\left[1 + \frac{\rho V}{g_{2}} (1 - \gamma) \right] \frac{T}{g_{2}^{c}} \left(\frac{\partial \varepsilon}{\partial T} \right)_{p,c}^{2} + \frac{(\partial \varepsilon / \partial c)}{(\partial \mu / \partial c)} \left(\frac{\rho VT}{g_{2}^{c}} \left[1 - \frac{1}{\gamma} \right] \left(\frac{\partial \varepsilon}{\partial T} \right)_{p,c}^{2} + \frac{2\alpha T}{g_{2}^{\beta} T^{c}} \left(\frac{\partial \varepsilon}{\partial p} \right)_{T,c} \left(\frac{\partial \varepsilon}{\partial T} \right)_{p,c} + \frac{1}{V^{\beta}} \left(\frac{\partial \varepsilon}{\partial p} \right)_{T,c}^{2} \right).$$
(65)

A tremendous amount of simplification results for small scattering angles, since $k \to 0$. For small scattering angles, $\mathbf{v} \to \mathbf{c}$, also, and we are left with

$$\frac{I_{C}}{2I_{B}} \simeq J_{O} , \qquad (66)$$

which is essentially the result obtained by Miller (39) using the fluctuation theory approach outlined by Landau and Lifshitz (47).

For the case of large scattering angles (i.e., $\theta \to 180^{\circ}$), k goes to $2n/\lambda_{\circ}$, which is very large in comparison with the k values for low-angle scattering. In this situation, we find that equation (64) can again be simplified, if we are willing to assume that $k \to \infty$ as $\theta \to 180^{\circ}$:

$$\frac{I_{c}}{2I_{B}} \simeq \frac{c_{\infty}^{2}}{c_{o}^{2}} - 1 + \frac{c_{\infty}^{2}}{c_{o}^{2}} J_{o} . \tag{67}$$

It is unfortunate that large-and small-angle scattering measurements are difficult to perform experimentally, because the reduction in complexity of the theoretical expressions for the Landau-Placzek ratio is enormous.

In spite of the complicated form for the Landau-Placzek ratio, $I_{C}/2I_{B}$, let us examine the situation for a binary mixture at constant temperature. For this type of system we note that $(\partial \epsilon/\partial c)_{p,T} \neq 0; \quad (\partial \mu/\partial c)_{p,T} \neq 0; \quad (\partial \epsilon/\partial p)_{T,C} \neq 0; \text{and} \quad (\partial \epsilon/\partial T)_{p,C} = 0.$

Equation (64) then becomes

$$\frac{I_{c}}{2I_{B}} \approx \begin{cases} v\beta_{S}(\partial \varepsilon/\partial c)^{2}_{p,T}/(\partial \mu/\partial c)_{p,T} \\ (\partial \varepsilon/\partial p)^{2}_{T,c} \end{cases} \\
\times \left[1 + \frac{\left[c_{\infty}^{2} - v^{2} k^{2}\tau^{2} \right] + \left[c_{o}/v \right]^{4} - \left[c_{o}/v \right]^{2}}{(vk\tau)^{2} + \left[c_{o}/v \right]^{4}} \right] \\
+ \frac{\left[c_{\infty}^{2} - c_{o}^{2} \right] k^{2}\tau^{2} + \left[c_{o}/v \right]^{4} - \left[c_{o}/v \right]^{2}}{(vk\tau)^{2} + \left[c_{o}/v \right]^{4}} \right] \\
\left\{ 1 - \frac{\left[c_{\infty}^{2} - c_{o}^{2} \right] k^{2}\tau^{2} + \left[c_{o}/v \right]^{4} - \left[c_{o}/v \right]^{2}}{(vk\tau)^{2} + \left[c_{o}/v \right]^{4}} \right\} \\
- V\beta_{S} \frac{\left(\partial \varepsilon/\partial c \right)_{p,T}^{2}}{\left(\partial \varepsilon/\partial p \right)_{T,C}^{2}} \left[\frac{\left[c_{\infty}^{2} - v^{2} \right] k^{2}\tau^{2} + \left[c_{o}/v \right]^{4} - \left[c_{o}/v \right]^{4}}{(vk\tau)^{2} + \left[c_{o}/v \right]^{4}} \right] \right\}. (68)$$

Fishman and Mountain have shown that the expression in the brackets in the denominator is a relatively unimportant term for the case of hypersonic waves detected by Brillouin scattering. Furthermore, Miller (39) has shown that the approximation

$$(\partial \varepsilon / \partial p)_{\mathbf{T,C}} = \rho \left(\frac{\partial \varepsilon}{\partial \rho} \right)_{\mathbf{T,C}} \beta_{\mathbf{T}}$$
 (69)

is valid for a binary solution, so that we can reduce equation (68) to

$$\frac{I_{c}}{2I_{B}} \simeq \frac{V\beta_{S}(\partial \varepsilon/\partial c)^{2}_{p,T}}{\beta_{T}^{2\rho^{2}(\partial \mu/\partial c)}_{p,T}(\partial \varepsilon/\partial \rho)^{2}_{T,c}} + \frac{\left[c_{\infty}^{2} - c_{o}^{2}\right]k^{2}\tau^{2} + \left[c_{o}/v\right]^{4} - \left[c_{o}/v\right]^{2}}{(vk\tau)^{2} + \left[c_{o}/v\right]^{4}} \cdot \frac{I_{c}}{1 - \frac{\left[c_{\infty}^{2} - c_{o}^{2}\right]k^{2}\tau^{2} + \left[c_{o}/v\right]^{4} - \left[c_{o}/v\right]^{2}}{(vk\tau)^{2} + \left[c_{o}/v\right]^{4}} \cdot \frac{1 - \left[c_{\infty}/v\right]^{4}}{(vk\tau)^{2} + \left[c_{o}/v\right]^{4}} \cdot \frac{1 - \left[c_{\infty}/v\right]^{4}}{(vk\tau)^{2} + \left[c_{o}/v\right]^{4}} \cdot \frac{1 - \left[c_{\infty}/v\right]^{4}}{(vk\tau)^{2} + \left[c_{\infty}/v\right]^{4}} \cdot \frac{1 - \left[c_{\infty}/v\right]^{4}}{(vk\tau)^{2} + \left[c_{\infty}/v$$

Equation (70) is valid for a binary mixture at constant temperature.

b. Relationship between the Brillouin linewidth, phenomenological coefficients and thermodynamic parameters

The Brillouin linewidth of a pure liquid is directly related to the sonic absorption coefficient of a thermal sound wave in the liquid such that (48, 49)

$$\Gamma_{\rm B} = \alpha V_{\rm s} . \tag{71}$$

 $\Gamma_{\rm B}$ is the half width at half height of the Brillouin peak (corrected for the effects of instrumental broadening), and α is the absorption coefficient of the thermally propagated sound wave. $V_{\rm S}$ is the velocity of the sound wave in the liquid, which is determined by the Brillouin shift, the refractive index of the medium, and the wavelength of the incident light, at a specific scattering angle.

The sonic absorption coefficient is describeable in terms of a classical ultrasonic experiment in which a plane sound wave traverses a distance x from the radiation source:

$$I = I_0 e^{-2\alpha x} . (72)$$

Here I is the intensity of the sound wave at a distance x from the source, I is the intensity at x = 0, and α is the absorption coefficient. The absorption coefficient is known to depend on the physical properties of the medium, on external temperature and pressure, and on the frequency of the propagating wave (50). The frequency-corrected absorption coefficient is denoted by α/ν^2 , where ν is the linear frequency of the sound wave.

Herzfeld and Litovitz (51) derived the classical absorption coefficient, $\alpha_{\rm class}$, for a plane sound wave traveling in a medium

which possesses viscosity and heat conductivity which dissipate the wave. Their result is

$$\alpha_{class} = \frac{2}{3} \frac{\omega^2}{v_s^3 \rho} \left[\eta + \frac{3\lambda}{4c_p} (\gamma - 1) \right] , \qquad (73)$$

where $\omega = 2\pi\nu$ is the angular frequency of the sound wave, ρ is the density of the medium, η is the shear viscosity, γ is the ratio of the specific heats at constant pressure and volume, respectively, λ is the thermal conductivity, and c_D is the specific heat at constant pressure.

Ultrasonic measurements (52, 53) of the absorption coefficient reveal that many pure liquids possess α values which do not correspond to $\alpha_{\rm class}$. Accordingly, Pinkerton (54) and Herzfeld and Litovitz (51) divided liquids into groups, depending on the ratio $\alpha/\alpha_{\rm class}$ and on the sign of the temperature coefficient of absorption, $(\partial \alpha/\partial T)$. The liquids investigated fell into three categories (Ref. 51, p. 357):

- Group I. "Normal liquids," for which $\alpha/\alpha_{class} \simeq 1.0$, and $(\partial \alpha/\partial T) \simeq 0$.
- Group II. "Kneser liquids," for which $\alpha/\alpha_{\rm class}$ > 1.0, and ($\partial\alpha/\partial T$) is positive.
- Group III. "Associated liquids," for which $\alpha/\alpha_{\rm class} > 1.0$, and $(\partial\alpha/\partial T)$ is negative.

It has been suggested by Hall (55) and confirmed experimentally by Rai, Singh, and Awasthi (56), that the abnormally high value of the measured absorption coefficient for associated liquids is due to the presence of a third type of dissipative mechanism, "structural absorption." The essence of the theory of structural absorption is that molecules in an associated liquid can undergo a transition from one type of structure to another under the influence of the passage of a

sound wave through the liquid. The total frequency-corrected absorption coefficient for associated liquids can be considered to be composed of two parts: a contribution from the viscosity and thermal relaxation mechanisms ($\alpha_{\rm class}$) and a term due to structural absorption ($\alpha_{\rm excess}$). Expressing this statement in terms of an equation, we have

$$(\alpha/\nu^2)_{\text{total}} = (\alpha/\nu^2)_{\text{class}} + (\alpha/\nu^2)_{\text{excess}}$$
 (74)

or
$$(\alpha/\nu^2)_{\text{total}} = \frac{2\pi^2}{v_s^3 \rho} \left[\frac{4}{3} \eta + \frac{\lambda}{c_p} (\gamma - 1) \right] + (\alpha/\nu^2)_{\text{excess}}.$$
 (75)

Hall (Ref. 55, p. 778) defines the excess absorption from structural relaxation to be

$$(\alpha/\nu^2)_{\text{excess}} = 2\pi^2 \rho V_{\text{s}} \beta_{\text{r}} \tau \tag{76}$$

where β_{r} is the relaxational part of the isothermal compressibility and τ is the structural relaxation time. β_{r} is considered to be the difference between the static isothermal compressibility, $\beta_{T,O}$, and the high frequency limit, $\beta_{T,\infty}$. The structural relaxation time, τ , can be calculated from the formula

$$\tau = \frac{v\eta}{RT} \left[1 + \exp(\Delta F/RT) \right]$$
 (77)

where v is the molal volume, ΔF is the difference in free energy between the two structural configurations of the molecule, and R is the universal gas constant.

If we assume that the behavior of binary mixtures of associated liquids is not too dissimilar from the behavior of pure liquids of this type, and that the sonic absorption coefficient for the mixtures can be given by equation (75) (using the values for the mixture), then we might expect our DMSO-pyridine solutions to fall into the Group III

classification. We might also expect the variation of α with respect to composition and temperature to give us further insight into the structural changes occurring in the DMSO-pyridine solutions.

Looking back at equation (71), we see that our primary task in the determination of α is the evaluation of the Brillouin linewidth, $2\Gamma_B$. It is a well-established fact (21, 49, 57-59) that in Brillouin scattering experiments, the linewidths of the spectral components are of the same order of magnitude as the combined linewidths of the incident source and detector, which is called the instrumental profile. The observed spectrum is, therefore, the convolution of the true light scattering spectrum with the instrumental profile of the light detection system. Mathematically speaking, we have (60)

$$O(v) = \int_{0}^{\infty} T(v, v') \int_{0}^{\infty} S(v', v'') I(v'') dv'' dv' , \qquad (78)$$

with $O(\nu)$ being the observed spectrum as a function of frequency, ν , $T(\nu,\nu')$ being the transmission function of the spectral analyzer (which is usually a Fabry-Perot etalon), $S(\nu',\nu'')$ being the scattering spectrum as a function of the incident frequency input, ν'' , and the scattering frequency output, ν' , and $I(\nu'')$ being the intensity spectrum of the incident source, with output frequency ν'' .

Leidecker and LaMacchia (60) have given a detailed account of the effects of instrumental profiles on the shape of Brillouin peaks.

Following their analysis, we will examine the generalized case of a Gaussian instrumental function convoluted with a Lorentzian scattering spectrum to produce an observed intensity spectrum which is a combination of the two (namely, a Voigt function). Then we will examine the special case of a Lorentzian instrumental profile convoluted with a

Lorentzian scattering spectrum to produce an observed Lorentzian intensity spectrum.

It has been shown experimentally (61) that most continuous wave lasers possess an intensity profile which can be adequately described by a Gaussian distribution function, $I_{C}(v)$:

$$I_{G}(v) = \sum_{i=1}^{N} \delta\left(v - v_{oi}^{i}\right) \exp\left\{-4\ln 2\left(\frac{v - v_{oi}^{i}}{\Gamma_{i}}\right)^{2}\right\}.$$
 (79)

In equation (79), N is the number of axial modes lasing, ν_{oi} is the central frequency of the ith axial mode, and Γ_{i} is the full width at half height of the ith spectral line. Many of the recently available commercial lasers have single mode outputs so that the intensity distribution reduces to

$$I_{\mathbf{G}}(\mathbf{v}) \propto \delta \left(\mathbf{v} - \mathbf{v}_{\mathbf{o}}\right) \exp \left\{-4\ln 2 \left(\frac{\mathbf{v} - \mathbf{v}_{\mathbf{o}}}{\Gamma}\right)^{2}\right\}. \tag{80}$$

The spectral analyzer employed in the majority of Brillouin scattering spectrometers (including the one used in this work) is the scanning Fabry-Perot interferometer. A simple theoretical analysis of a Fabry-Perot etalon yields the result that the transmission intensity, $T(\nu)$, for the etalon is

$$T(v) \propto \frac{1}{1 + \left(\frac{2}{\pi} \operatorname{F} \sin \varepsilon\right)^2}$$
 (81)

where F is the effective finesse of the etalon, $\varepsilon = 2\pi dn\nu/c$, and $T(\nu)$ has the form of an Airy function. In the expression for ε , n is the refractive index of the medium between the Fabry-Perot mirrors and d is the mirror separation. For cases in which the effective finesse is greater than 30, the Airy function reduces to Lorentzian form:

$$T_{L}(v) \propto \frac{1}{1 + \left[2\left(v - v_{o}\right)/\Gamma_{FP}\right]^{2}}.$$
 (82)

Here v_0 is again the central frequency of the transmitted beam, and Γ_{pp} is the full width at half height of the Fabry-Perot spectral peak. The restrictions on the validity of equation (82) are the conditions of absolute parallelism and flatness of the mirrors (62).

The linewidth of the instrumental profile is a combination of the linewidths of the laser beam and Fabry-Perot transmission function. Therefore, it can be seen a priori that in a situation in which the linewidth of the Fabry-Perot transmission function is very much larger than the linewidth of the light source, the resulting instrumental profile will possess the shape of the Fabry-Perot function; i.e., it will be a Lorentzian. In the less common situation in which the linewidth of the incident source is comparable in size to the linewidth of the transmission function, the resulting instrumental profile will be a Voigt function. From the theoretical discussion of the intensity profiles which are predicted for pure liquids (pp. 19, 27) and for binary mixtures (p. 33), and from reported experimental linewidth measurements for Brillouin spectra (49, 57-59, 63-65), one has every reason to expect the true shape of a Brillouin peak from a DMSO-pyridine spectrum to be Lorentzian. For the remainder of this discussion, we assume that this conclusion is correct, and proceed to an important discovery about the shape of an observed Brillouin peak when the instrumental function is a Lorentzian.

For the special case of the instrumental profile being

It will be demonstrated in Part IV-E that this assumption is indeed correct.

Lorentzian in nature, it can be shown (Ref. 60, p. 145) that the observed intensity distribution for a Brillouin peak in the light scattering spectrum is a Lorentzian with full width at half height given by

$$2\Gamma_{\text{B/obs}} = 2\Gamma_{\text{B}} + \Gamma_{\text{inst}}$$
 (83)

Here $2\Gamma_B$ is the true width of the Lorentzian-shaped Brillouin peak, and Γ_{inst} is the full width at half height of the Lorentzian-shaped instrumental profile (viz., the Fabry-Perot transmission function).

In conclusion of this discussion of Brillouin linewidths, it should be noted that the above analysis is not valid if other relaxational modes are observed in the experimental spectra (i.e., if the Rayleigh and/or Brillouin peaks are composed of more than one Lorentzian function).

D. Effects of Optical Properties of Polar Liquids on Light
Scattering

From equation (9) on p. 7, it is seen that the velocity of hypersound in a fluid is dependent upon both the observed Brillouin shift and the refractive index, measured at a given wavelength. Consequently, in order to obtain accurate values for the hypersonic velocities of the DMSO-pyridine solutions, it was necessary to determine the refractive index of each solution under the appropriate thermal conditions.

During the course of the data analysis on the refractive index measurements, it was discovered that there is a dearth of material available on the optical properties of mixtures of polar compounds.

Furthermore, it was recognized that the Clausius-Mosotti-LorentzLorenz equation 1 describing the relationship between the dielectric
constant, refractive index, and polarizability of a nonpolar compound,
would in no way be valid for the polar substances DMSO and pyridine.
Since the additivity of molar refractivities of mixtures of compounds
is based on the Clausius-Mosotti-Lorentz-Lorenz equation, we felt that
there was also doubt concerning the linearity of the molar refractivity
of the DMSO-pyridine solutions with mole fraction DMSO. We were cognizant of the fact that any abnormality in the values of the refractive
index would be transmitted directly to the hypersonic velocity in such
a manner as to render this data invalid. Therefore, we felt that it
would be advisable to confirm the additivity of the molar refractivities
of DMSO and pyridine, both experimentally and theoretically.

The following is a brief theoretical discussion concerning the optical properties of polar and nonpolar liquids which we hope will lend significance to the refractive index data presented in section IV.

For a uniform isotropic medium, the refractive index, n, is defined as

$$n = \frac{c}{v} \tag{84}$$

where c is the velocity of light in vacuo and v is the velocity of light in the medium.

$$\frac{\varepsilon - 1}{\varepsilon + 2} = \frac{n^2 - 1}{n^2 + 2} = \frac{4}{3} \pi N\alpha$$

where ϵ is the dielectric constant, n is the refractive index, N is the number of molecules per unit volume, and α is the polarizability of the molecules.

From Born and Wolf (66), p. 87, the Clausius-Mosotti-Lorentz-Lorenz equation is given by

Born and Wolf (Ref. 66, p. 11) discuss the relationship between the velocity of light in a medium, the dielectric constant, ϵ , and magnetic permeability, μ . They state that the solution of Maxwell's wave equations,

$$\nabla^{2}_{H} = \frac{\varepsilon \mu}{c^{2}} \frac{\partial^{2}_{H}}{\partial t^{2}} \qquad \nabla^{2}_{E} = \frac{\varepsilon \mu}{c^{2}} \frac{\partial^{2}_{E}}{\partial t^{2}}$$
(85)

"... suggest the existence of electromagnetic waves propagated with a velocity

$$\mathbf{v} = \mathbf{c}/\sqrt{\epsilon \mu} \cdot \mathbf{n}$$
 (86)

In equation (74), \vec{H} and \vec{E} are the magnetic and electric field vectors, respectively, $\partial^2 \vec{H}/\partial t^2$ and $\partial^2 \vec{E}/\partial t^2$ are second derivatives with respect to time, and

$$\nabla^{2} \vec{h} = \left(\frac{\partial^{2} H}{\partial x^{2}} + \frac{\partial^{2} H}{\partial y^{2}} + \frac{\partial^{2} H}{\partial z^{2}} \right)$$

$$\nabla^{2} \vec{h} = \left(\frac{\partial^{2} E}{\partial x^{2}} + \frac{\partial^{2} E}{\partial y^{2}} + \frac{\partial^{2} E}{\partial z^{2}} \right) . \tag{87}$$

From the definition of n, we have

$$n = (\varepsilon \mu)^{\frac{1}{2}} . \tag{88}$$

The form of this equation presented in most optics texts, $n^2 = \epsilon$, arises from the fact that $\mu = 1$ for "nonmagnetic" substances.

Although the relationship $n^2 = \varepsilon$ has proven valid for experimental observations on gases and many liquid hydrocarbons, it has been shown to be incorrect for certain other liquids (namely, highly associated ones). Values of n and $\sqrt{\varepsilon}$ given by Born and Wolf (Ref. 66, p. 14) for methyl alcohol, ethyl alcohol, and water are illustrative

Ref. 66, p. 11.

of the strong deviation from the $n^2 = \epsilon$ relation exhibited by highly polar compounds:

	n(yellow light)	$\sqrt{\varepsilon}$
сн 3он	1.34	5.7
C2H5OH	1.36	5.0
H ₂ O	1.33	9.0

The temperature for these measurements is assumed to be ambient, since no information was provided.

The values of n and $\sqrt{\epsilon}$ cited in Szmant's work (Ref. 1, p. 11) for DMSO exhibit a similar behavior:

$$n_D^{20} = 1.4783$$
 $\sqrt{\varepsilon} = \sqrt{48.9} = 6.99$ $n_D^{25} = 1.47674$ $\sqrt{\varepsilon} = \sqrt{46.4} = 6.81$

Experimental determinations of n and ε are made under quite different conditions. Refractive index measurements are made with electromagnetic radiation of rather high frequency (10^{15} sec^{-1}), whereas dielectric constant measurements take place with electric fields in the frequency range 5 x 10^5 to 5 x 10^6 sec⁻¹. Because of the extreme differences in frequency in the two cases, certain criteria must be met in order for the relation $n^2 = \varepsilon$ to be valid (67):

- (1) the molecules of the dielectric medium must possess no dipole moment
- (2) the measurement of refractive index should be made with long-wavelength infrared radiation so that both the electrons and the nuclei are affected by the electromagnetic wave
- (3) the wavelength of the infrared radiation should be far enough from an absorption band to insure that anomalous dispersion is not occurring.

The first restriction arises from the frequency dependence of the dielectric constant, and from the contribution of the permanent dipole moment, μ , to the dielectric constant at low frequencies. Lipson and Lipson (68) derive the frequency dependence of the dielectric constant for a medium consisting of polar molecules; a brief summary of their discussion follows.

The frequency dependent dielectric constant, ϵ (ω), is related to the electric susceptibility, χ (ω), by the equation

$$\varepsilon (\omega) = \varepsilon + 4\pi \chi (\omega)$$
 (89)

where ϵ_0 is the value of the frequency independent portion of the dielectric constant and $\chi(\omega)$ is found to be a complex function of the form

$$\chi(\omega) = \frac{\chi(0)}{1 + i\omega\tau}.$$
 (90)

Here ω is the frequency of the applied electric field, $\chi(0)$ is the zero-frequency electric susceptibility and τ is the relaxation time, or the time required for the electric dipoles to orient themselves in a state of minimum potential energy while under the influence of the external electric field.

Equations (89) and (90) lead to the result

$$\varepsilon(\omega) = \varepsilon_1 + i\varepsilon_2$$
, (91)

where

$$\varepsilon_1 = \varepsilon_0 + \frac{4\pi\chi(0)}{1 + \omega^2\tau^2}$$
 and $\varepsilon_2 = \frac{-4\pi\chi(0)\omega\tau}{1 + \omega^2\tau^2}$ (92)

In the limit of low frequencies,

$$\epsilon_1 \rightarrow \epsilon_0 + 4\pi\chi(0)$$
 $\epsilon_2 \rightarrow 0$ (93)

so that $\varepsilon(\omega)$ + ε \simeq ε + $4\pi\chi(0)$, which is the value of the static dielectric constant.

At high frequencies the molecules do not have time to change with the rapidly oscillating field so that

It can be seen from the expressions for the dielectric constant at the low and high frequency limits that experimental determinations of the dielectric constant must be made at low electromagnetic frequencies in order to obtain meaningful values of ε . Debye (69) has shown, however, that in this low frequency region the permanent dipole moment of a polar molecule can contribute to the total polarization of the medium.

Debye calculated the contribution of the average value of the permanent dipole moment, μ , to the dielectric constant for a polar liquid. He showed that the total molar polarization, P_M , in the region of low electromagnetic frequencies is due to the contributions from both the induced and permanent dipole moments:

$$P_{M} = \left(\frac{\varepsilon - 1}{\varepsilon + 2}\right) \frac{MW}{\rho} = \frac{4\pi N_{L}}{3} \left(\alpha + \frac{\mu^{2}}{3kT}\right) . \qquad (95)$$

In equation (95) MW is the molecular weight of the liquid, ρ is the density, α is the polarizability, N_L is the Avogadro-Loschmidt constant, and kT is the thermal energy of the system at temperature T.

What all of this means, of course, is that for polar molecules, the value of the low-frequency dielectric constant will contain a contribution due to the permanent dipole moment of the molecule. In the

high frequency region of the electromagnetic spectrum, where refractive index measurements are made, the dielectric constant will be much lower, due to the fact that at high frequencies the permanent dipole moment cannot contribute to the dielectric constant. Therefore, for polar molecules, the relation $\varepsilon = n^2$ is not valid. In order to obtain a suitable relationship between the dielectric constant and the refractive index for a polar fluid, Onsager (70) reviewed Mosotti's internal field theory of the polarization of dielectric media and found it to be unapplicable to polar molecules. From his subsequent analysis of the effect of the environment of a polar molecule on the permanent and induced dipole moments of that molecule during the presence of an external electric field, Onsager derived the following equation for a pure polar fluid:

$$\frac{\left[\varepsilon - n^2\right]\left(2\varepsilon + n^2\right)}{\varepsilon\left(n^2 + 2\right)^2} \left(\frac{MW}{\rho}\right) = \frac{4\pi N_L \mu^2}{9kT} . \tag{96}$$

The first step in solving (96) for the refractive index is to rewrite the equation in expanded form:

$$\frac{4\pi N_L \mu^2}{9kT} \left(\frac{\rho}{MW}\right) = \frac{2\epsilon^2 - \epsilon n^2 - n^4}{\epsilon \left(n^4 + 4n^2 + 4\right)} . \tag{97}$$

Let $c' = 4\pi N_{I,\rho}/(9kMW)$ so that

$$\frac{c'\mu^2}{T} = \frac{\left(2\varepsilon^2 - \varepsilon n^2 - n^4\right)}{\varepsilon\left(n^4 + 4n^2 + 4\right)} . \tag{98}$$

After cross multiplication and suitable algebraic manipulations, we find that

$$\left(1 + \varepsilon c' \mu^2 / T\right) n^4 + \left(\varepsilon + 4\varepsilon c' \mu^2 / T\right) n^2 - 2\varepsilon^2 + 4\varepsilon c' \mu^2 / T = 0. \tag{99}$$

Solving for the refractive index, n, we have

$$n = \left\{ \frac{\left[\left[\varepsilon + 4\varepsilon c' \mu^2 / T \right]^2 - 4 \left[1 + \varepsilon c' \mu^2 / T \right] \left(-2\varepsilon^2 + 4\varepsilon c' \mu^2 / T \right] \right]^{\frac{1}{2}}}{2 \left[1 + \varepsilon c' \mu^2 / T \right]} \right\}^{\frac{1}{2}}$$
(100)

for a polar liquid.

Applying equation (100) to the case of pure DMSO at $25^{\circ}C^{-1}$, we find that n = 1.12. The agreement between this value and the experimental value of n = 1.4767 cited by Szmant (Ref. 1, p. 5) is quite good, considering the errors inherent in the experimental measurements of ϵ and μ . Recall that the value of n calculated from the equation $\epsilon = n^2$ is 6.81.

The value of n calculated for pure pyridine from equation (100) is 1.16 at 22° C, as opposed to the value 3.54 obtained from the relation ϵ = n^2 . The values of ϵ and μ for pure pyridine were taken from the International Critical Tables.

The results for DMSO and pyridine tend to support Onsager's theoretical relationship between the refractive index of a polar liquid and its static dielectric constant.

It has been found empirically that the refractive index behavior of mixtures of molecules is directly related to the refractive index characteristics of the constituent molecules.

For pure nonpolar liquids, a quantity known as the molar refractivity, A, can be defined by

$$A = \frac{MW}{\rho} \left(\frac{n^2 - 1}{n^2 + 2} \right) \quad , \tag{101}$$

where the factor $(n^2 - 1)/(n^2 + 2)$ comes from the Clausius-Mosotti-Lorentz-Lorenz equation (see footnote, p.44)

The values of ϵ and μ for DMSO used in equation (100) were taken from Ref. 1, p. 5.

$$\frac{\varepsilon - 1}{\varepsilon + 2} = \frac{n^2 - 1}{n^2 + 2} = \frac{4}{3}\pi_N\alpha . \qquad (102)$$

The total molar refractivity, $\mathbf{A_T}$, for mixtures of nonpolar compounds is linearly dependent on the mole fraction of each component of the mixture. 1 Therefore, for a binary mixture of nonpolar substances,

$$A_{T} = X_{1}A_{1} + X_{2}A_{2} , \qquad (103)$$

where X_1 and X_2 are the mole fractions of substances 1 and 2, respectively, and A_1 and A_2 are the molar refractivities.

In view of the complicated functional relationship between ε and n for polar liquids, it is not intuitively obvious that the total molar refractivity of a binary mixture of two polar compounds should be linearly dependent on the mole fraction of component 1. Onsager (Ref. 70, p. 1490), however, hinted at a linear dependence in his derivation of the equation relating ε and n for a mixture of polar liquids. Onsager defined the effective polarizability, α_i , of species i in a mixture of polar fluids to be

$$\alpha_{i} = a_{i}^{3} \left[\frac{n_{i}^{2} - 1}{n_{i}^{2} + 2} \right] , \qquad (104)$$

where a_i is the radius of the ith spherical molecular species. In light of equation (104), we may define the molar refractivity, A_i' of polar species i to be

$$A_{i}' = \left(\frac{n_{i}^{2} - 1}{n_{i}^{2} + 2}\right) \frac{MW}{\rho} , \qquad (105)$$

This linear relationship is known as the law of Gladstone and Dale.

where n_{i} is the refractive index for the polar species i, and is given by equation (100). Note that equation (105) is exactly analogous to the molar refractivity equation for nonpolar substances.

The total molar refractivity for a binary mixture of polar species can then be expected to be linearly dependent on the mole fraction of component 1 such that

$$A' = X_1 A_1' + X_2 A_2' . (106)$$

Summarizing, we have the following equations relating the dielectric constant, refractive index, and molar refractivity for nonpolar and polar substances:

pure nonpolar fluids:

$$n^2 = \varepsilon$$

binary mixtures of nonpolar fluids: $A_{T} = X_1 A_1 + X_2 A_2$

$$\mathbf{A}_{\mathbf{T}} = \mathbf{X}_{1}\mathbf{A}_{1} + \mathbf{X}_{2}\mathbf{A}_{2}$$

pure polar fluids:

$$n^{2} = \frac{1}{2} \left\{ \left(\frac{\varepsilon + 4\varepsilon c' \mu^{2}/T}{1 + \varepsilon c' \mu^{2}/T} \right)^{2} + 8\varepsilon^{2} - 16\varepsilon c' \mu^{2}/T \right\}^{\frac{1}{2}}$$

binary mixtures of polar fluids:

$$A' = X_1 A_1' + X_2 A_2'$$

III. EXPERIMENTAL INFORMATION

A. The Brillouin Spectrometer

The Brillouin spectrometer employed in these light scattering studies was designed and constructed by S. J. Gaumer. A detailed description of the apparatus is contained in his Ph.D. thesis (71). For the sake of completeness, however, and in order to be able to discuss separate portions of the apparatus, a schematic diagram of the spectrometer is shown in Figure 2.

Omitted from the diagram is the temperature control cell which houses the glass sample tubes. The temperature control cell is placed on the rotating table and is constructed to allow the incident and scattered beams into and out of the sample tube while maintaining the temperature to + 0.1 °C of a prescribed setting. The design, construction and calibration of the temperature control cell are the subjects of section III B.

The incident, vertically polarized light of wavelength 5145 Å originates from a single mode, frequency stabilized Spectra Physics Model 165 Argon Ion laser. The incident beam travels to a front surface mirror mounted on a triangular optical rail, is reflected 90°, and passes into the sample on the rotating table. Light scattered at 90° from the incident beam in the horizontal plane is collected for analysis.

Optics housing I is a light-tight metal box which sits at the head of the detection train; it contains two adjustable iris diaphragms and an achromatic lens. The iris diaphragms are located on either end of a threaded aluminum pipe which is positioned in the front portion of the box. Scattered light passes through the ~ 1 mm diameter

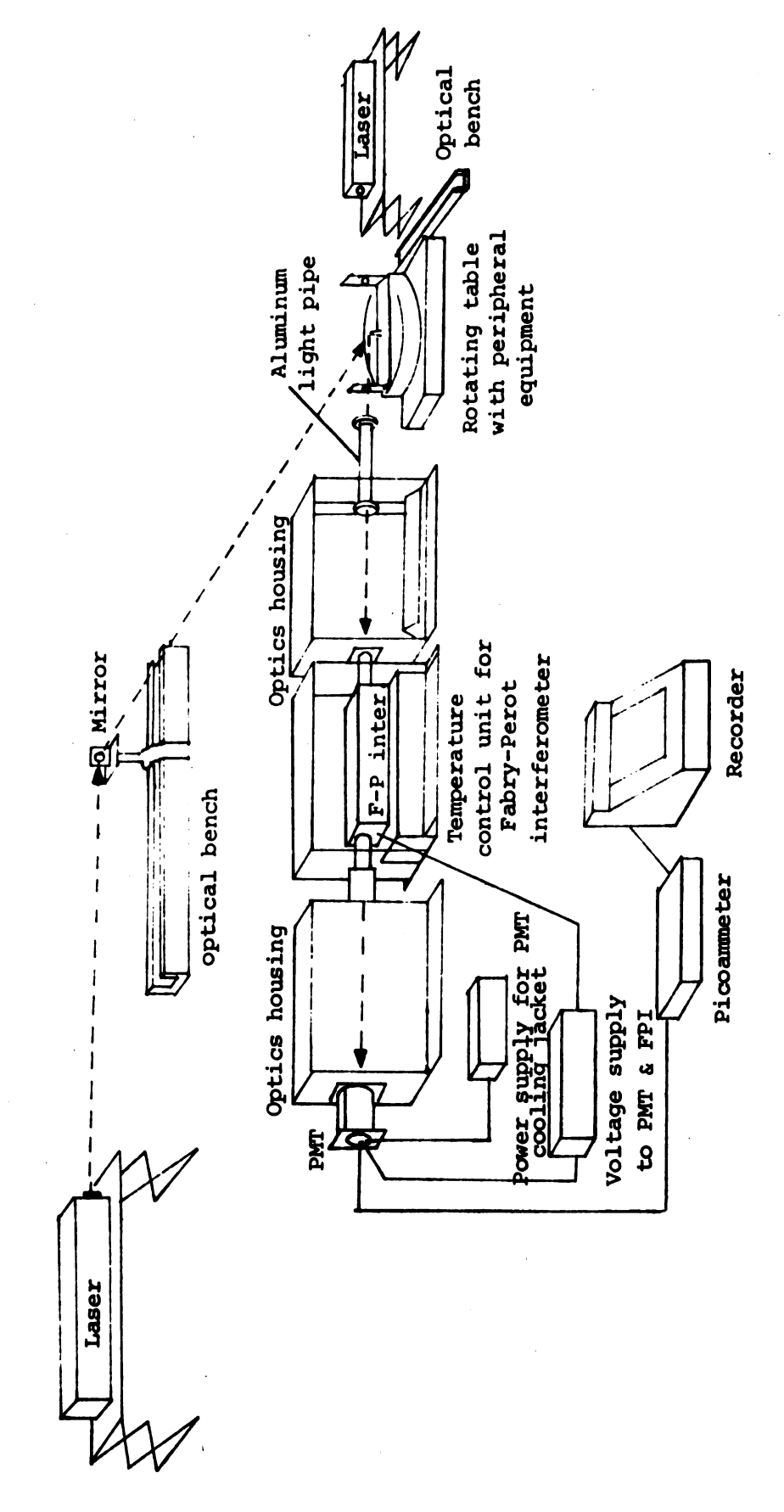


Figure 2. The Brillouin spectrometer.

diaphragms and is collimated by a 500 mm focal length achromatic lens. The collimated light then impinges on a Fabry-Perot interferometer to be resolved. The Fabry-Perot etalon possesses 1 inch diameter mirrors which have inside surfaces polished to $\lambda/100$ flatness; the etalon is scanned piezoelectrically.

The resolved light travels to a second light-tight metal box, optics housing II, to pass through (1) a third aperture (~ 5 mm diameter) (2) another achromatic lens (1000 mm focal length) (3) a final aperture (~ 1 mm diameter) and (4) a disc of polarizing material (HGCP-21, Eastman Kodak) set in the vertical position. The vertically polarized, resolved, scattered light then travels to a photomultiplier tube to be detected. The signal from the photomultiplier is amplified by a Keithley picoammeter and is fed into a Sargent recorder. The spectrum of the scattered light is traced by the recorder as the linear ramp voltage to the piezoelectric device is increased. Five spectral orders are obtained from a single 0-1700-volt scan of the interferometer. The finesse for the spectra obtained in this project ranged from 30 to 45.

In order to obtain accurate data from a Brillouin scattering experiment, it is necessary to remove the depolarized (horizontal) contribution to the total light scattering spectrum. The vertical polarizer included in the detection train is used to accomplish this task. The horizontal component appears to have been of little consequence, however, since the depolarization ratio for the two neat liquids was found to be < 0.02.

B. Design and Characterization of the Temperature Control Cell

In order to maintain a constant, controlled temperature within the DMSO-pyridine solutions and yet enable light to pass through, a special temperature control cell had to be constructed for use with the Brillouin spectrometer. An artist's sketch of the unit is shown in Figure 3, while a cut-away representation is given in Figure 4.

The basic component of the temperature control cell is a solid copper cylinder 4 1/2 inches in height. The diameter of the cylinder in the upper and lower flanges is 3 3/8 inches, while the diameter of the smaller central section is 2 1/2 inches. A slit 1/2 inch in width is positioned 1 3/4 inches from the bottom of the cylinder and extends 1 7/16 inches (horizontal depth) into the cylinder. The slit allows light to pass through a sample tube which sits in the center of the copper cylinder.

A piece of copper tubing 3/16 inch O.D. is wound around and soldered to the outside surface of the copper cylinder to serve as a cooling coil. The ends of the tubing are soldered to hollow posts on the top of the cylinder to provide an inlet and outlet, respectively, for cooling solutions. A layer of molded asbestos with 12 feet of #30 nichrome wire embedded in it forms the outermost layer of the central section of the copper cylinder. Each end of the nichrome wire is wound around a drilled and tapped, electrically insulated brass post which emerges on the top of the cylinder. Voltage applied to the nichrome wire via the brass posts serves to heat the copper cylinder.

The outer insulation material for the temperature control cell consists of a Transite board on the bottom, on which the copper cylinder

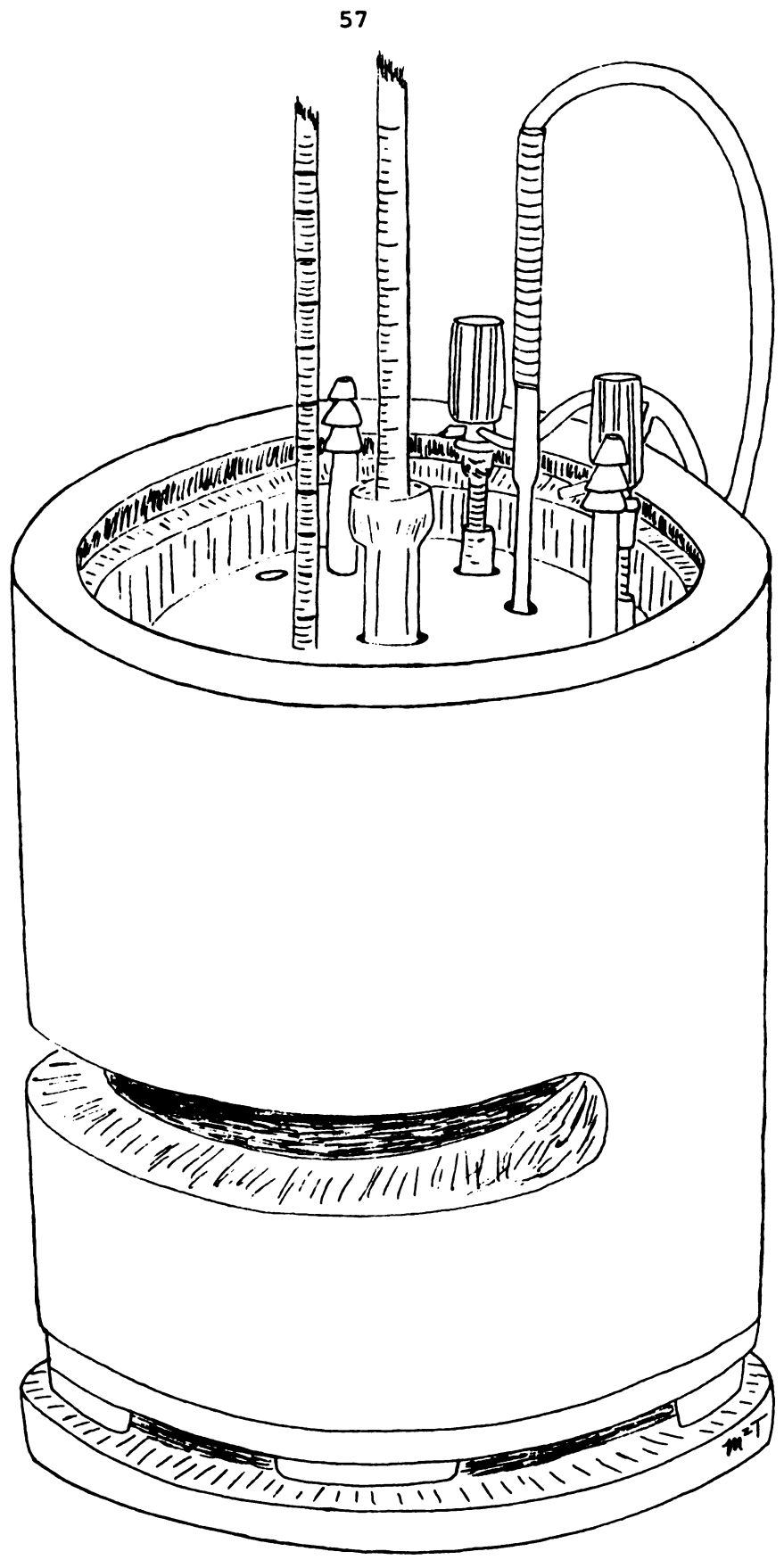


Figure 3. Sketch of the temperature control cell.

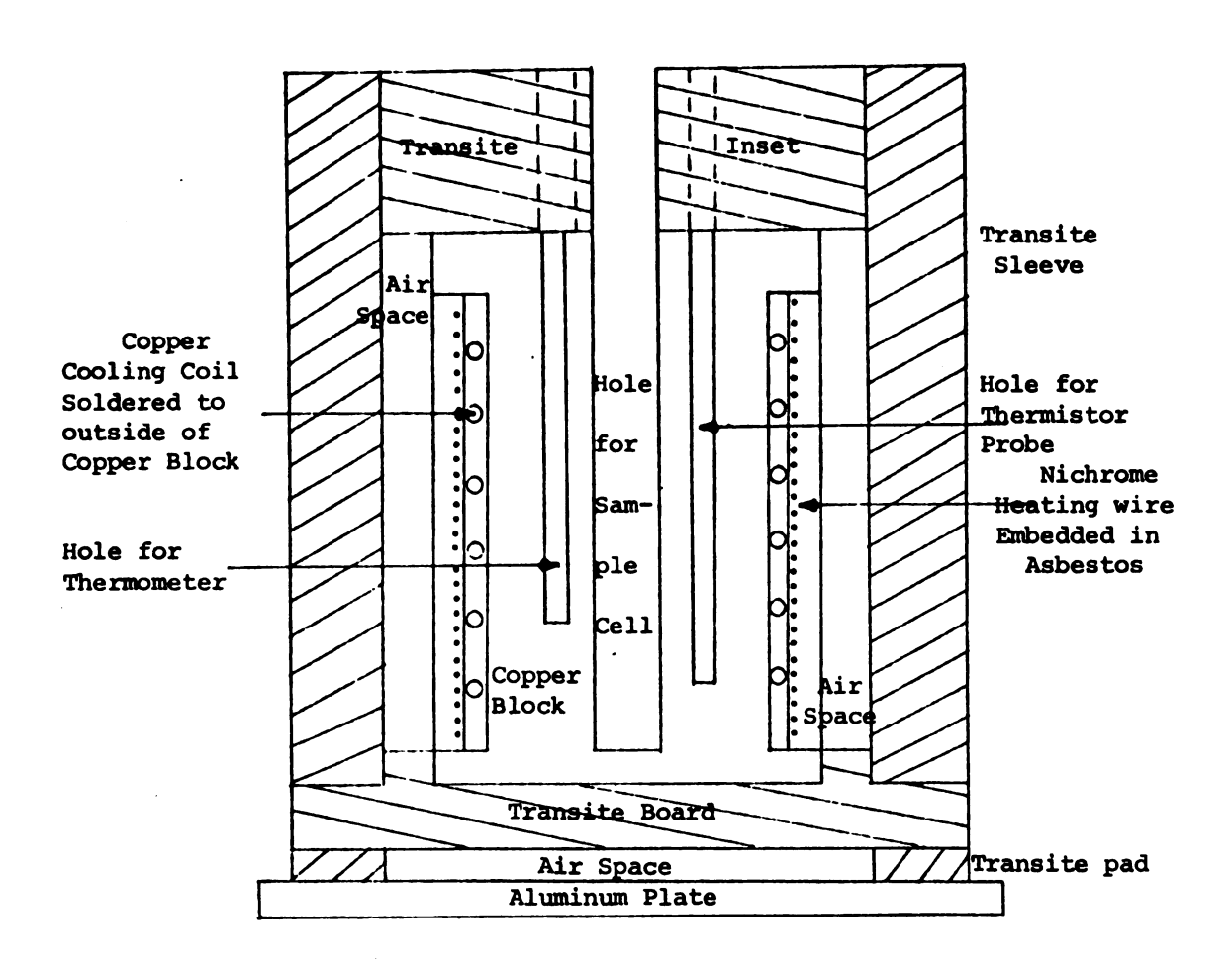


Figure 4. Cross-sectional view of the temperature control cell.

rests, a Transite sleeve around the periphery of the cylinder and a Transite inset on top. The Transite pipe and board were gifts of the Johns-Manville Corporation.

In order to provide a firm mounting for the heavy unit, the Transite board was cemented with epoxy glue to three 1/4 inch thick rectangular pieces of Transite, which were in turn epoxied to a 1/4 inch thick circular aluminum plate. An air space the thickness of the Transite pads helped to insulate the main portion of the temperature control cell from the aluminum base plate.

Holes for a thermometer, thermistor probe and sample tube were drilled through the vertical portion of the copper cylinder in suitable positions. The 1/2 inch diameter hole for the sample tube was placed in the center of the upper face of the cylinder, while the holes for the thermometer and thermistor probe were located one quarter inch to either side of the central hole.

Calibration of the temperature control cell was performed using glycerin as the sample and two accurate etched-stem mercury thermometers as the temperature monitors. An Owens-Illinois mercury thermometer, designated A, reading from -1 to 101 °C in divisions of 0.1 °C, was placed inside a glass sample tube 1 in the copper cylinder and was immersed in glycerin to the proper depth. A Nurnbero mercury thermometer, designated C, reading from -10 to 80 °C in divisions of 0.2 °C, was positioned in the thermometer hole in the copper cylinder. A thermistor probe from a YSI Model 72 temperature controller occupied

The glass sample tube was a 9 mm diameter Fischer-Porter joint sealed at the bottom.

the second small hole in the top of the copper cylinder. This particular arrangement, with thermometer C in the thermometer hole and the thermistor probe in the other small hole in the copper cylinder, constituted the experimental arrangement by which all of the temperatures for the DMSO-pyridine solutions were measured and controlled during the Brillouin scattering experiments.

In response to a signal from the YSI temperature controller, voltage was applied to the nichrome wire around the copper cylinder, causing the cylinder to be heated. The band width of the controller was adjusted to 0.1 °C, and temperatures could be set on the controller to the nearest tenth of a degree. It was found during the calibration procedure that the temperatures set on the controller agreed very closely with the temperatures read from thermometer C.

The calibration procedure was begun by immersing both of the thermometers in an ice bath to determine a correct zero point for each. After the zero points had been obtained, the temperature controller was set to + 70.0 °C, and the control cell was allowed to come to thermal equilibrium. The set-point was then lowered by five-degree increments down to 40 °C; below 40 °C, the controller set-point was lowered one degree at a time. At least 20 minutes was allowed for thermal equilibrium after each lowering of the set-point, even for the one degree increments. A summary of the data obtained is given in Appendix A; only the pertinent results are included here.

Figure 5 illustrates some of the data gathered from the temperature calibration experiments. The temperatures from the two thermometers are designated T_C and T_A , respectively. T_C refers to the temperature of the thermometer in the hole in the copper cylinder,

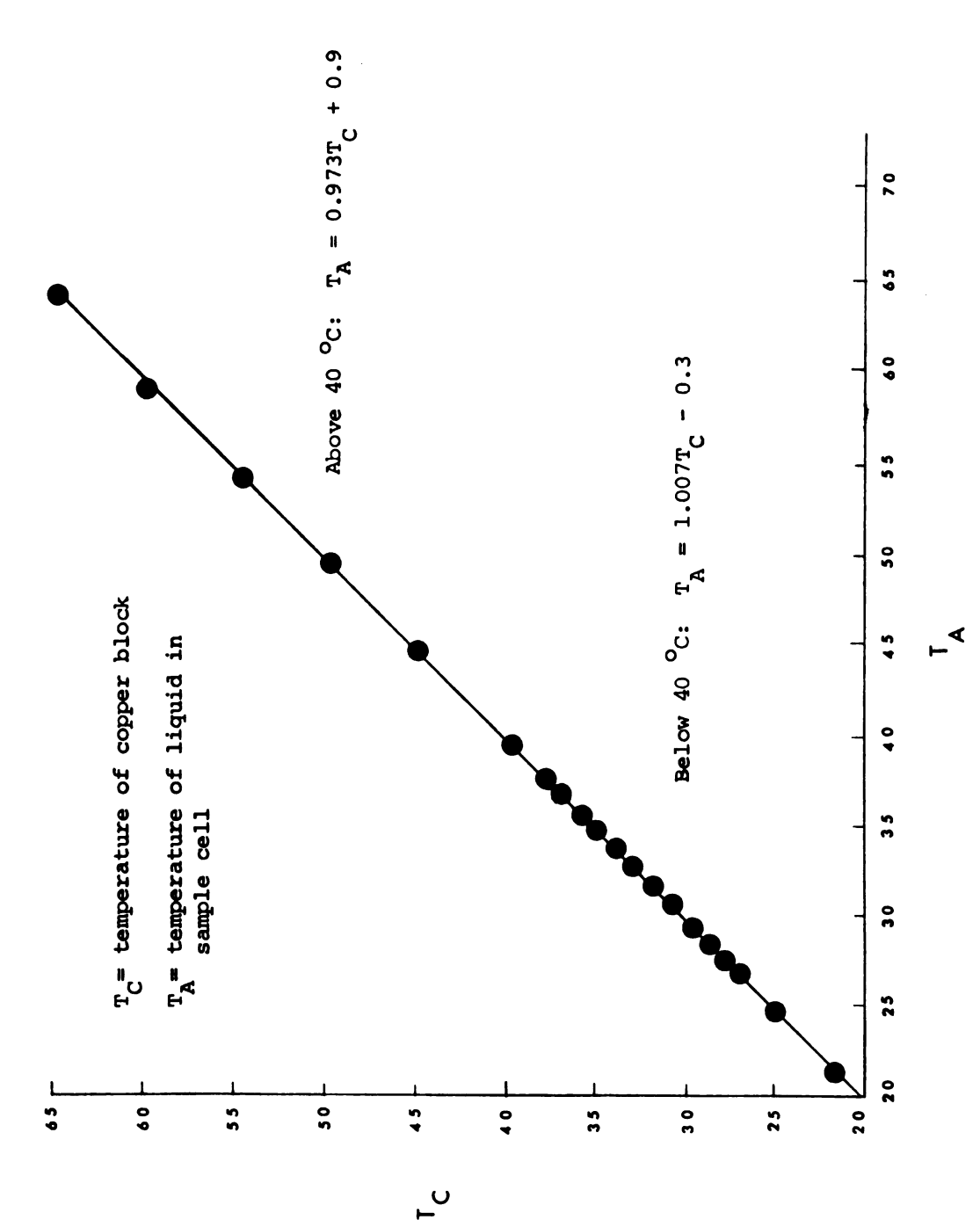


Figure 5. Calibration data for the temperature control cell.

while T_A refers to the temperature of the thermometer in the sample liquid. It was found that the data above 40 $^{\circ}$ C gave rise to a straight line of slightly different slope than the data between 20 and 40 $^{\circ}$ C. The linear relationships for each temperature region are shown on the respective portions of the graph. Not surprisingly, the similarity of the two temperatures (T_C and T_A) decreases at readings above 40 $^{\circ}$ C.

From the data obtained in this series of experiments, it was a simple matter to adjust the temperatures taken in the DMSO-pyridine light scattering experiments to the correct values established by the calibration curve in Figure 5. Typical temperature readings from thermometer C taken during light scattering measurements are given in Table 1, along with the corrected values. The precision of the measured and corrected temperatures is \pm 0.1 $^{\rm O}$ C.

TABLE 1

Measured and Corrected Temperatures Obtained During Brillouin
Scattering Measurements for Mixtures of DMSO and Pyridine

Measured Temperature T _C (^O C)	Corrected Temperature T _A (^O C)
64.7	63.9
59.8	59.0
54.6	54.2
49.6	49.3
44.7	44.5
39.6	39.4
34.8	34.5
29.6	29.5
26.8	26.7
21.6	21.6

It should be noted at this point that all the temperatures presented in other sections of this work are corrected values.

C. Preparation of the Samples

Purification of the two solvents, DMSO and pyridine, and preparation of eleven of their mixtures were carried out by M. S. Greenberg; details of these procedures are given in Ref. 72. It was found from Karl Fischer titrations that the residual water in the two pure fluids amounted to < 0.077% by weight. This corresponds to a maximum contribution of 0.33 mole per cent water to the DMSO-pyridine mixtures.

To insure that the samples were as free of dust as possible for the light scattering measurements, the solutions were passed repeatedly through an ultrafine-Millipore filter apparatus designed by H. K. Yuen (73). This filtering device was a closed-system type whereby the solution was forced under nitrogen pressure through an ultrafine filter, through a Millipore filter, and finally into a collection tube. The collection tubes consisted of 9 mm diameter Fischer-Porter joints which had been sealed at the bottom.

Filtration and collection of the samples proceeded according to the steps outlined below, beginning with neat pyridine and ending with neat DMSO.

Filtration Procedure

- 1. Flushed apparatus twice with 2 ml of the new sample.
- Passed five more 2-ml aliquots of sample through the filtration apparatus. Each sample was collected in a Fischer-Porter collection tube, was rolled around in the tube and discarded.
- 3. After the rinsing process was completed, 12 ml of solution was passed repeatedly through the filtering apparatus and collected until, upon examination with a laser beam, the resultant liquid appeared to be dust-free. (The small dust particles were visible

as tiny scintillators when the beam was passed through a dirty sample.)

After a dust-free solution had been obtained, the sample tube was sealed to prevent contamination from dust and moisture. Duplicate or triplicate samples were prepared for each composition for examination with the Brillouin spectrometer. This was done to eliminate the possibility of a sample being prepared with an incorrect composition. In all cases it was found that the light scattering data from the duplicate or triplicate samples agreed within the limits of experimental error.

D. Measurement of the Refractive Index

Refractive indices for the DMSO-pyridine mixtures were obtained on a Bausch and Lomb Abbe 3-L Refractometer at a wavelength of 5890 Å (the sodium D line). The refractive index for each of the thirteen solutions was measured at five different temperatures. Temperature control for the prisms of the refractometer was provided by a Haake circulating-bath temperature control unit.

The refractive indices for λ = 5145 A were calculated from information given in the dispersion table provided by the Bausch and Lomb Company, and from compensator readings obtained on the refractometer for each refractive index measurement made at 5890 $\overset{\text{O}}{\text{A}}$.

IV. RESULTS AND DISCUSSION

A. Variation of the Refractive Index with Temperature and Composition

Refractive indices for the DMSO-pyridine solutions were required at each temperature to calculate the velocities of sound. Since the light scattering observations were made using an incident wavelength of 5145 Å, and the refractive index measurements were made employing a wavelength of 5890 Å (the sodium D line), corrections to convert the refractive index data to obtain n_{5145} Å for the DMSO-pyridine mixtures were necessary. Details of the correction procedure are given in Appendix B; only the refractive indices measured at $\lambda = 5890$ Å and calculated for $\lambda = 5145$ Å are reported here.

Preceding the refractive index data is a table of actual and approximate compositions for the DMSO-pyridine solutions (Table 2). The rounded (nominal) values of the mole fraction are used throughout the remainder of this monograph to conserve space. The molecular weights of the two solvents are listed to illustrate their remarkable similarity.

The refractive indices of the DMSO-pyridine solutions at five different temperatures are given in Table 3. Typical graphs of the measured refractive index, n_{5890} $^{\rm O}_{\rm A}$, versus temperature are shown in Figure 6, while data for n_{5890} $^{\rm O}_{\rm A}$ and n_{5145} $^{\rm O}_{\rm A}$ versus temperature for pure DMSO are presented in Figure 7. Graphs of the refractive index versus temperature give rise to no discontinuities in the temperature range 22.0 to 39.0 $^{\rm O}_{\rm C}$, indicating that there are no anomalies in the refractive index behavior of the individual mixtures in this temperature region. The temperature coefficient of the refractive index,

Table 2

Nominal and Measured Compositions for Mixtures of DMSO and Pyridine

mole fraction DMSO (nominal)	mole fraction DMSO (measured)
0.00	0.0000
0.05	0.0495
0.10	0.0993
0.15	0.1506
0.20	0.1983
0.30	0.2997
0.40	0.3995
0.50	0.5005
0.60	0.6002
0.70	0.7001
0.80	0.8004
0.95	0.9453
1.00	1.0000

Molecular weight pyridine = 79.10

Molecular weight DMSO = 78.13

The average standard error in these values is \pm 0.0003.

The DMSO-pyridine mixtures were made up by M. S. Greenberg (72).

Table 3 Refractive Index as a Function of Temperature for λ = 5890 and 5145 Å

T(°C)	n ₅₈₉₀ A	n _{5145A}	T(OC)	n ₅₈₉₀ A	ⁿ 5145A
pı	ure pyridi	ne	0.05 m	ole fracti	on DMSO
22.0	1.5090	1.5164	22.0	1.5073	1.5146
26.4	1.5064	1.5138	26.4	1.5053	1.5126
30.1	1.5046	1.5120	30.1	1.5031	1.5104
30.3	1.5042	1.5116	30.3	1.5028	1.5101
39.0	1.4988	1.5062			
					
0.10 m	ole fracti	on DMSO	0.15 m	ole fracti	on DMSO
22.0	1.5056	1.5128	22.0	1.5052	1.5123
26.4	1.5035	1.5107	26.4	1.5020	1.5091
30.1	1.5017	1.5089	30.1	1.5003	1.5074
30.3	1.5008	1.5080	30.3	1.5000	1.5071
39.0	1.4957	1.5029	39.0	1.4942	1.5013
					
0.20 m	ole fracti	ion DMSO	0.30 m	ole fracti	ion DMSO
22.0	1.5044	1.5113	22.0	1.4979	1.5045
26.4	1.5010	1.5079	26.4	1.4962	1.5028
30.1	1.4993	1.5062	30.1	1.4941	1.5007
30.3	1.4988	1.5057	30.3	1.4950	1.5016
39.0	1.4931	1.5000			
					

The refractive index measurements were a joint effort of M. S. Greenberg and the author.

The average error for n_{5890A}^{O} is \pm 0.0002.

According to the Bausch and Lomb reference manual, values of the refractive index calculated for a wavelength other than 5890\AA are subject to a standard error of \pm 0.0005.

Table 3 (cont.)

T (°C)	ⁿ 5890A	n _{5145A}
0.40 m	ole fracti	on DMSO
22.0	1.4962	1.5025
26.4	1.4942	1.5005
30.1	1.4923	1.4986
30.3	1.4925	1.4988
0.60 m	ole fracti	on DMSO
22.0	1.4915	1.4973
26.4	1.4894	1.4952
30.1	1.4877	1.4935
30.3	1.4877	1.4935
39.0	1.4827	1.4885
0.80 m	ole fracti	on DMSO
22.0	1.4852	1.4909
26.4	1.4831	1.4888
30.1	1.4809	1.4866
	pure DMSO	
22.0	1.4784	1.4836
26.4	1.4763	1.4815
30.1	1.4748	1.4800
30.3	1.4748	1.4800
39.0	1.4709	1.4761

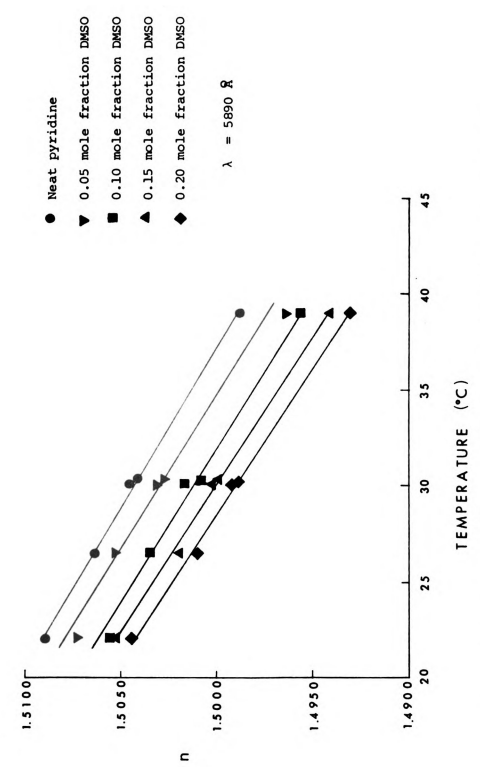


Figure 6. Refractive index versus temperature for mixtures of DMSO and pyridine.

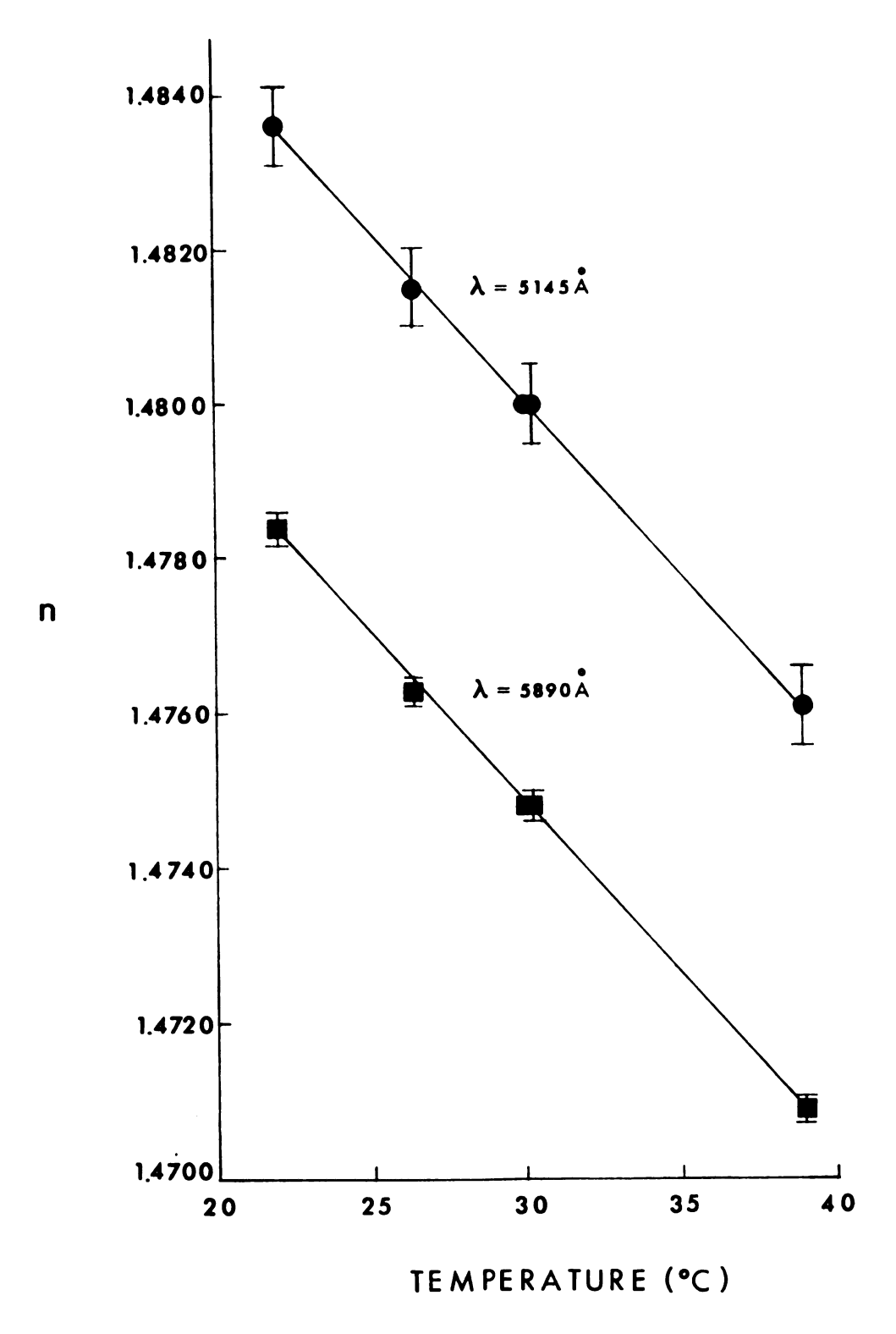


Figure 7. Refractive index versus temperature for neat DMSO.

dn/dT, does, however, exhibit some rather interesting discontinuities when plotted as a function of composition (Figure 8). The behavior of dn/dT with composition is probably a reflection of the change in dipole moment and dielectric constant of the aggregated species as the degree of association changes from one solution to the next. The break in the dn/dT curve between 0.20 and 0.30 mole fraction DMSO is particularly striking.

Variation of the refractive index with composition is illustrated in Figures 9 and 10. As can be seen from the graphs, the refractive index is a linear function of composition for the DMSO-pyridine mixtures.

B. Molar Refractivity at 22.0 °C

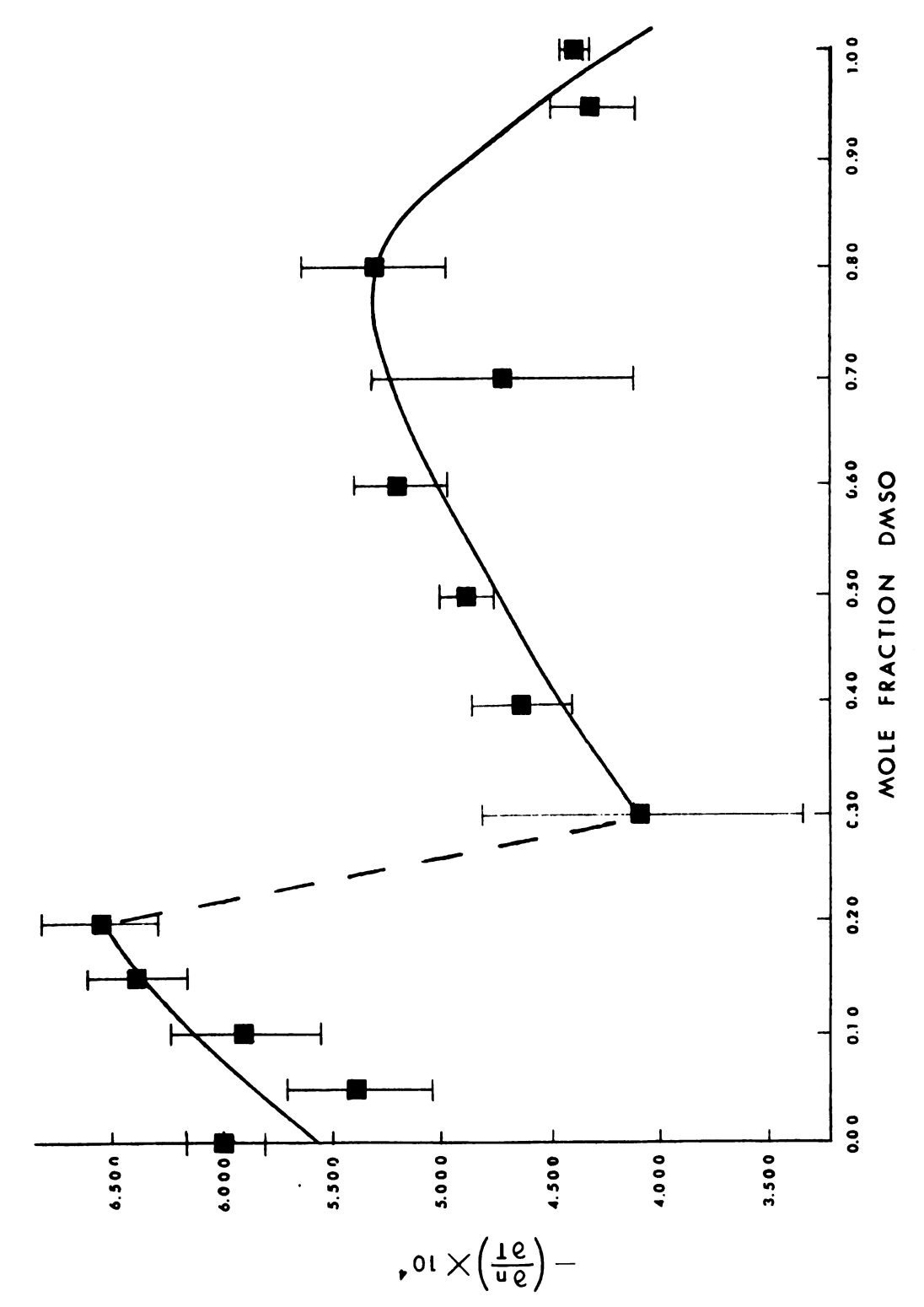
Another optical property which was evaluated for mixtures of DMSO and pyridine is the molar refractivity, A.

The molar refractivity of a pure fluid is given by

$$A = \frac{MW}{\rho} \left(\frac{n^2 - 1}{n^2 + 2} \right) , \qquad (101)$$

where MW is the molecular weight, ρ is the density and n is the refractive index of the fluid. One method of obtaining the molar refractivity of a binary mixture is to treat the mixture as an ordinary pure fluid and use MW, ρ and n values for the mixture in the equation above. The molar refractivity, A_{MIX} , calculated in this manner for the DMSO-pyridine solutions at 22.0 °C is given in Table 4. The densities given in this table were determined experimentally by

Large changes in the dipole moment and dielectric constant with composition have been recorded for binary mixtures of dimethyl sulfoxide and benzene (Ref. 10).



Variation of the temperature derivative of the refractive index with composition for mixtures of DMSO and pyridine. Figure 8.

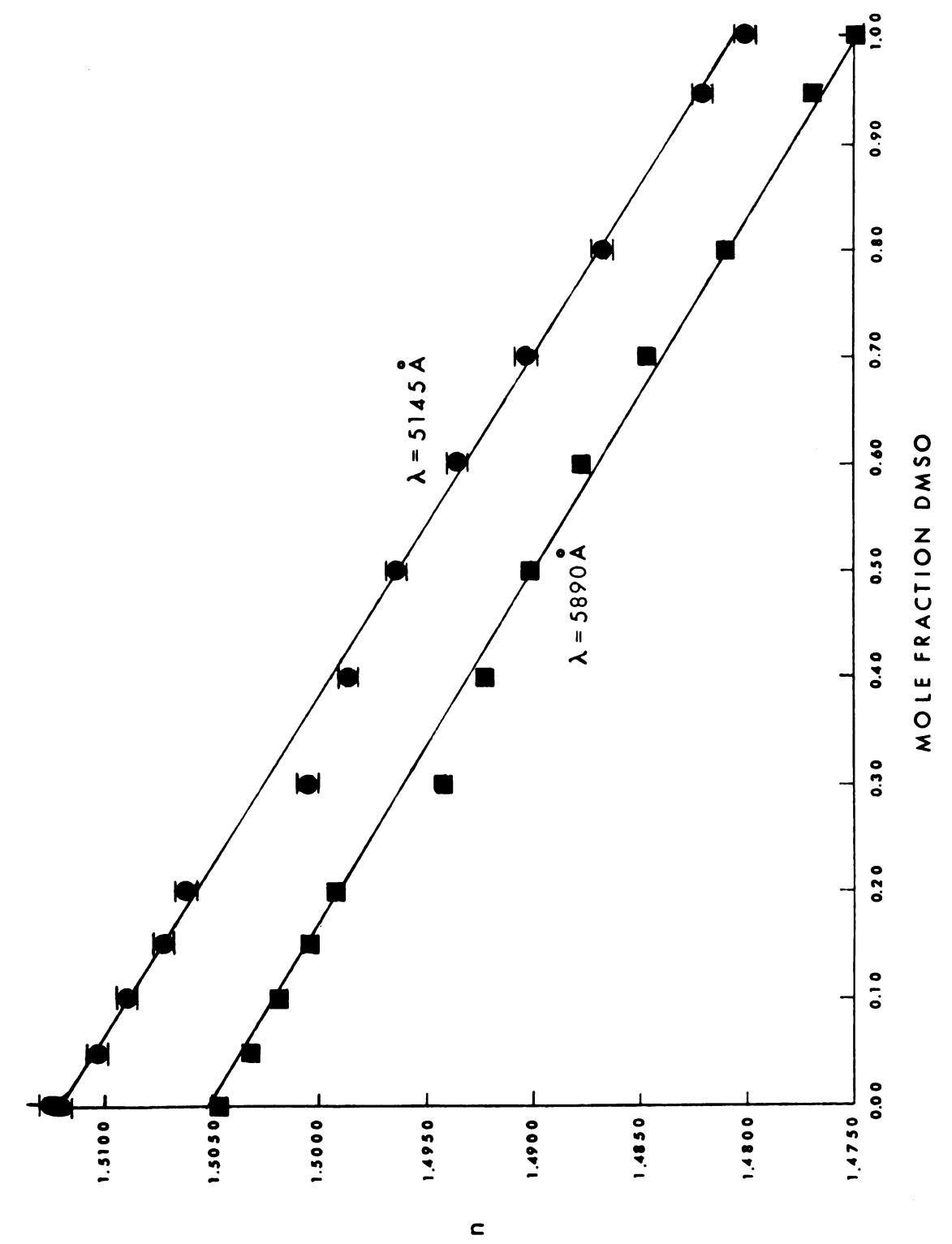


Figure 9. Refractive index versus composition for 30.1 °C.

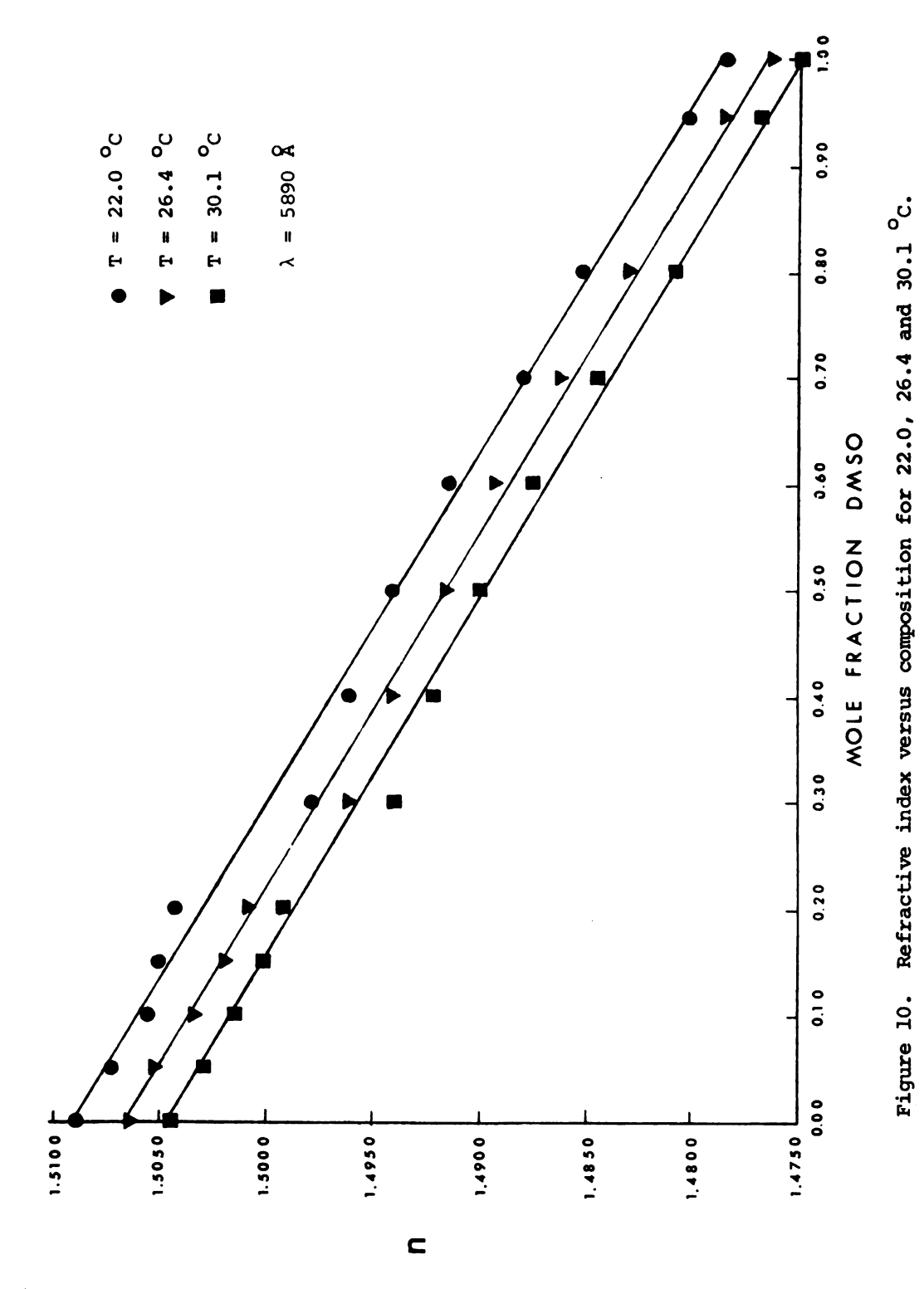


Table 4 $$\operatorname{\mathtt{Molar}}$ Refractivities for Mixtures of DMSO and Pyridine at 22.0 $^{\mathrm{O}}\mathrm{C}$

mole frac. DMSO, X _{DMSO}	MW'(g/mole)	ρ(g/ml)	n _D '	A _{mix} (ml/mole)	A'(ml/mole)
1.000	78.13	1.0936	1.4784	20.24	20.24
0.9453	78.18	1.0876	1.4802	20.43	20.46
0.8004	78.32	1.0678	1.4852	21.03	21.03
0.7001	78.42	1.0571	1.4880	21.37	21.43
0.6002	78.52	1.0448	1.4915	21.78	21.82
0.5005	78.62	1.0323	1.4942	22.18	22.22
0.3995	78.71	1.0203	1.4962	22.54	22.61
0.2997	78.81	1.0095	1.4979	22.88	23.01
0.1983	78.91	1.0003	1.5044	23.37	23.41
0.1506	78.96	0.9933	1.5052	23.58	23.61
0.0993	79. 00	0.9886	1.5056	23.73	23.80
0.0495	79.05	0.9829	1.5073	23.95	24.00
0.0000	79.10	0.9760	1.5090	24.20	24.20

M. S. Greenberg (72). In Figure 11 the density is seen to be a linear function of composition.

The molar refractivity, A', for a binary mixture of polar fluids has been defined on page 46 as

$$A' = X_1 A_1' + X_2 A_2',$$
 (106)

where A_1 and A_2 are the molar refractivities of the pure polar species 1 and 2, respectively. The molar refractivities for the DMSO-pyridine mixtures calculated from equation (106) are listed in Table 4 for comparison. The agreement between the molar refractivities calculated by the two methods is excellent, with the exception of the values for the 0.30 mole fraction DMSO mixture. The value of $A_{\rm MIX}$ for this solution is much lower than the value of A, so that one cannot ignore the possibility of having water present in excess of 0.33 mole per cent. An accurate theoretical analysis reveals that the presence of water in even a slightly greater amount (~ 0.50 mole %) could account for the observed difference between $A_{\rm MIX}$ and A.

A plot of A_{MIX} versus composition at 22.0 ^OC is shown in Figure 12. The linearity of the graph is proof of the overall credibility of the refractive index and density measurements for the DMSO-pyridine mixtures.

C. Variation of the Brillouin Shift with Temperature and Composition

The interaction of an incident beam of light with a thermal pressure wave (sound wave) in a liquid gives rise to a three-peaked intensity-frequency distribution known as a Brillouin spectrum. The two side peaks are symmetrically displaced about the central Rayleigh peak and are Doppler shifted from the central peak by an amount $v_{\rm B}$,

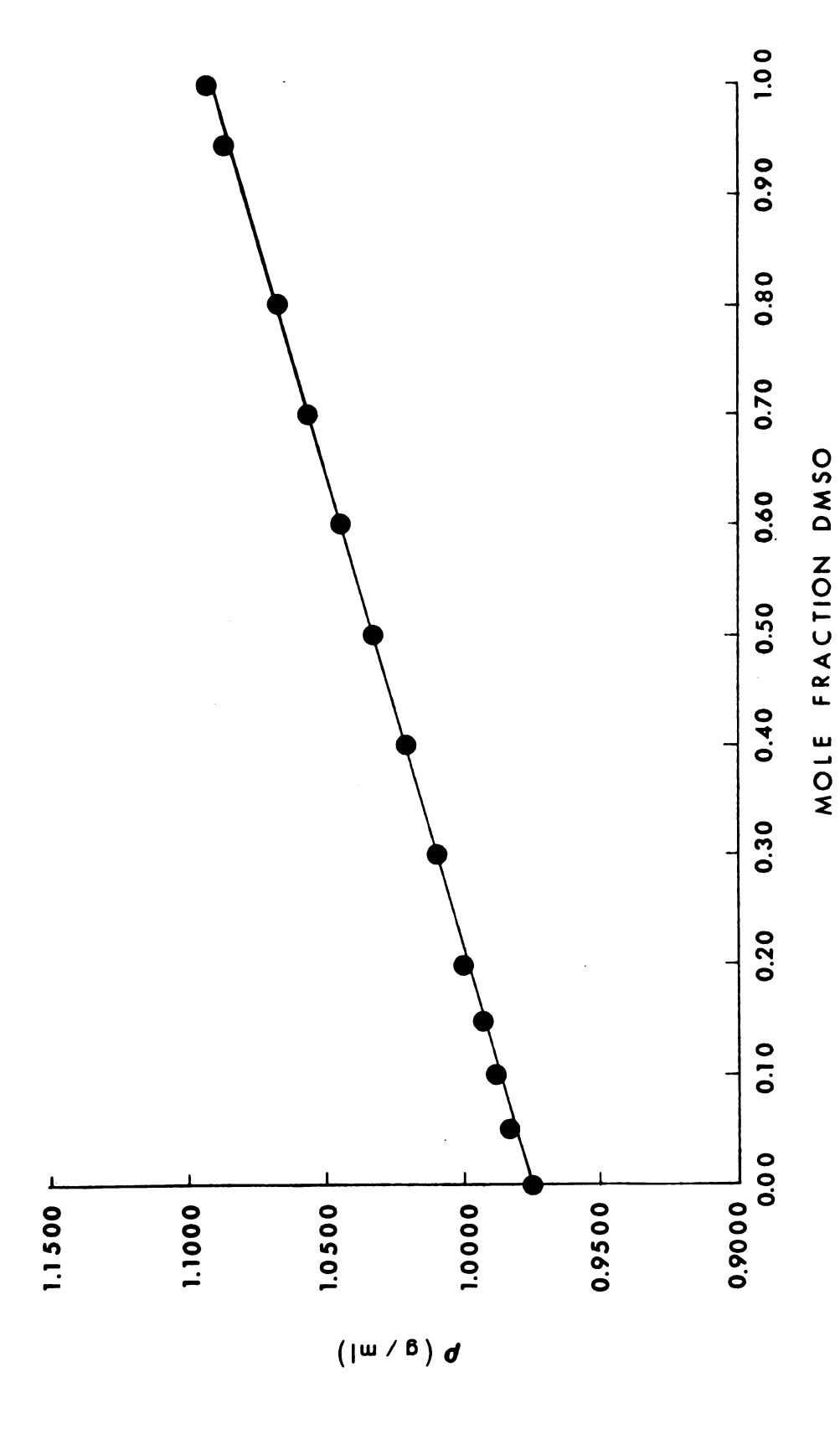


Figure 11. Variation of the density with composition for 22.0 $^{\rm O}{\rm C}.$

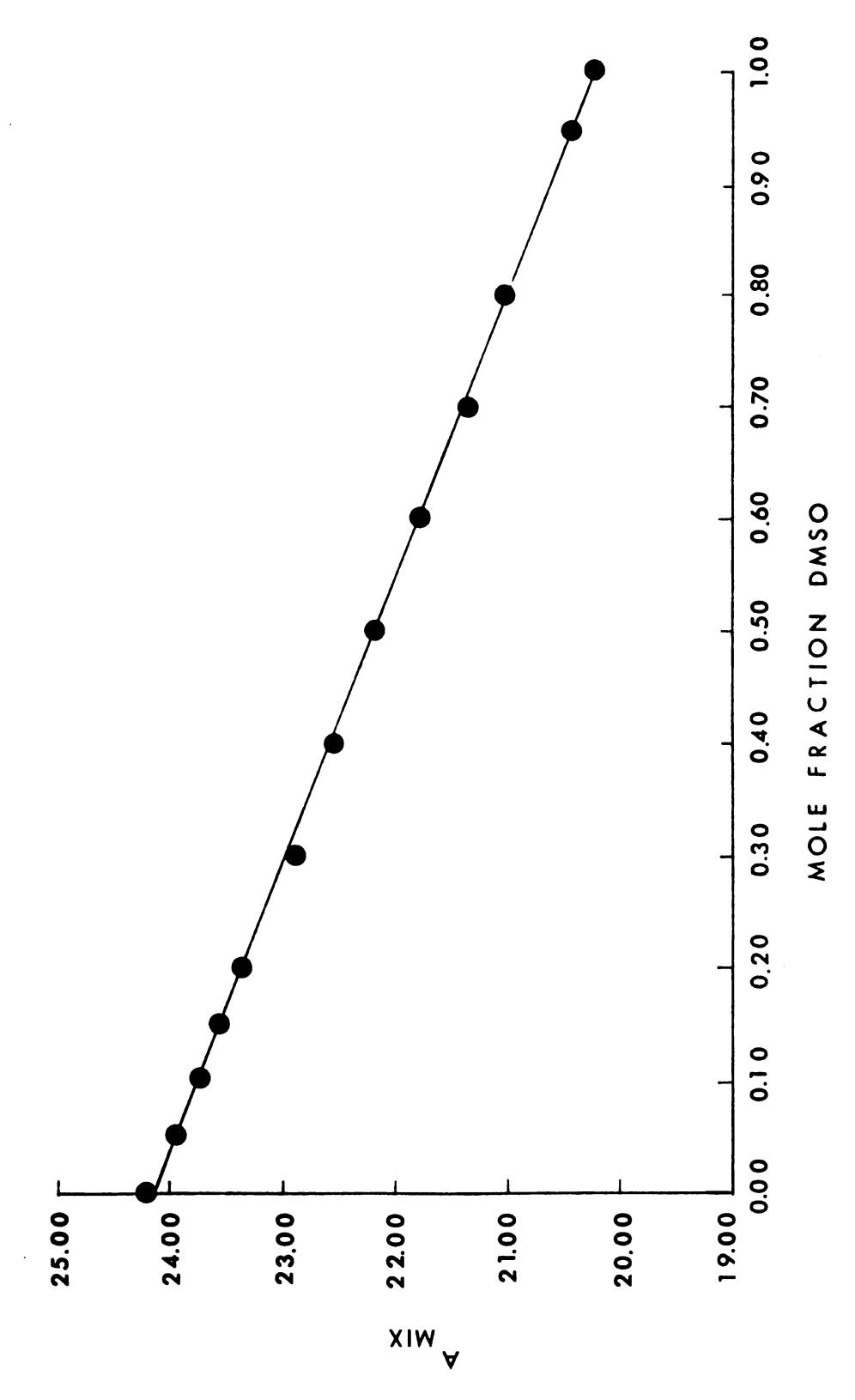


Figure 12. Molar refractivity versus composition at 22.0 $^{\rm O}_{\rm C}$.

the Brillouin shift. This displacement in frequency is defined by

$$v_{\rm B} = \pm \frac{2v_{\rm o}nV_{\rm s}}{c} \sin \theta/2 , \qquad (107)$$

 v_0 being the incident frequency, n, the refractive index, V_s , the velocity of sound, c, the velocity of light in vacuo and θ , the scattering angle. In terms of an actual light scattering experiment, v_B is the frequency and V_s the velocity, of the phonon (sound wave) in the liquid.

Measurement of the Brillouin shift from an experimental spectrum is shown in Figure 13; ν_B is the frequency interval, in gigaherz (GHz), between the central peak and a Brillouin side peak. As can be seen from the spectra in Figures 14-16, the Brillouin shift varies with both temperature and composition.

Values of the Brillouin shift for mixtures of DMSO and pyridine are presented in Table 5 as a function of temperature. Typical graphs of Brillouin shift with temperature are shown in Figures 17 and 18.

The Brillouin shift is a linear function of temperature for a given composition. This type of linear relationship has also been noted for pure liquids (49, 74-76). The individual DMSO-pyridine mixtures appear to be behaving as pure fluids with respect to the temperature dependence of the Brillouin shift.

An interesting comparison is given in Table 6, which contains values for the slope and intercept of the Brillouin shift-temperature curves. It can be seen immediately that the slope and intercept both change irregularly from one solution to another. Graphical illustrations of this behavior are presented in Figures 19 and 20. These graphs seem to indicate that although the alteration of the Brillouin shift with temperature for an individual mixture is analogous to that for

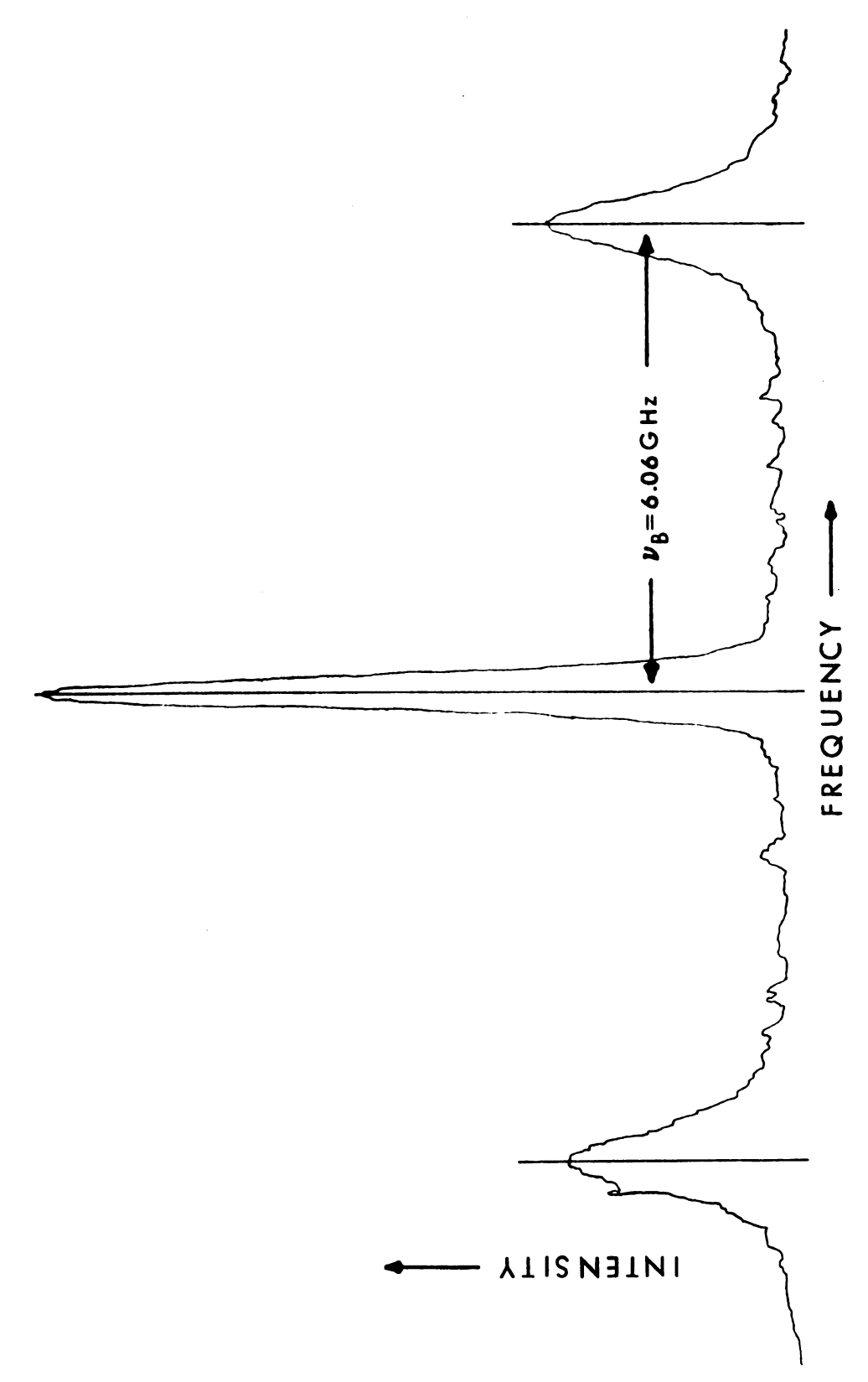


Figure 13. Brillouin spectrum for 0.15 mole fraction DMSO at 34.5 °C.

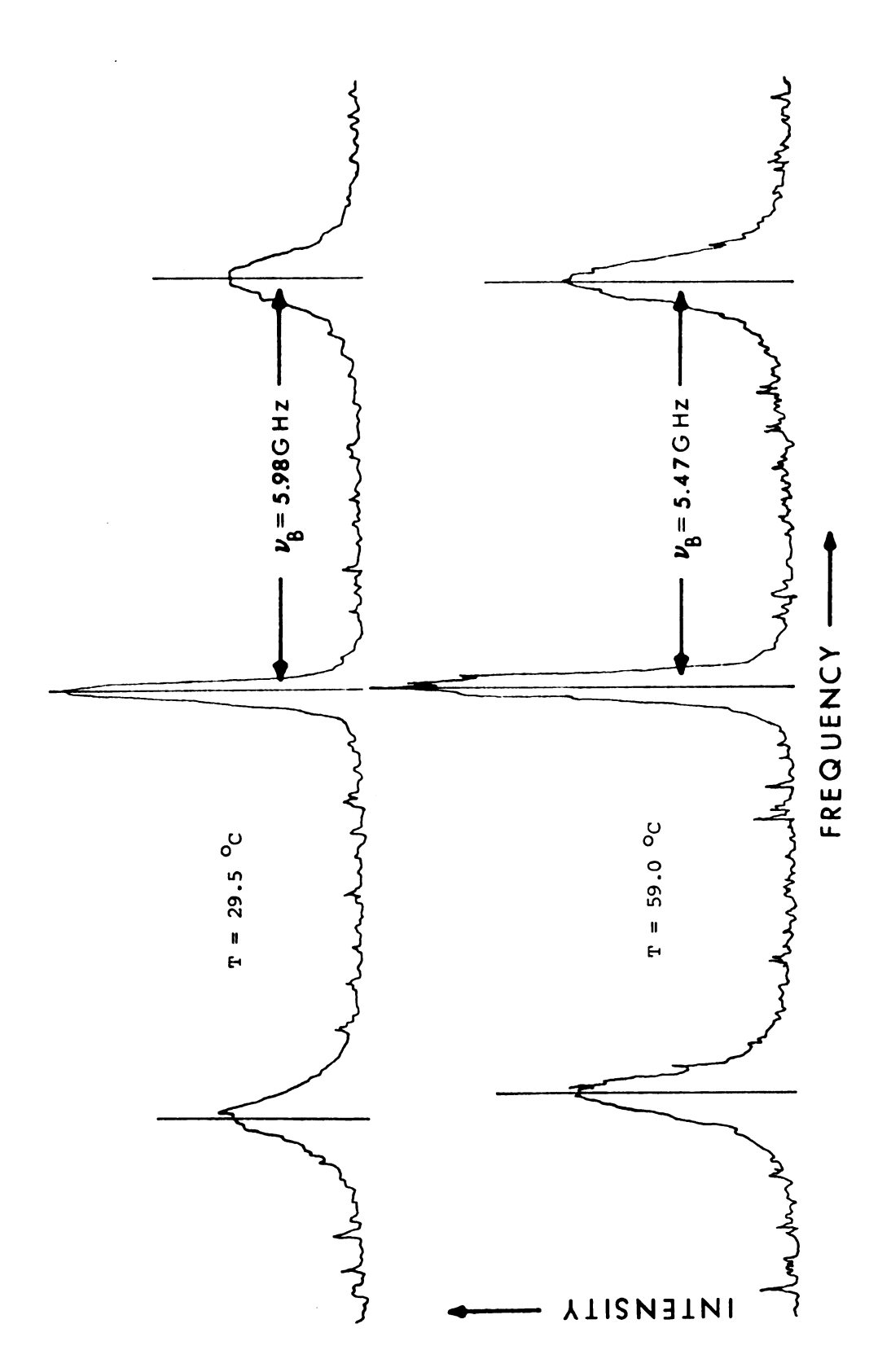


Figure 14. Brillouin spectra for neat DMSO at 29.5 and 59.0 °C.

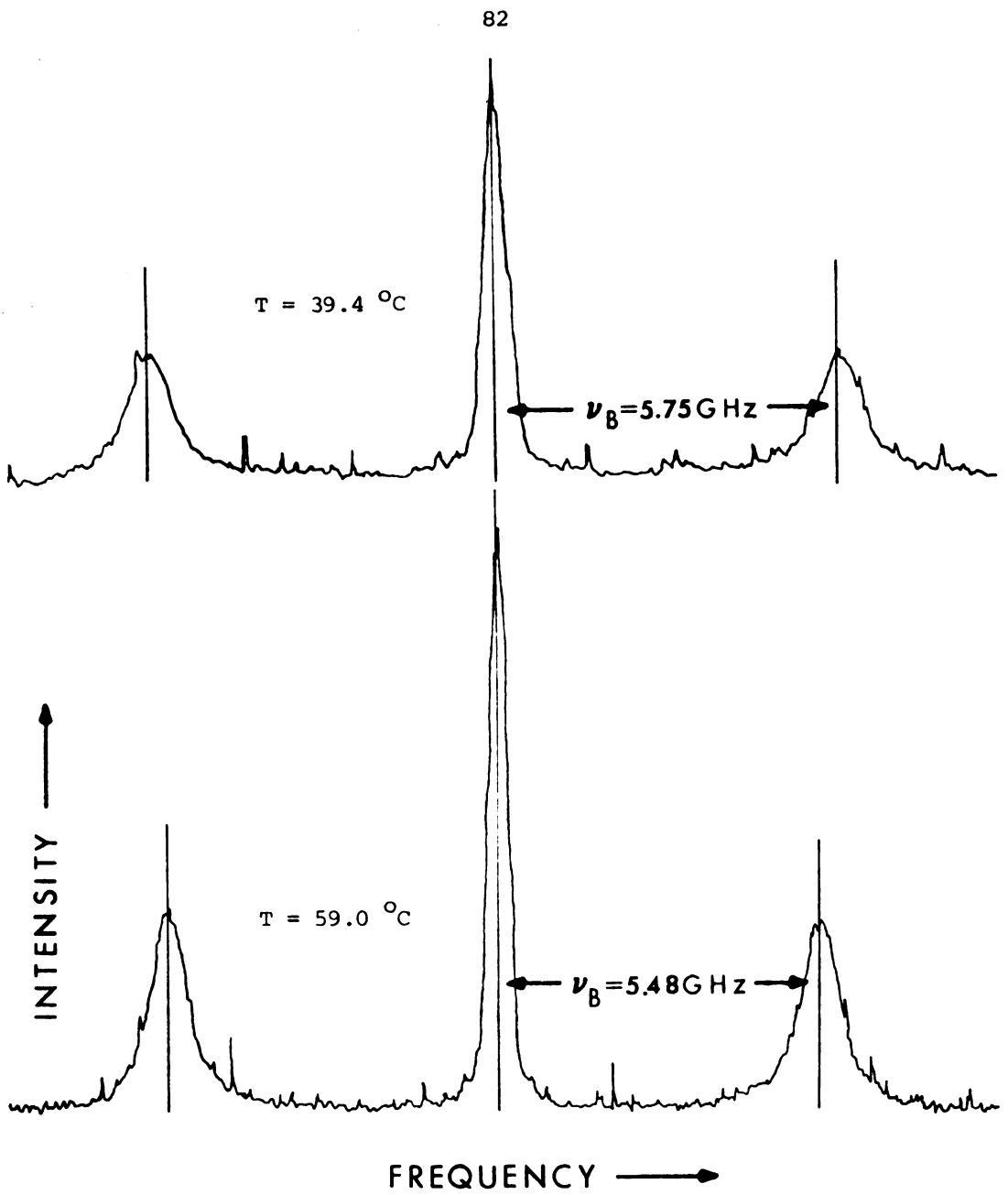


Figure 15. Brillouin spectra for 0.60 mole fraction DMSO at 39.4 and 59.0 °C.

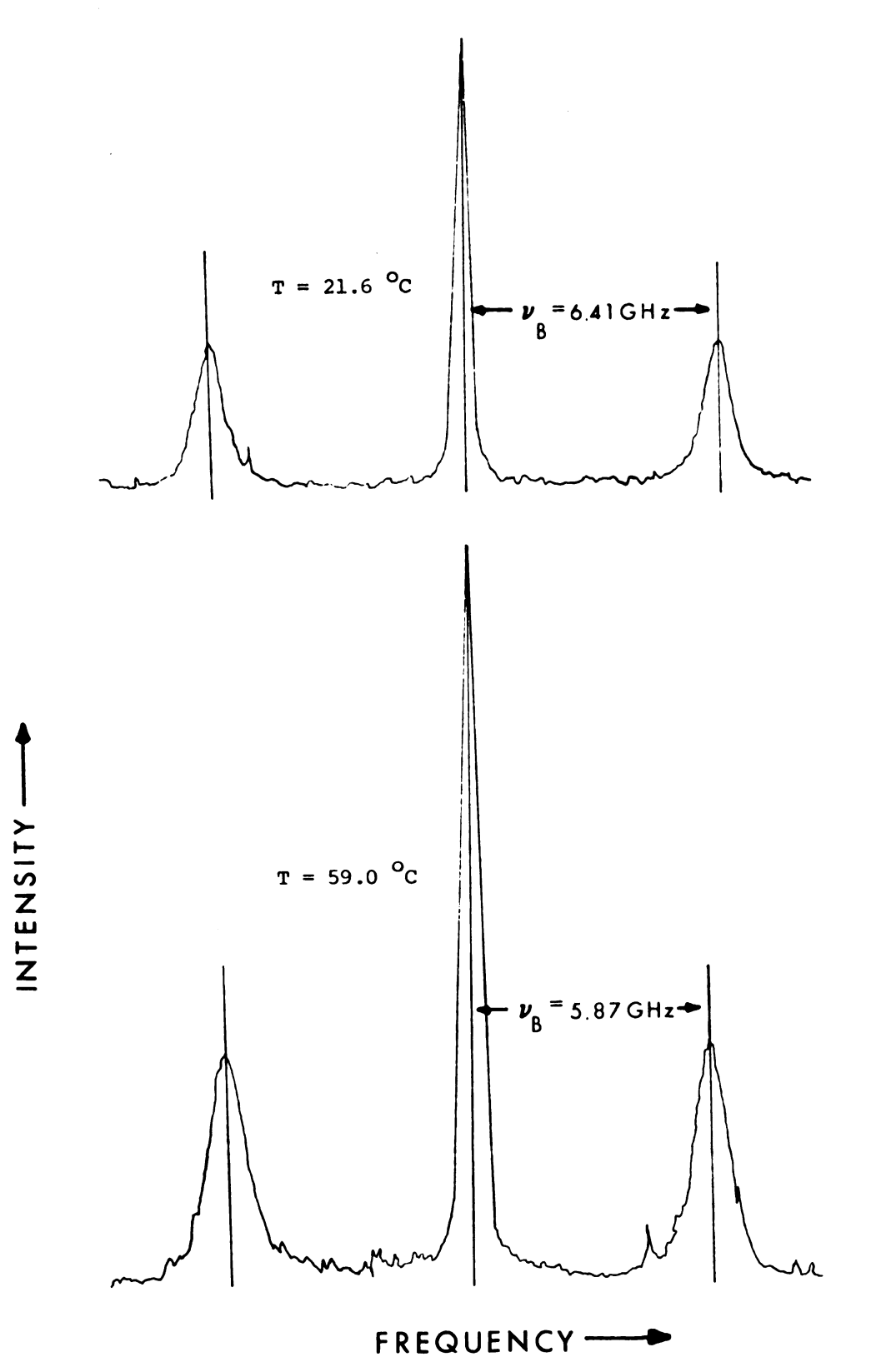


Figure 16. Brillouin spectra for neat pyridine at 21.6 and 59.0 $^{\circ}\text{C}.$

Table 5

Brillouin Shift as a Function of Temperature

T(°C)	ν _B (GHz)	T(OC)	v _B (GHz)	T(°C)	ν _B (GHz)	T(OC)	ν _B (GHz)
pure p	yridine	0.05 m	.f. DMSO	0.10 m	.f. DMSO	0.15 m	.f. DMSO
21.6	6.39	21.6	6.29	21.6	6.27	21.6	6.28
29.5	6.27	29.5	6.17	29.5	6.12	29.5	6.14
34.5	6.19	34.5	6.08	34.5	6.02	34.5	6.05
39.4	6.11	39.4	6.01	39.4	5.92	39.4	5.97
44.5	6.03	44.5	5.92	44.5	5.82	44.5	5.88
49.3	5.95	49.3	5.85	49.3	5.73	49.3	5.80
54.2	5.87	54.2	5.77	54.2	5.63	54.2	5.71
59.0	5 .7 9	59.0	5.69	59.0	5.54	59.0	5.63
							
0.20 m	.f. DMSO	0.30 m	.f. DMSO	0.40 m	.f. DMSO	0.50 m	.f. DMSO
	6.17		6.22		6.11	0.50 m	
21.6		21.6			6.11		
21.6	6.17	21.6	6.22	21.6	6.11 5.99	21.6	6.02
21.6 29.5 34.5	6.17	21.6	6.22	21.6	6.11 5.99 5.90	21.6	6.02 5.90 5.82
21.6 29.5 34.5	6.17 6.05 5.97	21.6 29.5 34.5	6.22 6.08 5.98	21.6 29.5 34.5	6.11 5.99 5.90 5.82	21.6 29.5 34.5	6.02 5.90 5.82 5.75
21.6 29.5 34.5 39.4	6.17 6.05 5.97 5.89	21.6 29.5 34.5 39.4	6.22 6.08 5.98 5.89	21.6 29.5 34.5 39.4	6.11 5.99 5.90 5.82	21.6 29.5 34.5 39.4	6.02 5.90 5.82 5.75
21.6 29.5 34.5 39.4 44.5	6.17 6.05 5.97 5.89 5.81	21.6 29.5 34.5 39.4 44.5	6.22 6.08 5.98 5.89 5.79	21.6 29.5 34.5 39.4 44.5	6.11 5.99 5.90 5.82 5.73	21.6 29.5 34.5 39.4 44.5	6.02 5.90 5.82 5.75 5.67
21.6 29.5 34.5 39.4 44.5 49.3 54.2	6.17 6.05 5.97 5.89 5.81 5.74	21.6 29.5 34.5 39.4 44.5 49.3 54.2	6.22 6.08 5.98 5.89 5.79 5.70	21.6 29.5 34.5 39.4 44.5 49.3	6.11 5.99 5.90 5.82 5.73 5.65 5.57	21.6 29.5 34.5 39.4 44.5 49.3	6.02 5.90 5.82 5.75 5.67 5.59

Table 5 (cont.)

T(°C)	ν _B (GHz)	T(OC)	VB (GHZ)	T(°C)	ν _B (GHz)	T(°C)	ν _B (GHz)
0.60 m	.f. DMSO	0.70 m.	f. DMSO	0.80 m.	f. DMSO	0.95 m.	f. DMSO
21.6	6.00	21.6	6.05	21.6	6.04	21.6	6.13
29.5	5.91	29.5	5.92	29.5	5. 95	29.5	6.00
34.5	5.84	34.5	5.83	34.5	5.88	34.5	5.92
39.4	5.78	39.4	5.75	39.4	5.82	39.4	5.83
44.5	5.72	44.5	5.66	44.5	5.75	44.5	5.75
49.3	5.66	49.3	5.57	49.3	5.69	49.3	5.67
54.2	5.60	54.2	5.49	54.2	5.63	54.2	5,59
59.0	5.54	59.0	5.41	59.0	5.57	59.0	5.51
pure	DMSO						

pure	DMSO
21.6	6.11
29.5	5.99
34.5	5.91
39.4	5.84
44.5	5.75
49.3	5.68
54.2	5.60
59.0	5.53

Average standard deviation for T is $\sigma_{\rm T}$ = ± 0.1 $^{\rm O}\text{C}\text{.}$

Average standard deviation for ν_B is σ_{ν} = ± 0.05 GHz.

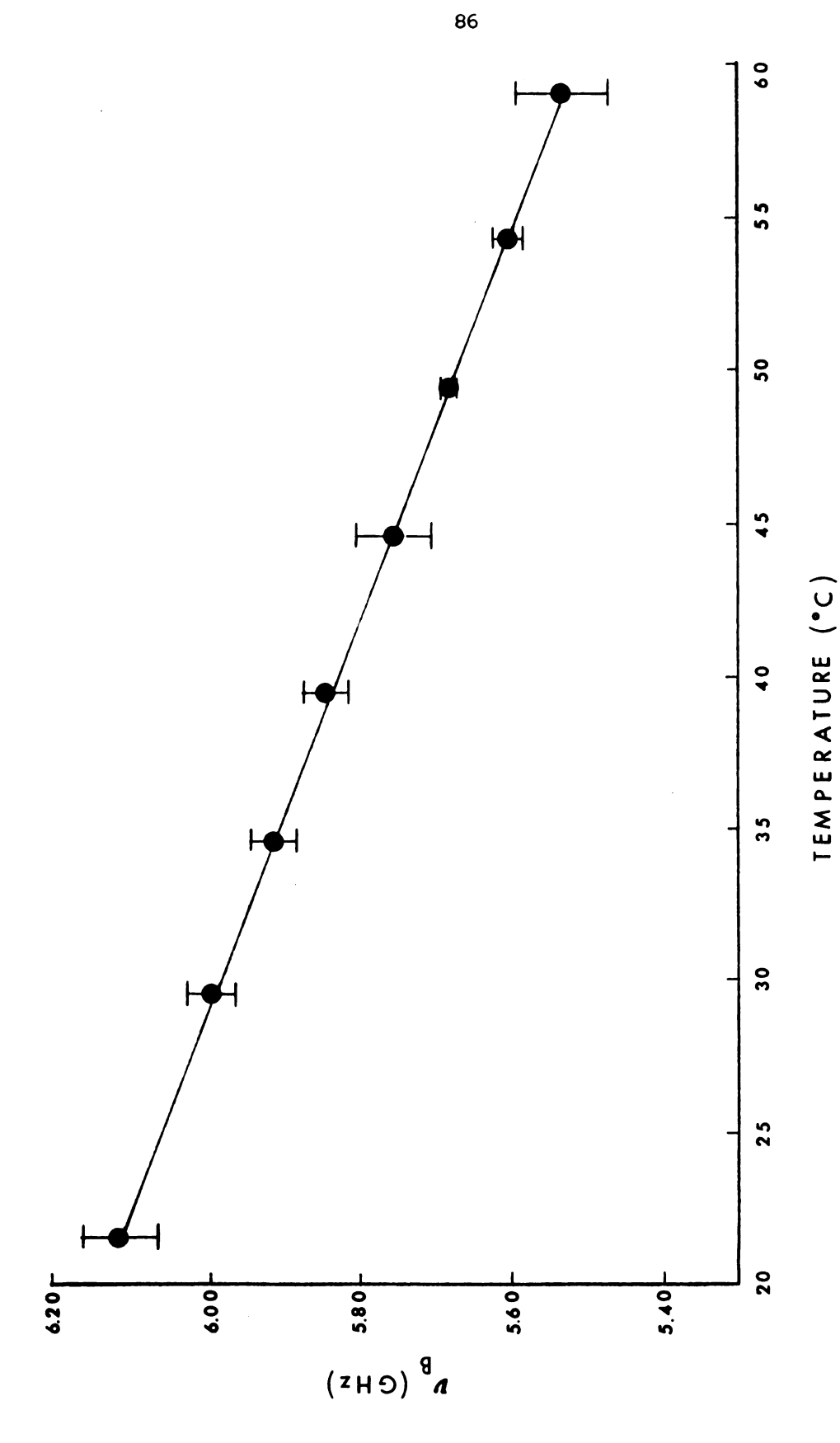
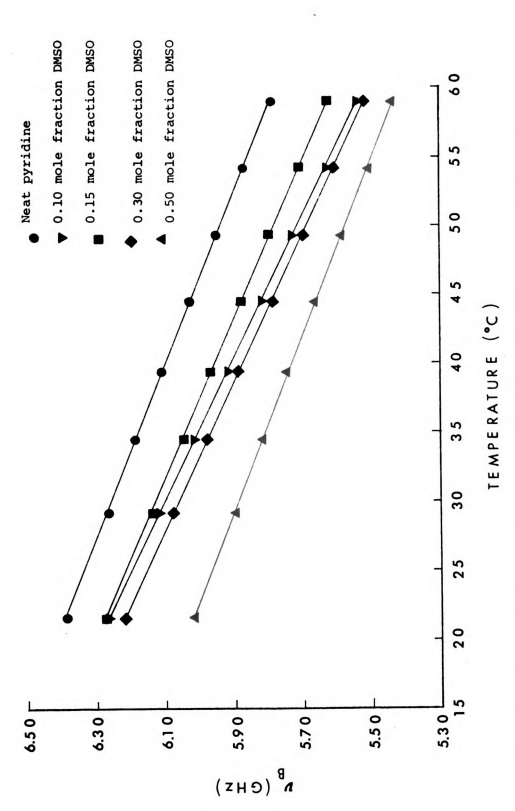


Figure 17. Brillouin shift versus temperature for neat DMSO.



Brillouin shift versus temperature for neat pyridine, 0.10, 0.15, 0.30 and 0.50 mole fraction DMSO. Figure 18.

Table 6 Intercept and Slope for the Brillouin Shift-Temperature Relationship ν_B = A + BT

mole fraction DMSO	A (GHz)	σ _A	-B (GHz/ ^O C)	σ _B
0.0000	6.74	±0.06	0.0160	±0.0014
0.0495	6.63	0.05	0.0159	0.0013
0.0993	6.70	0.09	0.0197	0.0024
0.1506	6.65	0.02	0.0174	0.0005
0.1983	6.50	0.03	0.0155	0.0006
0.2997	6.62	0.04	0.0186	0.0011
0.3995	6.47	0.03	0.0166	0.0008
0.5005	6.3 6	0.06	0.0156	0.0014
0.6002	6.27	0.02	0.0124	0.0005
0.7001	6.42	0.05	0.0172	0.0010
0.8004	6.31	0.14	0.0126	0.0030
0.9453	6.49	0.09	0.0166	0.0021
1.0000	6.45	0.05	0.0157	0.0011

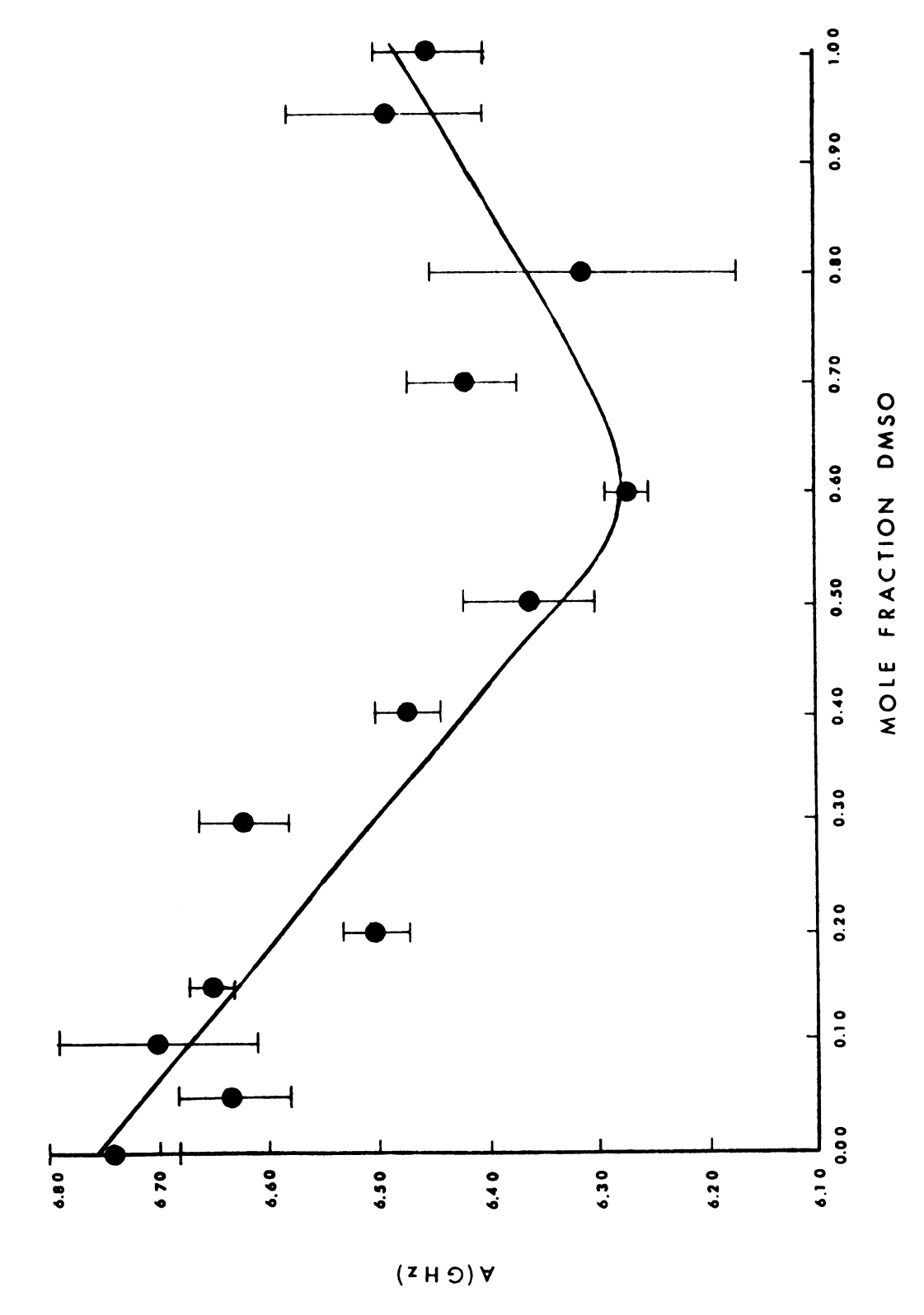


Figure 19. Variation of the intercept of $v_B = A + BT$ with composition for mixtures of DMSO and pyridine.

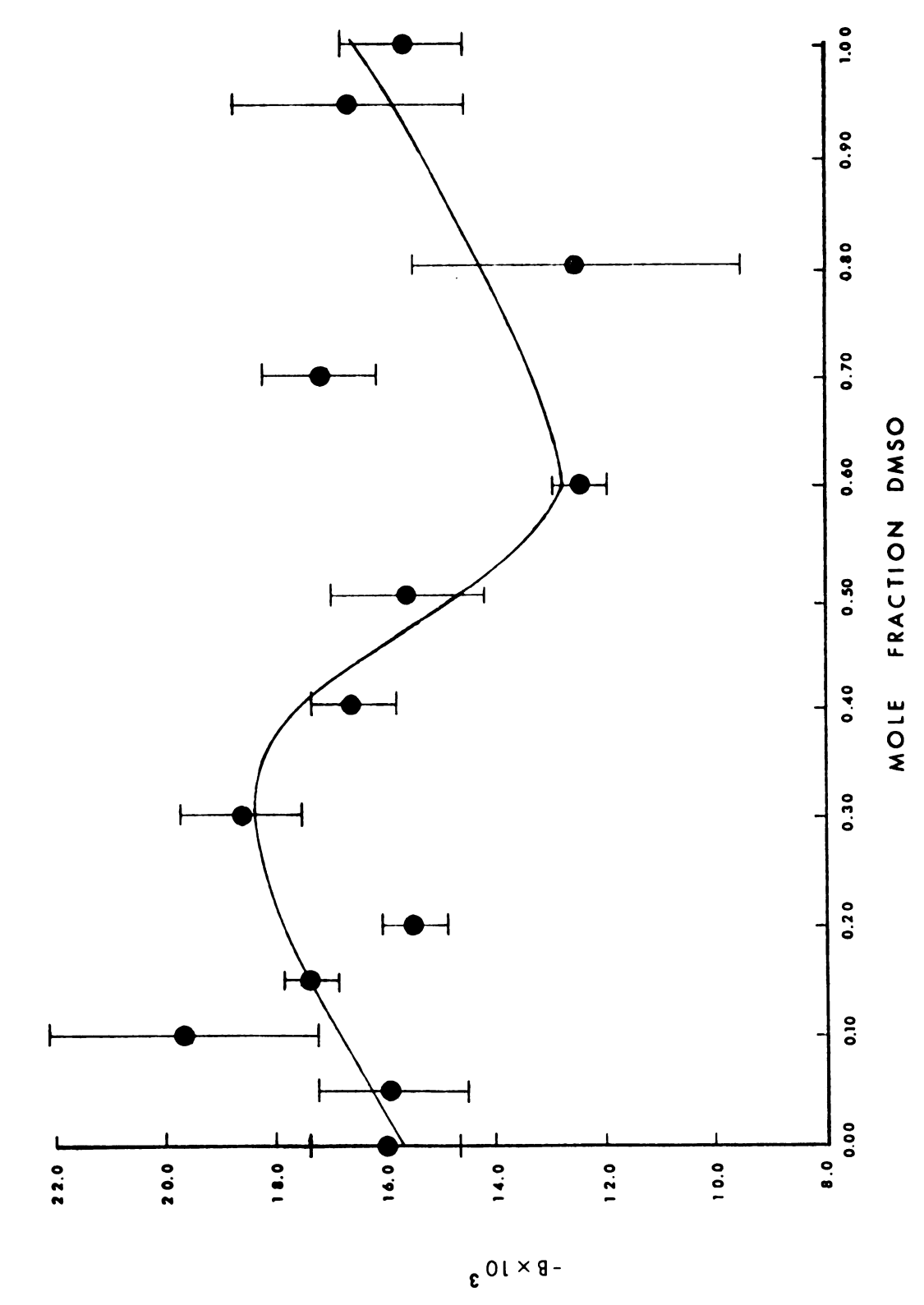


Figure 20. Variation of the slope of $v_B = A + BT$ with composition for mixtures of DMSO and pyridine.

a pure fluid, the physicochemical properties of the mixture which $\mbox{affect } \nu_{\rm B} \mbox{ differ significantly from one solution to another. }$

The variation of the Brillouin shift with composition at a specific temperature proves to be an interesting non-linear relationship, as illustrated in Figures 21-23. One might expect, a priori, that the change in Brillouin shift with composition at a given temperature for an ideal mixture of two pure fluids would be a smooth, continuous function. Below 40 $^{\circ}$ C, the curves seem to conform reasonably well to this expectation. However, as the temperature is raised above 40 $^{\circ}$ C, there appears to be considerable aberration from continuity, especially in the region between 0.50 and 1.00 mole fraction DMSO. Experimental error prevents our interpretation of the seemingly progressive discontinuity in $v_{\rm B}$ between 0.10 and 0.15 mole fraction DMSO; however the discontinuities in $v_{\rm B}$ between 0.50 and 1.00 mole fraction DMSO at 54.2 and 59.0 $^{\circ}$ C are well outside the limits of experimental error and can be looked upon as indications of changes in local structure in the liquid.

D. Velocity of Sound and Related Quantities

Just as ultrasonic data (50, 51, 77-81) have been used to monitor changes in the structure of liquids with changes in temperature, pressure and composition, hypersonic data obtained from Brillouin scattering experiments can be employed to obtain analogous information in a complementary frequency interval. The velocity of sound varies with the compressibility of the molecules; the compressibility, in turn, depends on liquid structure. The velocity of sound, therefore, is a direct measure of the strength of intermolecular forces, or degree of association, in a liquid.

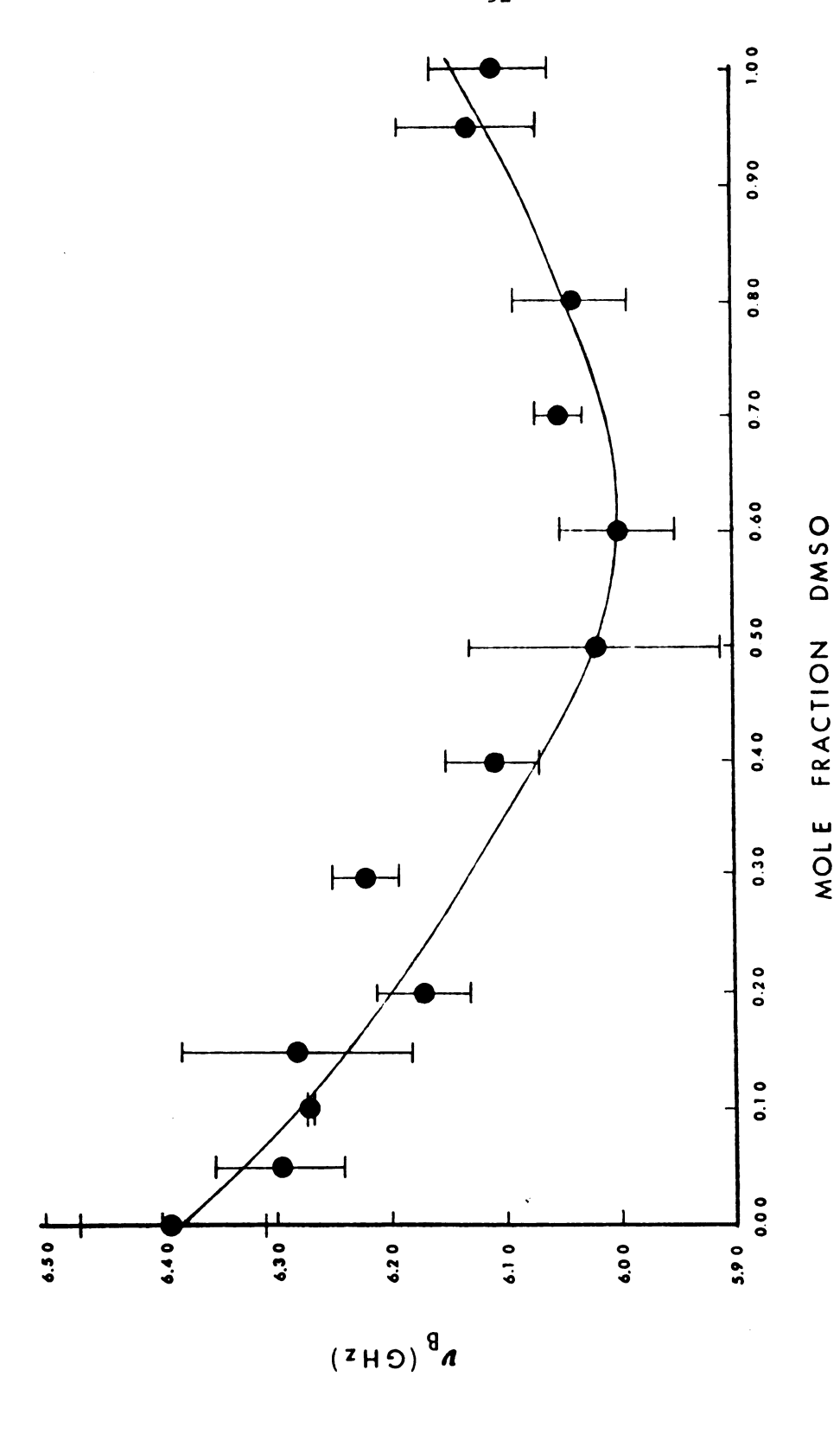


Figure 21. Brillouin shift versus composition at 21.6 °C.

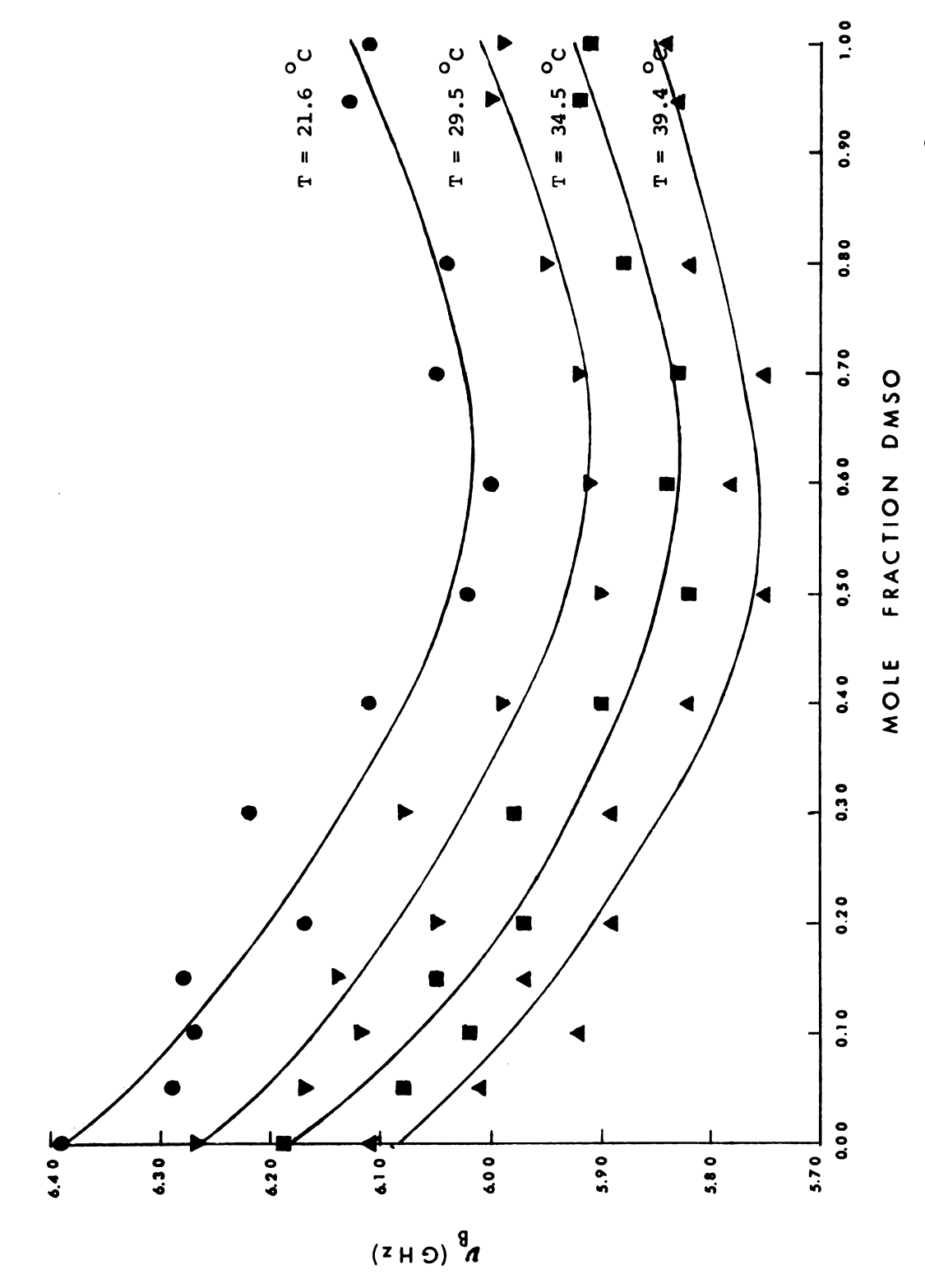


Figure 22. Brillouin shift versus composition for 21.6, 29.5, 34.5 and 39.4 °C.

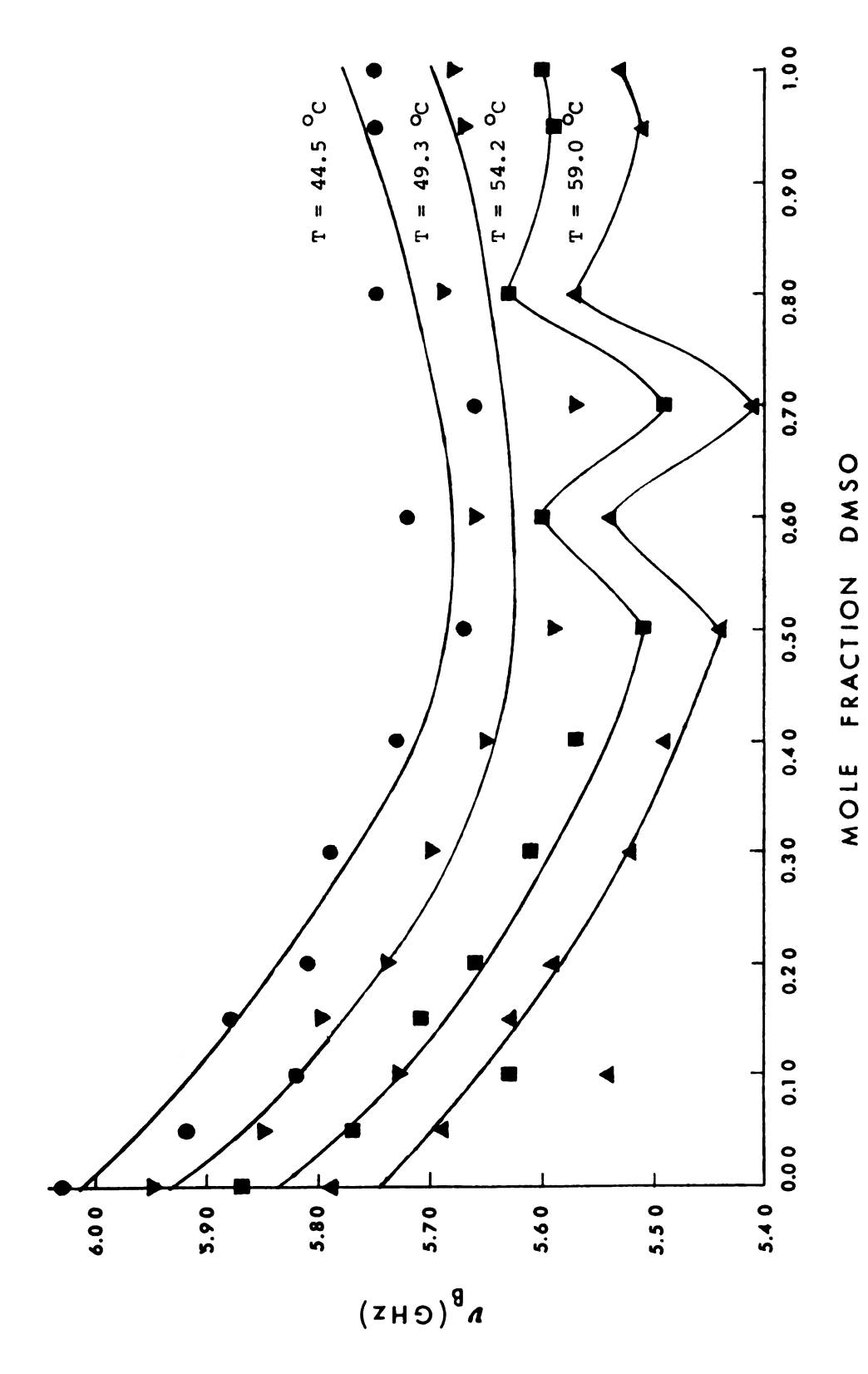


Figure 23. Brillouin shift versus composition for 44.5, 49.3, 54.2 and 59.0 °C.

An advantage of Brillouin scattering over ultrasonic measurements is that no transducer is required; the sound velocities detected are the products of thermal motion in the liquid. Velocity of sound data gathered by light scattering and by ultrasonics for a variety of liquids have been found to be in good agreement (29,49,82). A logical consequence would be to assume that one can use documented ultrasonic findings on mixtures to aid in the interpretation of data obtained from Brillouin scattering measurements. As seen in the remaining portion of this chapter, the author has drawn extensively from ultrasonic research to aid in the interpretation of the data from this study.

If there were no structural changes occurring in proceeding from pure pyridine to pure DMSO, one would expect two phenomena:

- (1) the change in the velocity of sound in proceeding from one pure fluid to the other would be a smooth, continuous function $(81)^{\frac{1}{2}}$
- (2) the change in dV_S/dT with composition would also be a smooth, continuous function.

In Table 7 are displayed the frequency shifts, refractive indices and velocities of sound for the DMSO-pyridine mixtures as a function of temperature. By numerical analysis the sonic velocity-temperature curves for each composition are fit by a linear relationship, $V_s = A + BT$. The parameters A and B obtained for each composition and their standard deviations are exhibited in Table 8. The

From Richardson, p. 178, "If two liquids of different density and elasticity are mixed in various proportions, one would expect the velocity to pass gradually from the value corresponding to one pure fluid to that of the other." This type of behavior has been observed for many liquid mixtures; cf. Ref. 81, pp. 178-181 and Ref. 77.

Table 7

Brillouin Shift and Velocity of Sound as a Function of

Temperature for Mixtures of DMSO and Pyridine

T(OC)	ν _B (GHz)	n _{5145A}	V _s (m/sec)	T(OC)	ν _B (GHz)	n _{5145A}	V _s (m/sec)
	pure	С ₅ н ₅ N			05 mo]	le % DMSO	
21.6	6.39	1.5168	1530	21.6	6.29	1.5149	1510
29.5	6.27	1.5121	1510	29.5	6.17	1.5107	1490
34.5	6.19	1.5091	1490	34.5	6.08	1.5080	1470
39.4	6.11	1.5061	1480	39.4	6.01	1.5053	1450
44.5	6.03	1.5031	1460	44.5	5.92	1.5026	1430
49.3	5.95	1.5002	1440	49.3	5.85	1.5000	1420
54.2	5.87	1.4974	1430	54.2	5 .7 7	1.4974	1400
59.0	5 .7 9	1.4944	1410	59.0	5.69	1.4948	1380
	10 mol	Le % DMSO	-		15 mo	le % DMSO	
21.6	6.27	1.5134	1510	21.6	6.28	1.5125	1510
29.5	6.12	1.5087	1480	29.5	6.14	1.5075	1480
34.5	6.02	1.5058	1460	34.5	6.05	1.5043	1460
39.4	5.92	1.5029	1430	39.4	5.97	1.5012	1450
44.5	5.82	1.5000	1410	44.5	5.88	1.4979	1430
49.3	5.73	1.4971	1390	49.3	5.80	1.4948	1410
54.2	5.63	1.4942	1370	54.2	5.71	1.4917	1390
59.0	5.54	1.4914	1350	59.0	5.63	1.4887	1380

Values for the average standard deviation for each of the entities listed in the table are as follows:

temperature $\sigma_{\rm T} = \pm \ 0.1$ °C refractive index $\sigma_{\rm n} = \pm \ 0.0005$ Brillouin shift $\sigma_{\rm V} = \pm \ 0.05$ GHz velocity of sound $\sigma_{\rm V} = \pm \ 10$ m/sec

Table 7 (cont.)

T(OC)	ν _B (GHz)	n _{5145A}	V _S (m/sec)	T(°C)	ν _B (GHz)	ⁿ 5145A	V _s (m/sec)
	20 mol	e % DMSO			30 mol	e % DMSO	
21.6	6.17	1.5115	1490	21.6	6.22	1.5047	1500
29.5	6.05	1.5063	1460	29.5	6.08	1.5015	1470
34.5	5.97	1.5030	1450	34.5	5.98	1.4994	1450
39.4	5.89	1.4998	1430	39.4	5.89	1.4974	1430
44.5	5.81	1.4965	1410	44.5	5.79	1.4953	1410
49.3	5.74	1.4933	1400	49.3	5.70	1.4934	1390
54.2	5.66	1.4901	1380	54.2	5.61	1.4914	1370
59.0	5.59	1.4870	1370	59.0	5.52	1.4894	1350
	40 mol	e % DMSO			50 mol	e % DMSO	
21.6	6.11	1.5027	1480	21.6	6.02	1.5005	1460
29.5	5.99	1.4990	1450	29.5	5.90	1.4966	1430
34.5	5.90	1.4967	1430	34.5	5.82	1.4942	1420
39.4	5.82	1.4944	1420	39.4	5.75	1.4918	1400
44.5	5.73	1.4921	1400	44.5	5.67	1.4893	1390
49.3	5.65	1.4899	1380	49.3	5.59	1.4869	1370
54.2	5.57	1.4876	1360	54.2	5.51	1.4846	1350
59.0	5.49	1.4854	1340	59.0	5.44	1.4822	1330

Table 7 (cont.)

T(OC)	ν _B (GHz)	n ₅₁₄₅ A	V _s (m/sec)	T(OC)	ν _B (GHz)	o n _{5145A}	V _s (m/sec)
	60 mol	e % DMSO			70 mol	e % DMSO	
21.6	6.00	1.4977	1460	21.6	6.05	1.4940	1470
29.5	5.91	1.4936	1440	29.5	5.92	1.4903	1450
34.5	5.84	1.4910	1430	34.5	5.83	1.4880	1430
39.4	5.78	1.4885	1410	39.4	5.7 5	1.4856	1410
44.5	5.72	1.4859	1400	44.5	5.66	1.4832	1390
49.3	5.66	1.4834	1390	49.3	5.57	1.4810	1370
54.2	5.60	1.4809	1380	54.2	5.49	1.4787	1350
59.0	5.54	1.4784	1360	59.0	5.41	1.4764	1330
	80 mol	e % DMSO			95 mol	e % DMSO	
21.6	6.04	1.4912	1470	21.6	6.13	1.4857	1500
29.5	5.95	1.4870	1460	29.5	6.00	1.4823	1470
34.5	5.88	1.4843	1440	34.5	5.92	1.4802	1460
39.4	5.82	1.4818	1430	39.4	5.83	1.4781	1440
44.5	5.75	1.4791	1410	44.5	5.75	1.4759	1420
49.3	5.69	1.4765	1400	49.3	5.67	1.4738	1400
54.2	5.63	1.4739	1390	54.2	5.59	1.4717	1380
59.0	5 .5 7	1.4714	1380	59.0	5.51	1.4696	1360

Table 7 (cont.)

T(OC)	ν _B (GHz)	n _{5145A}	V _s (m/sec)
	e DMSO		
21.6	6.11	1.4837	1500
29.5	5.99	1.4803	1470
34.5	5.91	1.4781	1460
39.4	5.84	1.4760	1440
44.5	5.75	1.4737	1420
49.3	5.68	1.4716	1400
54.2	5.60	1.4695	1390
59.0	5.53	1.4674	1370
			

Table 8 Intercept and Slope for the Sonic Velocity-Temperature Relationship $V_S = A + BT$

mole fraction DMSO	A (m/sec)	B (m/sec/ ^O C)
0.0000	1603±4	-3.23±0.09
0.0495	1589±4	-3.51±0.09
0.0993	1606±4	-4.36±0.09
0.1506	1585±4	-3.52±0.09
0.1983	1559±4	-3.25±0.09
0.2997	1588±1	-4.02±0.02
0.3995	1560±4	-3.68±0.09
0.5005	1534±5	-3.38±0.12
0.6002	1516±4	-2.60±0.09
0.7001	1560±5	-3.84±0.11
0.8004	1 52 9±5	-2.57±0.12
0.9453	1584±5	-3.74±0.11
1.0000	1575±4	-3.47±0.09

The errors listed are the standard deviations for each value.

quantity B, $|dV_s/dT|$, as a function of composition is shown in Figure 24. The variation in the velocity of sound with composition for each temperature is displayed in Figure 25. Within experimental precision in the measurements, neither the V_s versus X_1 nor $|dV_s/dT|$ versus X_1 curve is a smooth, continuous function over the entire temperature range, indicating that there are structural changes in the mixture as one progresses from pure pyridine to pure DMSO.

According to Kudriavtsev (83), the square of the velocity of sound for an ideal binary solution at a given temperature should vary linearly with composition:

$$(v')^2 = x_A \frac{M_A}{M_{mix}} v_A^2 + x_B \frac{M_B}{M_{mix}} v_B^2$$
 (108)

In equation (108), X_A and X_B are the mole fractions of components A and B, M_A and M_B are the molecular weights of pure A and B, and V_A and V_B are the sonic velocities of the pure species, respectively. M_{mix} is the molecular weight of the mixture. Deviations from this linear relationship occur when association takes place.

Values of $(V')^2$ for mixtures of DMSO and pyridine at 21.6 $^{\circ}C$ are given in Table 9, along with values for the square of the experimentally determined velocity of sound, V_c^2 .

Table 9 Squares of the Ideal and Experimental Velocities of Sound for 21.6 $^{
m o}{
m C}$

mole fraction DMSO, X _{DMSO}	Ideal $(v')^2 x 10^{-6}$ (m^2/sec^2)	Experimental $V_s^2 \times 10^{-6}$ (m^2/sec^2)	
0.0000	2.341	2.34	
0.0495	2.338	2.28	
0.0993	2.332	2.28	
0.1506	2.326	2.28	
0.1983	2.323	2.22	

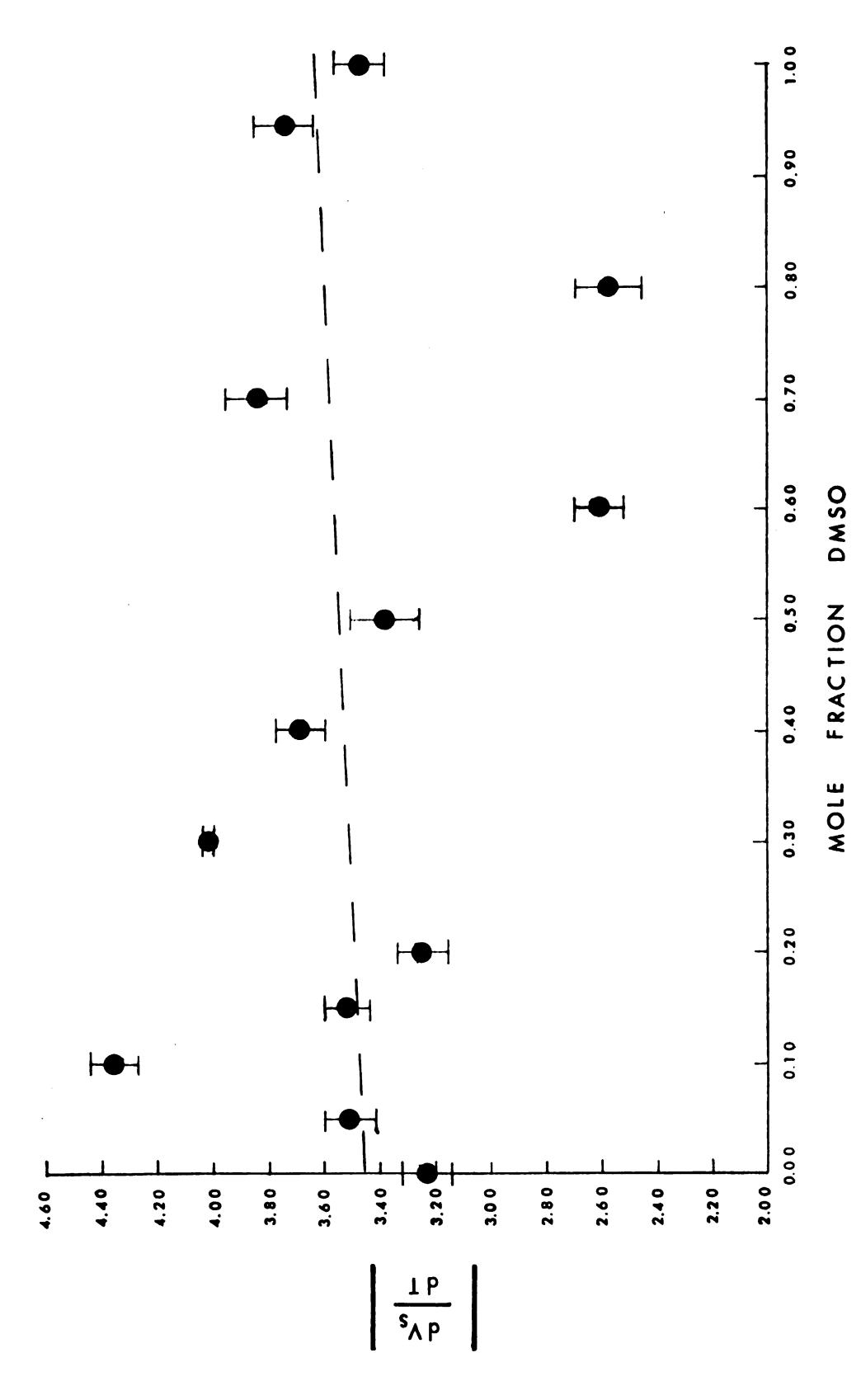
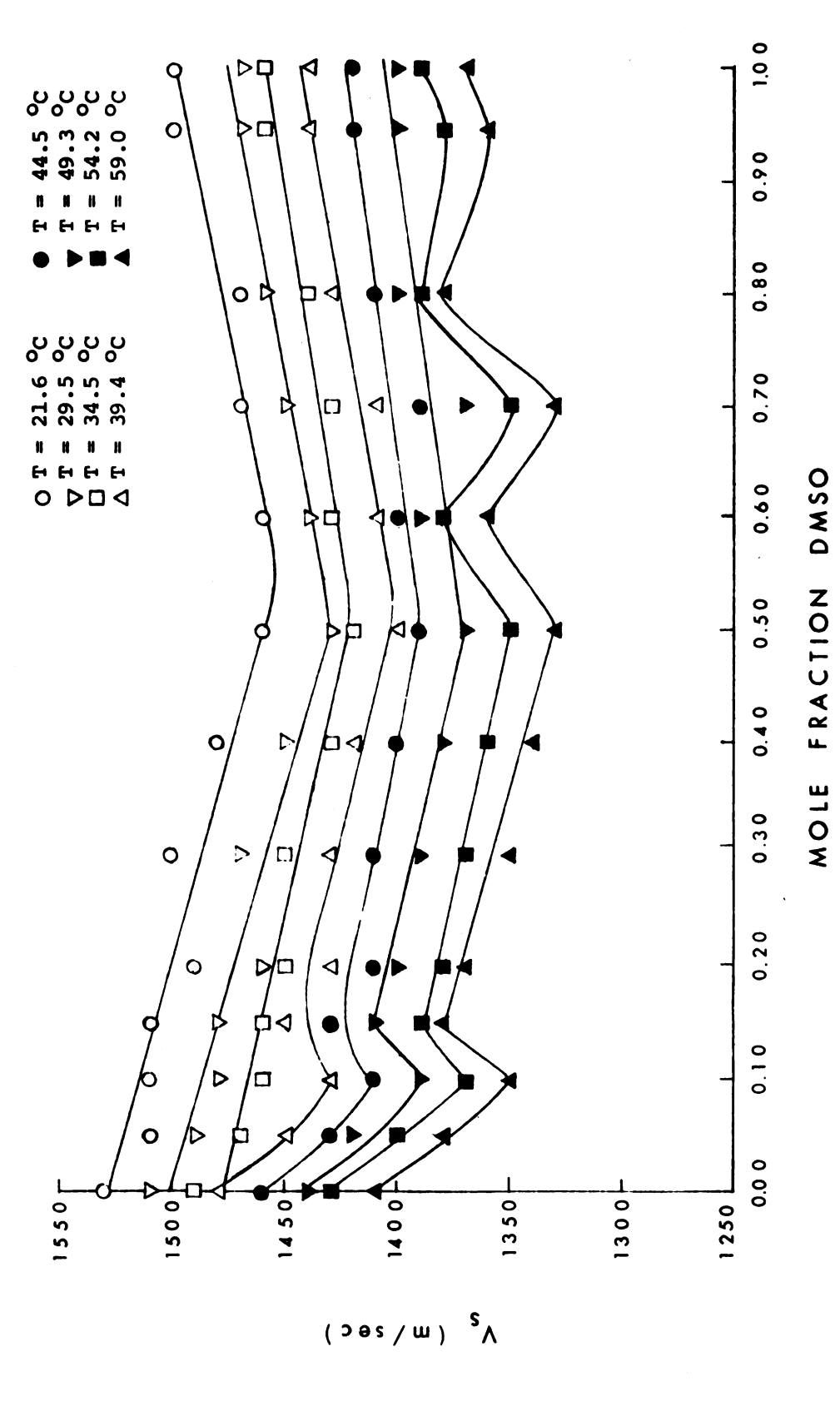


Figure 24. Temperature coefficient of the velocity of sound.



Variation of the velocity of sound with composition for 21.6, 29.5, 34.5, 39.4, 44.5, 49.3, 54.2 and 59.0 $^{\circ}$ C. Figure 25.

Table 9 (cont.)

mole fraction DMSO, X _{DMSO}	Ideal $(V')^2 \times 10^{-6}$ (m^2/sec^2)	Experimental $V_s^2 \times 10^{-6}$ (m^2/sec^2)
0,2997	2.313	2.25
0.3995	2.304	2.19
0.5005	2,295	2.13
0.6002	2.286	2.13
0.7001	2.277	2.16
0.8004	2.268	2.16
0.9453	2.256	2.25
1.0000	2.250	2.25

Average standard deviation for V' and V_s is $\sigma_V = \pm 10 m/sec$. Average standard deviation for $(V')^2$ and V_s^2 is $\sigma V^2 = \pm 0.03 \times 10^6$ m²/sec².

Variations of $(v')^2$ and v_s^2 with composition at 21.6 °C, plus the standard deviations, are shown in Figure 26. The DMSO-pyridine solutions exhibit extremely large deviations from ideality, indicating that a considerable amount of association is present in these mixtures at 21.6 °C.

The adiabatic compressibility, β_S , is another quantity of interest and can be calculated from velocity of sound and density data according to

$$\beta_{S} = \frac{1}{\rho v_{S}^{2}} \qquad (109)$$

Table 10 contains values of the adiabatic compressibility for the DMSO-pyridine mixtures at 21.6 °C.

Table 10 $\label{eq:Adiabatic Compressibility as a Function of Composition for 21.6 } ^{\rm O}{\rm C}$

X _{DMSO}	$\beta_S \times 10^{11}$ (cm ² /dyne)
0.0000	4.38
0.0499	4.4 6

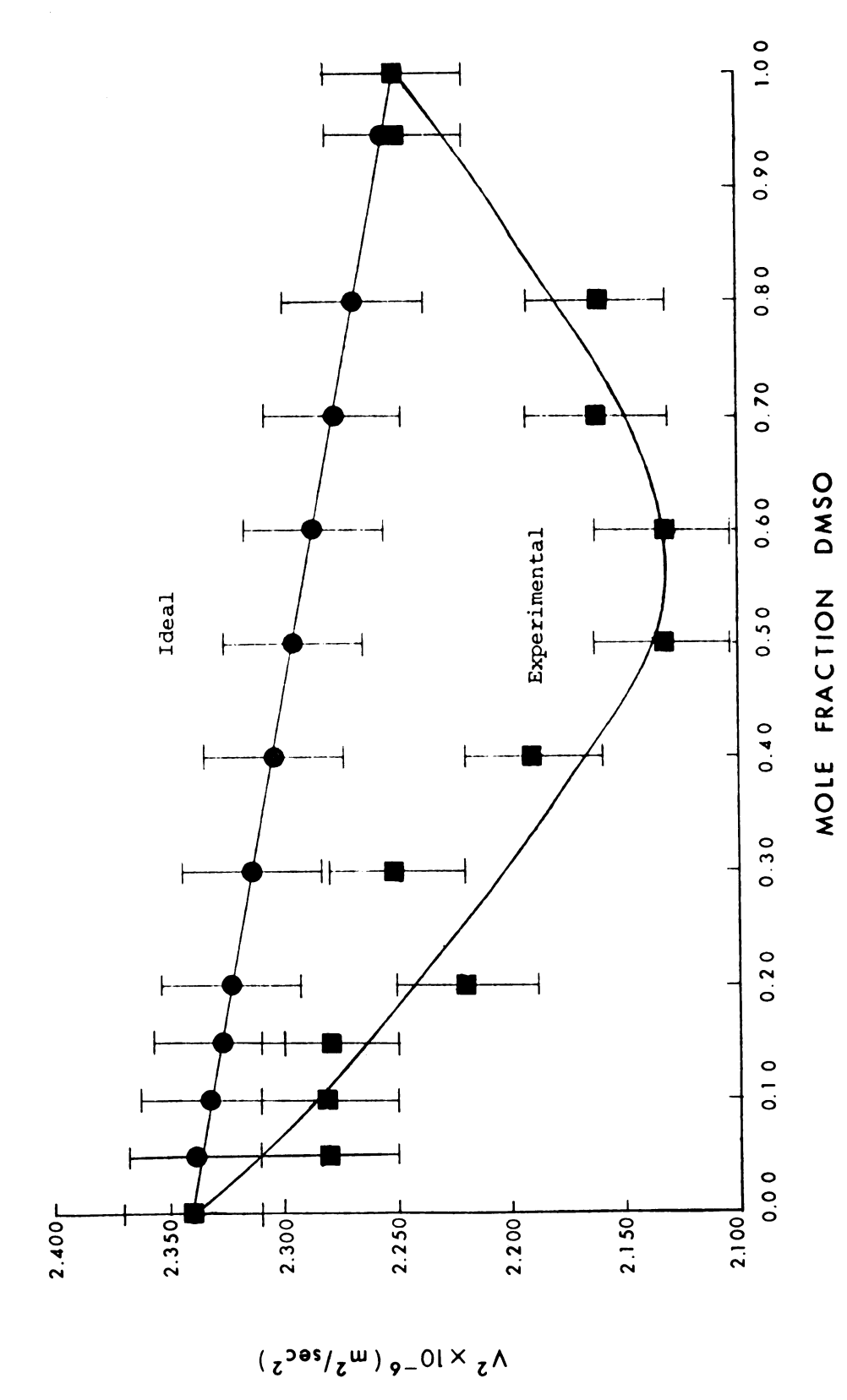


Figure 26. Square of the velocity of sound versus composition for 21.6 $^{\rm o}{\rm C}.$

Table 10 (cont.)

	$\beta_{S} \times 10^{11}$
X _{DMSO}	(cm ² /dyne)
0.1005	4.44
0.1500	4.42
0.2000	4.50
0.2996	4.40
0.4016	4.48
0.4993	4.55
0.6002	4.49
0.7005	4.38
0.8004	4.34
0.9453	4.09
1.0000	4.06

Average standard deviation for β_S is $\sigma_{\beta S} = \pm 0.05 \times 10^{-11}$ cm²/dyne.

The apparent adiabatic compressibility as a function of composition is plotted in Figure 27.

Several interesting observations can be made about Figure 27 and part b of Figure 26. The most noticeable one is that the two functions are almost mirror images of one another. This indicates that the structural changes which produce the characteristic behavior in the β_s versus X_1 curve at 21.6 °C produce a similar but opposite effect in the plot of V_s^2 with X_1 .

The compressibility of a liquid is inversely proportional to the strength of the intermolecular forces or degree of association in the liquid. The velocity of sound is directly proportional to the strength of attraction between the molecules. By examining changes in adiabatic compressibility, sonic velocity and $dV_{\rm S}/dT$ with composition for a series of binary fluids, one can gain insight into the local structural modifications occurring over the full range from one pure fluid to the other.

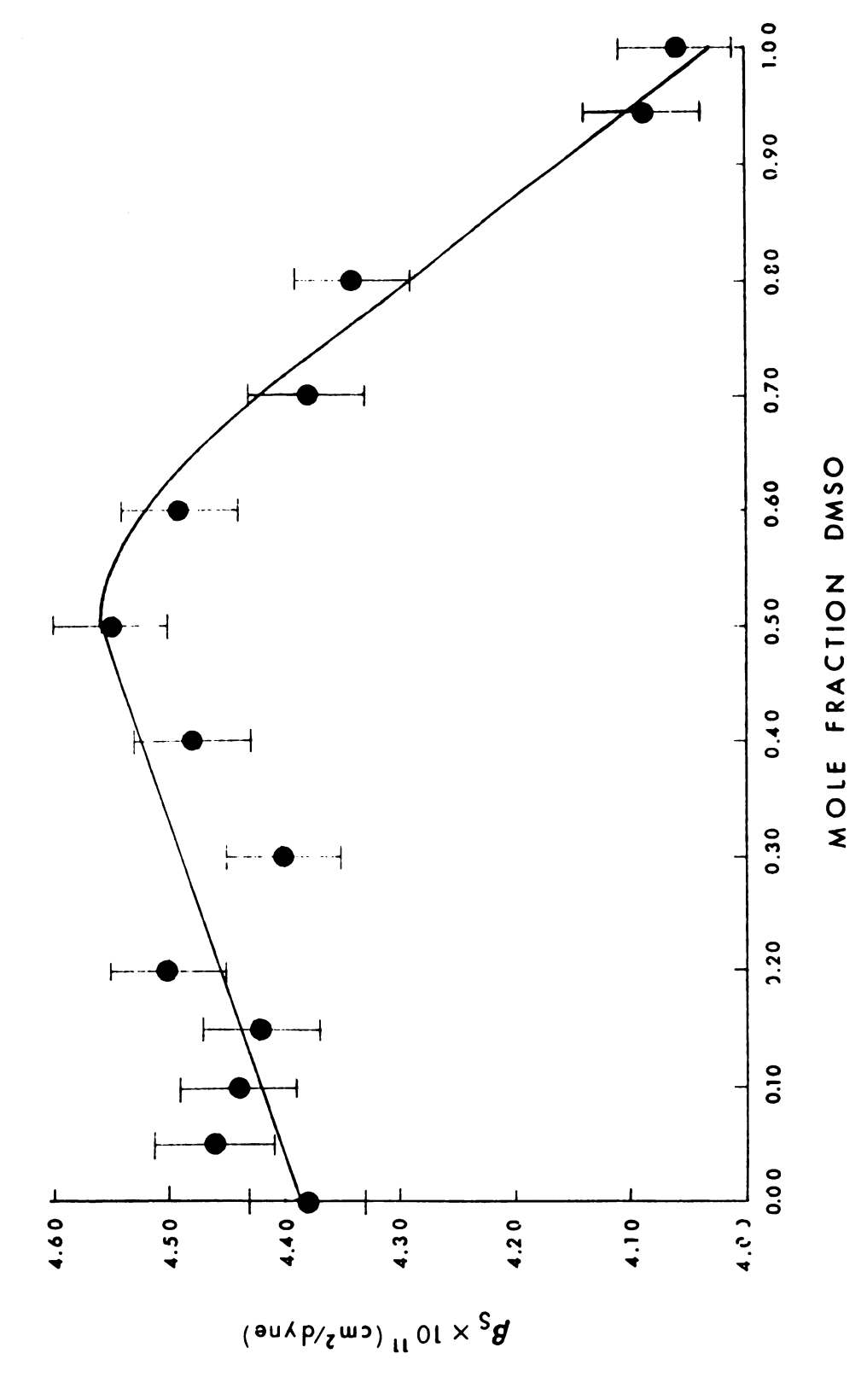


Figure 27. Variation of the adiabatic compressibility with composition for 21.6 °C.

Referring to Figures 26-b and 27, one sees that the addition of dimethyl sulfoxide to pyridine up to ~ 0.55 mole fraction DMSO causes a continuing decrease in the square of the velocity of sound and a slight increase in the adiabatic compressibility. This type of behavior, in general, is associated with a decrease in order or a disorganization of local structure in a liquid. The point of maximum disorganization appears to occur at ~ 0.55 mole fraction DMSO, where V_S^2 reaches a minimum and β_S attains a maximum.

These observations are interesting in view of the fact that the S-O stretching frequency (Figure 28) declines steadily in the region from pure pyridine to 0.60 mole fraction DMSO at 21.6 °C, indicating increased dipole-dipole interaction and alignment of the S-O dipoles (72). Evidently the microscopic changes in the bond order of the S-O bond are not reflected by the light scattering behavior of the fluid, which is dependent upon dimethyl sulfoxide and pyridine.

In the compositional region from 0.00 to 0.50 mole fraction DMSO, in which there are more pyridine molecules present than DMSO molecules, it is entirely possible that the attempts of the dimethyl sulfoxide molecules to form aggregated species (as indicated by the behavior of the S-O stretch frequency) are masked by the pyridine-pyridine, pyridine-DMSO interactions, which also influence the light scattering behavior of the liquid. 1

The dramatic fall in the adiabatic compressibility and rise in ${\rm V_s}^2$ between 0.50 and 1.00 mole fraction DMSO are accompanied by a

ahau 1 d

It should be noted that these observations pertain to one temperature only, 21.6 °C, and that the behavior of the molecules at higher temperatures may be entirely different.

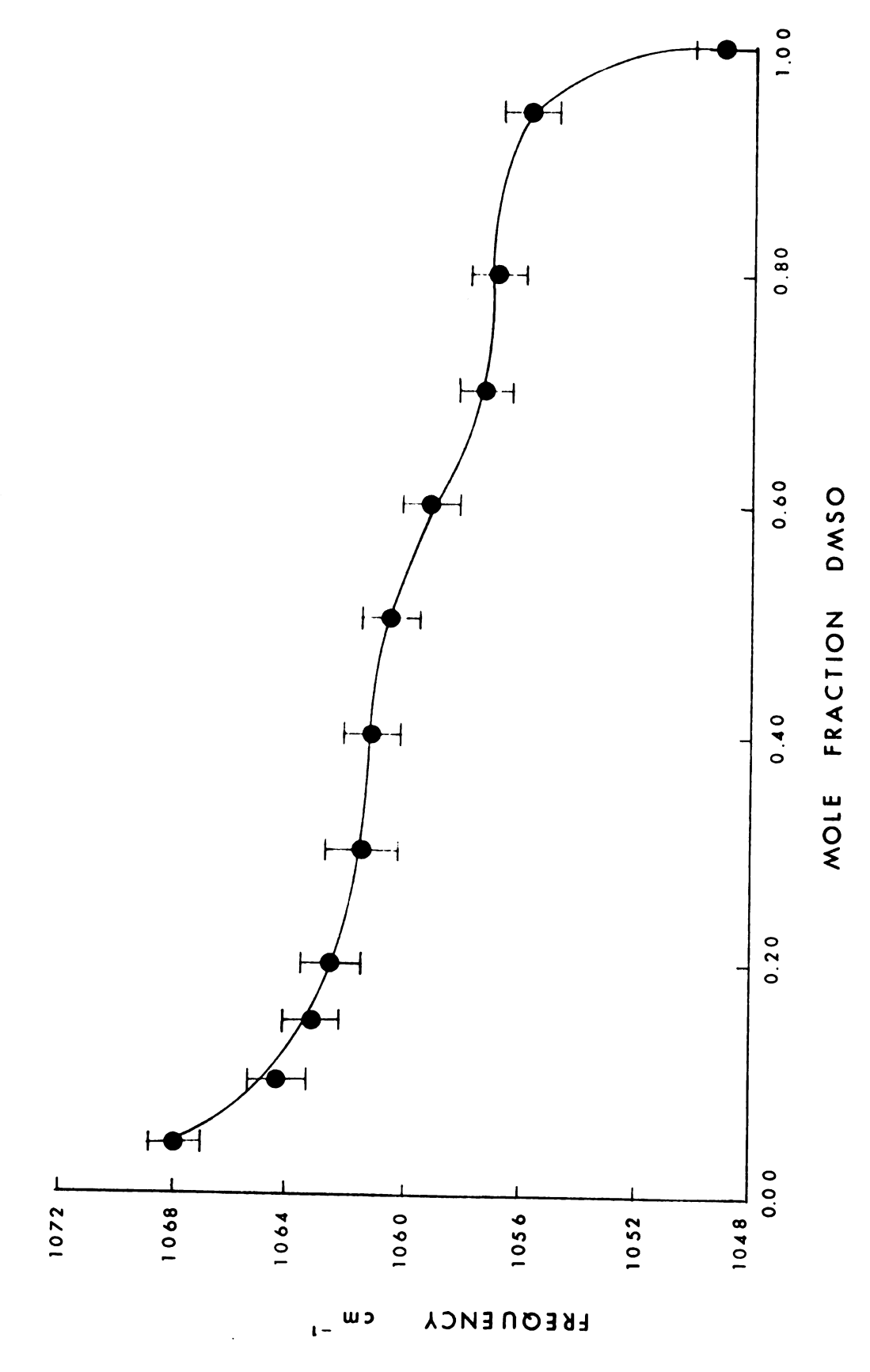


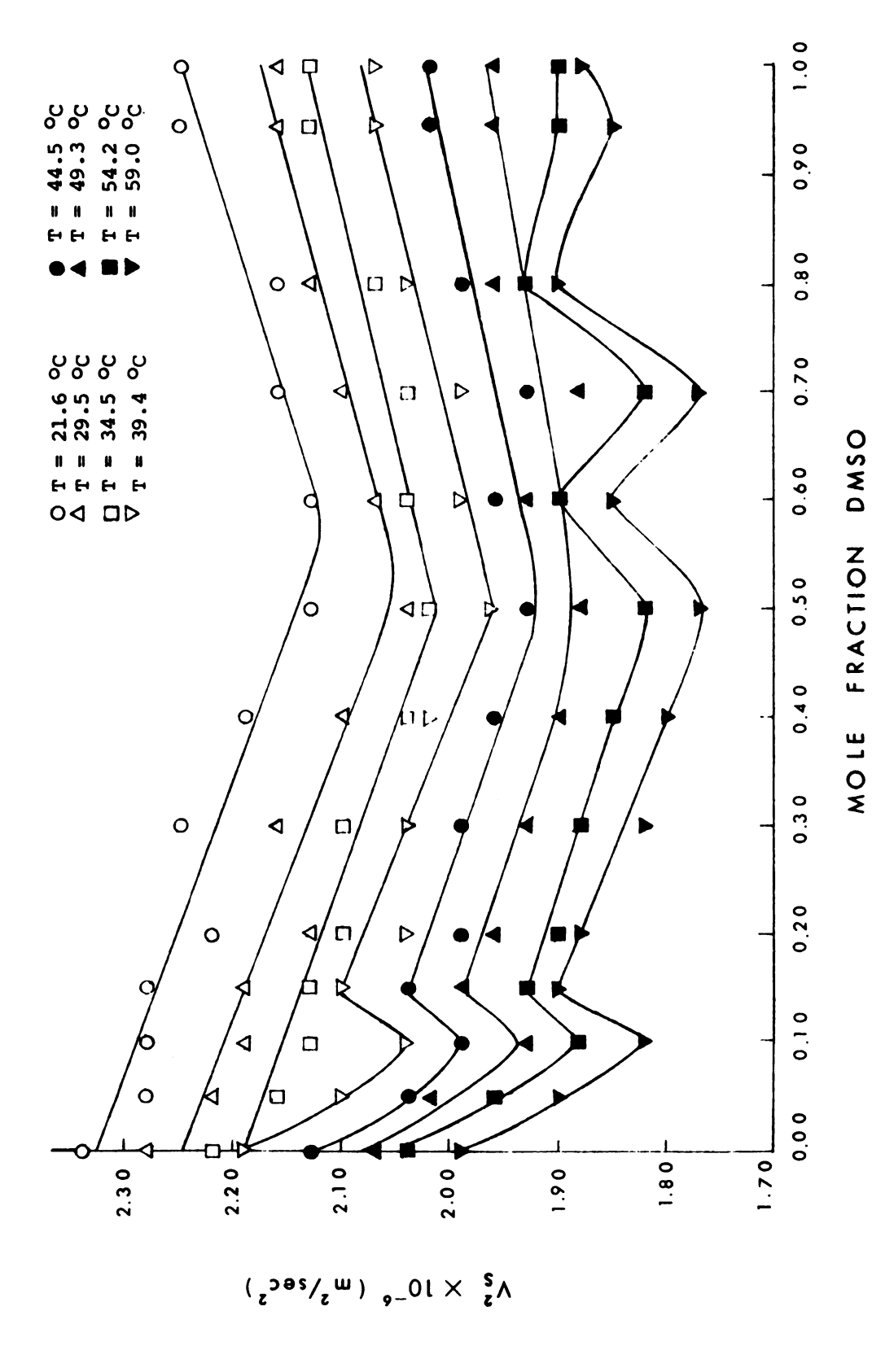
Figure 28. Variation of the S-O stretching frequency with composition at 21.6 °C.

significant decrease in the S-O stretching frequency (72). These data indicate the introduction of more and more association, and more rigid alignment of the S-O dipoles as the proportion of DMSO molecules is increased. The DMSO molecules seem to be undergoing self-association into aggregated species in this composition region at 21.6 °C. Unfortunately, Brillouin scattering data alone give no insight into the exact nature of the associated species present in the DMSO-pyridine mixtures.

The adiabatic compressibility at 21.6 °C reaches a minimum for pure DMSO; the S-O stretching frequency does likewise. These data demonstrate that pure DMSO at 21.6 °C possesses a higher degree of order than pyridine or any of the binary mixtures, and that the structural order involves an alignment of the S-O dipoles.

Interpretation of the structural changes occurring between 29.5 and 59.0 $^{\circ}$ C must be confined to an analysis of velocity of sound information only, since neither density nor infrared spectroscopy data are available for any of the higher temperatures. Because the square of the sonic velocity was found to mirror exactly the behavior of the adiabatic compressibility at 21.6 $^{\circ}$ C, it was decided to plot V_s^2 against composition for each of the remaining seven temperatures. The resultant curves are exhibited in Figure 29. Plots of V_s , V_s^2 and dV_s/dT versus X_1 are all used for interpretive purposes in the remainder of this section.

Examination of the variation in the square of the sonic velocity with composition for the eight different temperatures reveals some interesting fluctuations. The most striking transitions in the curves occur in the regions from 0.05 to 0.20 and 0.50 to 0.80 mole fraction



Square of the velocity of sound versus composition for 21.6, 29.5, 34.5, 39.4, 44.5, 49.3, 54.2 and 59.0 $^{\circ}$ C. Figure 29.

DMSO at the higher temperatures. The temperature coefficient of the hypersonic velocity, $\left| dV_{S}/dT \right|$, is seen to fluctuate dramatically in these compositional regions also.

From the ultrasonic work of Lutskii and Solon'ko (79,80) concerning variations of V_S and $\left| dV_S/dT \right|$ with association for aliphatic carboxylic acids, substituted phenols and anisole derivatives, one can make the following observations:

- (1) Association causes a significant increase of V_S and a sharp lowering of $\left| dV_S / dT \right|$.
- (2) In passing from a chain-like structure to cyclic dimer, there is a sharp decrease in V_S and a sharp increase in $\left| dV_S / dT \right|$.
- (3) Branched chain complexes exhibit an even larger increase in V_s and decrease in dV_s/dT than do linear complexes.

From these facts one can draw several reasonable conclusions concerning the behavior of the DMSO-pyridine mixtures. In particular, the significant increase in the velocity of sound (at the higher temperatures) and sharp decrease in the temperature coefficient between 0.10 and 0.15 mole fraction DMSO signify the formation of a more associated species from a less associated one. This could mean the formation of DMSO dimers, trimers or more highly associated chain-like aggregates in this region. Infrared spectroscopy measurements (72) of the S-O stretching frequency tend to support this interpretation, as does the cryoscopic and dipole moment data of Lindberg, et al. for

The chain-like association of formic acid has been confirmed by infrared studies, while the cyclic dimerization of acetic acid has been studied by proton magnetic resonance (80).

mixtures of DMSO and benzene (9,10).

Infrared spectroscopic data for binary mixtures of DMSO and benzene have been interpreted by Szmant and his coworkers (2) to be indicative of the formation of cyclic dimers of DMSO in the composition range from 0.002 to 0.029 mole fraction DMSO. The difference in compositional region required for the formation of the DMSO dimers can be attributed to the difference in interaction between the S-O dipole and the pi electrons of the benzene ring, on one hand, and the polarizable electron cloud of the spherical carbon tetrachloride molecule, on the other.

The minimum in the velocity of sound recorded for the 0.50-0.50 mole fraction mixture at each temperature signifies a maximum in disorganization of the liquid structure at this composition. These minima in the velocity of sound are indirect evidence for the presence of more substantial attractive forces between DMSO species than between DMSO and pyridine molecules. If the association noted in this study were caused primarily by the interaction of DMSO with pyridine, one would expect to see a maximum in organization of the liquid structure at the equimolar composition. This is exactly opposite of the behavior observed experimentally. One can conclude, then, with a reasonable degree of certainty, that the associated species present in binary mixtures of dimethyl sulfoxide and pyridine are aggregates of DMSO, not DMSO-pyridine species.

The complex pattern of variations in V_S and $|dV_S/dT|$ between 0.50 and 0.80 mole fraction DMSO could be due to the formation and rearrangement of more highly associated species in the liquid, possibly chain-like and/or ring-like aggregates of dimethyl sulfoxide. The sequence of formation, breakdown and recombination of the species, however, remains obscure.

In the composition region between 0.80 and 1.00 mole fraction DMSO the velocity of sound increases at temperatures below 40 °C, signifying an increase in association. Presumably, more and more DMSO molecules are rearranging into the long-chain ring structure which has been proposed for the neat liquid at temperatures below 40 °C (84,85). The types of associated species present at temperatures above 40 °C are difficult to approximate because of the apparent breakdown in association that occurs in the pure liquid at these higher temperatures. 1

E. Variation of the Brillouin Linewidth with Temperature and Composition

It appears to be a straightforward process to determine the linewidth of a Brillouin peak in a light scattering spectrum; however, this information has been obtained for relatively few liquids (49, 57-59, 63-65). The reason for the lack of information on Brillouin linewidths is that it is exceptionally difficult to obtain a liquid which is free enough from dust so that accurate peak heights (and widths) can be measured. This difficulty holds true for both pure liquids and multicomponent fluids and explains in large measure why there is only slightly more linewidth data available for pure liquids (49, 57-59, 65) than for binary mixtures (63,64). The dearth of information on experimental Brillouin linewidths, therefore, renders this work the first major attempt to correlate effects of temperature and composition on the linewidths of Brillouin peaks for binary solvent systems.

This breakdown in association is evidenced by the change in slope of the Landau-Placzek ratio-temperature curve at ~ 45 °C (see section III G).

One realizes from the theoretical discussion of Brillouin linewidths on pp. 40-43, that a vast simplification of the data analysis occurs if the instrumental profiles and the observed Brillouin peaks can be shown to be Lorentzian in nature. Specifically, one finds that

$$2\Gamma_{\rm B} = 2\Gamma_{\rm B/obs} - \Gamma_{\rm inst}$$
, (110)

where $2\Gamma_{\rm B}$ is the true linewidth of the Brillouin peak, $2\Gamma_{\rm B/obs}$ is the observed linewidth of the Brillouin peak and $\Gamma_{\rm inst}$ is the linewidth of the instrumental function. In this particular situation, the true Brillouin linewidths can be obtained without the use of complicated computer methods for the deconvolution of the instrumental profile. Furthermore, if one shows that the instrumental profile is approximated by the central peak of the Brillouin spectrum, the instrumental linewidth, $\Gamma_{\rm inst}$, can be replaced by the linewidth of the central peak, $\Gamma_{\rm C}$.

In order to justify the use of such a simplification in our Brillouin linewidth analysis, we felt that we must demonstrate the following:

- The central and Brillouin peaks for the spectra of the DMSO-pyridine solutions are Lorentzian in shape.
- 2. The instrumental profile of the detection system is equivalent to the profile of the central peak of a Brillouin spectrum, via the fact that the linewidths of the central peaks for pure DMSO, pure pyridine and one of their mixtures are equal at a given value of finesse.
- The linewidth of the central peak for a given solution is a linear function of the experimental finesse.

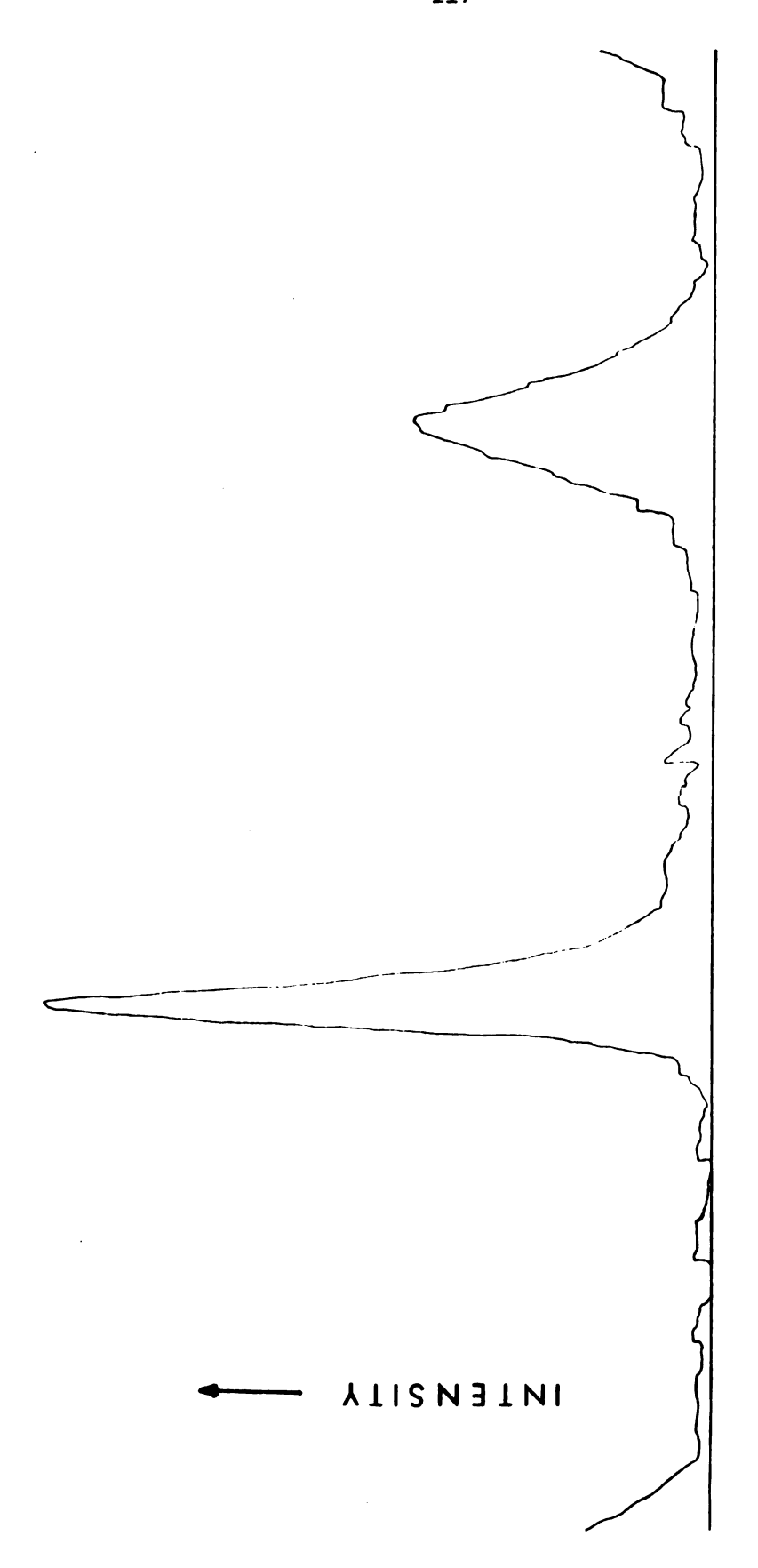
Portions of experimental Brillouin spectra which were used in testing the Lorentzian nature of the component peaks are shown in Figures 30-34. The central peak and one Brillouin peak from each spectrum were used in this analysis. Each peak was divided at the center so that the left and right portions could be fit to appropriate Lorentzian functions. 1

Numerical values for the intensities and graphical comparisons of the experimental and calculated intensities for the peaks of 0.80 mole fraction DMSO are presented in Tables 11 and 12 and Figures 35-38, respectively. As one can see from the computer plots of the 0.80 mole fraction DMSO data, 2 each side of each peak fits a Lorentzian function, especially in the tail regions of the peaks, where one would expect the greatest discrepancies to occur for an incorrect choice of mathematical function. Experimental and calculated intensities for analogous peaks of the two neat liquids are given in Tables 13-16.

mental and calculated peaks when one attempts to fit a Lorentzian profile to a Gaussian mathematical function, one finds an experimental profile in Figure 39, and the respective Gaussian and Lorentzian computer fits to this profile in Figures 40-42. A beam of monochromatic (5145 Å), vertically polarized radiation was passed through the detection system to obtain the experimental spectrum. The natural profile of the laser is superimposed on the transmission function of the Fabry-Perot interferometer to produce an instrumental profile which

¹This was done for computational simplicity.

²Similar computer plots were obtained for the central and Brillouin peaks of pure DMSO and pure pyridine, but were omitted to conserve space.



FREQUENCY ----

Figure 30. Portion of Brillouin spectrum for neat pyridine at 29.5 °C.

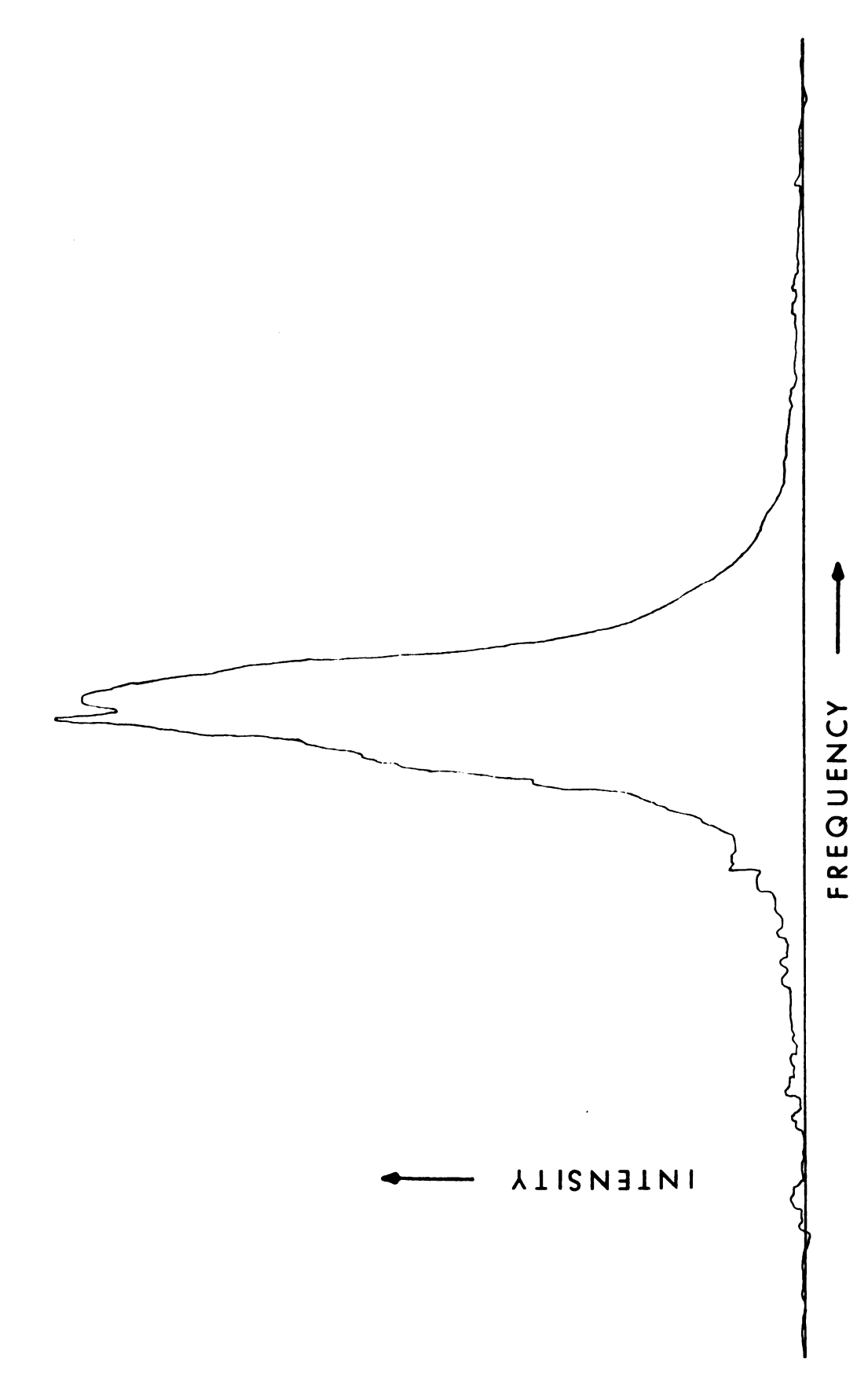
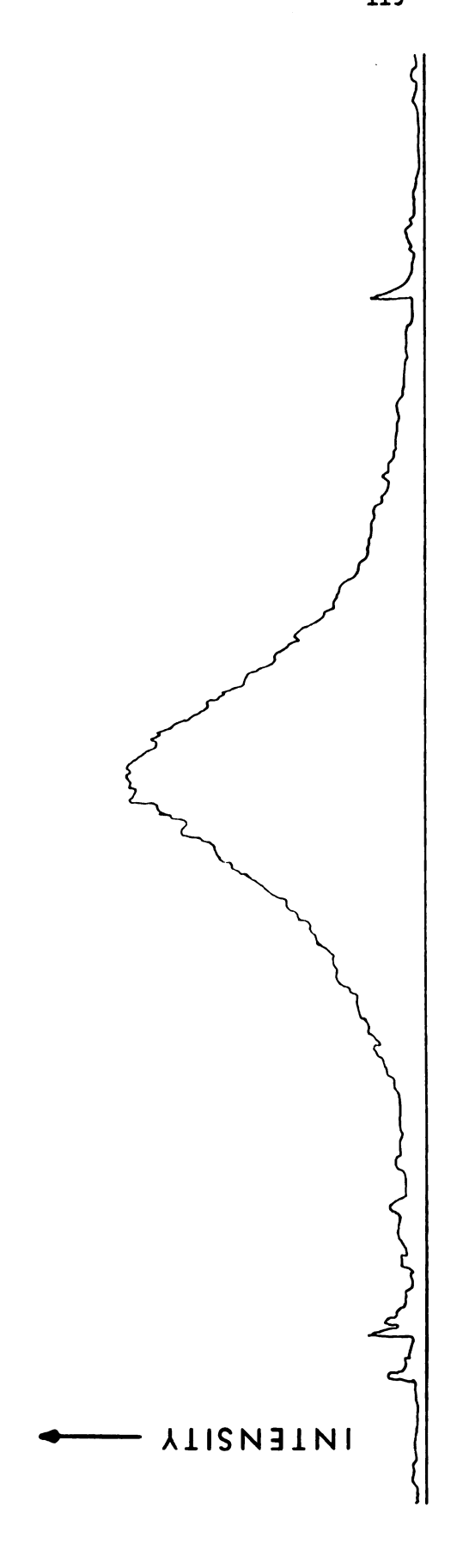


Figure 31. Central peak of Brillouin spectrum for 0.80 mole fraction DMSO at $59.0^{\circ}\mathrm{C}.$



FREQUENCY ---

Figure 32. Left Brillouin peak of Brillouin spectrum for 0.80 mole fraction DMSO at 59.0 °C.

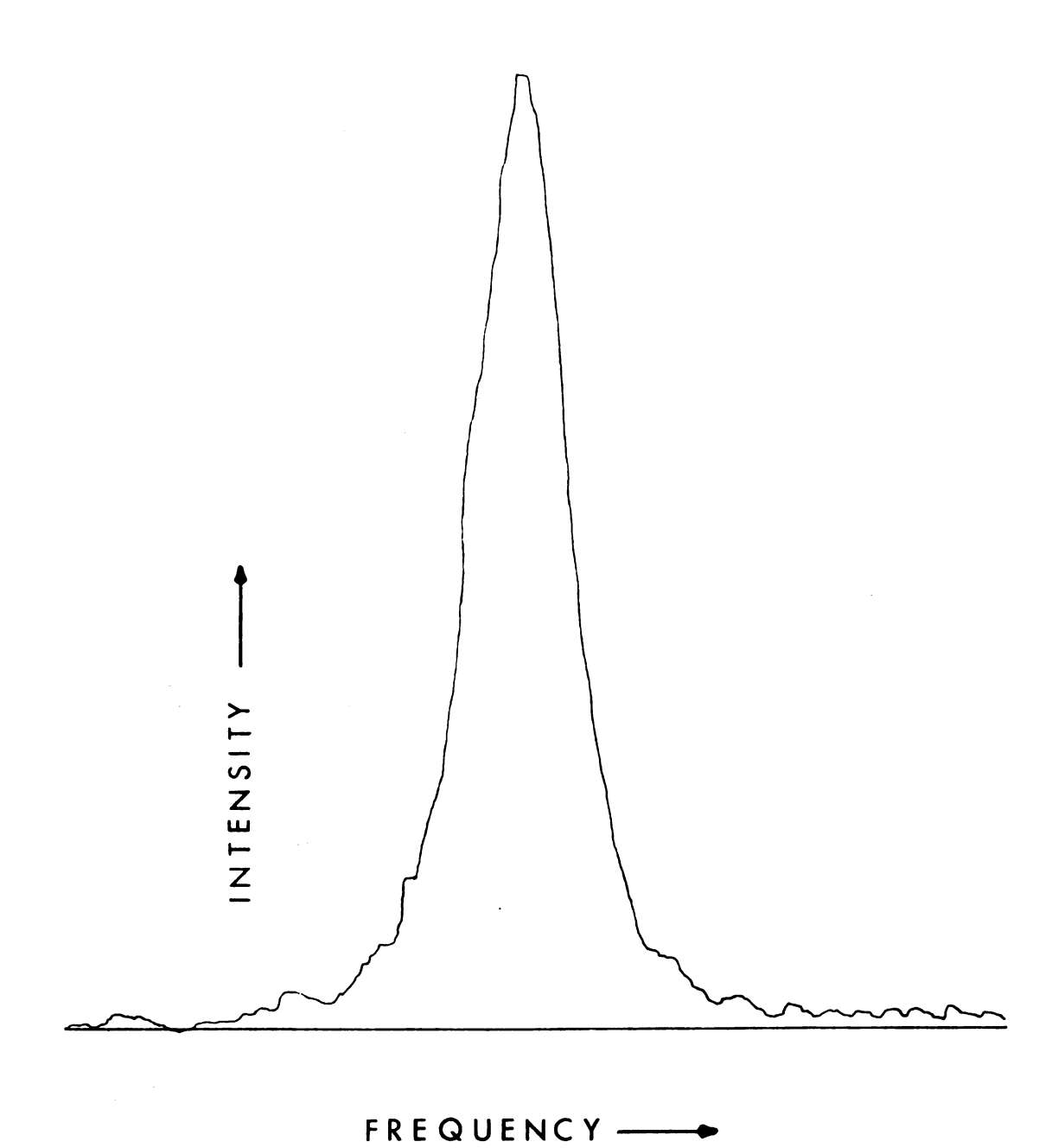


Figure 33. Central peak of Brillouin spectrum for neat DMSO at 59.0 °C.

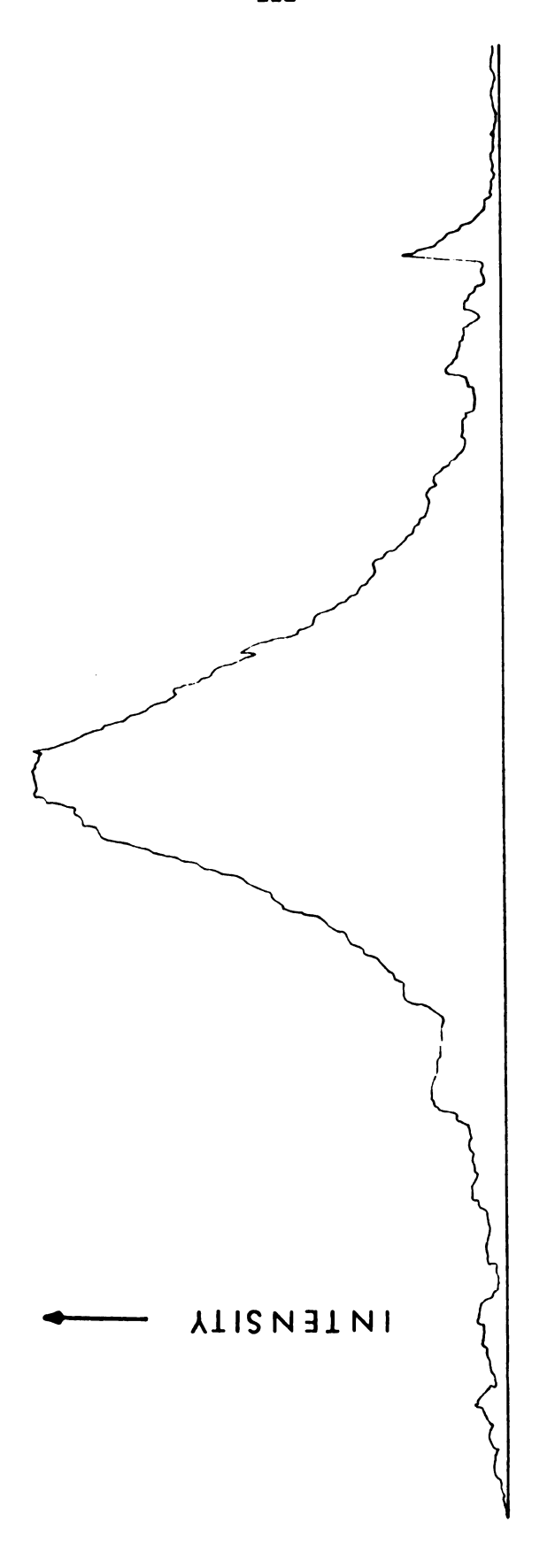


Figure 34. Left Brillouin peak of Brillouin spectrum for neat DMSO at 59.0 °C.

FREQUENCY

Table 11 Experimental and Calculated Intensities for the Central Peak of 0.80 Mole Fraction DMSO at $59.0\,^{\circ}\text{C}$

0.80 mole fraction DMSO; March 18, 0.80 mole fraction DMSO; March 18, 1972, No. 6; Central peak, left 1972, No. 6; Central peak, right hand side; fit to Lorentzian hand side; fit to Lorentzian Point Intensity Intensity* Point Intensity Intensity Number (exptl.) (calcd.) Number (exptl.) (calcd.) 1 0.0 1.095 289.5 1 259.1 2 0.0 1.148 2 280.0 284.1 3 0.0 1.204 3 240.0 243.8 4 0.0 1.265 4 190.0 179.4 5 0.0 1.331 5 118.0 124.8 6 0.0 1.402 87.79 6 83.5 7 0.0 1.478 7 64.5 64.12 8 0.0 1.561 8 51.0 48.01 9 0.0 1.652 9 42.5 37.25 10 1.0 1.750 10 33.0 29.47 11 1.0 1.857 11 25.0 23.94 12 1.5 1.974 12 21.0 19.72 13 2.0 2.104 13 17.0 16.57 14 2.0 2.245 14 14.0 14.05 15 2.5 2.402 15 10.5 12.10 16 2.5 2.576 16 9.0 10.50 17 3.0 2.769 17 8.0 9.184 18 3.5 2.984 18 7.0 8.125

3.225

3.498

19

20

7.0

6.0

7.219

6.471

4.0

4.0

19

20

^{*}Intensities are given in arbitrary units.

Table 11 (cont.)

0.80 mole fraction DMSO; March 18, 1972, No. 6; Central peak, left hand side; fit to Lorentzian

0.80 mole fraction DMSO; March 18, 1972, No. 6; Central peak, right hand side; fit to Lorentzian

Point Number	Intensity (exptl.)	•	Point Number	Intensity (exptl.)	
21	4.5	3.806	21	5.0	5.819
22	4.5	4.155	22	5.0	5.273
23	5.0	4.555	23	4.0	4.789
24	5.0	5.014	24	4.0	4.377
25	5.0	5.553	25	4.0	4.008
26	6.0	6.168	26	3.0	3.691
27	6.5	6.909	27	3.0	3.404
28	7.0	7.767	28	3.0	3.148
29	8.0	8.821	29	3.0	2.926
30	9.0	10.07	30	3.0	2.721
31	10.0	11.64	31	2.5	2.542
32	12.0	13.60	32	2.5	2.375
33	15.5	16.02	33	2.5	2.228
34	19.5	19.22	34	2.0	2.091
35	24.5	23.33	35	1.5	1.969
36	31.5	29.01	36	1.5	1.855
37	39.5	36.69	37	1.5	1.753
38	54.0	47.94	38	1.0	1.657
39	68.0	64.17	39	1.0	1.568
40	98.5	89.43	40	0.5	1.488
41	137.0	128.4	41	0.0	1.413
42	184.0	183.5	42	0.0	1.345

Table 11 (cont.)

0.80 mole fraction DMSO; March 18, 1972, No. 6; Central peak, left hand side; fit to Lorentzian

0.80 mole fraction DMSO; March 18, 1972, No. 6; Central peak, right hand side; fit to Lorentzian

Point Number	Intensity (exptl.)	Intensity (calcd.)	Point Number	Intensity (exptl.)	Intensity (calcd.)
43	241.5	246.9	43	0.0	1.280
44	270.5	273.3	44	0.0	1.221
45	289.5	235.0	45	0.0	1.164
			46	0.0	1.112

Table 12 $\label{table 12}$ Experimental and Calculated Intensities for the Left Brillouin Peak of 0.80 Mole Fraction DMSO at 59.0 $^{\rm O}{\rm C}$

0.80 mole fraction DMSO; March 18, 1972, No. 6; Left Brillouin peak, left hand side; fit to Lorentzian

0.80 mole fraction DMSO; March 18, 1972, No. 6; Left Brillouin peak, right hand side; fit to Lorentzian

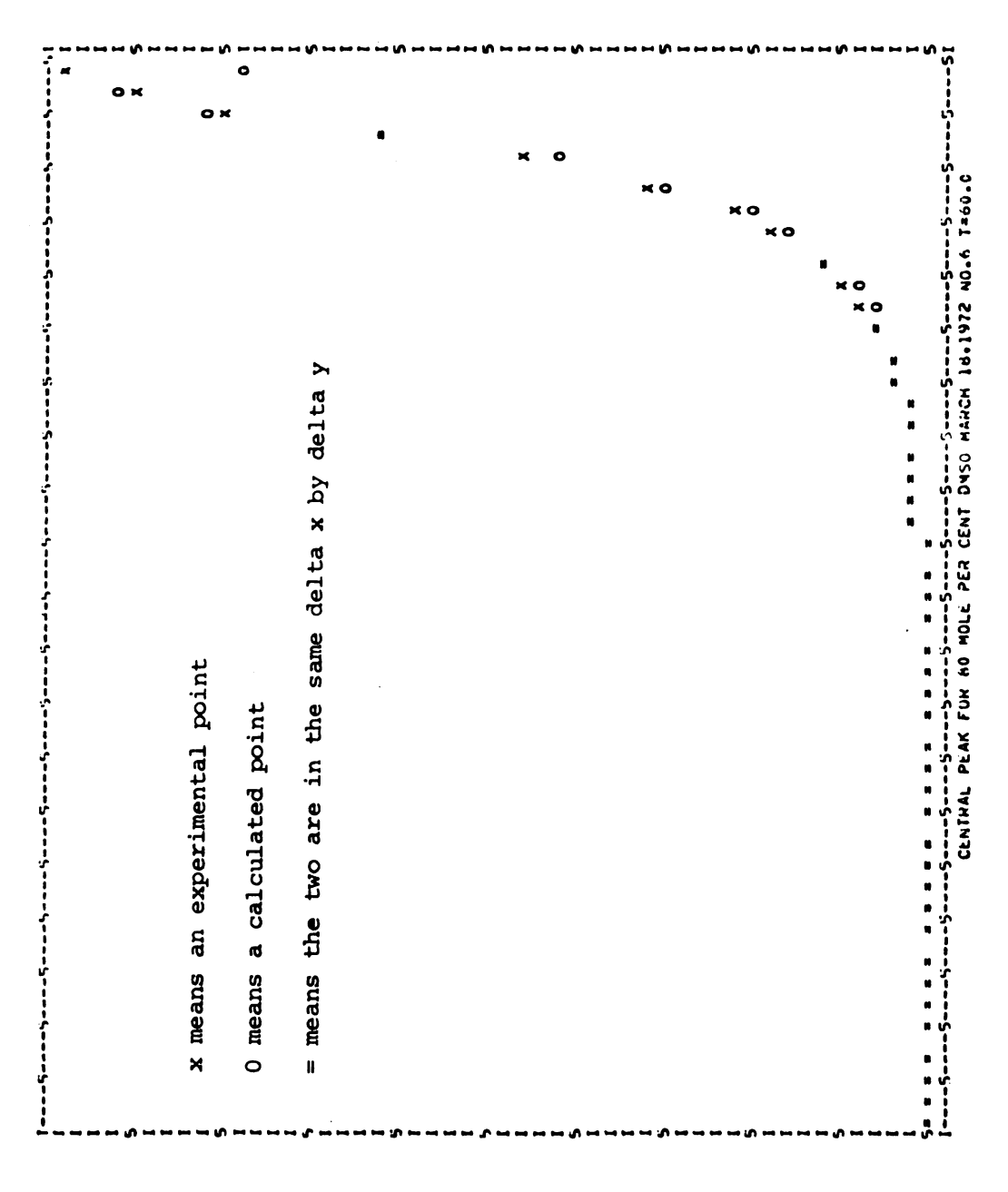
Point Number	Intensity (exptl.)	Intensity (calcd.)	Point Number	Intensity (exptl.)	Intensity (calcd.)
1	0.0	1.716	1	110.0	109.8
2	1.5	1.834	2	100.5	102.0
3	2.0	1.966	3	81.5	82.98
4	2.0	2.111	4	64.0	63.11
5	3.0	2.274	5	48.5	47.20
6	4.0	2.455	6	35.0	35.51
7	3.5	2.659	7	26.0	27.31
8	4.0	2.890	8	21.0	21.45
9	3.5	3.151	9	20.0	17.19
10	3.0	3.449	10	16.0	14.03
11	3.5	3.7 91	11	11.0	11.64
12	4.0	4.185	12	10.0	9.794
13	5.0	4.643	13	8.0	8.344
14	5.5	5.179	14	7.0	7.188
15	6.0	5.811	15	5.5	6.251
16	7.0	6.574	16	5.0	5.476
17	8.0	7.482	17	5.0	4.841
18	9.0	8.586	18	4.5	4.309
19	9.5	9.944	19	4.0	3.859
20	10.0	11.64	20	3.0	3.476

Table 12 (cont.)

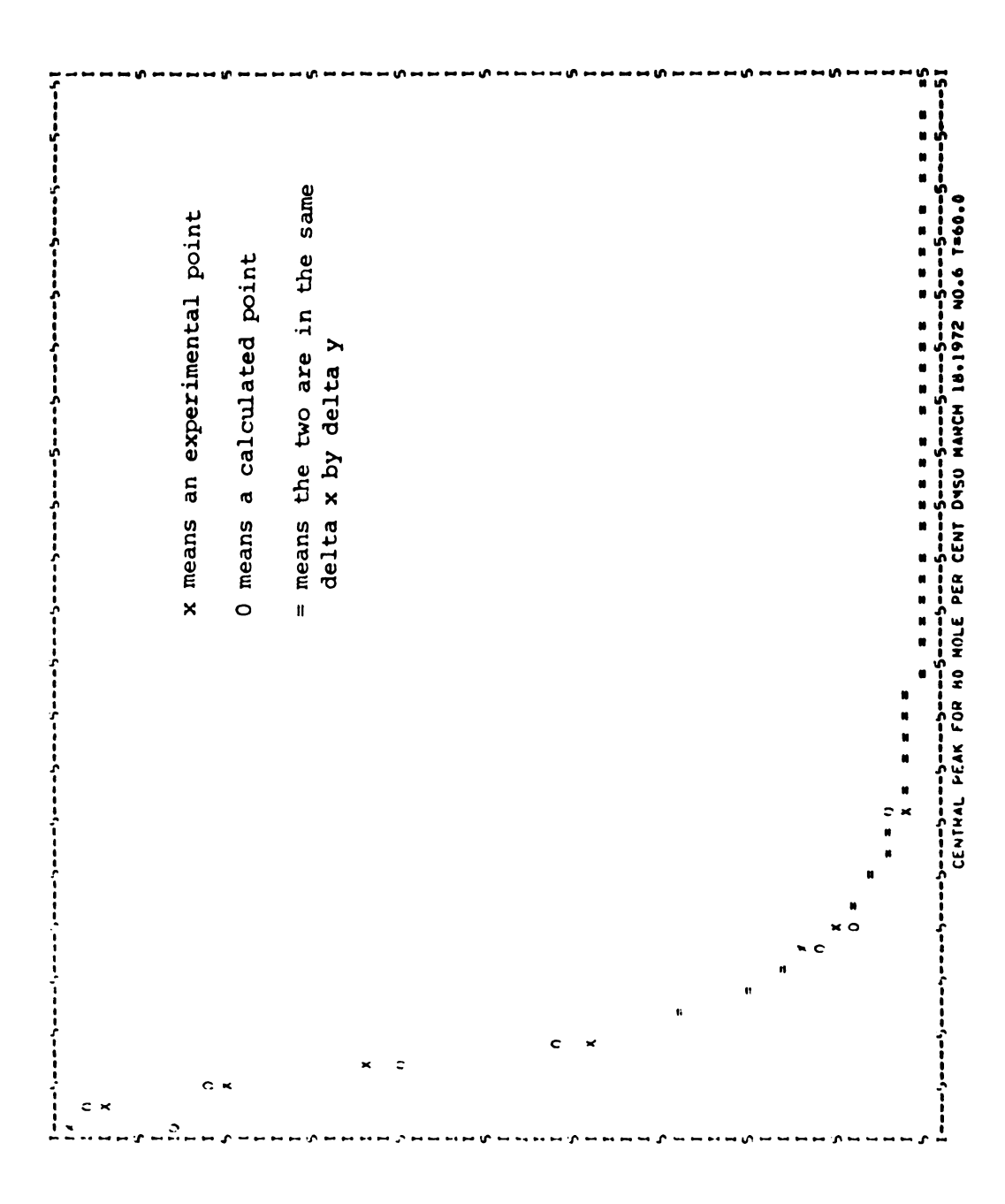
0.80 mole fraction DMSO; March 18, 1972, No. 6; Left Brillouin peak, left hand side; fit to Lorentzian

0.80 mole fraction DMSO; March 18, 1972, No. 6; Left Brillouin peak, right hand side; fit to Lorentzian

Point Number	Intensity (exptl.)	Intensity (calcd.)	Point Number	<pre>Intensity (exptl.)</pre>	Intensity (calcd.)
21	12.0	13.78	21	2.5	3.146
22	14.0	16.53	22	3.0	2.861
23	20.0	20.13	23	3.0	2.613
24	26.0	24.91	24	2.0	2.395
25	34.0	31.44	25	1.0	2.220
26	42.0	40.27	26	0.5	2.032
27	52.5	52.25	27	0.5	1.881
28	69.5	67.93	28	0.0	1.746
29	83.5	86.38	29	0.0	1.626
30	102.0	103.0	30	0.0	1.517
31	110.0	109.8	31	0.0	1.419
			32	0.0	1.330



Left-hand side of central peak for 0.80 mole fraction DMSO at 59.0 $^{\circ}\mathrm{C}$ fit to a Lorentzian. Figure 35.



Right-hand side of central peak for 0.80 mole fraction DMSO at 59.0 °C fit to a Lorentzian. Figure 36.

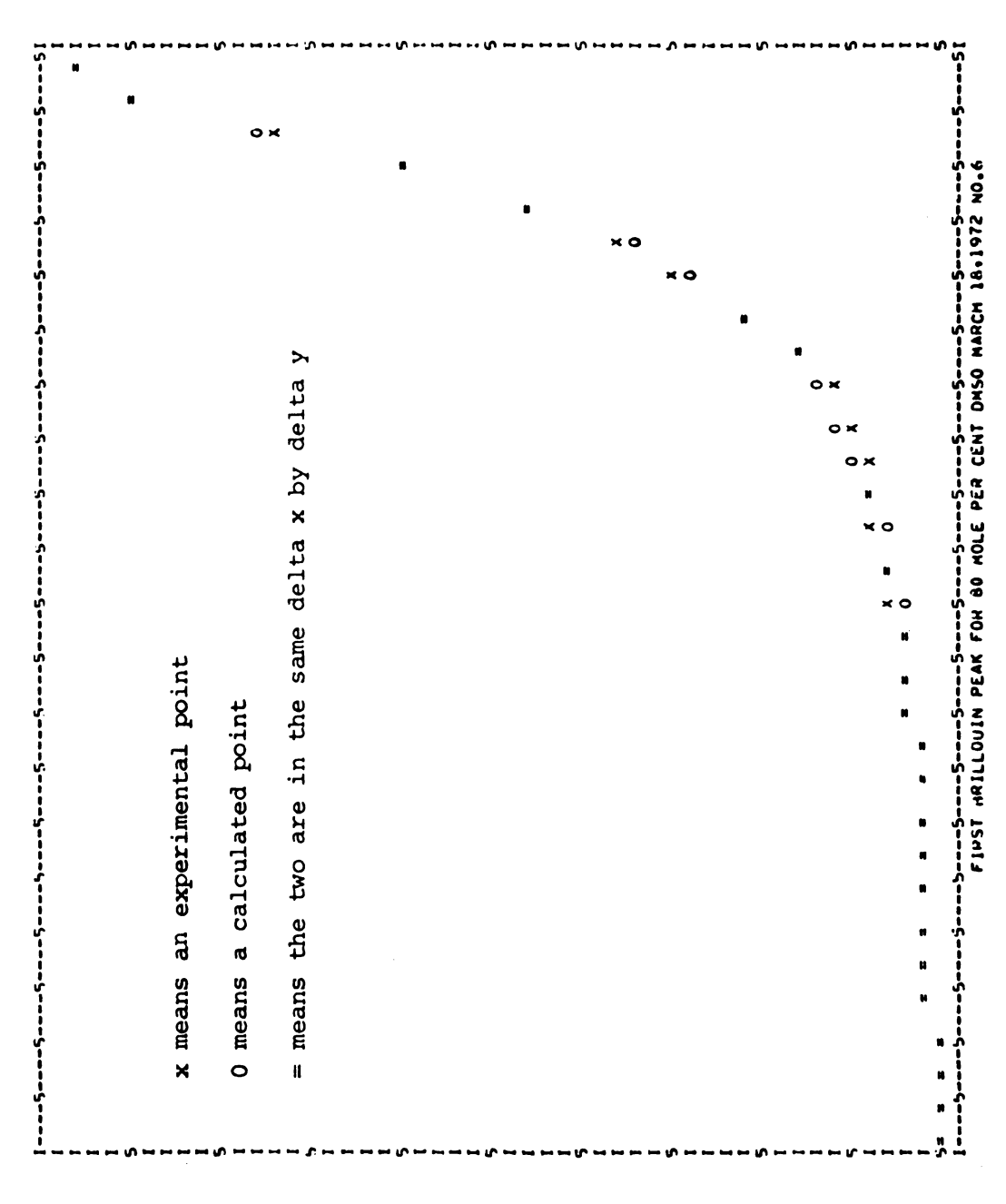
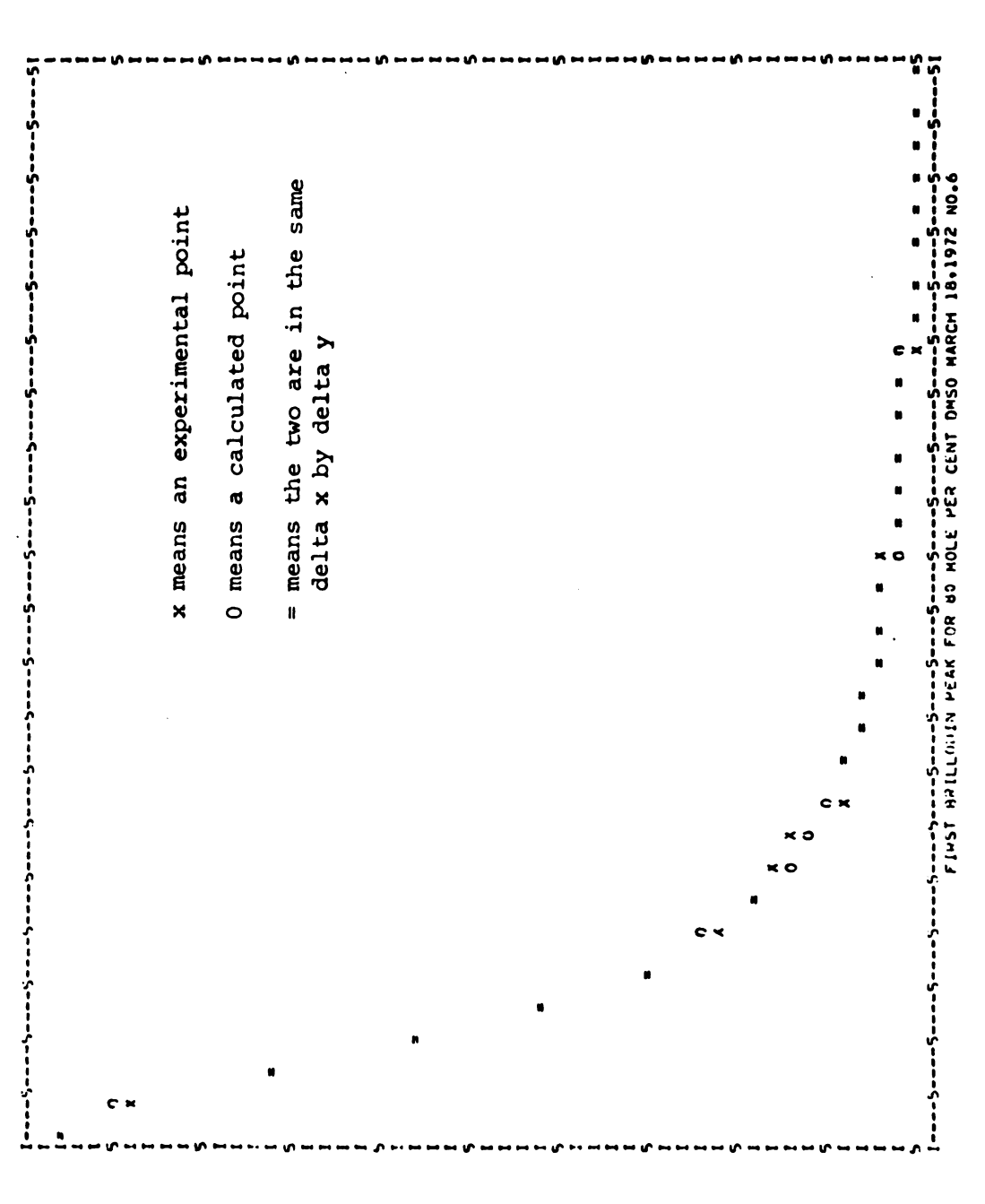


Figure 37. Left-hand side of left Brillouin peak for 0.80 mole fraction DMSO at 59.0 OC fit to a Lorentzian.



Right-hand side of left Brillouin peak for 0.80 mole fraction DMSO at 59.0 °C fit to a Lorentzian. Figure 38.

Table 13

Experimental and Calculated Intensities for the

Central Peak of Neat DMSO at 59.0 °C

Pure DMSO; December 15, 1971, No. 6; <u>Central peak</u> , left hand side; fit to <u>Lorentzian</u>		No. 6; C	Pure DMSO; December 15, 1971, No. 6; Central peak, right hand side; fit to Lorentzian		
Point Number	Intensity (exptl.)	Intensity (calcd.)	Point Number	Intensity (exptl.)	Intensity (calcd.)
1	0.0	2.021	1	485.0	456.4
2	0.0	2.191	2	427.0	476.6
3	0.5	2.383	3	261.0	251.0
4	1.0	2.602	4	148.7	128.2
5	2.0	2.852	5	84.5	73.77
6	2.2	3.140	6	44.0	46.81
7	2.5	3.474	7	34.0	32.23
8	3.5	3.864	8	22.0	23.37
9	4.0	4.322	9	17.0	17.74
10	4.5	4.868	10	12.3	13.91
11	5.0	5.524	11	10.0	11.16
12	5.5	6.319	12	7.5	9.175
13	6.0	7.303	13	6.0	7.671
14	7.5	8.523	14	6.0	6.495
15	9.0	10.10	15	6.0	5.579
16	11.5	12.12	16	5.5	4.835
17	14.0	14.80	17	5.5	4.237
18	15.0	18.52	18	5.5	3.744
19	20.5	23.73	19	5.5	3.326
20	33.7	31.42	20	5.0	2.979

Table 13 (cont.)

Pure DMSO; December 15, 1971, No. 6; Central peak, left hand side; fit to Lorentzian

Pure DMSO; December 15, 1971, No. 6; Central peak, right hand side; fit to Lorentzian

Point Number	Intensity (exptl.)	Intensity (calcd.)	Point Number	Intensity (exptl.)	Intensity (calcd.)
21	48.5	43.57	21	4.0	2.684
22	80.0	63.52	22	4.0	2.427
23	124.0	99.23	23	4.0	2.208
24	199.0	169.2	24	3.0	2.017
25	330.5	298.8	25	2.0	1.848
26	427.5	430.6	26	2.0	1.701
27	485.0	349.2	27	1.0	1.570
			28	0.0	1.454

Pure DMSO; December 15, 1971, Pure DMSO; December 15, 1971, No. 6; Left Brillouin peak, No. 6; Left Brillouin peak, left hand side; fit to Lorentzian right hand side; fit to Lorentzian Point Intensity Intensity Point Intensity Intensity Number (exptl.) Number (exptl.) (calcd.) (calcd.) 1 6.343 0.0 1 429.0 422.2 2 1.0 6.711 2 421.8 421.5 2.0 3 7.112 3 372.7 385.9 3.0 7.550 4 330.5 318.2 5.0 5 8.029 5 272.7 272.1 6.0 6 8.555 6 220.3 233.6 7 6.0 9.134 7 187.3 177.9 8 8.0 9.774 8 153.6 144.6 9 10.0 10.48 9 127.3 118.7 10 10.0 11.27 10 107.3 98.52 11 12.0 12.15 86.4 82.70 11 12 14.0 13.13 12 70.0 70.19 13 14.0 14.24 13 57.3 60.18 14 16.0 15.50 14 45.4 52.07 15 17.0 16.92 45.44 15 36.4 16 17.0 18.54 16 30.0 39.96 20.41 17 19.0 17 24.5 35.39 18 20.0 22.57 31.54 18 23.6 19 22.7 25.08 19 22.7 28.29

20

20.0

25.48

20

28.2

28.03

Table 14 (cont.)

Pure DMSO; December 15, 1971, No. 6; <u>Left Brillouin peak</u>, left hand side; fit to <u>Lorentzian</u> Pure DMSO; December 15, 1971, No. 6; Left Brillouin peak, right hand side; fit to Lorentzian

Point Number	Intensity (exptl.)	Intensity (calcd.)	Point Number	Intensity (exptl.)	Intensity (calcd.)
21	32.7	31.51	21	17.3	23.08
22	34.5	35.66	22	17.3	20.99
23	39.1	40.65	23	13.6	19.17
24	43.6	46.73	24	10.0	17.57
25	50.0	54.20	25	10.0	16.17
26	57.3	63.51	26	9.1	14.92
27	68.2	75.24	27	8.2	13.81
28	89.1	90.23	28	6.4	12.82
29	112.7	109.6	29	6.4	11.93
30	141.8	134.9	30	5.4	11.13
31	172.7	168.2	31	5.4	10.41
32	216.3	211.4	32	4.5	9.751
33	264.5	265.8	33	3.6	9.155
34	335.4	328.8	34	2.7	8.612
35	383.6	389.4	35	2.7	8.115
36	420.9	426.8	36	1.8	7.660
37	429.0	422.7	37	1.4	7.242
			38	0.0	6.857

Table 15 $\label{table 15}$ Experimental and Calculated Intensities for the Central Peak of Neat Pyridine at 29.5 $^{\rm O}{\rm C}$

Pure pyridine, December 20, 1971, No. 4; Central peak, left hand side; fit to Lorentzian

Pure pyridine, December 20, 1971, No. 4; Central peak, right hand side; fit to Lorentzian

_			•			
Point Number	Intensity (exptl.)	Intensity (calcd.)	Point Number	Intensity (exptl.)	Intensity (calcd.)	
1	0.0	0.8891	1	337.5	337.12	
2	0.0	0.9783	2	273.5	282.60	
3	0.0	1.0817	3	185.0	196.83	
4	0.0	1.2023	4	132.0	131.30	
5	0.0	1.3443	5	90.0	89 .7 90	
6	0.0	1.5130	6	65.5	63.920	
7	0.0	1.7155	7	48.0	47.415	
8	0.0	1.9623	8	38.0	36.283	
9	0.0	2.2635	9	29.2	28.557	
10	0.0	2.6429	10	24.5	23.047	
11	1.0	3.1259	11	20.5	18.936	
12	1.5	3.7485	12	17.0	15.819	
13	2.2	4.5840	13	15.0	13.404	
14	3.5	5.7318	14	12.2	11.510	
15	5.5	7.3679	15	10.5	9.9765	
16	8.5	9.7877	16	8.0	8.7279	
17	12.5	13.648	17	6.0	7.7055	
18	20.2	20.276	18	4.5	6.8455	
19	37.5	32.855	19	2.8	6.1211	
20	78.0	61.243	20	1.2	5.5097	

Table 15 (cont.)

Pure pyridine, December 20, 1971, No. 4; Central peak, left hand side; fit to Lorentzian

Pure pyridine, December 20, 1971, No. 4; Central peak, right hand side; fit to Lorentzian

Point Number	Intensity (exptl.)	Intensity (calcd.)	Point Number	Intensity (exptl.)	Intensity (calcd.)
21	188.0	139.62	21	0.0	4.9813
22	288.0	275.36	22	0.0	4.5251
23	337.5	338.74	23	0.0	4.1315
			24	0.0	3.7844

Table 16

Experimental and Calculated Intensities for the Right Brillouin Peak of Neat Pyridine at 29.5 °C

Pure pyridine, December 20, 1971, Pure pyridine, December 20, 1971, No. 4; Right Brillouin peak, left No. 4; Right Brillouin peak, right hand side; fit to Lorentzian hand side; fit to Lorentzian Point Point Intensity Intensity Intensity Intensity Number (exptl.) (calcd.) Number (exptl.) (calcd.) 0.0 3.1568 152.0 149.49 1 1 2 0.0 3.4179 2 134.0 143.91 0.0 3 3.7125 3 109.5 117.74 1.0 4 4.0466 89.5 88.130 5 2.0 4.4273 5 70.0 64.505 6 3.0 4.8638 6 54.0 47.817 7 4.0 5.3674 42.0 7 36.149 8 4.5 5.9541 8 32.0 27.999 9 5.2 6.6346 9 23.0 22.188 10 7.0 7.4434 10 17.5 17.973 8.2 11 8.4065 11 13.2 14.796 9.0 12 9.5546 12 10.5 12.370 13 10.5 10.960 7.5 10.496 13 14 12.2 12.690 14 5.5 8.9995 15 13.5 14.847 15 4.0 7.7964 16.5 16 17.552 16 3.8 6.8229 19.2 3.3 6.0130 17 21.056 17 18 24.0 25.641 18 2.5 5.3376 4.7729 19 30.0 31.695 2.0 19 39.0 20 1.5 4.2890 20 39.960

Table 16 (cont.)

Pure pyridine, December 20, 1971, No. 4; Right Brillouin peak, left hand side; fit to Lorentzian

Pure Pyridine, December 20, 1971, No. 4; Right Brillouin peak, right hand side; fit to Lorentzian

Point Number	Intensity (exptl.)	Intensity (calcd.)	Point Number	Intensity (exptl.)	Intensity (calcd.)
21	59.0	51.315	21	1.5	3.8745
22	76.0	66.803	22	1.0	3.5169
23	95.0	87.724	23	0.5	3.2086
24	116.5	113.42	24	0.0	2.9369
2 5	132.0	138.30	25	0.0	2.6981
26	149.0	151.15	26	0.0	2.4886
27	152.0	143.09	27	0.0	2.3012
			28	0.0	2.1340

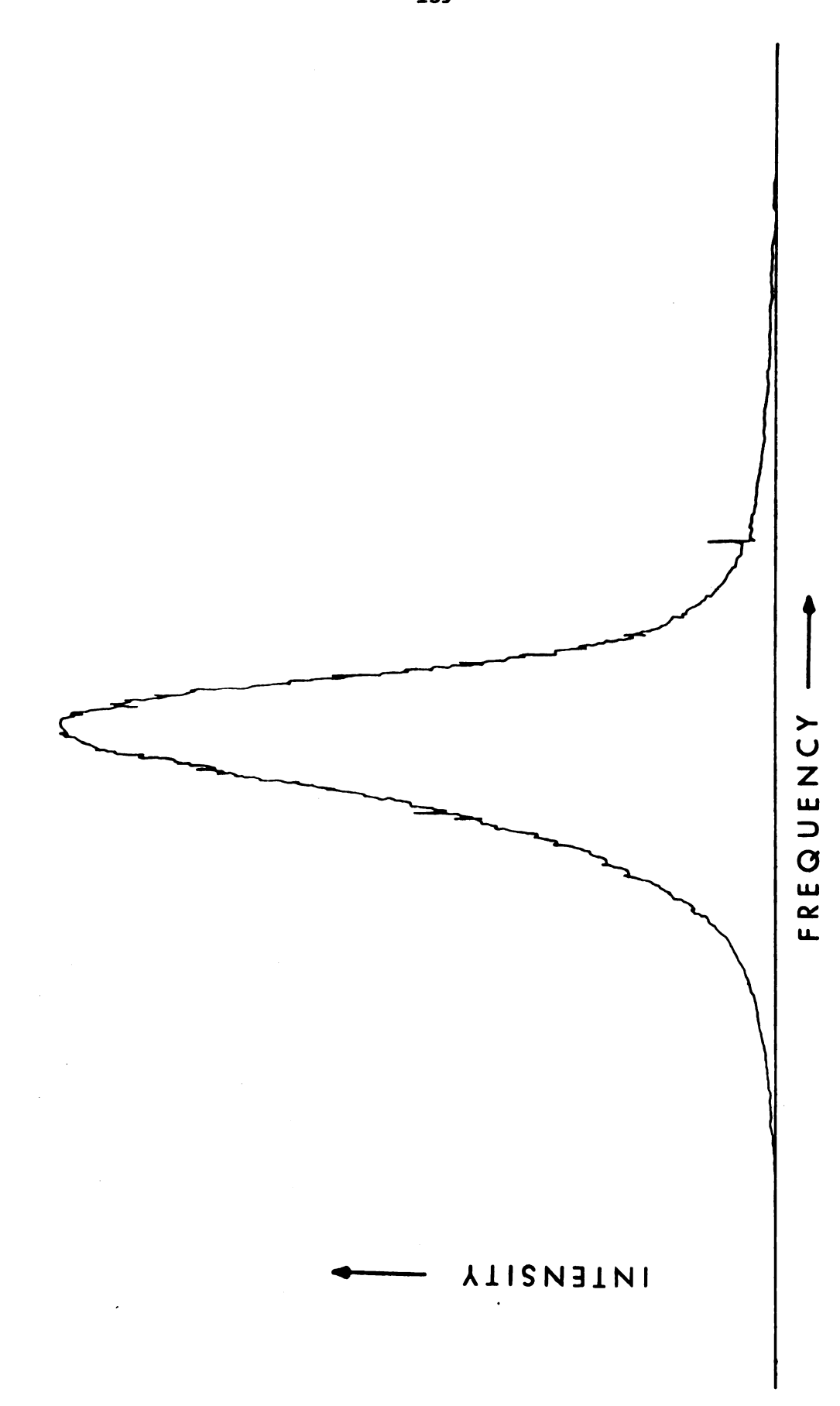


Figure 39. Laser-line instrumental profile, spectrum 1-b, August 17, 1971.

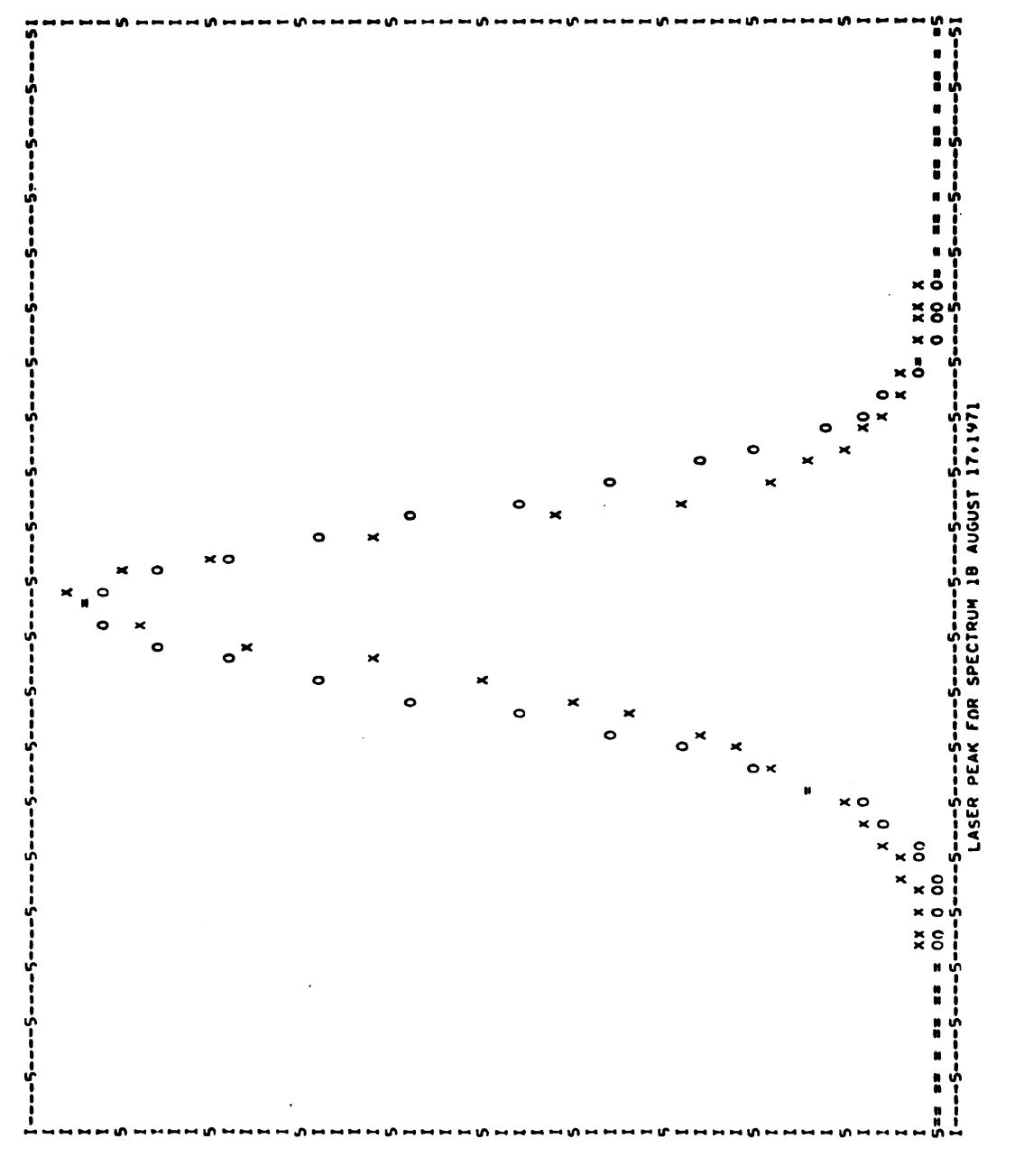
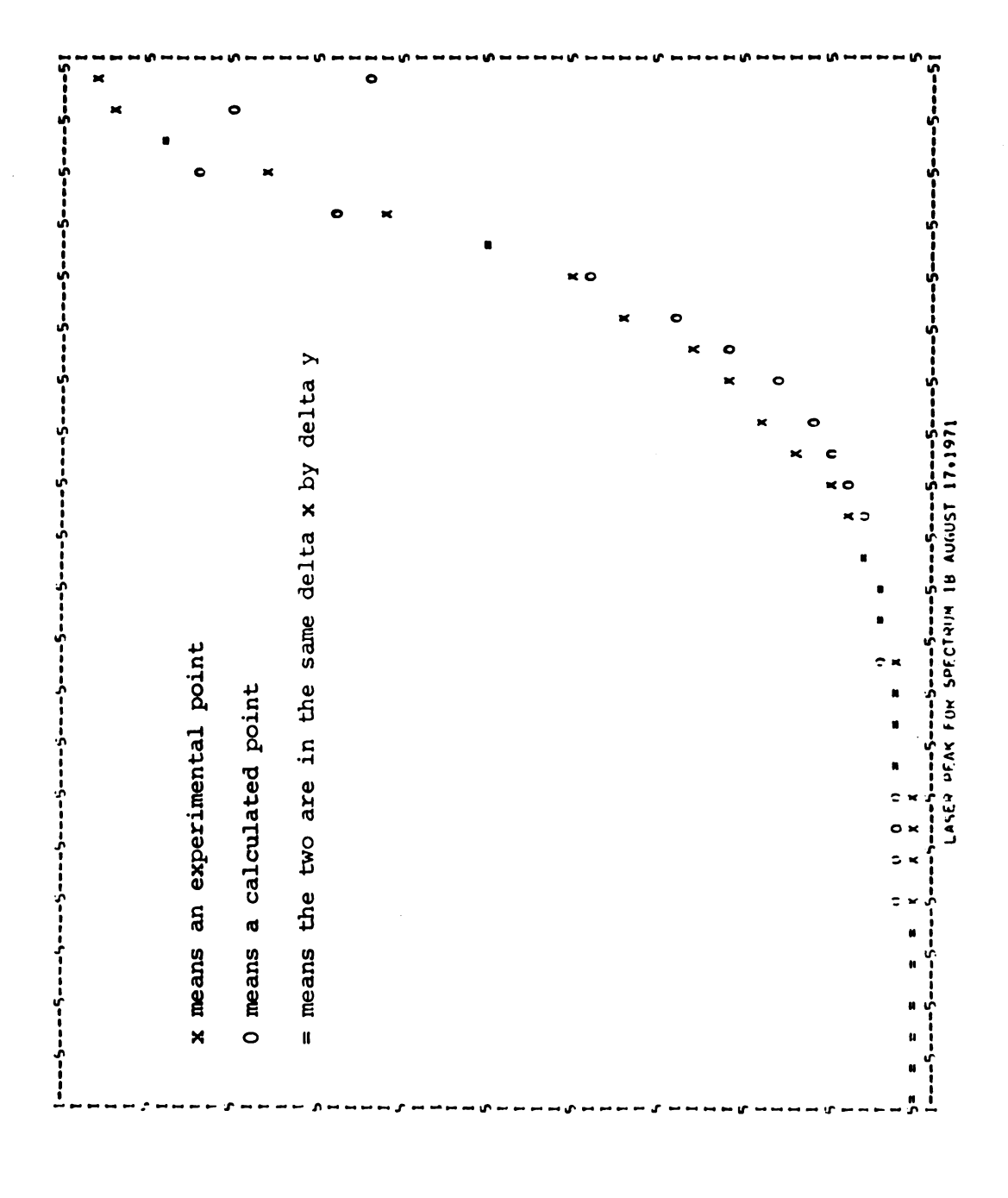
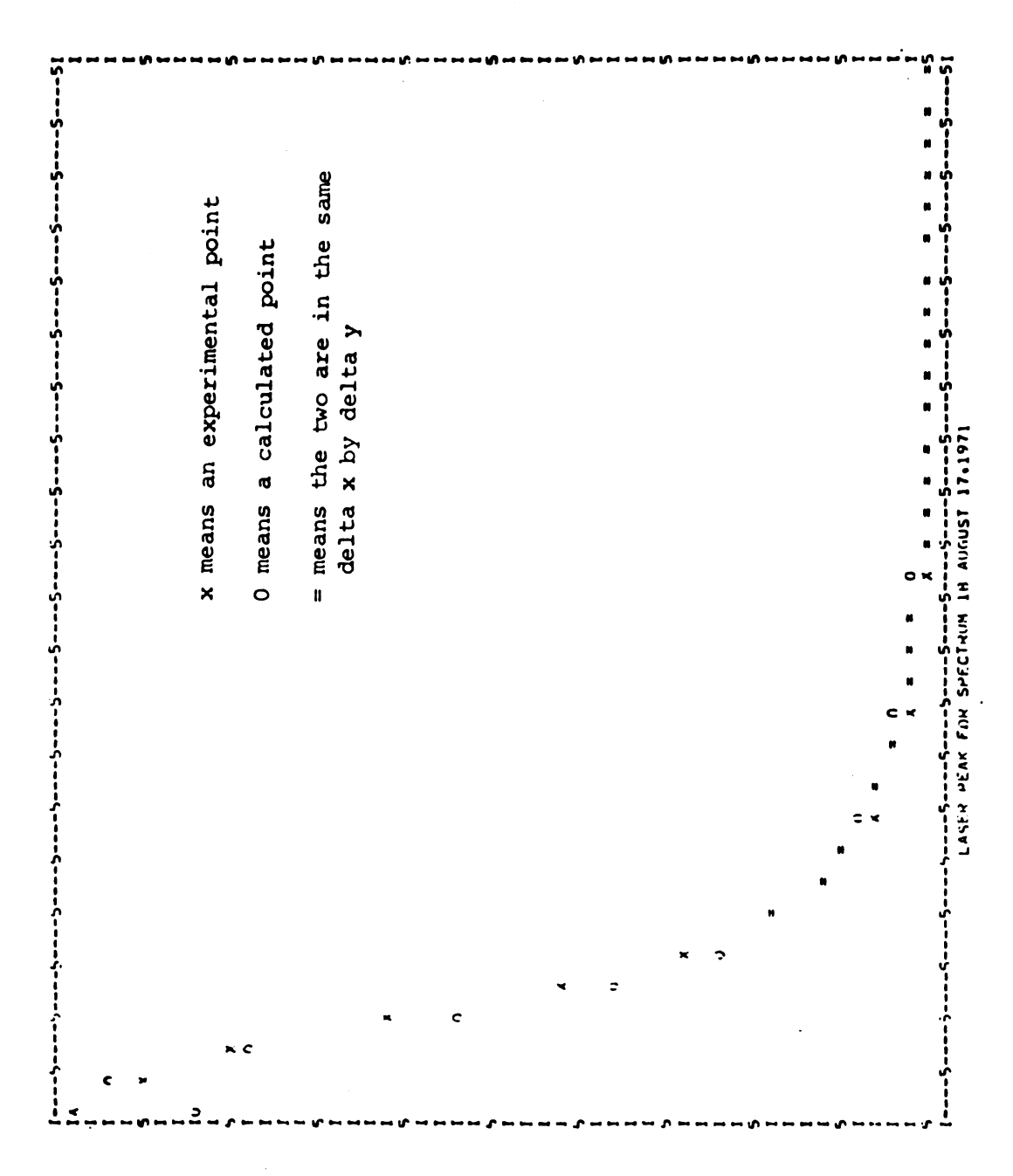


Figure 40. Laser-line instrumental profile, spectrum 1-b, August 17, 1971, fit to a Gaussian.



Left-hand side of laser-line instrumental profile, 1-b, August 17, 1971, fit to a Lorentzian. Figure 41.



Right-hand side of laser-line instrumental profile, 1-b, August 17, 1971, fit to a Lorentzian. Figure 42.



we call a "laser-line instrumental profile." This instrumental profile is for pure coherent light, whereas the instrumental profile of a scattering spectrum is the frequency distribution of incoherent scattered light.

As one can see from the graphical comparisons of the experimental profile to Gaussian and Lorentzian functions, the laser-line instrumental profile is Lorentzian in nature. The great difference between the experimental profile and the Gaussian distribution function helps to reinforce the conclusion that the experimental peaks for the 0.80 mole fraction DMSO mixture and for the two neat liquids are true Lorentzians.

Having proven that the experimental light scattering peaks are Lorentzians functions, the next step in the endeavor to simplify the analysis of the Brillouin linewidth data is to prove that the central peak of a Brillouin scattering spectrum is equivalent to the instrumental profile of the incoherent scattered light. One knows from statements in the Brillouin scattering literature (21), that the true Rayleigh linewidth is often a factor of 10^2-10^3 smaller than the observed linewidth of the central peak. In order to test the validity of this assumption for our particular case of the light scattering from binary mixtures of DMSO and pyridine, we compared the linewidths of the central peaks of several different solutions at a given finesse. We were cognizant of the fact that if the central peak were a true representation of the instrumental profile of the scattered light, we would obtain similar linewidth values for the various solutions. The linewidths of the central peaks for three solutions are listed in Table 17, and individual graphs of Γ_{C} versus finesse for each of the

Table 17

Linewidth of the Central Peak as a Function of Finesse

Pure DMSO

Date	Spectrum Number	Finesse	Γ _C (MHz)	Mirror Spacing, d(cm)
December 15, 1971	1-b	40.1	415	0.879
December 17, 1971	9	41.3	428	0.875
December 17, 1971	9	41.3	435	0.875
December 17, 1971	10	27.6	620	0.875
December 18, 1971	5	46.5	383	0.875
December 18, 1971	5	46.5	376	0.875
December 16, 1971	1	46.5	383	0.874
December 15, 1971	2	41.2	414	0.879
December 19, 1971	2	33.6	512	0.872
December 19, 1971	2	34.4	499	0.872
December 19, 1971	1	45.7	376	0.872
December 19, 1971	1	43.7	394	0.872

Table 17 (cont.)

Pure Pyridine

Date	Spectrum Number	Finesse	Γ _C (MHz)	Mirror Spacing, d(cm)
December 20, 1971	4	29.8	575	0.872
December 20, 1971	3	39.8	432	0.872
February 18, 1972	3	36.7	467	0.874
December 19, 1971	3	41.4	416	0.872
December 19, 1971	3	34.0	505	0.872
December 18, 1971	28	33.9	505	0.875
December 18, 1971	28	27.3	628	0.875
December 14, 1971	14	49.0	348	0.879
December 14, 1971	14	45.7	373	0.879
December 18, 1971	17	36.3	473	0.875
December 18, 1971	16	47.4	362	0.875
December 18, 1971	16	42.7	401	0.875
December 17, 1971	1	32.7	524	0.875
December 17, 1971	1	29.7	577	0.875

Table 17 (cont.)

0.40 Mole Fraction DMSO

Date	Spectrum Number	Finesse	Γ _C (MHz)	Mirror Spacing, d(cm)
January 3, 1972	7	27.3	622	0.882
January 3, 1972	6	37.8	450	0.882
January 10, 1972	19	38.2	449	0.875
January 10, 1972	20	28.8	595	0.875
January 10, 1972	7	32.8	522	0.875
January 10, 1972	8	26.8	639	0.875
January 8, 1972	9	32.0	533	0.878
January 8, 1972	8	40.2	425	0.878
January 9, 1972	14	33.6	502	0.875
January 9, 1972	13	41.1	417	0.875
January 9, 1972	7	44.3	387	0.875
January 9, 1972	8	31.8	539	0.875
January 3, 1972	11	35.2	483	0.882
January 2, 1972	6	34.4	493	0.882

three solutions are given in Figures 43-45.

A comparison is given in Table 18 of the full width at half height, $\Gamma_{\rm C}$, at a given finesse, for pure DMSO, pure pyridine, and 0.40 mole fraction DMSO. Considering that the standard deviation in a typical linewidth measurement is \pm 8 MHz, the values of $\Gamma_{\rm C}$ are in excellent agreement. We may conclude that the central peaks of our Brillouin scattering spectra are equivalent to the instrumental profiles of the scattered light at specific values of the finesse. In addition, we can couple this knowledge with the conclusion reached earlier that the peaks in a Brillouin scattering spectrum are Lorentzian, to arrive at the following equation for the true Brillouin linewidth, $2\Gamma_{\rm B}$:

$$2\Gamma_{B} = 2\Gamma_{B/obs} - \Gamma_{C} . \qquad (111)$$

In equation (111), $2\Gamma_{\rm B/obs}$ is the observed full width at half height of the Brillouin peak while $\Gamma_{\rm C}$ is the full width at half height of the central peak.

The results of the calculations of the Brillouin linewidths for each solution at the various temperatures are tabulated in Table 19. Typical plots of Brillouin linewidth versus temperature at a specific composition are shown in Figure 46. The Brillouin linewidth is found to decrease linearly with temperature for each composition. These results represent the first deliberate effort at correlating the variation in Brillouin linewidth with temperature for either pure or multicomponent fluids. The only other reported study concerning the change in Brillouin linewidth with temperature (64) was published in terms of the decrease in the frequency-corrected absorption coefficient, α/ν^2 , with temperature. No Brillouin linewidths were



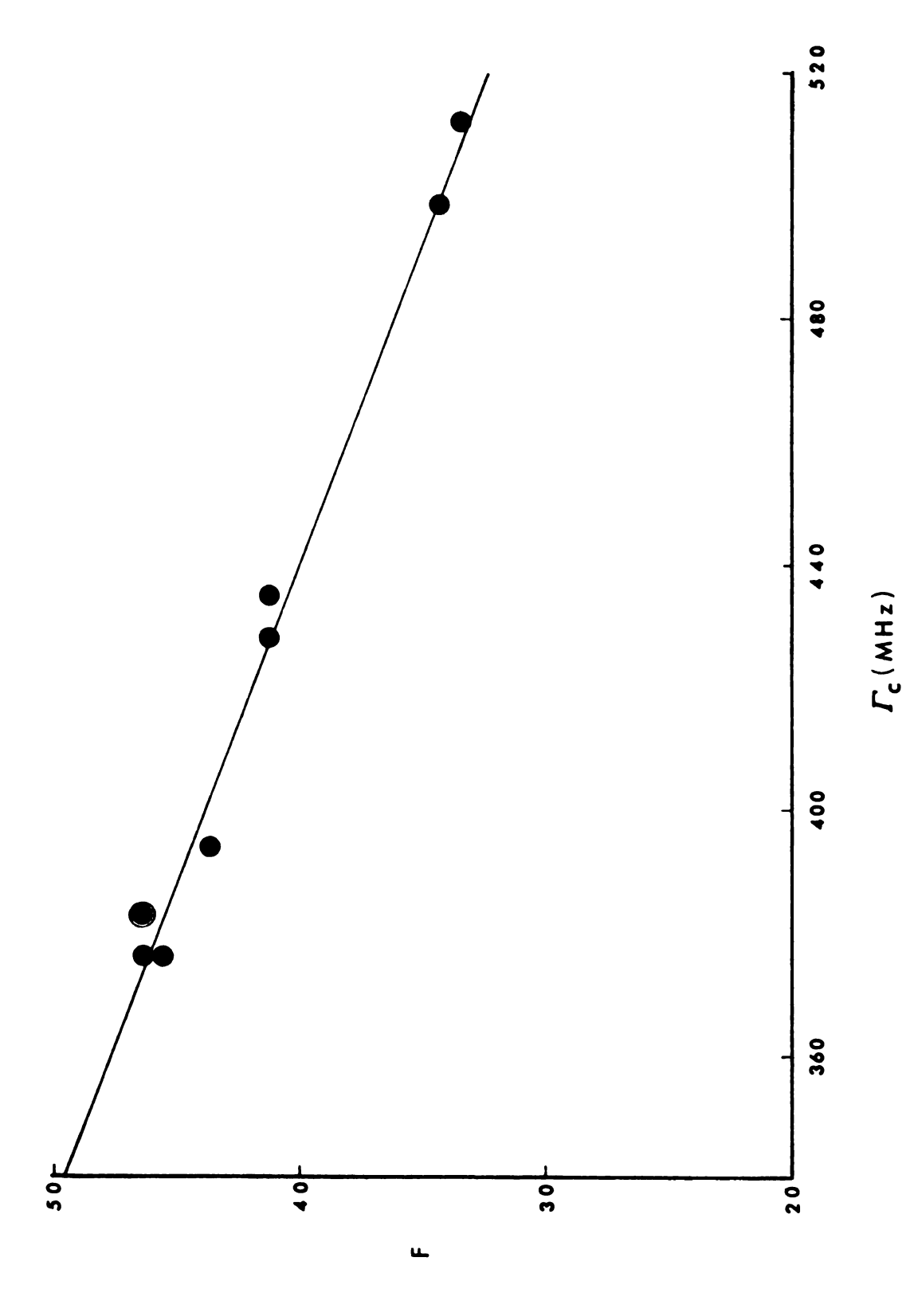


Figure 43. Linewidth versus finesse for central peak of neat DMSO.

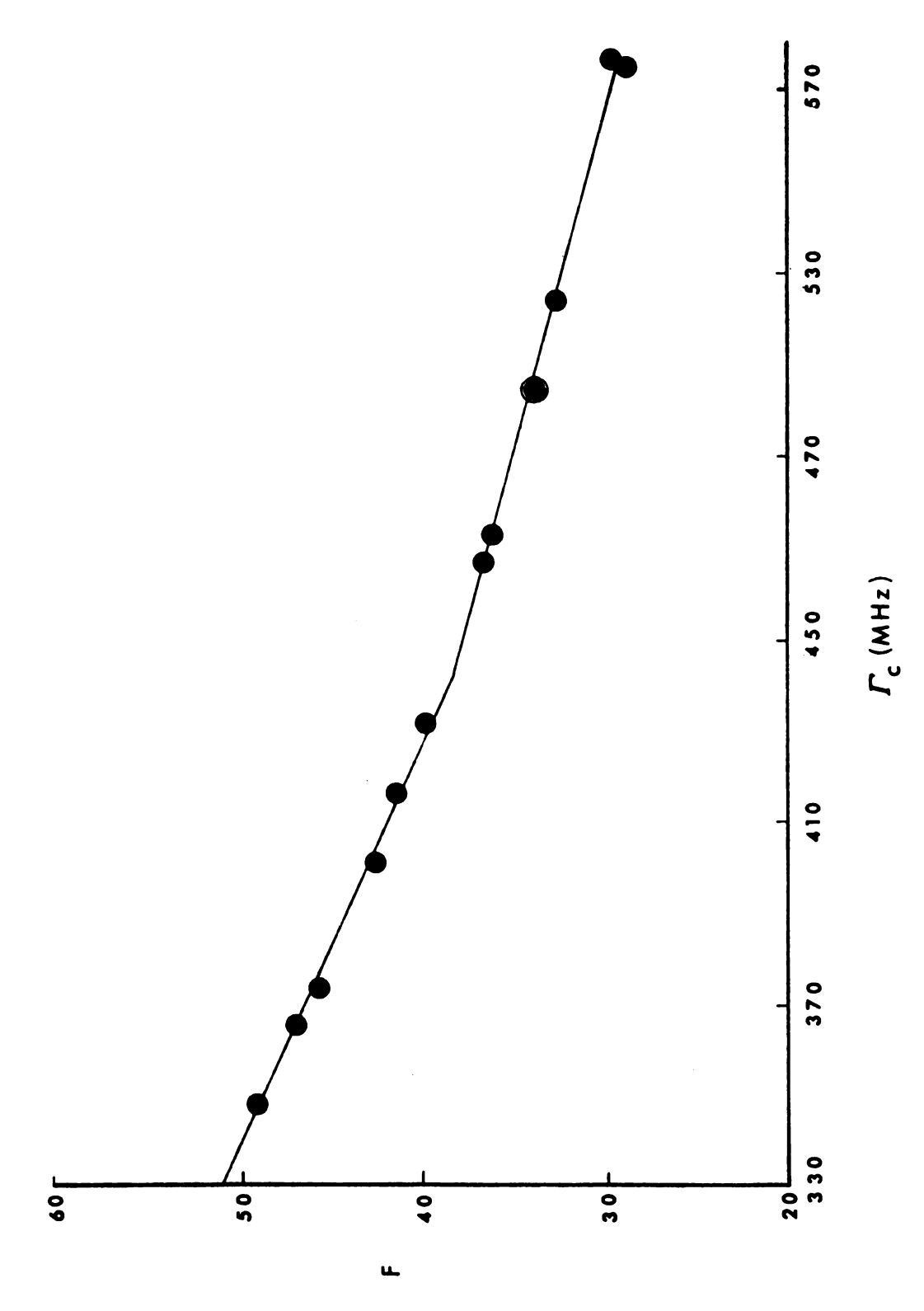


Figure 44. Linewidth versus finesse for central peak of neat pyridine.

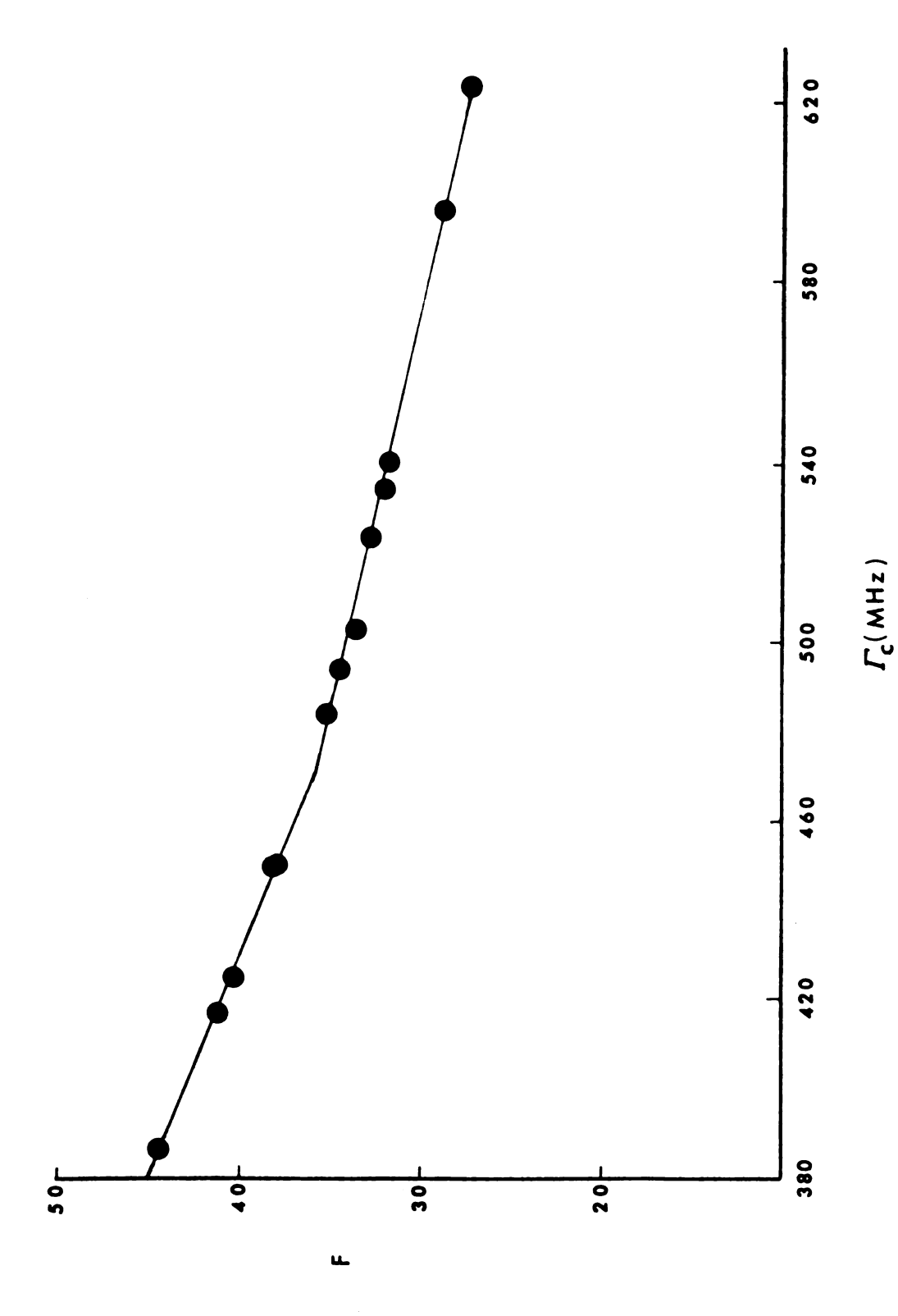


Figure 45. Linewidth versus finesse for central peak of 0.40 mole fraction DMSO.

Table 18

Comparison of the Linewidths of the Central Peaks of Neat DMSO,

Neat Pyridine and 0.40 Mole Fraction DMSO at a Given Finesse

Sample	Finesse	Full Width at Half Height of Central Peak (δ_C)
neat pyridine	45	382 ± 8 MHz
0.40 mole fraction DMSO	45	380
neat DMSO	45	387
	••	307
neat pyridine	43	400
0.40 mole fraction DMSO	43	400
neat DMSO	43	410
neat pyridine	41	419
0.40 mole fraction DMSO	41	419
neat DMSO	41	430
neat pyridine	39	436
0.40 mole fraction DMSO	39	439
neat DMSO	39	451
neat pyridine	36	477
0.40 mole fraction DMSO	36	468
neat DMSO	36	482
neat pyridine	35	491
0.40 mole fraction DMSO	35	484
neat DMSO	35	493
	- 4	
neat pyridine	34	506
0.40 mole fraction DMSO	34	502
neat DMSO	34	503
mant muniding	22	503
neat pyridine 0.40 mole fraction DMSO	33	521
neat DMSO	33	520 514
neac briso	33	514
neat pyridine	32	536
0.40 mole fraction DMSO	32	537
neat DMSO	32	525
		023
neat pyridine	30	565
0.40 mole fraction DMSO	30	572
		- · -

Table 19

Brillouin Linewidth as a Function of Temperature

for Mixtures of DMSO and Pyridine

	neat pyridine			0.05 mole fraction DMSO		
temp.(°C)	2Γ _B (MHz)	21 Bavg (MHz)	temp.(°C)	2Γ _B (MHz)	2F _B avg (MHz)	
21.6	454,498,448	467	21.6	472,459	466	
29.5	436,466,449	4 50	29.5	445,450	448	
34.5	441,437,439	439	34.5	432,435,435	434	
39.4	430,430,431	430	39.4	421,422	422	
44.5	415,404	410	44.5	396,407,422	408	
49.3	388,411	400	49.3	397,397	397	
54.2	406,374	3 90	54.2	397,390,381	389	
59.0	369,376,404	383				
0.	10 mole fract	ion DMSO	0.15	mole fractio	n DMSO	
21.6	459,4 69,459, 45 6	461	21.6	471,449,442, 468	458	
29.5	469,442,420, 439	442	29.5	401,450,475, 439	441	
34.5	439,423	431	34.5	426,424,441	430	
39.4	426,424	425	39.4	418,418	418	
44.5	411,407	409	44.5	401,407	404	
49.3	379,379,403, 410	393	49.3	406,384,390	393	
54.2	379,388,377	381	54.2	382,382	382	

Table 19 (cont.)

0.20 mole fraction DMSO			0.30	0.30 mole fraction DMSO		
temp. (°C)	2Γ _B (MHz)	2Γ _B avg(MHz)	temp.(OC)	2Γ _B (MHz)	2Γ _B avg(MHz)	
21.6	434,470,470	458	21.6	446,446	446	
29.5	441,436,436	438	29.5	432,435,417	428	
34.5	431,431,426	429	34.5	418,418,418, 418	418	
39.4	421,416	418	39.4	419,400,396	405	
44.5	396,412	404	44.5	402,386	394	
49.3	387,387	387	49.3	356,409	382	
54.2	39 4, 365,383, 377	380	54.2	398,349	373	
			59.0	364,358	361	
0.40	mole fractio	n DMSO	0.50	0.50 mole fraction DMSO		
21.6	429,460,436	442	21.6	4 36,440,443, 433	438	
29.5	429,403,435, 425	423	29.5	426,423,411	420	
34.5	411,418	414	34.5	396,417	406	
39.4	408,395	402	39.4	413,365,396, 400	394	
44.5	406,367,384	386	44.5	399,383,371	384	
49.3	398,355	376	49.3	394,348	371	
54.2	344,344,388, 398	368	54.2	359,356	358	
59.0	334,376	355	59.0	363,332	348	

Table 19 (cont.)

0.60 mole fraction DMSO			0.70 mole fraction DMSO		
temp.(°C)	2Γ _B (MHz)	2Γ _B avg(MHz)	temp.(OC)	2Γ _B (MHz)	2Γ _B avg(MHz)
29.5	393,414,422, 405,416,416	411	21.6	435,418,423, 423	425
34.5	412,398	405	29.5	406,406	406
39.4	372,372,412, 402	390	34.5	388,410,410, 388,382	396
44.5	37 4,37 0,388, 385,375	378	39.4	388,372,379, 391,387,387	384
49.3	385,385,349, 343,361	365	44.5	370,374,368 379,355	369
54.2	361,361, 356	359	49.3	371,370,354, 338	35 8
59.0	355,352,318, 355,353,320	342	54.2	332,355,351, 349	347
			59.0	335,335	335
0.80	mole fraction	DMSO	0.95	mole fraction	DMSO
29.5	430,388,404, 396,355,422	399	21.6	408,425,401 400,421	411
34.5	389,389,392, 396	392	29.5	394,394,401, 384	393
39.4	392,422,363, 337	378	34.5	380,370,402 379	383
44.5	349,367,370, 367,385	368	39.4	373,373	373
49.3	366,363,363, 335	357	44.5	366,318,395 349	357
54.2	318,348,348, 355	342	49.3	338,352,352	347
59.0	363,325,309	328	54.2	348,364,400, 231	336
			59.0	318,329	324

Table 19 (cont.)

neat DMSO

temp.(°C)	2Γ _B (MHz)	2Γ _B avg (MHz)	
21.6	407,407,390,417	405	
29.5	38 4,3 95	390	
34.5	394,350,382	375	
39.4	353,379,373	368	
44.5	363,346	354	
49.3	334,343	338	
54.2	337,323	330	
59.0	318,318	318	

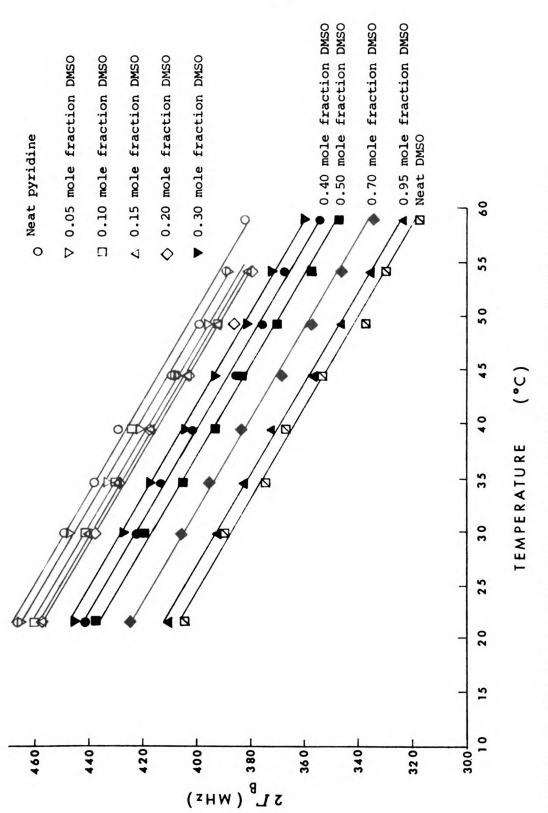


Figure 46. Brillouin linewidth versus temperature for mixtures of DMSO and pyridine.

given in this paper.

The Brillouin linewidth plotted against composition at a specific temperature yields another linear function. A typical graph of this type for T = 34.5 °C is shown in Figure 47. The linear nature of this graph is not a totally uninteresting result, in view of the fact that it is the first evaluation of the change in Brillouin linewidth with composition for a two-component fluid. The standard deviation for each point is shown on the graph; it was found that the average standard deviation for all the points is 8 MHz. The plots of Brillouin linewidth versus composition for each of the eight temperatures are found to be linear, as shown in Figure 48.

As interesting as this concentration dependence of the Brillouin linewidth is, the real significance of the Brillouin linewidths is manifested in the calculations of the sonic absorption coefficient, α , which are given in the next section.

F. Sonic Absorption Coefficient and Related Quantities

To complete the Brillouin scattering study of the acoustical properties of dimethyl sulfoxide-pyridine mixtures, the sonic absorption coefficient, α , and its frequency-corrected analogue, α/ν^2 , were calculated for thirteen mixtures at eight temperatures in the range 20 to 60 °C. Results of these calculations are shown in Table 20. The equation used to evaluate the absorption coefficient is

$$\alpha = \Gamma_{\rm B/V_{\rm S}} . \tag{112}$$

The frequency used in the determination of α/ν^2 is the Brillouin shift, or the frequency of the sound wave in the liquid.

Ultrasonic physicists regard the absorption of sound as being related to the effectiveness of the transfer of internal vibrational

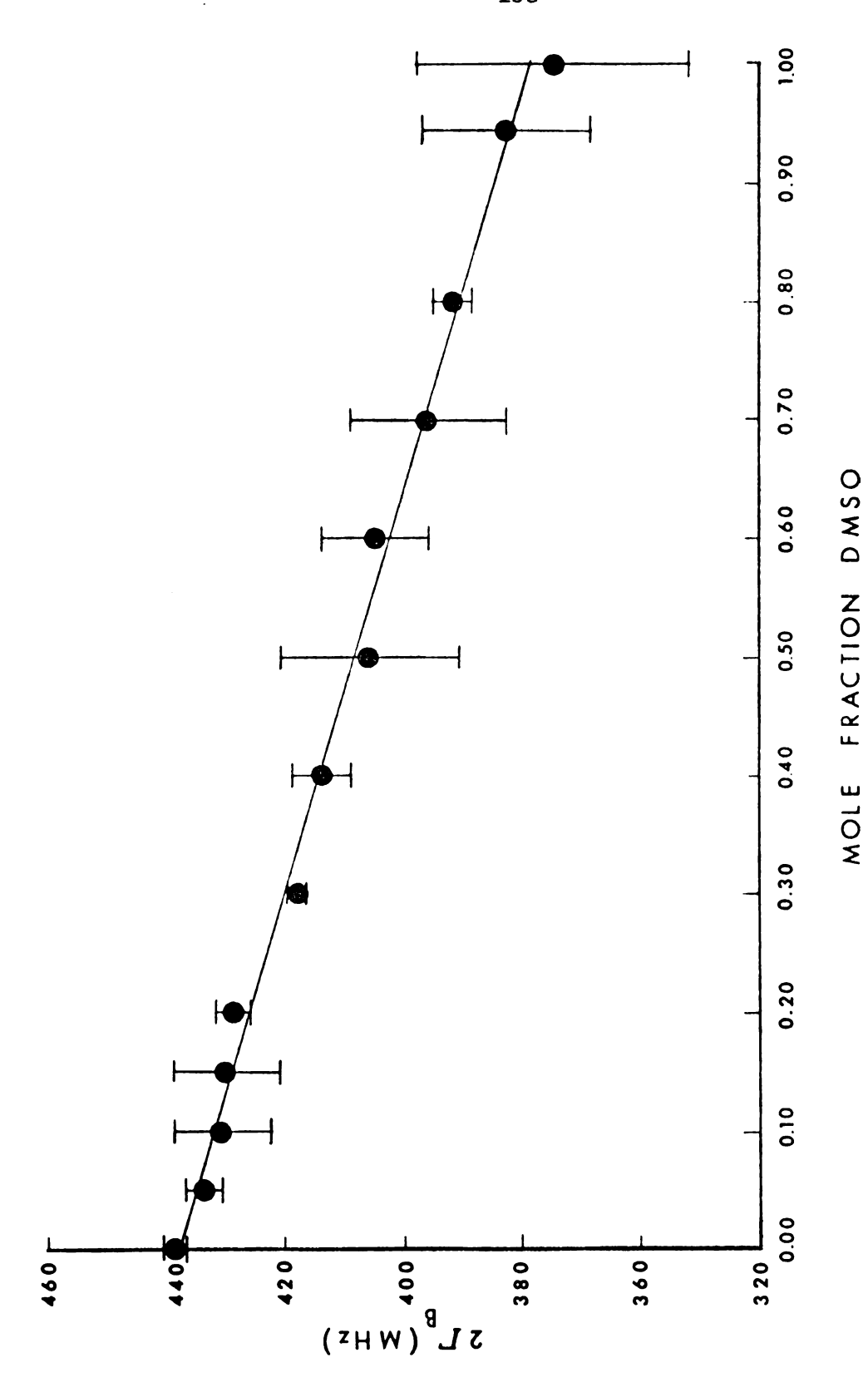


Figure 47. Brillouin linewidth versus composition for 34.5 $^{\rm o}{\rm C}_{\rm \cdot}$

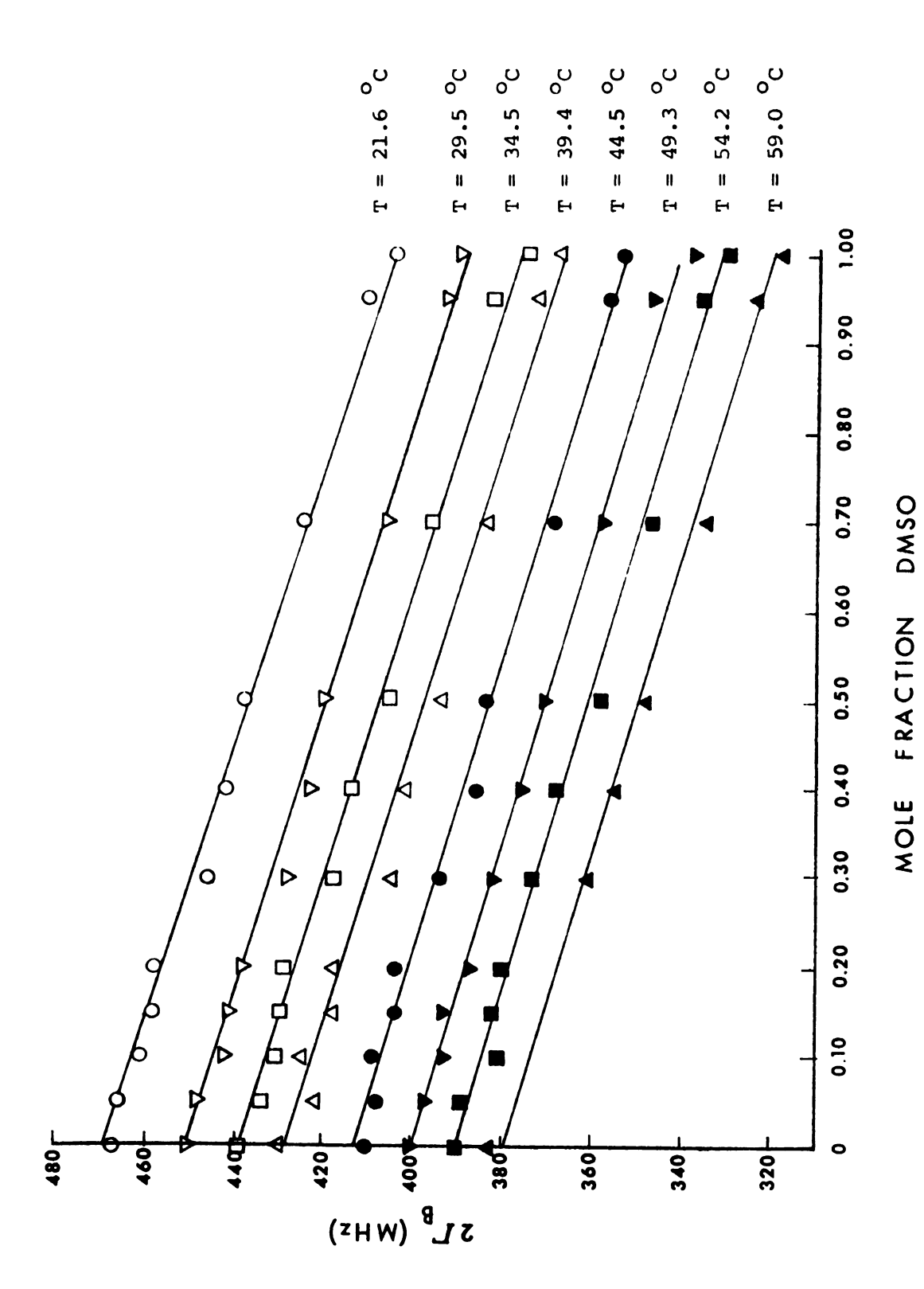


Figure 48. Brillouin linewidth versus composition for 21.6, 29.5, 34.5, 39.4,44.5,49.3,54.2 and 59.0 °C.



Table 20
Absorption Coefficient as a Function of Temperature
for Mixtures of DMSO and Pyridine

temp.	Brill. shift,v (GHz)	velocity of sound, V _S (m/sec)	Brillouin half-width Γ _B (MHz)	absorp. coeff., α(cm ⁻¹)	freq-correc. absorption coefficient, $\alpha/\nu^2 \times 10^{18}$ (sec ² /cm)			
pure C5H5N								
21.6	6.3 9	1530	234	1530	37.5			
29.5	6.27	1510	224	1480	37 .7			
34.5	6.19	1490	219	1470	38.4			
39.4	6.11	1480	213	1440	38.6			
44.5	6.03	1460	207	1420	39.0			
49.3	5.95	1440	202	1400	39.6			
54.2	5.87	1430	196	1370	39.8			
59.0	5.79	1410	190	1350	40.2			
0.05 mole fraction DMSO								
21.6	6.29	1510	233	1540	39.0			
29.5	6.17	1490	224	1500	39.5			
34.5	6.08	1470	217	1480	39.9			
39.4	6.01	1450	211	1460	40.3			
44.5	5.92	1430	205	1430	40.8			
49.3	5.85	1420	199	1400	40.9			
54.2	5.77	1400	193	1380	41.4			
59.0	5.69	1380						

Table 20 (cont.)

temp.	Brill. shift,v (GHz)	velocity of sound, V _S (m/sec)	Brillouin half-width Γ _B (MHz)	absorp. coeff., α(cm ⁻¹)	absorption coefficient, $\alpha/\nu^2 \times 10^{18}$ (sec ² /cm)
		0.10 mol	e fraction D	MSO	
21.6	6.27	1510	232	1540	39.1
29.5	6.12	1480	222	1500	40.0
34.5	6.02	1460	216	1480	40.8
39.4	5.92	1430	210	1470	41.9
44.5	5.82	1410	204	1450	42.8
49.3	5.73	1390	198	1420	43.4
54.2	5.63	1370	192	1400	44.2
59.0	5.54	1350			
		0.15 mol	e fraction D	MSO	
21.6	6.28	1510	230	1520	38.6
29.5	6.14	1480	220	1490	39.4
34.5	6.05	1460	214	1470	40.0
39.4	5.97	1450	208	1430	40.2
44.5	5.88	1430	202	1410	40.9
49.3	5.80	1410	197	1400	41.6
54.2	5.71	1390	191	1370	42.2
59.0	5.63	1380			

Table 20 (cont.)

temp.	Brill. shift,v	velocity of sound, V _S (m/sec)	Brillouin half-width Γ _B (MHz)	absorp. coeff., α(cm ⁻¹)	freq-correc. absorption coefficient, $\alpha/\nu^2 \times 10^{18}$ (sec ² /cm)
		0.20 mol	e fraction D	MSO	
21.6	6.17	1490	230	1540	40.4
29.5	6.05	1460	220	1510	41.2
34.5	5.97	1450	214	1480	41.5
39.4	5.89	1430	208	1450	41.8
44.5	5.81	1410	202	1430	42.4
49.3	5.74	1400	196	1400	42.5
54.2	5.66	1380	190	1380	43.1
59.0	5.59	1370			
		0.30 mol	e fraction D	MSO	
21.6	6.22	1500	223	1490	38.5
29.5	6.08	1470	214	1460	39.5
34.5	5.98	1450	208	1430	40.0
39.4	5.89	1430	203	1420	40.9
44.5	5.79	1410	197	1400	41.8
49.3	5 .7 0	1390	192	1380	42.5
54.2	5.61	1370	186	1360	43.2
59.0	5.52	1350	180	1330	43.6

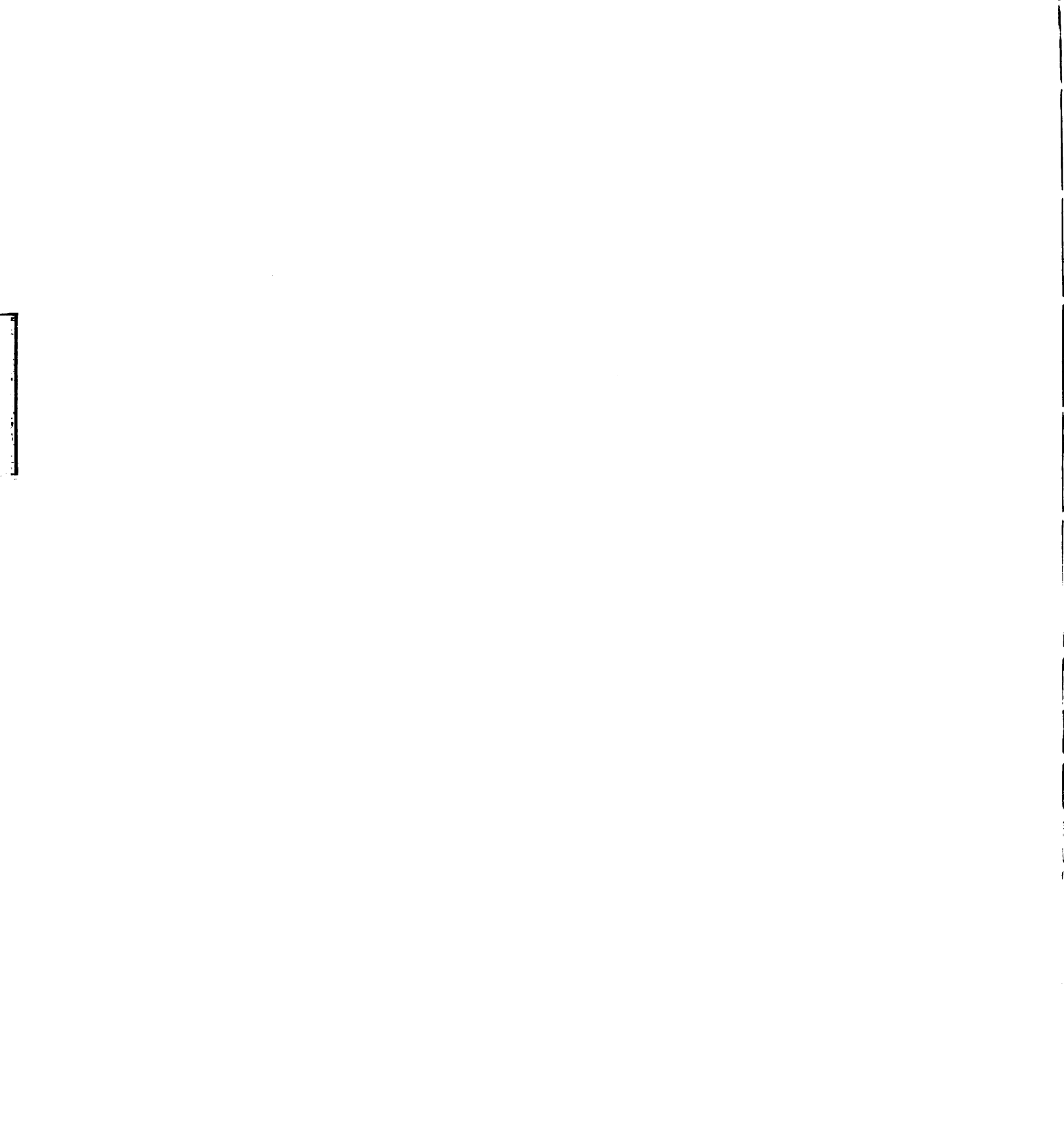


Table 20 (cont.)

temp.	Brill. shift,v (GHz)	velocity of sound, V _S (m/sec)	Brillouin half-width Γ _B (MHz)	absorp. coeff., α(cm ⁻¹)	freq-correc. absorption coefficient, $\alpha/\nu^2 \times 10^{18}$ (sec ² /cm)
		0.40 mol	e fraction D	MSO	
21.6	6.11	1480	221	1490	39.9
29.5	5.99	1450	212	1460	40.7
34.5	5.90	1430	206	1440	41.4
39.4	5.82	1420	200	1410	41.6
44.5	5.73	1400	194	1390	42.3
49.3	5.65	1380	189	1370	42.9
54.2	5.57	1360	183	1350	43.5
59.0	5.4 9	1340	178	1330	44.1
		0.50 mol	e fraction D	MSO	
21.6	6.02	1460	219	1500	41.4
29.5	5.90	1430	210	1470	42.2
34.5	5.82	1420	204	1440	42.5
39.4	5.7 5	1400	198	1410	42.6
44.5	5.67	1390	192	1380	42.9
49.3	5.59	1370	186	1360	43.5
54.2	5.51	1350	180	1330	43.8
59.0	5.44	1330	174	1310	44.3

Table 20 (cont.)

temp.	Brill. shift,v	velocity of sound, V _S (m/sec)	Brillouin half-width Γ _B (MHz)	absorp. coeff., α(cm ⁻¹)	freq-correc. absorption coefficient, $\alpha/\nu^2 \times 10^{18}$ (sec ² /cm)
		0.60 mol	e fraction D	MSO	
21.6	6.0 0	1460	216	1480	41.1
29.5	5.91	1440	206	1430	40.9
34.5	5.84	1430	201	1410	41.3
39.4	5.78	1410	195	1380	41.3
44.5	5.72	1400	189	1350	41.3
49.3	5.66	1390	184	1320	41.2
54.2	5.60	1380	178	1290	41.1
59.0	5.54	1360	172	1260	41.1
		0.70 mol	e fraction D	MSO	
21.6	6.05	1470	213	1450	39.6
29.5	5.92	1450	204	1410	40.2
34.5	5.83	1430	197	1380	40.6
39.4	5.75	1410	192	1360	41.1
44.5	5.66	1390	185	1330	41.5
49.3	5.57	1370	180	1310	42.2
54.2	5.49	1350	174	1290	42.8
59.0	5.41	1330	168	1260	43.0

Table 20 (cont.)

temp.	Brill. shift,v (GHz)	velocity of sound V _S (m/sec)	Brillouin half-width 「B(MHz)	absorp. coeff., α(cm ⁻¹)	freq-correc. absorption coefficient, $\alpha/\nu^2 \times 10^{18}$ (sec ² /cm)
		0.80 mol	e fraction D	MSO	
21.6	6.04	1470	210	1430	39.2
29.5	5.95	1460	200	1370	38.7
34.5	5.88	1440	195	1350	39.0
39.4	5.82	1430	189	1320	39.0
44.5	5.75	1410	184	1300	39.3
49.3	5.69	1400	178	1270	39.2
54.2	5.63	1390	172	1240	39.1
59.0	5.57	1380	166	1200	38.7
		0.95 mol	e fraction D	MSO	
21.6	6.13	1500	206	1370	36.5
29.5	6.00	1470	197	1340	37.2
34.5	5.92	1460	191	1310	37.4
39.4	5.83	1440	185	1280	37.7
44.5	5.75	1420	179	1260	38.1
49.3	5.67	1400	174	1240	38.6
54.2	5.59	1380	168	1220	39.0
59.0	5.51	1360	162	1190	39.2

Table 20 (cont.)

temp.	Brill. shift,v	velocity of sound V _S (m/sec)	Brillouin half-width 「B(MHz)	absorp. coeff., a(cm ⁻¹)	freq-correc. absorption coefficient, $\alpha/v^2 \times 10^{18}$ (sec ² /cm)
			pure DMSO		
21.6	6.11	1500	204	1360	36.4
29.5	5.99	1470	194	1320	36.8
34.5	5.91	1460	188	1290	36.9
39.4	5.84	1440	182	1260	36.9
44.5	5.75	1420	176	1240	37.5
49.3	5.68	1400	170	1210	37.5
54.2	5.60	1390	165	1190	37.9
59.0	5.53	1370	159	1160	37.9

energy to translational energy in a liquid. More specifically, it is believed that a greater amount of absorption will occur when collisions between the molecules in a liquid are inefficient in producing a transfer of energy. A high efficiency of transfer of internal vibrational energy to translational energy will result in a sustained propagation of the sound wave, or decreased absorption. The effectiveness of the molecular collisions, of course, is directly related to the degree of interaction between the molecules.

As the temperature of a liquid is changed the degree of order or structure of the liquid changes. Variation in the sonic absorption coefficient with temperature can be expected to reflect these alterations in structure, via alterations in the interactions between molecules.

Values for the temperature derivative of the sonic absorption coefficient were calculated for the thirteen DMSO-pyridine mixtures and are given in Table 21.

Table 21

Temperature Derivative of the Sonic Absorption Coefficient

mole fraction DMSO	(3\alpha/3\tau) (cm-1 \cdot 0C-1)
0.0000	-4.81
0.0495	-4.91
0.0993	-4.29
0.1506	-4.60
0.1983	-4.91
0.2997	-4.28
0.3995	-4.28
0.5005	-5.08
0.6002	-5.88
0.7001	-5.08
0.8004	-6.15
0.9453	-4.81
1.0000	-5. 35

The negative values of $\partial \alpha/\partial T$ render the mixtures "associated fluids" according to the classification scheme of Herzfeld and Litovitz (see p. 38). The sonic absorption coefficient as a function of temperature for a typical DMSO-pyridine mixture is illustrated in Figure 49. The absorption coefficient decreases linearly with an increase in temperature for all the solutions studied. The principal contribution to the error in these values is the error in measurement of the Brillouin linewidth.

A comparison of the measured sonic absorption coefficient and the calculated "classical" absorption coefficient (see p. 34) for DMSO at 25 OC reveals an unexpected result. The classical absorption coefficient can be evaluated from the equation

$$\alpha_{class} = \frac{8\pi^2 v_B^2}{3v_S^3 \rho} \left[\eta + \frac{3\lambda}{4c_p} (\gamma - 1) \right], \qquad (73)$$

where the first term in the brackets represents the shear viscosity of the medium and the second term involves thermal conduction parameters. For all liquids except liquid metals the heat conduction term is negligible (51,86), so that the classical absorption coefficient can be approximated by

$$^{\alpha} class = \frac{8\pi^2 v_B^2 \eta}{3V_s^3 \rho} . \tag{113}$$

For dimethyl sulfoxide at 25 $^{\rm O}{\rm C}$, one obtains a value of $\alpha_{\rm class} = 5320~{\rm cm}^{-1}$. The experimentally determined value of the sonic absorption coefficient is $\alpha_{\rm meas} = 1350 \pm 40~{\rm cm}^{-1}$. The ratio $\alpha_{\rm meas}/\alpha_{\rm class}$ is 0.254, which is much lower than would be expected from ultrasonic measurements for analogous associated fluids in lower frequency regions (51). This abnormally low value of $\alpha_{\rm meas}/\alpha_{\rm class}$

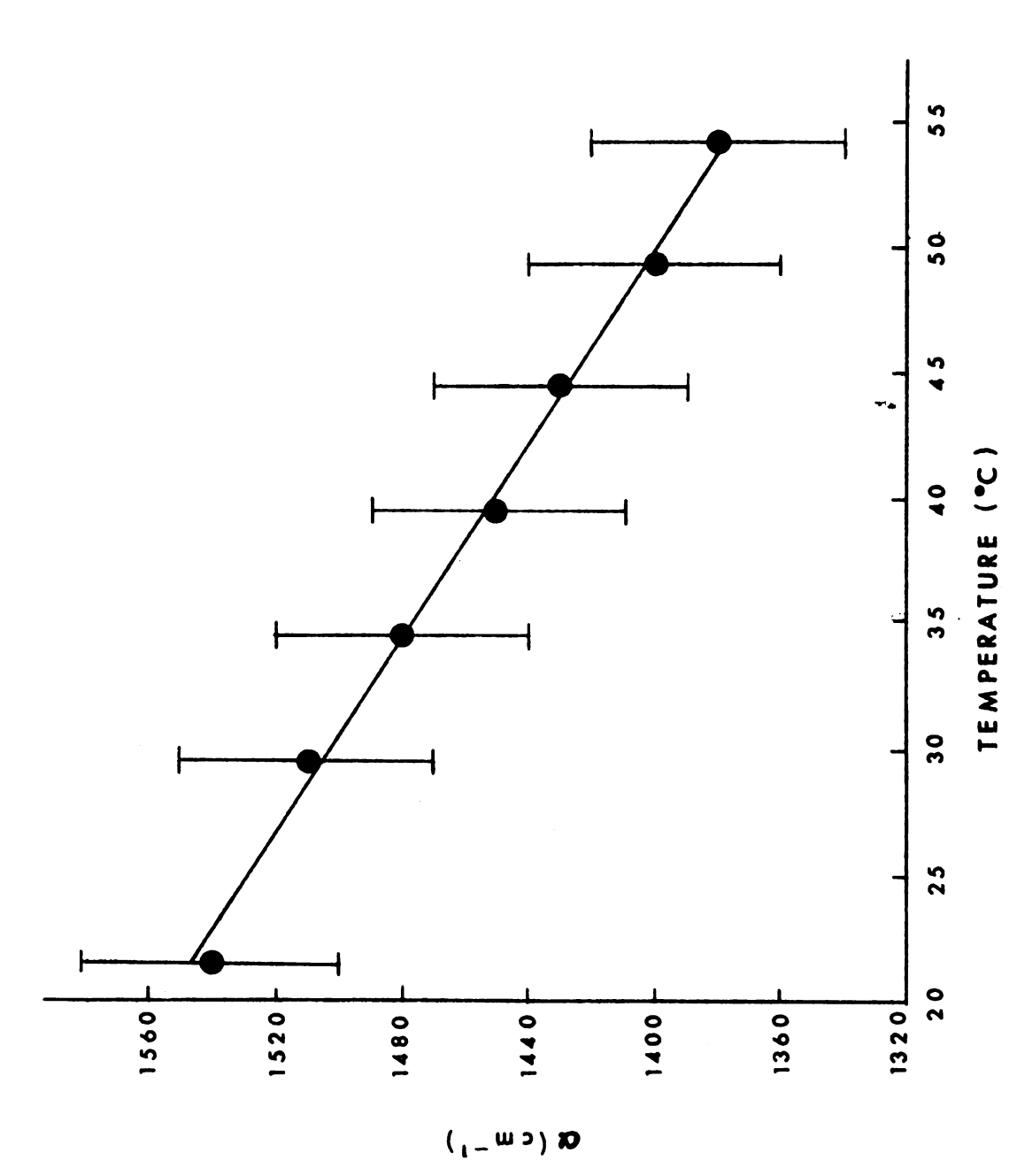


Figure 49. Absorption coefficient versus temperature for 0.20 mole fraction DMSO.

suggests that the relaxation mechanisms responsible for the absorption of ultrasonic waves in a liquid have response times that are slower than the period of the high frequency (~6 GHz) waves detected by Brillouin scattering.

Variation in the sonic absorption coefficient with composition for two different temperatures is plotted in Figures 50 and 51.

Within experimental error, the absorption coefficient is found to be a linear function of composition. As would be expected, the absorption coefficient reaches a minimum value for pure DMSO at each temperature. Highly associated neat DMSO is expected to possess a maximal amount of intermolecular interaction, thereby causing a minimal amount of absorption to take place.

Because the absorption coefficient usually varies with frequency, ultrasonics researchers prefer to use the term α/ν^2 , the frequency-corrected absorption coefficient, when reporting acoustical data. Typical plots of α/ν^2 versus temperature are exhibited in Figures 52 and 53. The change in the frequency-corrected absorption coefficient with temperature is found to be a monotonically increasing function for each of the solutions studied. The linearity of these plots again suggests that each of the DMSO-pyridine mixtures is behaving like a pure fluid with regard to temperature variations in the acoustical properties.

As in the case of the sonic absorption coefficient, the frequency-corrected absorption coefficient that is determined experimentally for pure DMSO at 25 $^{\circ}$ C is found to be ~1/4 the value calculated using the "classical" absorption coefficient, α_{class} , of equation (113). Instead of there being an "excess" absorption present in pure

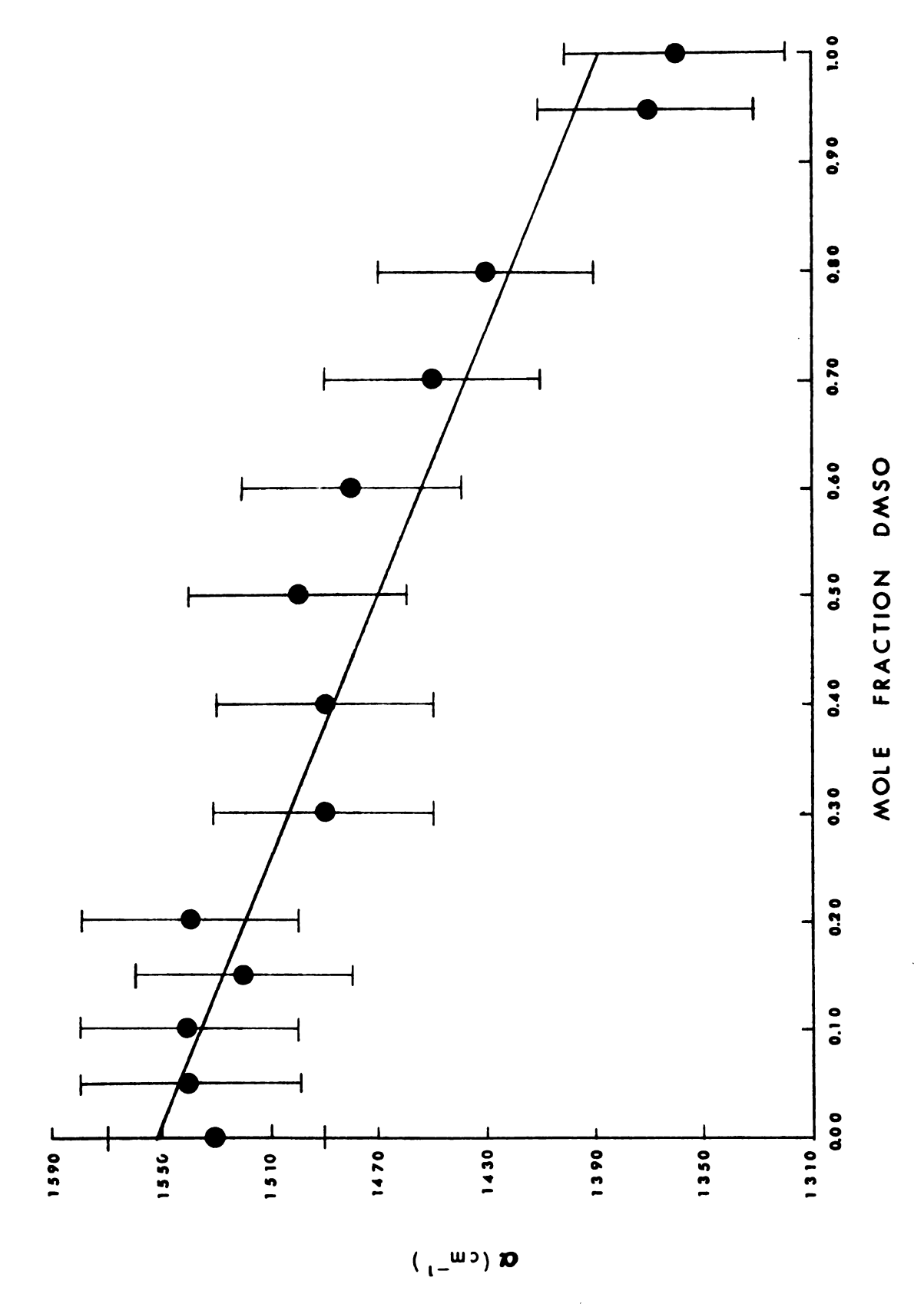


Figure 50. Absorption coefficient versus composition at 21.6 $^{\rm O}{\rm C}$.

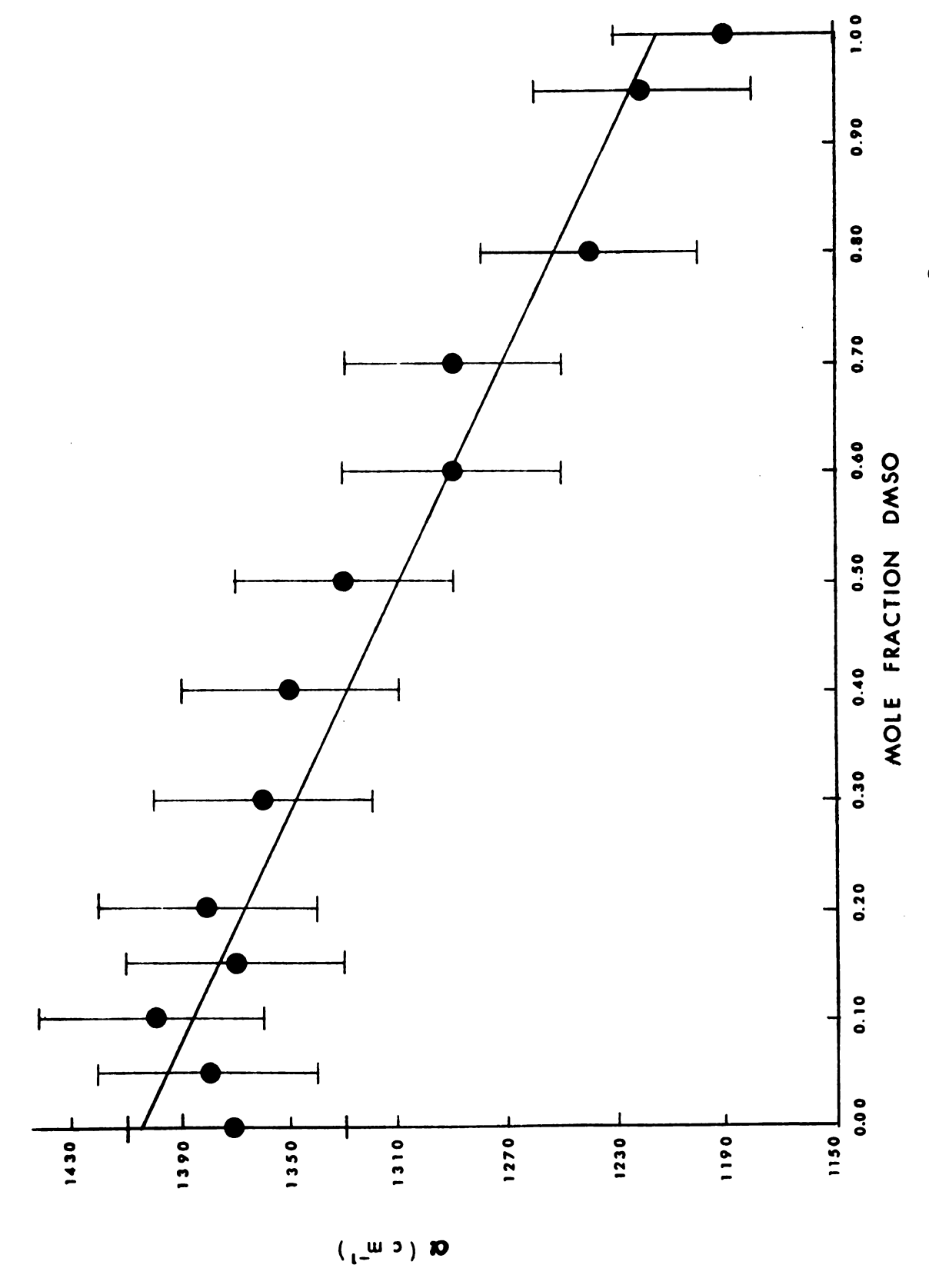


Figure 51. Absorption coefficient versus composition at 54.2 °C.

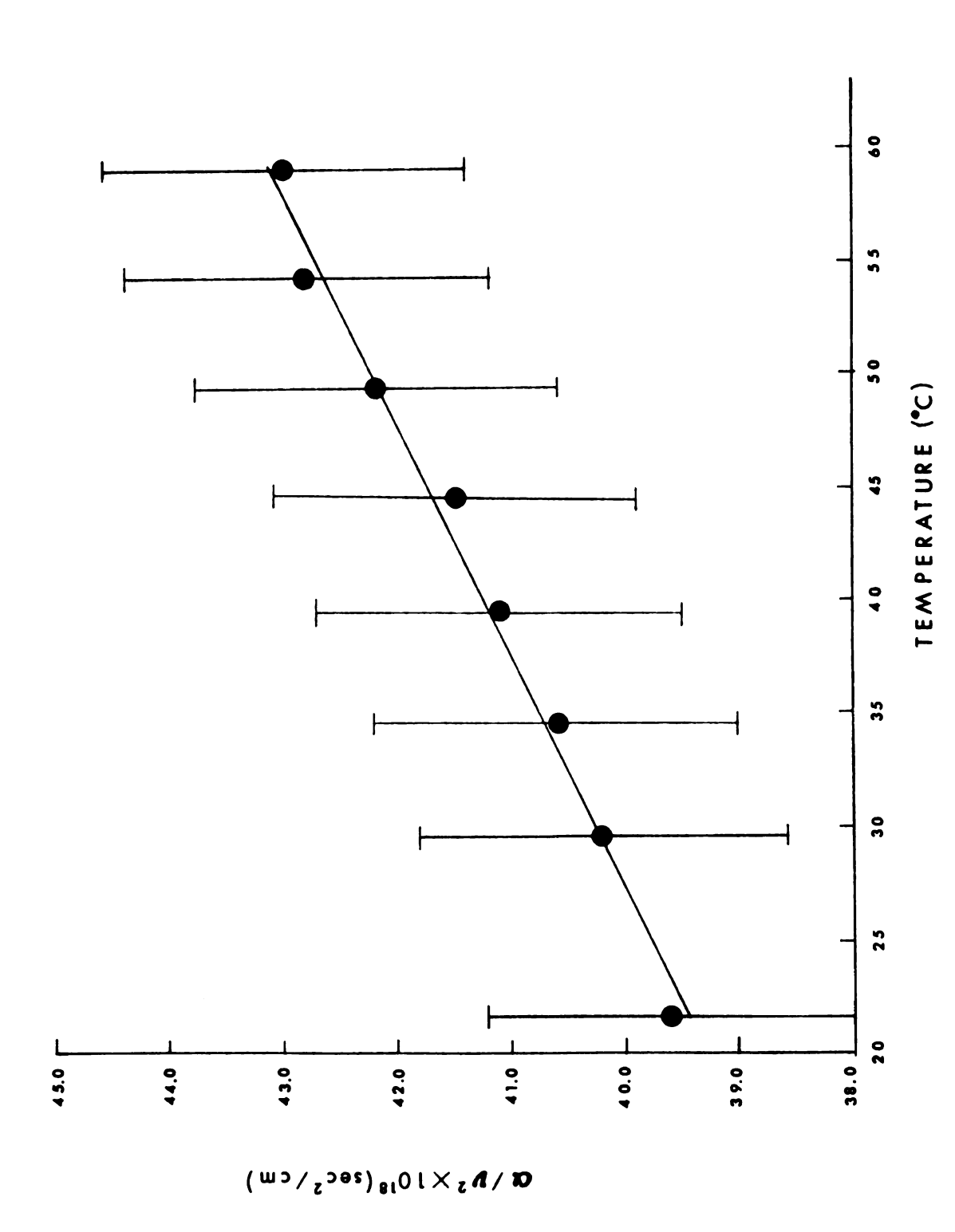
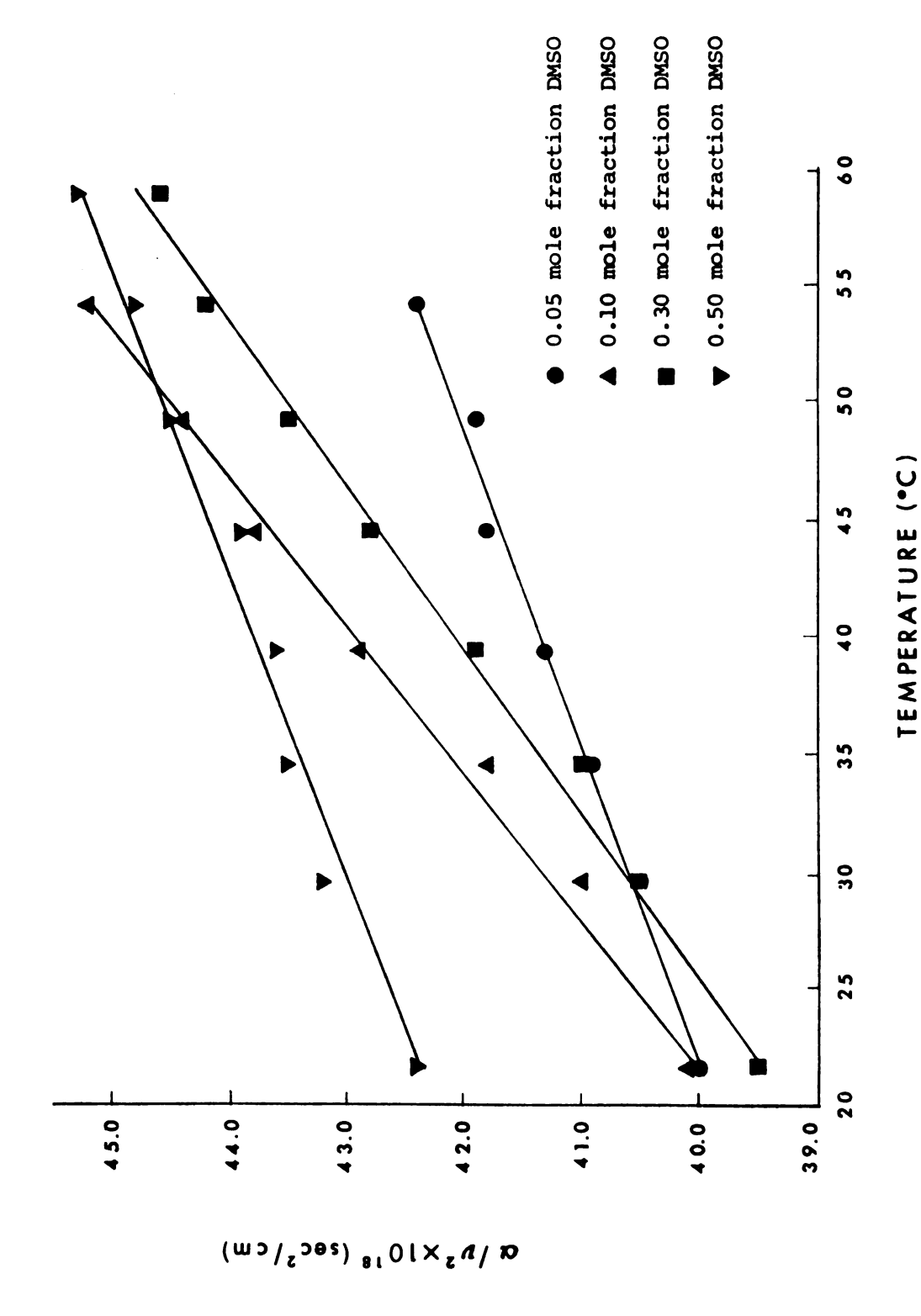


Figure 52. Frequency-corrected absorption coefficient versus temperature for 0.70 mole fraction DMSO.



Frequency-corrected absorption coefficient versus temperature for 0.05, 0.10, 0.30 and 0.50 mole fraction DMSO. Figure 53.

dimethyl sulfoxide at 25 °C as would be expected from ultrasonic theory for associated fluids (see pp. 38-39), there is actually a deficit of absorption for these high-frequency sound waves. Evidently the viscometric and structural relaxation mechanisms responsible for absorption of the lower frequency ultrasonic waves cannot absorb energy from the high frequency waves passing through the liquid. The hypersonic waves, therefore, suffer only minor attenuation.

The frequency-corrected absorption coefficient as a function of composition yields the set of curves shown in Figures 54-56. Although there are several persistent irregularities in the curves (especially in the region between 0.00 and 0.20 mole fraction DMSO), the lack of precision of these data prevents one from being able to assess the significance of the discontinuities. The overall increase in α/ν^2 between 0.00 and 0.50 mole fraction DMSO suggests an increase in disorganization of the liquid structure in this region; i.e., the local structure of neat pyridine is considerably more organized than the local structure of the 50-50 mole per cent mixture. If there is molecular association present, it is masked by the simultaneous repulsive interactions which are taking place. The drop in α/ν^2 between 0.50 and 1.00 mole fraction DMSO, however, indicates substantially increased association as one progresses from the 50-50 mole per cent mixture to pure DMSO.

For comparison purposes the frequency-corrected absorption coefficient and the velocity of sound are plotted in Figure 57 as a function of composition at 21.6 $^{\circ}$ C. On the next page (Figure 58) is a graph of α/ν^2 and the adiabatic compressibility versus composition at 21.6 $^{\circ}$ C. These two sets of curves reveal several interesting correlations between the frequency-corrected absorption coefficient and other properties of the DMSO-pyridine mixtures.

ĺ
\
, ,
I.
!

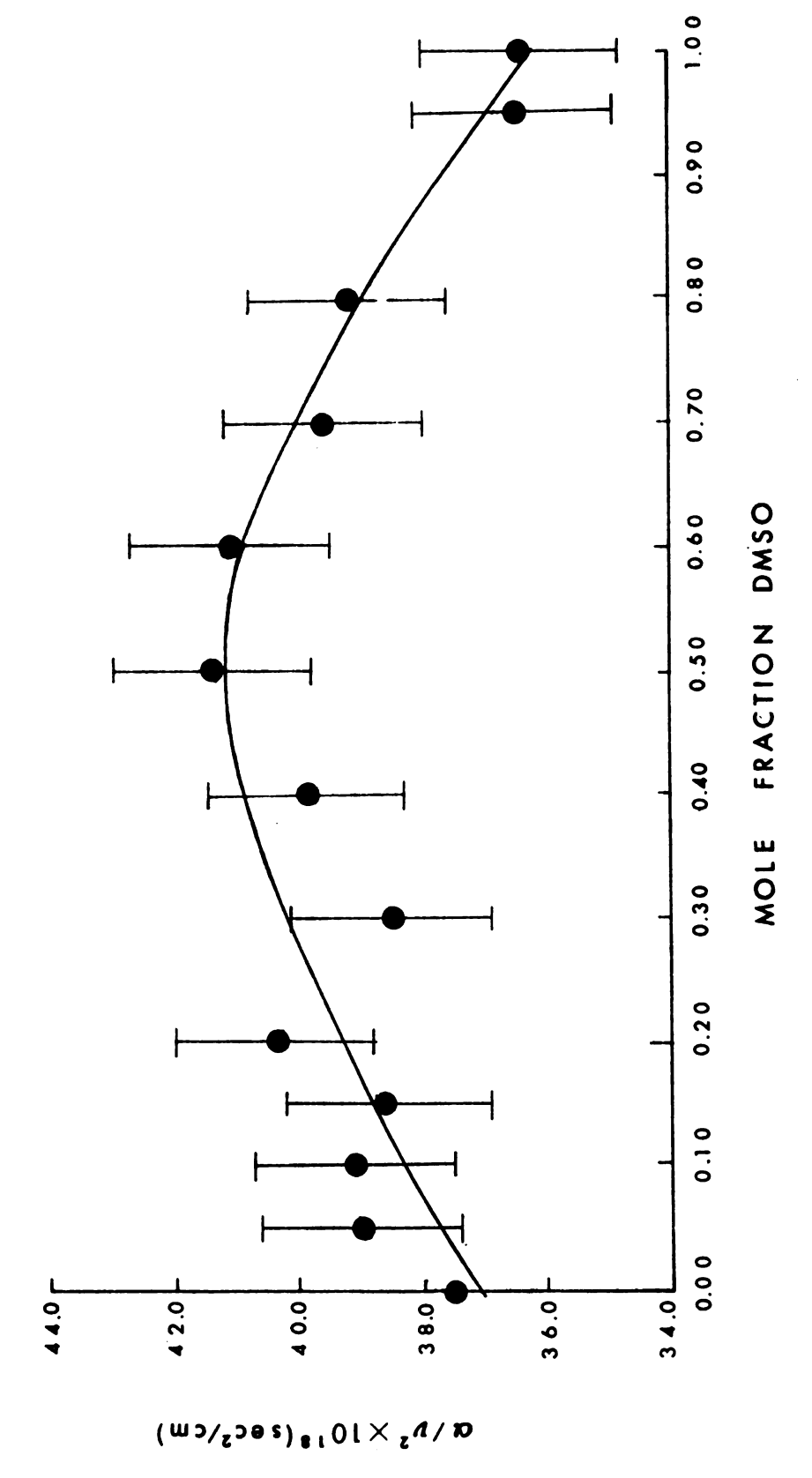


Figure 54. Frequency-corrected absorption coefficient versus composition at 21.6 °C.

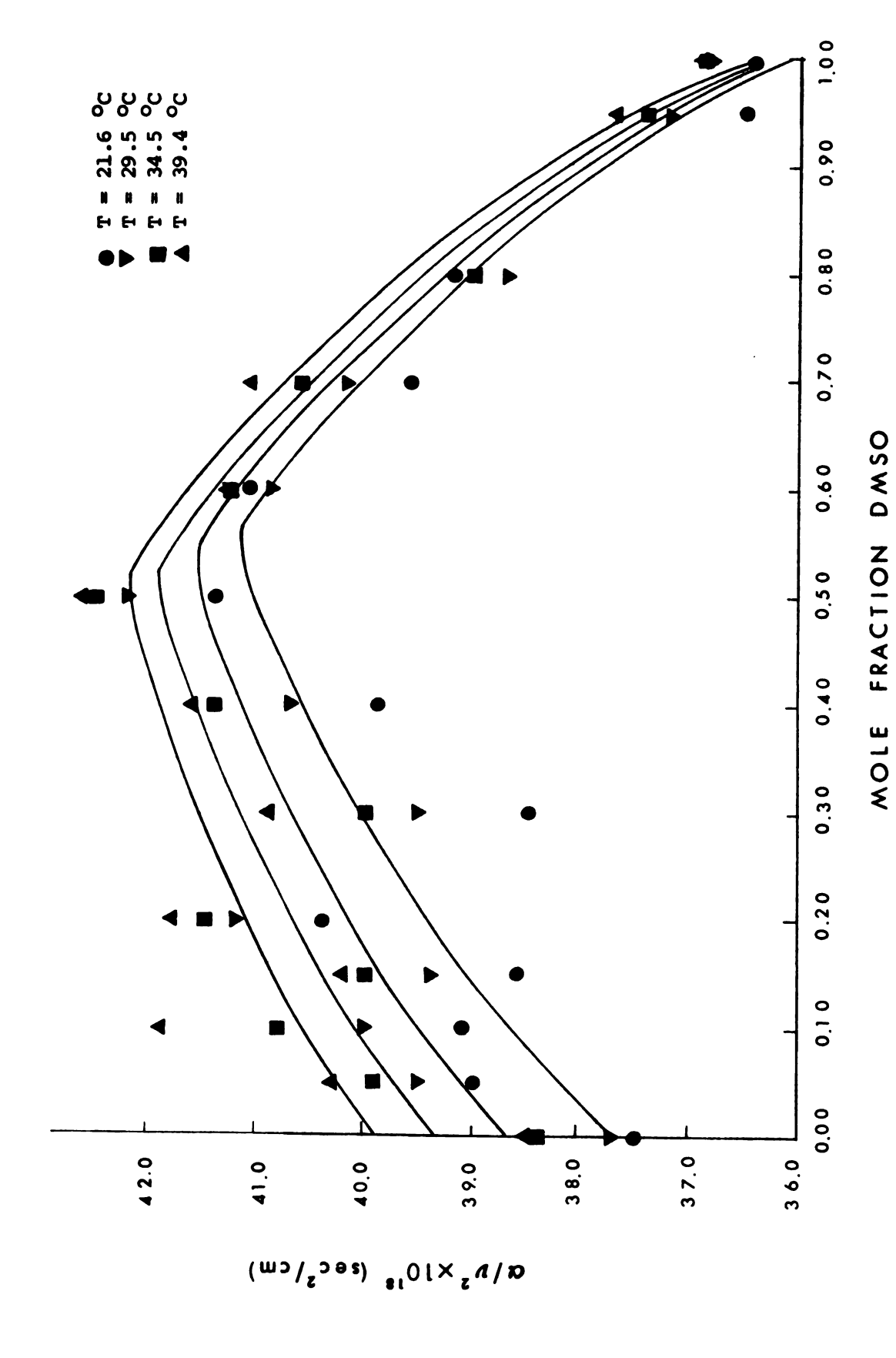


Figure 55. Frequency-corrected absorption coefficient versus composition for 21.6, 29.5, 34.5 and 39.4 °C.

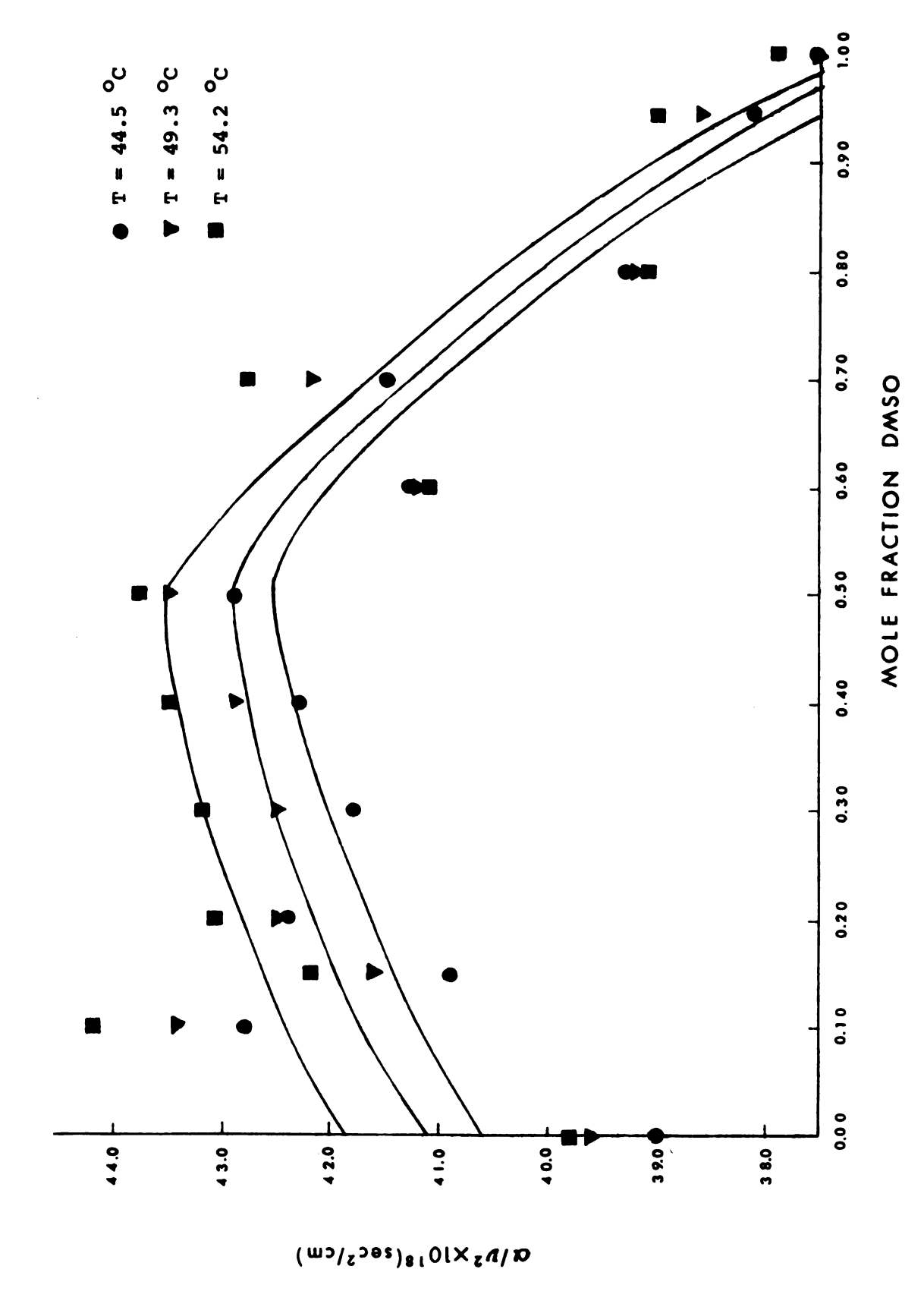
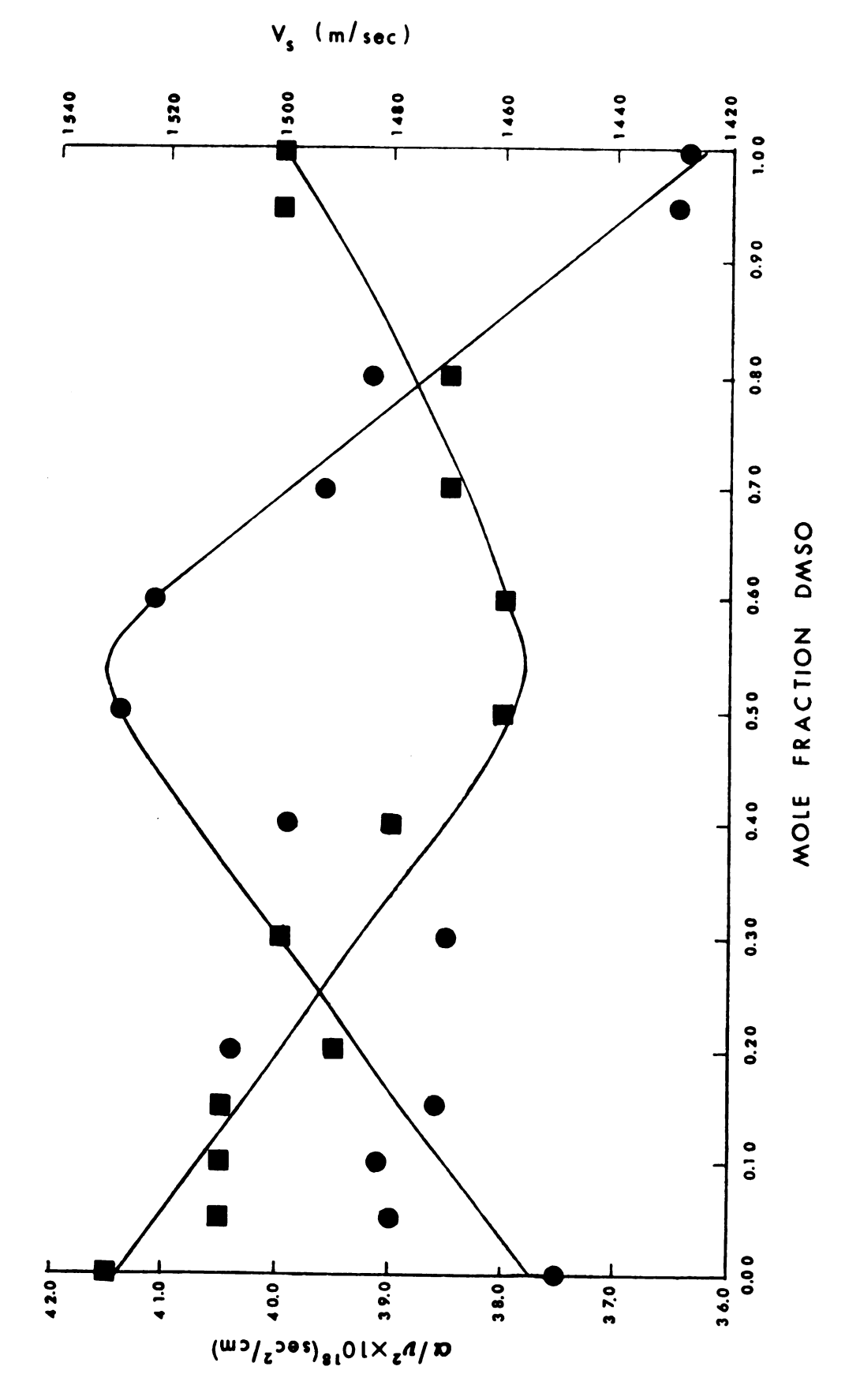
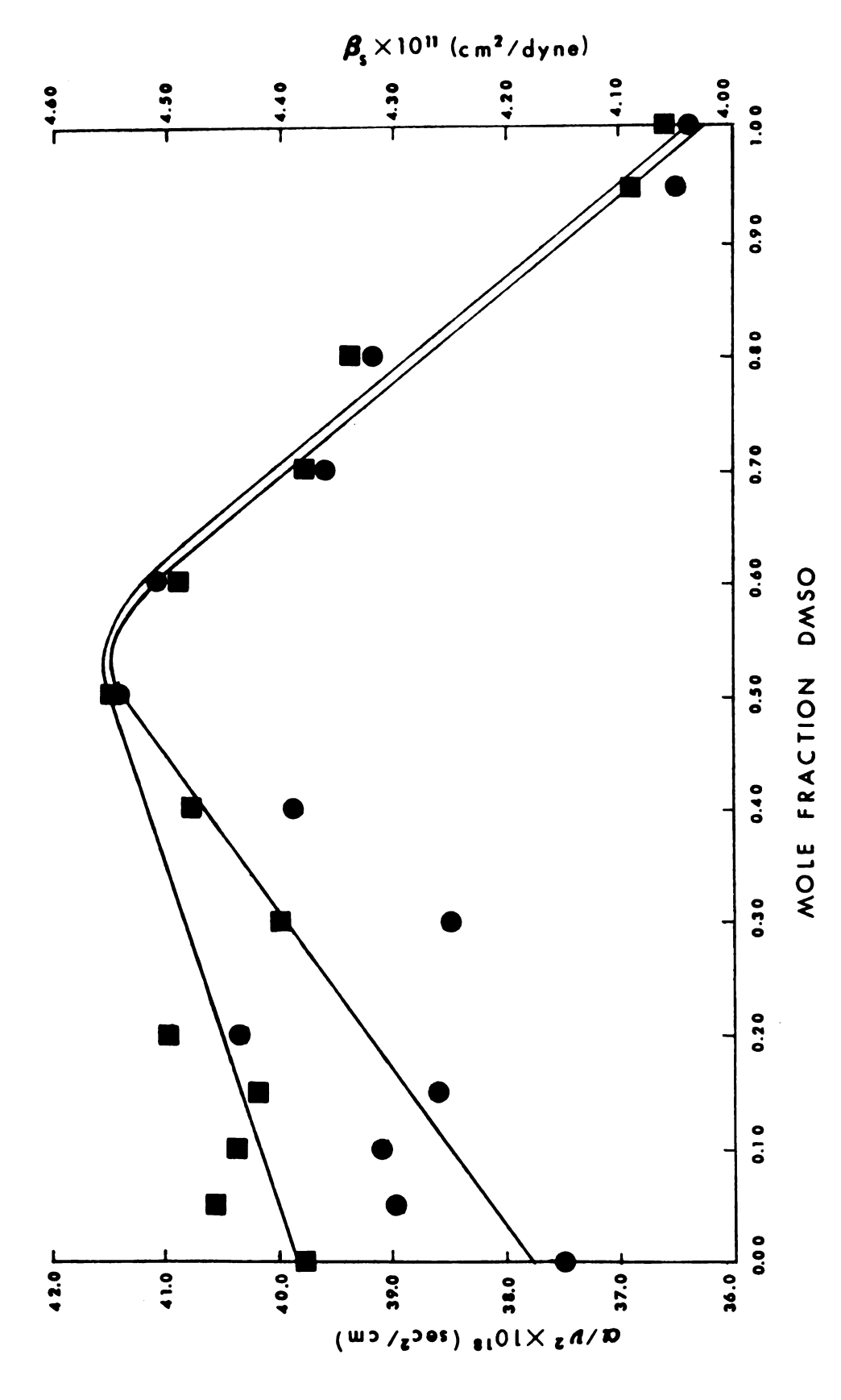


Figure 56. Frequency-corrected absorption coefficient versus composition for 44.5, 49.3 and 54.2 °C.



Velocity and absorption of sound for mixtures of DMSO and pyridine at 21.6 $^{\rm O}{\rm C}.$ Squares represent $V_{\rm S}$, circles represent $\alpha/\nu^2.$ Figure 57.



Absorption of sound and adiabatic compressibility for mixtures of DMSO and pyridine at 21.6 °C. Squares represent adiabatic compressibility, circles represent absorption of sound. Figure 58.

Examining Figure 57, one sees that the maximum of the α/ν^2 curve correspond to the minimum of the velocity of sound curve. This observation fits quite well with the concept of increased absorption being the result of inefficient transfer of internal vibrational energy to translational energy in the liquid, and decreased absorption being the result of efficient transfer of energy of sustained propagation of the sound wave between highly interacting molecular species.

Variations in α/ν^2 and β_s with composition at 21.6 °C follow the same trends, with the maximum in the α/ν^2 curve falling at the same x_1 value as the maximum for the β_s curve. These results indicate that changes in the adiabatic compressibility with intermolecular forces in an associated binary fluid are reflected accurately by changes in the frequency-corrected absorption coefficient. The structural changes which are presumed to account for the variations in both properties with composition have been elaborated in Section IV D.

G. Variation of the Landau-Placzek Ratio with Temperature and Composition

Although it had been hoped that a direct comparison could be made between the theoretical relationship for the Landau-Placzek ratio (equation (70)) and the values obtained experimentally for mixtures of dimethyl sulfoxide and pyridine, lack of information on quantities in the theoretical expression rendered this impossible. Consequently, only a semi-quantitative explanation for the change in Landau-Placzek ratio with temperature and composition is presented here.

Table 22 contains values for the Landau-Placzek ratio of DMSOpyridine solutions at seven temperatures. The effect of temperature

,
1

Table 22

Landau-Placzek Ratio as a Function of Temperature

for Mixtures of DMSO and Pyridine

T = 29.5	°c	T = 34.5	T = 34.5 °C		
mole fraction		mole fraction			
DMSO	RLP	DMSO	$\frac{R_{LP}}{}$		
0.00	0.56	0.00	0.60		
0.10	0.59	0.10	0.62		
0.15	0.65	0.15	0.67		
0.30	0.57	0.30	0.60		
0.40	0.61	0.40	0.66		
0.60	0.64	0.60	0.63		
0.80	0.72	0.80	0.71		
0.95	0.70	0.95	0.69		
1.00	0.45	1.00	0.46		
T = 39.4	°C	T = 44.5	°c		
0.00	0.63	0.00	0.67		
0.10	0.65	0.10	0.67		
0.15	0.69	0.15	0.71		
0.30	0.62	0.30	0.65		
0.40	0.71	0.40	0.77		
0.60	0.63	0.60	0.63		
0.80	0.70	0.80	0.69		
0.95	0.67	0.95	0.66		
1.00	0.46	1.00	0.47		

Table 22 (cont.)

T = 49.3 °C		T = 54.2 °C		
mole fraction DMSO	RLP	mole fraction DMSO	$^{ m R}_{ m LP}$	
0.00	0.70	0.00	0.74	
0.10	0.71	0.10	0.73	
0.15	0.73	0.15	0.75	
0.30	0.67	0.30	0.70	
0.40	0.82	0.40	0.87	
0.60	0.62	0 .60	0.62	
0.80	0.68	0.80	0.67	
0.95	0.65	0.95	0.64	
1.00	0.46	1.00	0.44	
T = 59.0	o °c			
0.00	0.77			
0.10	0.76			
0.15	0.77			
0.30	0.72			
0.40	0.93			
0.60	0.62			
0.80	0.67			
0.95	0.63			
1.00	0.43			

on the Landau-Placzek ratio for the two neat liquids and one of their mixtures is illustrated in Figures 59-61. The most surprising of these graphs is the one for pure DMSO. There is a distinct break in the curve at 45 °C, indicating a change in the degree of association in the liquid at this temperature. An analogous discontinuity observed by Schlafer and Schaffernicht (6) for refractive index data of pure DMSO between 40 and 50 °C was interpreted to signify a breakup in association of the DMSO molecules.

It should be noted in Figures 59-61 that although the Landau-Placzek ratio increases with temperature for the two pure fluids (up to 45 $^{\circ}$ C), $I_{\text{C}}/2I_{\text{B}}$ decreases with temperature for the 0.80 mole fraction DMSO mixture.

The compositional dependence of the Landau-Placzek ratio for temperatures in the range 29-59 °C is shown in Figure 62. The Landau-Placzek ratio is seen to decrease between 0.00 and 0.60 mole fraction DMSO, increase slightly between 0.60 and ~ 0.90 and finally plummet between 0.90 and 1.00 mole fraction DMSO to a minimum value for pure DMSO at all temperatures.

In an attempt to explain the significance of the compositional dependence of the Landau-Placzek ratio, we turn to equation (70), which was derived for the specific case of a binary mixture at constant temperature. According to equation (70), the Landau-Placzek ratio is dependent upon several physical and thermodynamic properties, including ρ , β_S and β_T . It is also dependent upon the infinite-and zero-frequency sound velocities, c_{∞} and c_{0} , respectively, for which we have no data.

At 21.6 °C we have values for the density and adiabatic compressibility, so that a semi-quantitative comparison can be made

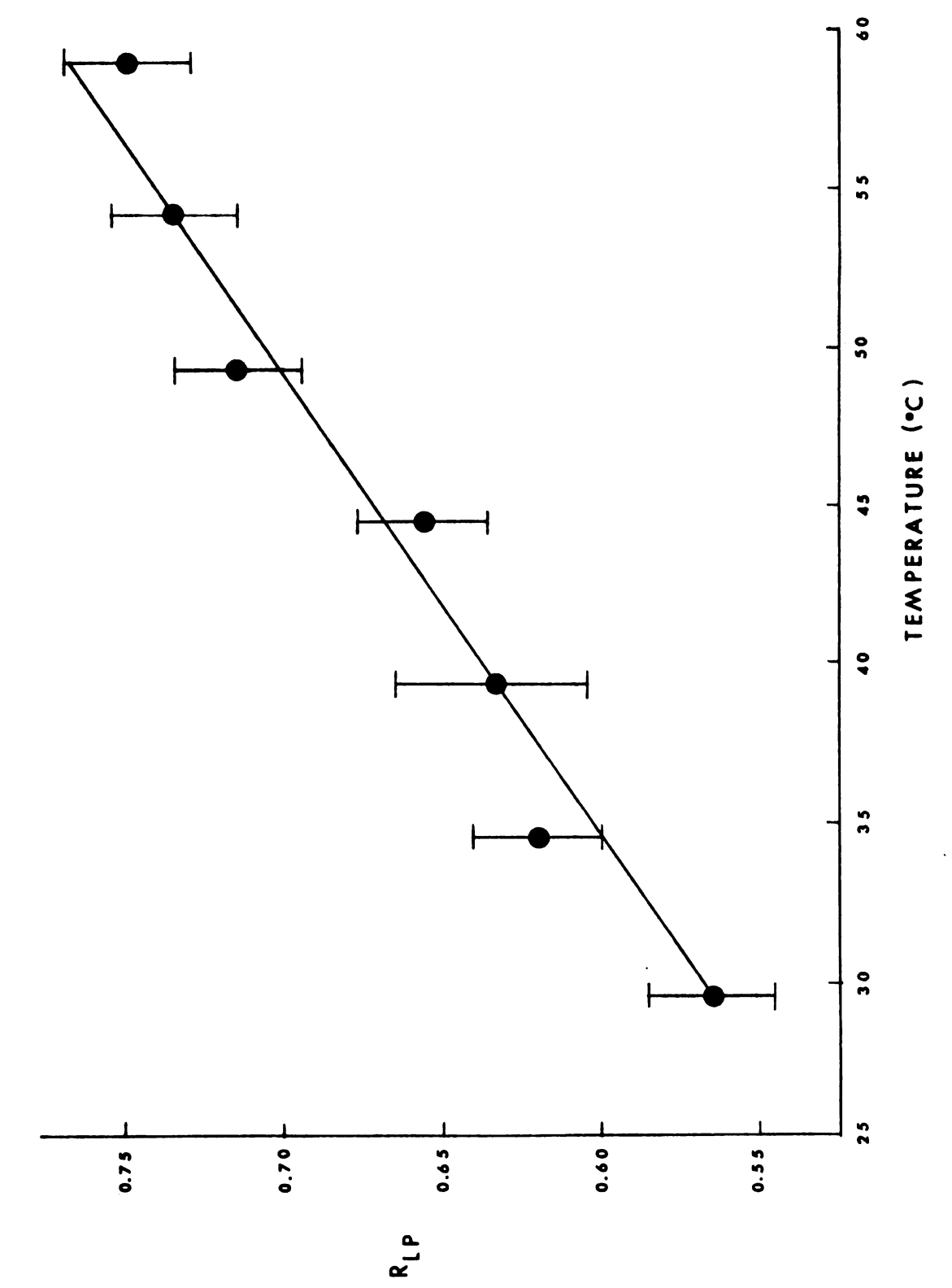


Figure 59. Landau-Placzek ratio versus temperature for neat pyridine.

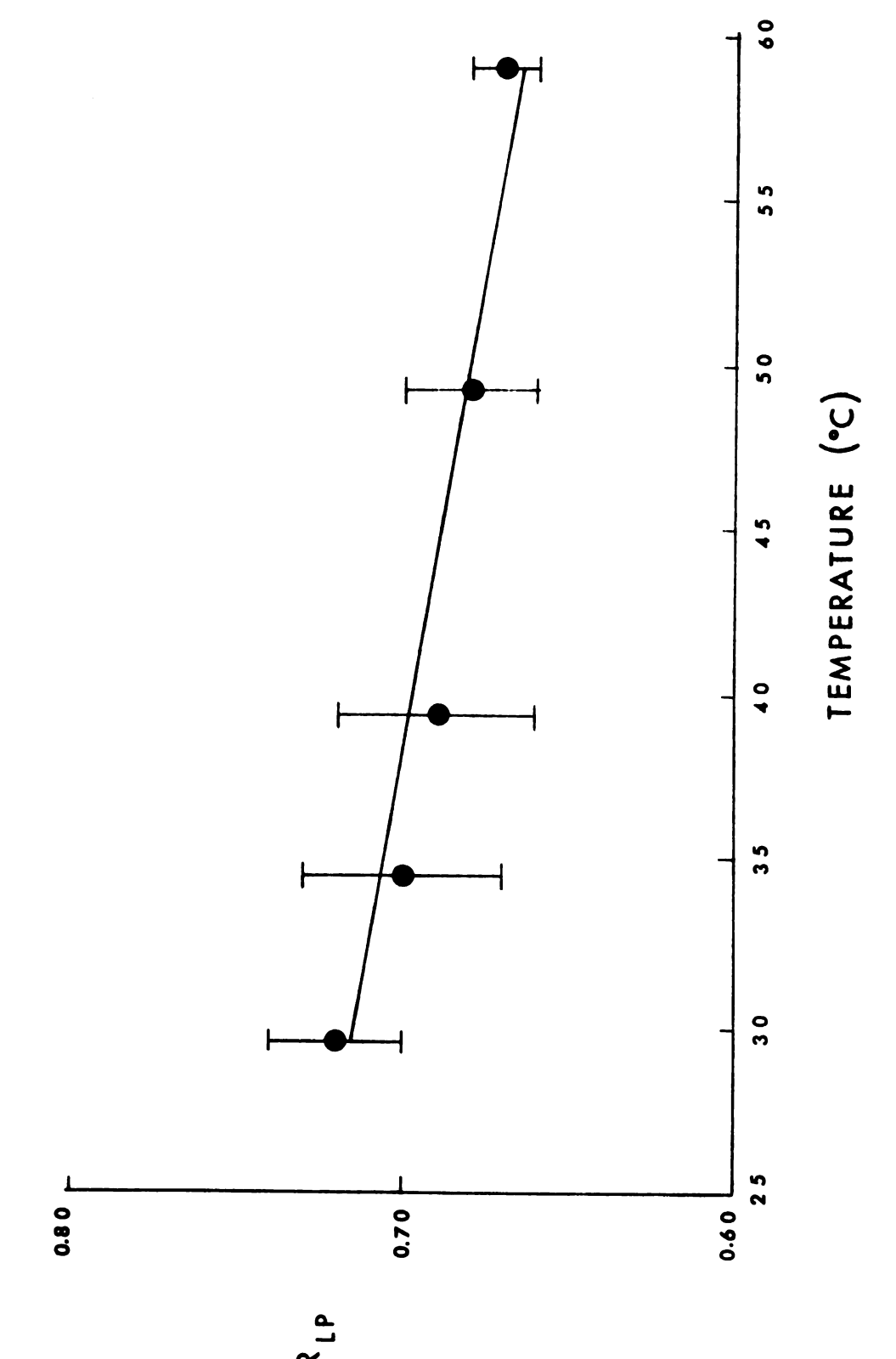


Figure 60. Landau-Placzek ratio versus temperature for 0.80 mole fraction DMSO.

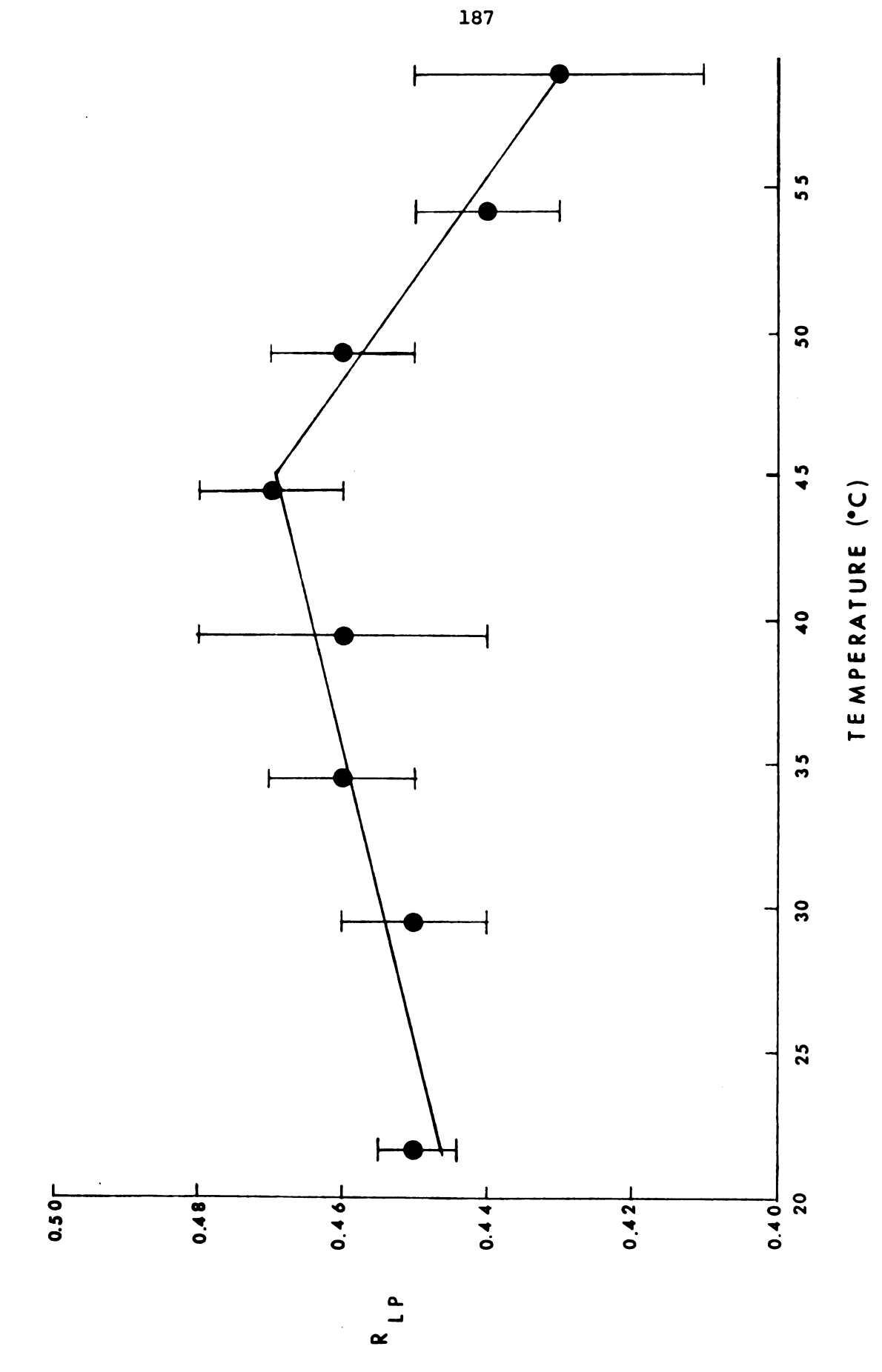
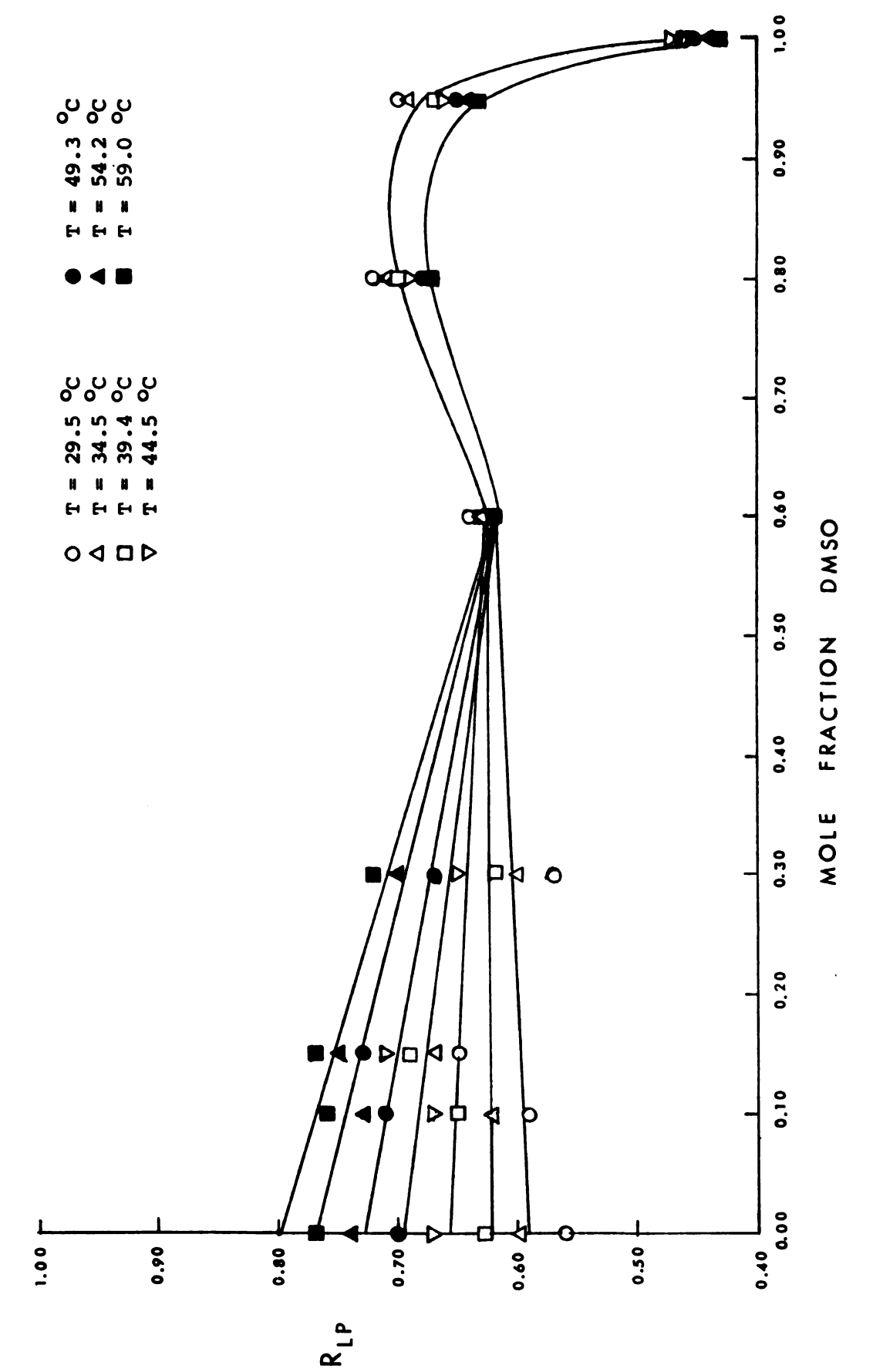


Figure 61. Landau-Placzek ratio versus temperature for neat DMSO.

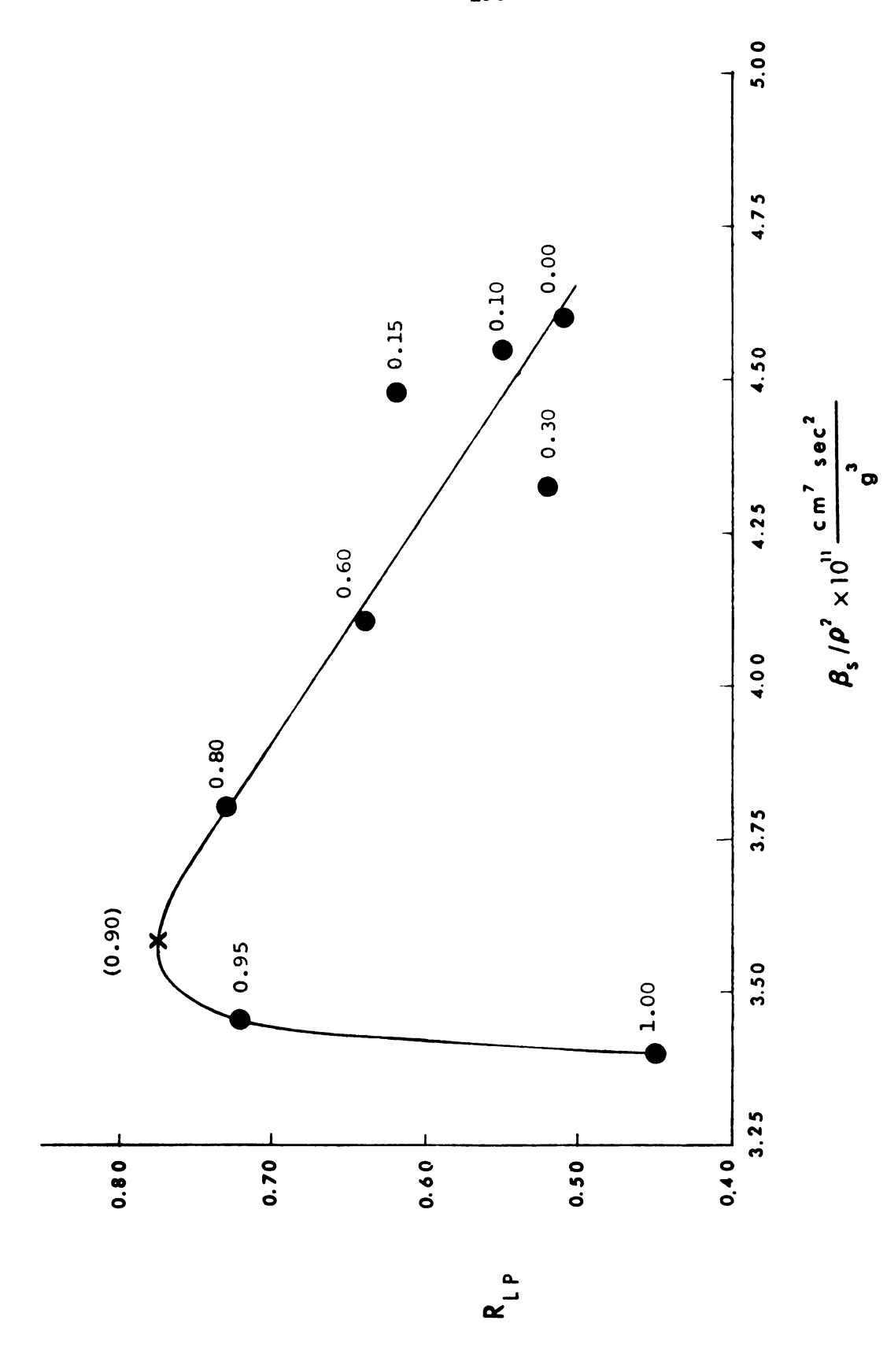


Variation of the Landau-Placzek ratio with composition for 29.5, 34.5, 39.4, 44.5, 49.3, 54.2 and 59.0 $^{\rm O}{\rm C}.$ Figure 62.

between theory and experiment for the change in $I_{\rm C}/2I_{\rm B}$ with $\beta_{\rm S/\rho}^{\ 2}$ at this temperature. From equation (70) we would expect a linear relationship between the Landau-Placzek ratio and $\beta_{\rm S/\rho}^{\ 2}$ at constant temperature; however, we should remember that equation (70) was derived under the tacit assumption that the binary mixture is ideal in nature. We know from the results of sections III A-F, that DMSO-pyridine mixtures exhibit distinctly non-ideal behavior, so that the variation in Landau-Placzek ratio with adiabatic compressibility and density can be expected to be linear only so long as the degree of association in the liquid affects $I_{\rm C}/2I_{\rm B}$ and $\beta_{\rm S/o}^{\ 2}$ to the same extent.

Figure 63 demonstrates the variation in the Landau-Placzek ratio with $\beta_{S/\rho}2$ for DMSO-pyridine mixtures at 21.6 $^{\rm O}{\rm C}$. The values of $I_{\rm C}/2I_{\rm B}$ were obtained from the respective Landau-Placzek ratio-temperature curves for each of the mixtures. The variation of $I_{\rm C}/2I_{\rm B}$ with $\beta_{\rm S/\rho}2$ in the range from pure pyridine to 0.80 mole fraction DMSO is seen to be a linear function, which is the type of relationship predicted from equation (70). The fact that the Landau-Placzek ratio increases with decreasing values of $\beta_{\rm S/\rho}2$ indicates that the change in chemical potential with concentration, $(\partial\mu/\partial c)_{\rm p,T}$, is negative as one progresses from pure pyridine to 0.80 mole fraction DMSO (see equation (70)).

At ~0.90 mole fraction DMSO, the change in Landau-Placzek ratio with $\beta_{\rm S/\rho}^{}2$ reverses sign and the Landau-Placzek ratio falls precipitously to a minimum for pure DMSO. A qualitative explanation of this abrupt drop in the Landau-Placzek ratio involves the assumption of a decrease in the damping forces in the liquid between 0.90 and 1.00 mole fraction DMSO due to an increase in association of the



Variation of the Landau-Placzek ratio with β_S/ρ^2 for mixtures of DMSO and pyridine at 21.6 $^{\circ}$ C. Numbers beside the data points indicate composition, in mole fraction DMSO. Figure 63.

DMSO molecules. A decrease in the damping forces in a liquid causes an increase in the magnitude of the pressure fluctuations which are responsible for the Brillouin peaks, thereby decreasing the Landau-Placzek ratio. The decrease in damping forces is also reflected by a concomitant decrease in the frequency-corrected absorption coefficient.

A glance at Figure 54 reveals that the frequency-corrected absorption coefficient decreases significantly between 0.80 and 1.00 mole fraction DMSO at 21.6 $^{\circ}$ C, lending credence to the qualitative explanation given above for the decrease in Landau-Placzek ratio. The fact that the change in Landau-Placzek ratio with $\beta_{\text{S/p}}^2$ takes on a positive slope between ~0.90 and 1.00 mole fraction DMSO indicates that the change in chemical potential with concentration reverses sign and becomes positive in this region. The changes in sign are undoubtedly due to the influence of increased association of the DMSO molecules in the compositional region from 0.80 to 1.00 mole fraction DMSO.

Variations in the Landau-Placzek ratio with $\beta_{\rm S/\rho}^{}2$ for temperatures above 21.6 $^{\rm O}$ C can be expected to follow the same general trends as those observed for $\rm I_C/2I_B$ at 21.6 $^{\rm O}$ C, although these variations cannot be monitored because of lack of density data.

V. CONCLUSIONS

Brillouin scattering parameters and acoustical properties have been used to monitor structural changes occurring in dimethyl sulfoxide-pyridine mixtures in the temperature range from 20 to 60 °C.

Linear variation of the refractive index, Brillouin shift, velocity of sound and sonic absorption coefficient with temperature indicated that each of the mixtures was behaving like a pure fluid with respect to these physicochemical properties. It was also noted that the refractive index and Brillouin linewidth were linear functions of composition in this temperature range. The Brillouin linewidth data represent the first reported measurements of the variation of Brillouin linewidth with temperature or composition for pure or multicomponent liquids.

Fluctuations in the velocity of sound and frequency-corrected absorption coefficient with composition denoted changes in the degree of association in the liquid. These changes were observed for each of the eight temperatures in the range from 20 to 60 °C.

Neat DMSO and neat pyridine were both found to be rather highly structured liquids, although it appeared that neat DMSO was the more ordered of the two at any given temperature. The binary mixtures were found to be less structured than the two pure solvents, with maximum disorganization of the liquid structure appearing to occur at approximately the equimolar composition. This behavior indicated, of course, that the species responsible for the highly associated nature of the mixtures of DMSO and pyridine were not complexes between DMSO and pyridine, but were homomolecular aggregates of DMSO and/or pyridine. Infrared spectroscopic data for the S-O stretching frequency for

mixtures of DMSO and pyridine at 22 °C support the concept of self-association of DMSO.

A linear relationship was observed between the Landau-Placzek ratio and the temperature for each of the DMSO-pyridine mixtures.

There was a distinct break, however, in the Landau-Placzek ratio-temperature curve for pure DMSO at 45 °C, indicating a rearrangement of the liquid structure at this temperature.

The overall changes in the Landau-Placzek ratio with composition gave supporting evidence to the interpretation of the velocity of sound and absorption coefficient data. In particular, a vast increase in association between 0.80 and 1.00 mole fraction was indicated by a precipitous drop in the Landau-Placzek ratio in this region.

The linear variation of the Landau-Placzek ratio with $\beta_{\rm S}/\nu^2$ between 0.00 and 0.80 mole fraction DMSO at 21.6 °C lent validity to the theoretical expression derived for ideal binary mixtures at constant temperature (equation (70)). The deviation from linearity observed for the mixtures between 0.80 to 1.00 mole fraction DMSO at 21.6 °C was interpreted to be a consequence of the substantial increase in association presumed to be taking place in this compositional region.

LIST OF REFERENCES

LIST OF REFERENCES

- H. Harry Szmant, "Chemistry of DMSO", in <u>Dimethyl Sulfoxide</u>,
 S. W. Jacob, E. E. Rosenbaum and D. C. Wood, eds. (Marcel Dekker, Inc., New York, 1971).
- 2. R. Figueroa, E. Roig and H. H. Szmant, Spectrochim. Acta 22, 587 (1966). Cited in Ref. 1.
- 3. F. A. Cotton, R. Francis and W. D. Horrocks, J. Phys. Chem. 64, 1534 (1960).
- 4. G. Kaufmann, M. J. F. Leroy and B. Pasche, Bull Soc. Chim. France, 3766, (1966). Cited in Ref. 1.
- 5. P. Biscarini and S. Ghersetti, Gazz. Chim. Ital. 92, 61 (1962). Cited in Ref. 1.
- 6. H. L. Schläfer and W. Schaffernicht, Angew. Chem. 72, 618 (1960).
- 7. D. Martin, A. Weise and H. J. Niclas, Angew. Chem. 79, 340 (1967).
- 8. W. S. MacGregor, Ann. N. Y. Acad. Sci. 141, 3 (1967).
- 9. J. J. Lindberg, J. Kenttamaa and A. Nissema, Suomen Kemistilehti 34B, 98 (1961).
- 10. J. J. Lindberg, J. Kenttamaa and A. Nissema, Suomen Kemistilehti 348, 156 (1961).
- 11. W. A. Millen and D. W. Watts, J.Am. Chem. Soc. 89, 6858 (1967).
- 12. R. F. Watson and J. F. Eastham, J. Am. Chem. Soc. 87, 664 (1965).
- 13. Lord Rayleigh, Scientific Papers 1, 87 (1871), Phil.Mag. 41, 447(1871).
- 14. A. D. Buckingham, lecture at Michigan State University, Dec. 8, 1970.
- 15. S. Bhagavantam, Scattering of Light and the Raman Effect (Andhra University, Waltair, India, 1940).
- 16. L. Brillouin, Ann. Physique (Paris) 17, 88 (1922).
- 17. P. Debye, Ann. Physik 39, 789 (1912).

- 18. A. Einstein, Ann. Physik 33, 1275 (1910).
- L. Brillouin, in International Conference on Light Scattering Spectra in Solids, G. B. Wright, ed. (Springer Verlag, New York, 1969).
- 20. L. Brillouin, Comp. Rendus 158, 1331 (1914). Cited in Ref. 19.
- 21. H. C. Lucas, D. A. Jackson, J. G. Powles and B. Simic-Glavaski, Molec. Phys. 18, 505 (1970).
- 22. L. Landau and G. Placzek, Physik Z. Sowjetunion 5, 172 (1934).
- 23. D. A. Pinnow, S. J. Candau, J. T. LaMacchia and T. A. Litovitz, J. Acous. Soc. Am. 43, 131 (1968).
- 24. R. D. Mountain, Rev. Mod. Phys. 38, 205 (1966).
- 25. H. Z. Cummins and R. W. Gammon, J. Chem. Phys. 44, 2785 (1966).
- 26. C. J. Montrose, V. A. Solovyev and T. A. Litovitz, <u>J. Acous. Soc.</u>
 <u>Am.</u> 43, 117 (1968).
- 27. R. D. Mountain, <u>J. Res. Natl. Bur. Std. 70A</u>, 207 (1966).
- 28. I. L. Fabelinskii, <u>Usp. Fiz. Nauk 63</u>, 355 (1957); English trans.: <u>Advan. Phys. Sci. 63</u>, 474 (1957).
- 29. G. B. Benedek and T. Greytak, Proc. IEEE 53, 1623 (1965).
- 30. C. S. Venkateswaran, Proc. Indian Acad. Sci. 15, 322 (1942).
- 31. I. L. Fabelinskii, Soviet Phys.-Doklady 1, 115 (1956).
- 32. D. J. Coumou, E. L. Mackor and J. Hijmans, <u>Trans. Far. Soc. 60</u>, 1539 (1964).
- 33. R. C. Tolman, The Principles of Statistical Mechanics (Oxford University Press, London, 1938), Ch. XIV.
- 34. L. van Hove, Phys. Rev. 95, 249 (1954).
- 35. L. I. Komarov and I. Z. Fisher, Soviet Physics JETP 16, 1358 (1963).
- 36. P. Biquard, Ann. Phys. (Paris) 6, 195 (1936). Cited in Ref. 26.
- H. B. Callen and T. A. Welten, Phys. Rev. 83, 34 (1951).
- 38. J. E. Piercy and G. R. Hanes, J. Acous. Soc. Am. 3, 1001 (1971).
- 39. G. A. Miller, J. Phys. Chem. 71, 2305 (1967).
- 40. R. Pecora, J. Chem. Phys. 48, 4126 (1968).

- 41. G. A. Miller and C. S. Lee, J. Phys. Chem. 72, 4644 (1968).
- 42. L. Blum, J. Chem. Phys. 50, 17 (1969).
- 43. R. D. Mountain and J. M. Deutch, J. Chem. Phys. 50, 1103 (1969).
- 44. L. Fishman and R. D. Mountain, J. Phys. Chem. 74, 2178 (1970).
- 45. F. H. Horne, lecture notes from the course "Advanced Thermodynamics" taught at Michigan State University, January-March, 1967.
- 46. L. D. Landau and E. M. Lifshitz, <u>Fluid Mechanics</u> (Addison-Wesley Publishing Co., Inc., Reading, Mass., 1959), Ch. 6.
- 47. L. D. Landau and E. M. Lifshitz, <u>Statistical Physics</u> (Addison-Wesley Publishing Co., Inc., Reading, Mass., 1958), Ch. 12.
- 48. H. G. Danielmeyer, J. Acous. Soc. Am. 47, 151 (1970).
- 49. D. P. Eastman, A. Hollinger, J. Kenemuth and D. H. Rank, J. Chem. Phys. 50, 1567 (1969).
- 50. I. E. Él'piner, <u>Ultrasound</u> (trans. by F. L. Sinclair, Consultants Bureau, New York, 1964).
- 51. K. F. Herzfeld and T. A. Litovitz, Absorption and Dispersion of Ultrasonic Waves (Academic Press, New York, 1959).
- 52. J. R. Pellam and J. K. Galt, J. Chem. Phys. 14, 608 (1946).
- 53. J. K. Galt, J. Chem. Phys. 16, 505 (1948).
- 54. J. M. M. Pinkerton, <u>Proc. Phys. Soc. London B 62</u>, 129 (1949); Ibid., p. 286.
- 55. L. Hall, Phys. Rev. 73, 775 (1948).
- 56. G. Rai, B. K. Singh and O. N. Awasthi, Phys. Rev. A5, 918 (1972).
- 57. S. L. Shapiro, M. McClintock, D. A. Jennings and R. L. Barger, <u>IEEE Trans. Quantum Elec. QE2</u>, 89 (1966).
- 58. S. Gewurtz, W. S. Gornall, and B. P. Stoicheff, <u>J. Acous. Soc. Am.</u> 49, 994 (1971).
- 59. G. I. A. Stegeman, W. S. Gornall, V. Volterra and B. P. Stoicheff, J. Acous. Soc. Am. 49, 979 (1971).
- 60. H. W. Leidecker, Jr., and J. T. LaMacchia, J. Acous. Soc. Am. 43, 143 (1968).
- 61. A. L. Bloom, Appl. Opt. 5, 1500 (1966).

- 62. V. N. Del Piano, Jr, and A. F. Quesada, Appl. Opt. 4, 1386 (1965).
- 63. I. M. Are'fev, V. S. Starnov and I. L. Fabelinskii, Sov. Phys. JETP Letters 6, 163 (1967).
- 64. C. J. Montrose and K. Fritsch, J. Acous. Soc. Am. 47, 786 (1970).
- 65. H. C. Lucas, D. A. Jackson and H. T. A. Pentecost, Opt. Comm. 2, 239 (1970).
- 66. M. Born and E. Wolf, <u>Principles</u> of <u>Optics</u>, 3rd ed. (Pergamon Press, London, 1965).
- 67. J. W. Moore, <u>Physical Chemistry</u>, 3rd ed. (Prentice-Hall, Inc., Englewood Cliffs, New Jersey, 1962).
- 68. S. G. Lipson and H. Lipson, Optical Physics (Cambridge University Press, London, 1969).
- 69. P. Debye, Polar Molecules (Chemical Catalog Co., Inc., New York, 1929).
- 70. L. Onsager, J. Am. Chem. Soc. 58, 1486 (1936).
- 71. S. J. Gaumer, "A Brillouin Spectrophotometer," Ph.D. Thesis, Department of Chemistry, Michigan State University, 1972.
- 72. J. B. Kinsinger, M. M. Tannahill, M. S. Greenberg and A. I. Popov, "Studies of Dimethylsulfoxide Association in Dimethylsulfoxide-Pyridine Mixtures," to be published.
- 73. H. K. Yuen, "Low Angle and Brillouin Light Scattering from Inhomogeneous Amorphous Polymers," Ph.D. Thesis, Department of Chemistry, Michigan State University, 1972.
- 74. L. Y. Wong and A. Anderson, J. Opt. Soc. Am. 62, 1112 (1972).
- 75. C. L. O'Connor and J. P. Schlupf, J. Acous. Soc. Am. 40, 663(1966).
- 76. D. H. Rank, E.M. Kiess and U. Fink, J. Opt. Soc. Am. 56, 163(1966).
- 77. G. W. Marks, J. Acous. Soc. Am. 41, 103 (1967).
- 78. A. Giacomini, Acta Pontificia Acad. Sci. 6, 87(1942).
- 79. A. E. Lutskii and V. N. Solon'ko, Russ. J. Phys. Chem. 38, 217(1964).
- 80. A. E. Lutskii and V. N. Solon'ko, Russ. J. Phys. Chem. 39, 414(1965).
- 81. E. G. Richardson, <u>Ultrasonic Physics</u> (Elsevier Publishing Company, Amsterdam, 1952).
- 82. I. L. Fabelinskii, Molecular Scattering of Light (trans. by R. T. Beyer, Plenum Press, New York, 1968).

- 83. B. B. Kudriavtsev, Soviet Phys.-Acoust. 2, 36 (1956). Cited in Ref. 77.
- 84. A. J. Parker, in Advances in Organic Chemistry, Methods and Results, Vol. 5 (R. A. Raphall, E. C. Taylor and H. Wynberg, eds., Wiley Interscience, New York, 1965). Cited in Ref. 1.
- 85. R. Thomas, C. B. Shoemaker and K. Eriks, Acta Cryst. 21, 12 (1966).
- 86. M. Greenspan, in <u>American Institute of Physics Handbook</u>, 3rd ed. (D. E. Gray, coordinating ed., McGraw-Hill Book Company, New York, 1972).



Appendix A

Temperature Calibration Data for the Thermal Characterization of the Control Cell Employed in the Brillouin Scattering Measurements

- T_C = temperature of thermometer C in the copper block
- T_A = actual temperature of the glycerin sample used for the calibration procedure
- T_C and T_A are both equilibrium temperatures

Table 23
Temperature Calibration Data

T _C (°C)	T _A (OC)
69.9	68.8
64.7	63.9
59.8	58.9
54.6	53.9
49.6	49.3
44.7	44.5
39.6	39.3
37.8	37.4
36.8	36.5
35.7	35.4
34.8	34.5
33.7	33.5
32.8	32.6
31.7	31.5
30.6	30.5

Table 23 (cont.)

T _C (°C)	T _A (OC)
29.6	29.5
28.6	28.6
27.8	27.7
26.8	26.7
24.9	24.9
21.6	21.6

Appendix B

Calculation of the Refractive Index at 5145A

Following the equations given in the Bausch and Lomb Abbe 3-L Refractometer instrument manual, the refractive index for λ = 5145A was calculated for each of the DMSO-pyridine solutions at five different temperatures. The equations used in the calculations are

$$n_{5145A}^{T} = A' + \frac{B'}{(514.5 \text{nm})^2}$$

$$A' = n_{D}^{T} - 2.8796 \times 10^{-6} B'$$

$$B' = 0.52364 \times 10^{6} (n_{F} - n_{C})$$

$$(n_{F} - n_{C}) = A + BC,$$

where A, B, and C are empirical constants for the system under investigation.

The dispersion, (n_F-n_C) , is the difference in the refractive index of the liquid at two known wavelengths, 656 and 486 nm, respectively. Because of the construction of the compensators in the Bausch and Lomb Abbe 3-L Refractometer, the dispersion can be accurately determined from values of A, B, and C, which are given in the Bausch and Lomb Dispersion Table. A, B, and C depend on the refractive index of the sample and on the drum readings of the refractometer obtained during measurements of n_D .

In Table 24 are given values for n_D , the average drum reading, A, B, and C, and the calculated dispersion, (n_F-n_C) , for the DMSO-pyridine mixtures at 26.4 $^{\rm O}$ C. Calculations of the dispersion at other temperatures followed the same format. Table 25 presents the

results for A', B' and $n_{5145\text{A}}^{\circ}$ for the DMSO-pyridine mixtures at 26.4 °C. The accuracy in the calculation of $n_{5145\text{A}}^{\circ}$ using this dispersion correction procedure is \pm 0.0005.

After the refractive index at λ = 5145Å had been calculated in a similar manner for the DMSO-pyridine mixtures at the four other temperatures, it was determined that the refractive index at 5145Å was a linear function of the refractive index at 5890Å. For each mixture it was found that

$$n_{5145A}^{T} \stackrel{O}{=} n_{D}^{T} + k,$$

 $(n_F - n_C) = A + BC$

mole frac. DMSO	n _D	average drum reading	A	В	c	(n _F - n _C)
1.000	1.4763	20.4	0.02417	0.02704	-0.482	0.01114
0.9453	1.4785	20.5	0.02417	0.02694	-0.477	0.01132
0.8004	1.4831	21.0	0.02415	0.02676	-0.454	0.01200
0.7005	1.4863	21.0	0.02415	0.02662	-0.454	0.01206
0.6002	1.4894	21.5	0.02414	0.02650	-0.431	0.01272
0.4993	1.4917	21.8	0.02414	0.02641	-0.416	0.01315
0.4016	1.4942	21.8	0.02413	0.02630	-0.416	0.01319
0.2996	1.4962	22.5	0.02413	0.02621	-0.383	0.01409
0.2000	1.5010	23.0	0.02412	0.02600	-0.358	0.01481
0.1500	1.5020	23.4	0.02412	0.02595	-0.339	0.01532
0.1005	1.5035	23.4	0.02411	0.02588	-0.339	0.01534
0.0499	1.5053	23.4	0.02411	0.02582	-0.339	0.01536
0.0000	1.5064	24.0	0.02411	0.02576	-0.309	0.01615

$$n_{5145}^{O} = A' + \frac{B'}{(514.5 \text{nm})^2}$$

mole frac. DMSO	_A'	в'	n5145Å
1.000	1.4595	5.833 x 10 ³	1.4815 ± 0.0005
0.9453	1.4614	5.928 x 10 ³	1.4838
0.8004	1.4650	6.284×10^3	1.4887
0.7005	1.4681	6.315 x 10 ³	1.4920
0.6002	1.4702	6.661×10^3	1.4954
0.4993	1.4719	6.886×10^3	1.4979
0.4016	1.4743	6.907×10^3	1.5004
0.2996	1.4750	7.378 \times 10 ³	1.5029
0.2000	1.4787	7.755×10^3	1.5080
0.1500	1.4789	8.022×10^3	1.5092
0.1005	1.4804	8.033×10^3	1.5108
0.0499	1.4821	8.043×10^3	1.5125
0.0000	1.4820	8.457 x 10 ³	1.5140

Table 26 Temperature Dependence of the Refractive Index for λ = 5890 and 5145A

j -	pure C ₅ H ₅ N	i -	(05 r	nole % DN	iso
k	= 0.0074			k	= 0.0073	3
T(°C)	n ₅₈₉₀ A	n ₅₁₄₅ A	T(°C))	n ₅₈₉₀ A	n _{5145A}
59.0	1.4870	1.4944	59.0		1.4875	1.4948
54.2	1.4900	1.4974	54.2		1.4901	1.4974
49.3	1.4928	1.5002	49.3		1.4927	1.5000
44.5	1.4957	1.5031	44.5		1.4953	1.5026
39.4	1.4987	1.5061	39.4		1.4980	1.5053
34.5	1.5017	1.5091	34.5		1.5007	1.5080
29.5	1.5047	1.5121	29.5		1.5034	1.5107
21.6	1.5094	1.5168	21.6		1.5076	1.5149
10 1	mole & DMS	<u> </u>	·	15 r	nole % Di	<u>450</u>
k	= 0.0072			k	= 0.007	L
59.0	1.4842	1.4914	59.0		1.4816	1.4887
54.2	1.4870	1.4942	54.2		1.4846	1.4917
49.3	1.4899	1.4971	49.3		1.4877	1.4948
44.5	1.4927	1.5000	44.5		1.4908	1.4979
39.4	1.4957	1.5029	39.4		1.4941	1.5012
34.5	1.4986	1.5058	34.5		1.4972	1.5043
29.5	1.5015	1.5087	29.5		1.5004	1.5075
21.6	1.5062	1.5134	21.6		1.5054	1.5125

Table 26 (cont.)

20	mole & DM	<u>50</u>	3	00 mole % D	MSO
k	- 0.0069			k = 0.006	6
T(OC)	n ₅₈₉₀ A	ⁿ 5145A	T(OC)	n ₅₈₉₀ A	ⁿ 5145A
59.0	1.4801	1.4870	59.0	1.4828	1.4894
54.2	1.4832	1.4901	54.2	1.4848	1.4914
49.3	1.4864	1.4933	49.3	1.4868	1.4934
44.5	1.4896	1.4965	44.5	1.4887	1.4953
39.4	1.4929	1.4998	39.4	1.4908	1.4974
34.5	1.4961	1.5030	34.5	1.4928	1.4994
29.5	1.4994	1.5063	29.5	1.4949	1.5015
21.6	1.5046	1.5115	21.6	1.4981	1.5047
40 1	mole % DMS	<u>50</u>	<u>5</u>	0 mole % D	MSO_
k	= 0.0063			k = 0.006	2
59.0	1.4791	1.4854	59.0	1.4760	1.4822
54.2	1.4813	1.4876	54.2	1.4784	1.4846
49.3	1.4836	1.4899	49.3	1.4807	1.4869
44.5	1.4858	1.4921	44.5	1.4831	1.4893
39.4	1.4881	1.4944	39.4	1.4856	1.4918
34.5	1.4904	1.4967	34.5	1.4880	1.4942
29.5	1.4927	1.4990	29.5	1.4904	1.4966
21.6	1.4964	1.5027	21.6	1.4943	1.5005

Table 26 (cont.)

k				70 mole % DMSO		
	= 0.0058		3	c = 0.005	7	
T(OC)	n ₅₈₉₀ A	n ₅₁₄₅	T(OC)	n ₅₈₉₀ A	n ₅₁₄₅ A	
59.0	1.4726	1.4784	59.0	1.4707	1.4764	
54.2	1.4751	1.4809	54.2	1.4730	1.4787	
49.3	1.4776	1.4834	49.3	1.4753	1.4810	
44.5	1.4801	1.4859	44.5	1.4775	1.4832	
39.4	1.4827	1.4885	39.4	1.4799	1.4856	
34.5	1.4852	1.4910	34.5	1.4823	1.4880	
29.5	1.4878	1.4936	29.5	1.4846	1.4903	
21.6	1.4919	1.4977	21.6	1.4883	1.4940	
80 r	nole % DMS	5O	95	mole % DM	4 SO	
		-				
59.0	1.4657	1.4714	59.0	1.4643		
54.2	1.4682	1.4739	54.2	1.4664	1.4717	
49.3	1.4708	1.4765	49.3	1.4685	1.4738	
44.5	1.4734	1.4791	44.5	1.4706	1.4759	
39.4	1.4761	1.4818	39.4	1.4728	1.4781	
34.5	1.4786	1.4843	34.5	1.4749	1.4802	
29.5	1.4813	1.4870	29.5	1.4770	1.4823	
21.6	1.4855	1.4912	21.6	1.4804	1.4857	
	59.0 54.2 49.3 44.5 39.4 34.5 29.5 21.6 80 r k 59.0 54.2 49.3 44.5 39.4 34.5 29.5	59.0 1.4726 54.2 1.4751 49.3 1.4776 44.5 1.4801 39.4 1.4827 34.5 1.4852 29.5 1.4878 21.6 1.4919 80 mole % DMS k = 0.0057 59.0 1.4657 54.2 1.4682 49.3 1.4708 44.5 1.4734 39.4 1.4761 34.5 1.4786 29.5 1.4813	59.0 1.4726 1.4784 54.2 1.4751 1.4809 49.3 1.4776 1.4834 44.5 1.4801 1.4859 39.4 1.4827 1.4885 34.5 1.4852 1.4910 29.5 1.4878 1.4936 21.6 1.4919 1.4977 80 mole % DMSO k = 0.0057 59.0 1.4657 1.4714 54.2 1.4682 1.4739 49.3 1.4708 1.4765 44.5 1.4734 1.4791 39.4 1.4761 1.4818 34.5 1.4786 1.4843 29.5 1.4813 1.4870	59.0 1.4726 1.4784 59.0 54.2 1.4751 1.4809 54.2 49.3 1.4776 1.4834 49.3 44.5 1.4801 1.4859 44.5 39.4 1.4827 1.4885 39.4 34.5 1.4852 1.4910 34.5 29.5 1.4878 1.4936 29.5 21.6 1.4919 1.4977 21.6 80 mole % DMSO 95 k = 0.0057 95 59.0 1.4657 1.4714 59.0 54.2 1.4682 1.4739 54.2 49.3 1.4708 1.4765 49.3 44.5 1.4734 1.4791 44.5 39.4 1.4761 1.4818 39.4 34.5 1.4786 1.4843 34.5 29.5 1.4813 1.4870 29.5	59.0 1.4726 1.4784 59.0 1.4707 54.2 1.4751 1.4809 54.2 1.4730 49.3 1.4776 1.4834 49.3 1.4753 44.5 1.4801 1.4859 44.5 1.4775 39.4 1.4827 1.4885 39.4 1.4799 34.5 1.4852 1.4910 34.5 1.4823 29.5 1.4878 1.4936 29.5 1.4846 21.6 1.4919 1.4977 21.6 1.4883 80 mole % DMSO 95 mole % DM k = 0.0057 59.0 1.4657 1.4714 59.0 1.4643 54.2 1.4682 1.4739 54.2 1.4664 49.3 1.4708 1.4765 49.3 1.4685 44.5 1.4734 1.4791 44.5 1.4706 39.4 1.4761 1.4818 39.4 1.4728 34.5 1.4813 1.4870 29.5 1.4770	

Table 26 (cont.)

pure DMSO

k = 0.0052

T(OC)	n5890A	n _{5145A}
59.0	1.4622	1.4674
54.2	1.4643	1.4695
49.3	1.4664	1.4716
44.5	1.4685	1.4737
39.4	1.4708	1.4760
34.5	1.4729	1.4781
29.5	1.4751	1.4803
21.6	1.4785	1.4837